ELECTRICAL INDUCED POLARISATION PROPERTIES

OF SATURATED BUNTER SANDSTONES

F.A. COLLAR

Thesis submitted for
the degree of Doctor of Philosophy,
to the Faculty of Science and Engineering
University of Birmingham.

UNIVERSITY OF BIRMINGHAM

University of Birmingham Research Archive

e-theses repository

ACKNOWLEDGEMENTS

UNITS

Most of the units used in this thesis conform to the SI
specification. It should be noted however that whereas
the units of electrical conductivities are written as
$(\Omega m)^{-1}$ in the diagrams, in the text they are referred
to as mhos m^{-1} for typewriting convenience. A departure
from SI units occurs in Chapter 10 where field measure-
ments are described in feet, retaining the calibration
of the field cables. So although these field data are
presented and interpreted in imperial units for convenience,
in discussion of the results they are converted to SI units.

CONTENTS

CHAPTER 1

INTRODUCTION

With the growing demand for supplies of potable water, in the UK as well as elsewhere, the efficient utilisation of aquifers is becoming increasingly important. However, for a groundwater extraction scheme to be planned and developed to maximum advantage the aquifer parameters must be known beforehand. In England, the Permo-Triassic sandstones constitute one of the more important and widespread aquifers. The hydrological parameters of these formations are geographically very variable, not only throughout the country as a whole (e.g. Crook, Daw, Howell and Morgan 1971; Crook, Howell, Woodhead and Worthington 1973) but sometimes also within the confines of individual aquifers (Barker and Worthington 1973a) and therefore it is necessary to determine the distribution of permeabilities or transmissibilities. Conventionally these parameters are estimated from controlled pumping tests on boreholes, ideally the surrounding water levels being monitored in a number of observation holes (Johnson Division UOP Co. 1966). Using this method to locate areas of potentially high yield from aquifers on which there is little or no geological control, for example those that are drift covered, requires a very costly programme of drilling arbitrarily located boreholes.

For those aquifers where the water flow is predominantly intergranular rather than fissure controlled, it may be possible to estimate the flow parameters from surface geophysical measurements which are made in conjunction with a few carefully sited boreholes (Worthington and Griffiths 1975). This approach could offer a considerable saving of time and money over the usual arbitrarily sited boreholes method.

Although there are a number of different geophysical measurements that can be made in boreholes to estimate local hydraulic properties (Lynch

- 1 -

1962) the seismic and electrical methods are the most practical for surface work, and these are usually employed to determine porosity. Applications of the seismic method to some Bunter sandstones have been studied by Forshaw 1975, Worthington 1976, Worthington and Griffiths 1975, Barker and Worthington 1973 and are not considered further here.

Of the electrical methods, the measurement of resistivity has been most often used to estimate aquifer hydraulic properties, and with reference to English Bunter sandstones, much research on this topic has already been done at Birmingham University geophysics department. Induced polarisation (IP) is another electrical property which several authors have compared with the hydraulic properties of sandstones, although generally the small amount of research done in this field has been restricted to the empirical approach. At Birmingham, IP has been studied in conjunction with the resistivity research on Bunter sandstones. This was first done by Barker (1971) measuring in the frequency domain but without positive conclusion, and subsequently in this case using the time domain.

1.a **Resistivity Techniques to estimate Porosity**

The initial work in this field was directed principally towards interpretation of well resistivity logs in the search for hydrocarbon reservoirs. Archie (1942) established an expression relating the resistivity of a water saturated clean sandstone to its porosity:

$$F = \emptyset^{-m}$$

where $\emptyset$ is the sandstone porosity

m   is a constant

F, the formation resistivity factor, he defined by

$$F = \frac{\rho_s}{\rho_w}$$

where ρ_s and ρ_w are the resistivities of the saturated sandstone and

saturating solution respectively. The expression, known as 'Archie's formula', was generalised by Wyllie and Gregory (1953) to the form

$$F = a\emptyset^{-m}$$ 1.1

where 'a' is also a constant.

Various workers have since assigned different values to the constants 'a' and 'm' in relation to particular sandstone formations.

Strictly, the expression is applicable only to 'clean' sands and sandstones i.e. those types in which there is no conducting matrix component and all ionic conduction occurs through the pore fluid. For a sand or sandstone which has a conducting matrix, the ratio ρ_s / ρ_w is not constant for a given sample over a range of pore water salinities and Archie's formula cannot be directly applied. This was recognised by Patnode and Wyllie (1950) who re-defined the ratio ρ_s / ρ_w as an apparent formation factor F_a and showed that the true formation factor F, for which Archie's formula is still valid, may be obtained via an espression of the form -

$$\sigma_s = \sigma_m + \frac{\sigma_w}{F}$$ 1.2

where $\sigma_s = \dfrac{1}{\rho_s} = $ conductivity of the sample

$\sigma_m = $ bulk conductivity of the matrix (constant)

$\sigma_w = \dfrac{1}{\rho_w} = $ conductivity of the saturating solution

$F = $ true formation factor.

This expression, in support of which the authors presented experimental data, implies that the rock matrix and the pore water may be considered as parallel and independent conductors and a graph of σ_s against σ_w has a slope $\dfrac{1}{F}$ with an intercept σ_m. Winsauer and McCardell (1953) showed this expression to be inadequate over wide ranges of pore water conductivity. They attributed matrix conduction to an ionic double

layer about the surfaces of charged clay particles and showed it to be dependent upon pore water salinity. They attributed the departure of their experimental data from the Patnode and Wyllie expression to this ionic interaction. For similar reasons Hill and Milburn (1956) rejected the equation of Patnode and Wyllie and invoked the empirical equation

$$F_a = F_{.01} \ (\rho_w \cdot 100)^{b.\log (\rho_w \cdot 100)} \quad \ldots\ldots\ldots \ 1.3$$

to fit their experimental data. In this expression F_a is the apparent formation factor corresponding to a pore water resistivity ρ_w, $F_{.01}$ is the apparent formation factor corresponding to $\rho_w = 0.01$ ohm m and 'b' is a constant for a given sandstone. These authors suggested that for low ρ_w, the clay mineral resistivity effects were negligible in contrast to the overall resistivity and therefore $F_{.01}$ could be regarded as a reasonable estimate of F. With a knowledge of b, ρ_s and ρ_w for a particular sandstone, F could therefore be calculated and hence also porosity $\emptyset$. Experimental data suggested that the 'b' factor of a sandstone sample could be evaluated by measuring its cation exchange capacity.

Although the above studies were directed toward petroleum exploration and production, the problems and concepts discussed are equally relevant to the study of electrical properties of sandstone aquifers. In this sphere Worthington (1970 and subsequently) has made significant progress by planning a field resistivity technique for estimating the porosities of saturated Bunter sandstones. Concentrating his efforts upon the Bunter sandstone aquifer in the Fylde (Lancs), he firstly established that the sandstone matrix was conductive and therefore adopted the approach of Hill and Milburn (1956). From electrical conductivity measurements upon a number of saturated sandstone samples he calculated 'b' factors as a measure of matrix conduction, and the formation factors $F_{.01}$, the latter being taken as a good approximation to the true formation factor F. He noted that for samples taken from any one

borehole, the value of 'b' did not vary greatly. Furthermore by measuring porosities, $\emptyset$, he showed that the data satisfied Archie's formula in the form

$$F = a\emptyset^{-m}$$

where m = 1.75   a = 1.49

By sampling from a large number of boreholes Worthington was able to construct distribution maps of averaged 'b' factors and groundwater conductivity. Incorporating with these maps the apparent formation factors F_a , calculated from surface resistivity measurements, he then obtained areal distributions of averaged porosities through expressions 1.3 and 1.1 . Although his attempt to relate these data with well yields met with only limited success, the work provided a useful basis for further research.

Later, Barker (1971) showed that the empirical expression (1.3) derived by Hill and Milburn incorporating the formation factor $F_{.01}$ was inadequate to describe the conductivity data for these Bunter sandstones over a range of low pore water salinities and demonstrated that the 'b' factors determined by Worthington were therefore of limited use. Barker also showed that in fact the relatively simple expression (1.2) proposed by Patnode and Wyllie described the sandstone conductivity data adequately over the range of low groundwater conductivities encountered in the Fylde.

1.b Studies of membrane IP in saturated sandstones as a possible method to determine permeability

There are two main types of induced electrical polarisation in the ground. One of these, known as electrode polarisation, may be observed in rocks which contain electronically conductive minerals. In this case the polarisation develops through electrolytic reactions at the faces of these mineral grains, where the mode of electrical conduction changes from ionic in the pore moisture to electronic in the crystal lattice (Loeb 1976).

This type of polarisation is commonly employed in prospecting for disseminated sulphide mineralisation (Bertin 1976) and is not relevant to this work. The other type of polarisation, referred to as the normal or membrane effect, is usually observed in saturated porous rocks and unconsolidated sediments. Although opinions differ on the exact causes of this IP, the effect is usually associated with the ion selective properties of active clays within the rock matrix (Keller and Frischknecht 1966).

A number of authors have shown membrane IP in frequency and time domains to be related to various rock properties including permeability and cation exchange capacity, and have demonstrated a dependence of IP upon pore water salinity. Their investigations, usually carried out on a small number of samples, have not so far led to a unique account of the origin of membrane IP; in fact some apparently contradictory conclusions have been drawn.

The first comprehensive study of membrane IP was by Vacquier, Holmes, Kintzinger and Lavergne (1957). They showed that for saturated clay coated sands, the observed IP was approximately proportional to the cation exchange capacity of the clay, and that whilst the type of cation within the pore water influenced the magnitude of the IP, anions had little or no effect. However they concluded that as a general rule IP decreased as pore water conductivity increased, and further that IP decay rate decreased with increased grain size. These authors introduced a membrane concept to explain the IP phenomenon. They suggested that at the constrictions of the pore spaces, the clays effectively form an electro-negative membrane in which electrodialysis is induced by the applied field. The IP decay is observed when, on removal of the applied field, the displaced cations return to exchange positions within the clay.

Ogilvy and Kuzmina (1972) showed an inverse bi-logarithmic proportionality between IP decay rate and grain size and also claimed to show that IP decay rate varied according to the salinity of the saturating solution. An interesting aspect of their work, consistent with the findings of Keller and Frischknecht (1966), was to demonstrate the dependence of chargeability upon the content and type of clay within a sandstone sample. Their results indicated that as clay content increased from zero, IP also increased from zero but eventually reached a maximum and thereafter decreased. The relative amplitude and position of this maximum varied according to the type of clay present.

Measuring in the frequency domain, Schoeppel and Thrasher (1966) reported that for sandstones saturated with highly saline pore water, IP increased for decreasing cation exchange capacity, increasing permeability and increasing salinity. They also showed a relationship between permeability and cation exchange capacity which they described with an empirical logarithmic equation.

On the basis of laboratory results such as these, several workers have measured IP in the field to investigate the locations and permeabilities of aquifers, with particular reference to unconsolidated sediments. Possibly the first of these were Vacquier et al (1957) who reported surveys made in New Mexico. They measured IP to determine areas of relatively pure groundwater and high permeability in volcanic alluvium and buried river channels, although they did not attempt to quantify their analyses. They associated high IP values with low salinity water, and a slow decay rate with high permeability. More recently Bodmer, Ward and Morrison (1968) conducted an IP survey in California, measuring in the frequency domain, and located clayey intercalations within a shallow sand and gravel aquifer.

Worthington (1970) recognised that instead of interpolating averaged 'b' factors between boreholes in the Bunter sandstone, these parameters might be determined directly from IP field measurements. This seems appropriate as 'b' factors and IP have been shown to be related to cation exchange capacity (Hill and Milburn 1956; Vacquier et al 1957; Schoeppel and Thrasher 1966). Research was carried out for this purpose by Barker (1971) who tackled the problem by measuring frequency domain IP in the laboratory and the field. In neither instance though was he able to demonstrate any systematic variations between the IP frequency effect (FE) and matrix properties of the sandstones, and attempts to relate FE to porosity and permeability were similarly unsuccessful. This may have been largely due to insufficient sampling from individual boreholes.

1.c Outline of this research

The research described in this thesis primarily investigates the scope of IP as a method of determining the permeabilities of Bunter sandstones in situ. Although a limited amount of preliminary fieldwork has been completed, the project has been largely confined to the laboratory, directed toward identification of the petrophysical factors involved, rather than determination of aquifer geometry. In contrast to all of the previous studies, the conclusions are supported by a large number of measurements.

IP has been measured in the time domain exclusively. Compared to the frequency domain method this offers the advantages of a wider scope of information from which a suitable measure of chargeability may be selected, together with the facility to monitor the potential decay for spurious results.

Without established quantitative theory from which a start could be made, the approach was to seek for relationships amongst experimental data.

Before the laboratory electrical measurements were carried out, some preliminary petrological examinations were made on a few sandstone samples. These studies, using scanning electron microscopy and x-ray diffraction methods, were designed to obtain information on the types, distribution and habit of the clay fractions.

Initial electrical measurements were designed to test the apparatus, to establish that the observed potential decay obtained with sandstones was wholly an induced polarisation of the sample and not partly polarisation of the electrodes or concentration effects across the measuring cell. A preliminary series of IP and sandstone conductivity measurements were taken on a few Fylde samples over a very wide range of pore water salinities so that on the basis of the results further measurements with appropriate controls could be planned. A simple electrical model of the sandstone was invoked to account for the observed variation of the conductivity data. The variation of IP with permeability was investigated for a large number of sandstones with suitable pore water control, and because of the diversity of the results a representative selection of the samples was then subjected to further measurements of IP over a range of pore water salinities. All these data have been described by empirical expressions which relate IP, permeability and matrix conductivity, and some geological implications of these results have been considered. Preliminary fieldwork has been done in the Fylde to find out whether an empirical relationship determined in the laboratory can be used to evaluate field permeabilities directly. The problems involved have been considered and further work in this direction is suggested.

CHAPTER 2

PETROLOGICAL AND MINERALOGICAL STUDIES ON THE CLAY MATRIX

Keller and Frischknecht (1966), Ogilvy and Kuzmina (1972) showed that both the abundance and the mineralogical type of a clay within a real or artificial sandstone influenced the magnitude of the IP. Their data indicate that generally for the clay fraction increasing from zero, IP also increased from zero but reached a maximum value and thereafter decreased. The relative position and amplitude of the IP maximum was determined according to the clay mineralogy.

In this instance suitable clay analyses from the Bunter sandstones were not readily available for comparison, therefore some elementary petrological and mineralogical studies were made. A few unweathered samples from the sandstones of St. Bees (Cumberland), the Fylde (Lancashire), Shropshire and the Vale of Clwyd were examined using mainly the scanning electron microscope (S.E.M.) optical microscope and x-ray diffraction (X.R.D.) equipment.

2.a Optical microscopy

Thin sections of sandstone and whole rock fragments were studied in transmitted and reflected light respectively. High magnification of thin sections revealed a semi-continuous thin red margin around each quartz grain which appeared to thicken about the points of contact. More complete descriptions of this type of thin section are given in texts such as Greensmith (1978).

The reflected light method was restricted by the limited depth of focus upon the rough fragments but could be used to reveal some typical features. Fig: 1 is a photomicrograph of a fragment of sandstone from the Fylde, magnified by 400. The picture shows two types of clay mineral upon a plane surface of colourless re-crystallised quartz. One of these
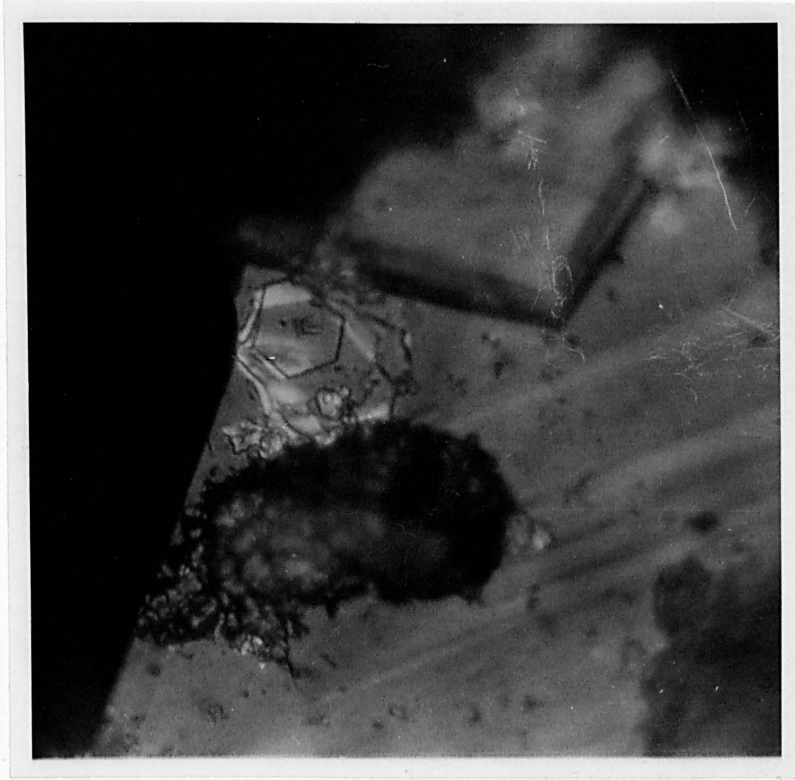
X 400

Photomicrograph in reflected light of a fragment of
Bunter sandstone from the Fylde. Colourless kaolinite
plate upon a surface of re-crystallised quartz. Darker
adjacent mineral is bright red-orange in reflected light
and appears to comprise a cellular network.

FIG.1
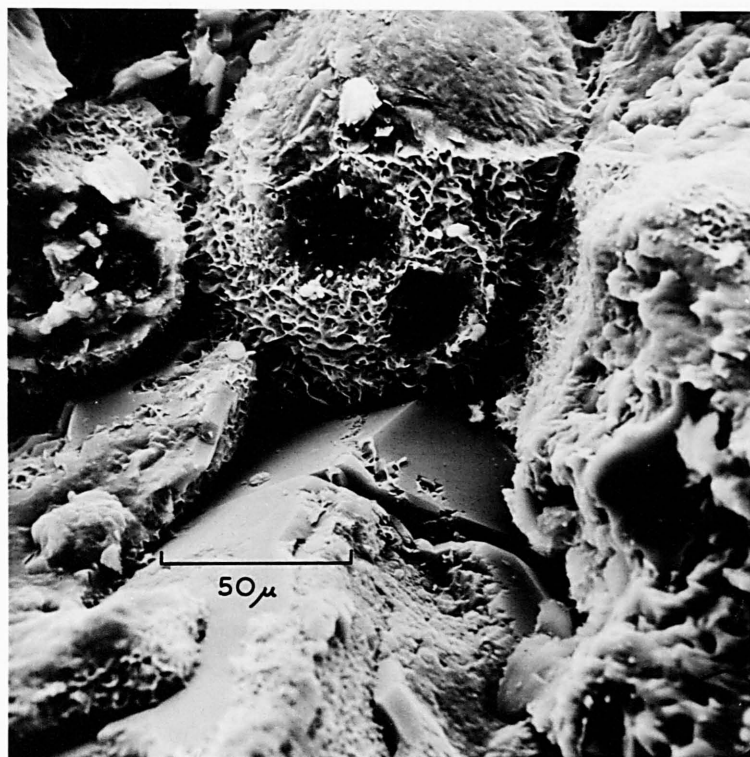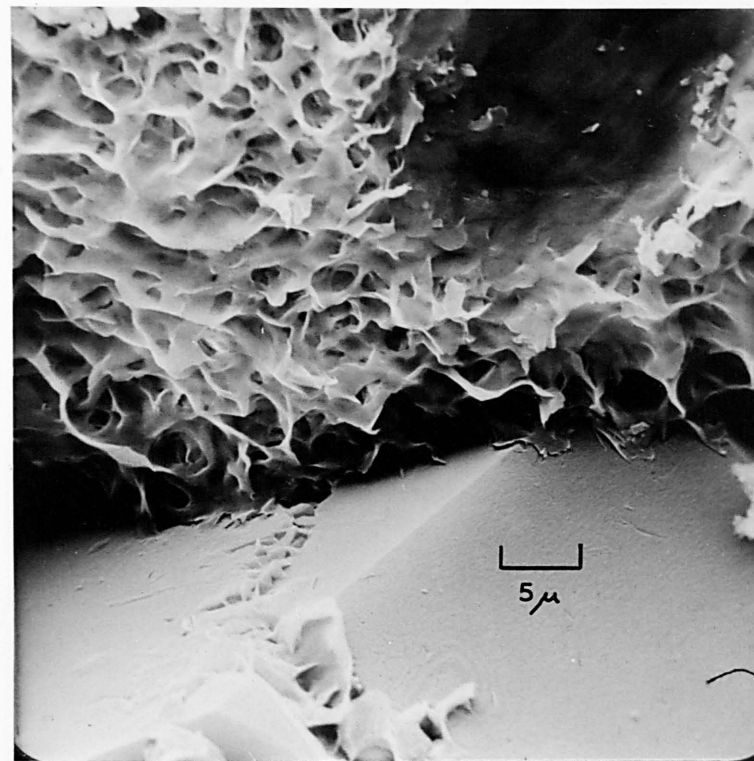
(a)   Fylde. Typical membrane-cellular coating of sub-crystalline clay on a rounded
        quartz grain. Note how the clay coating is interconnected between the grains,
        and the areas where adjacent grains were in contact.

(b)   Enlargement of (a). from which the clay is shown to extend onto the well formed
        re-crystallised quartz. In the contact area above, the membrane clay coating
        appears to blend into a smooth sheet.

FIG. 2 a,b

(c)
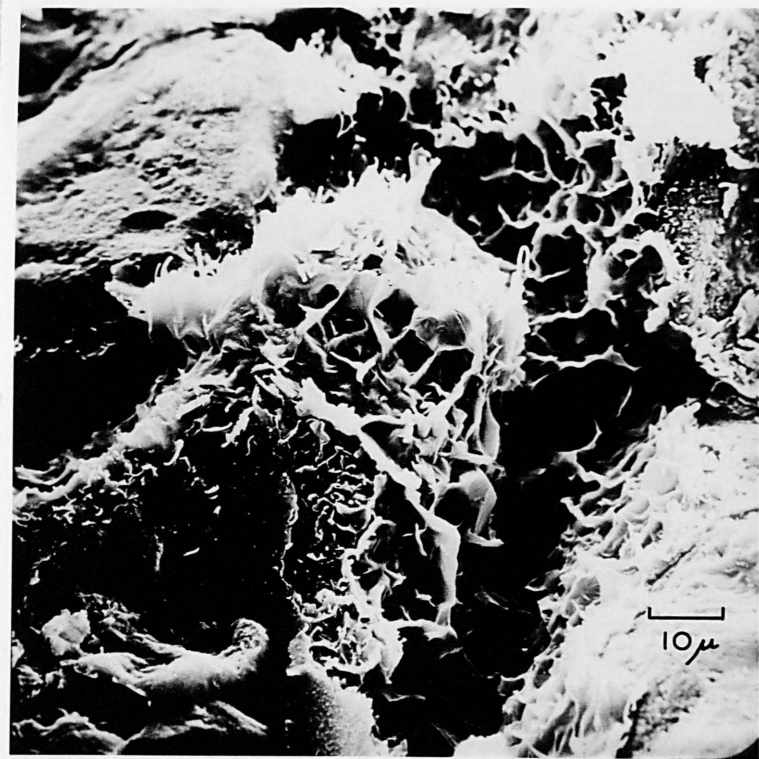
(d)
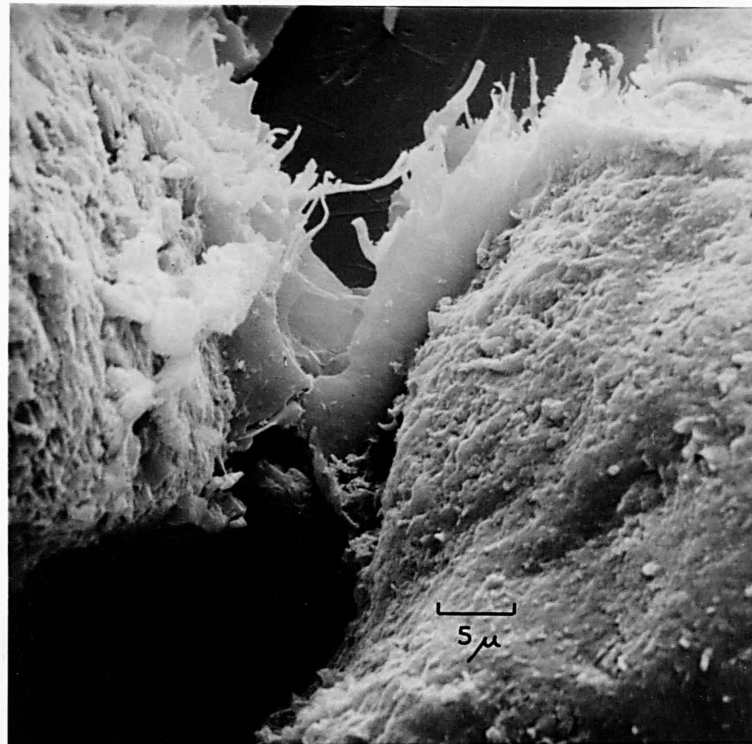
(c) St. Bees sandstone, Cumberland. Cellular clay coating four sand grains and
developing into thick membranes which cross the pore spaces perpendicularly.
The membranes show a form of parting or cleavage possibly exaggerated by
de-hydration, which suggests a crystalline structure for these clays. In
the lower part broken edges of the continuous coating or skin can be seen.

(d) A sample from the same area showing well developed platy membranes adjoining
two sand grains.

FIG.2 c,d
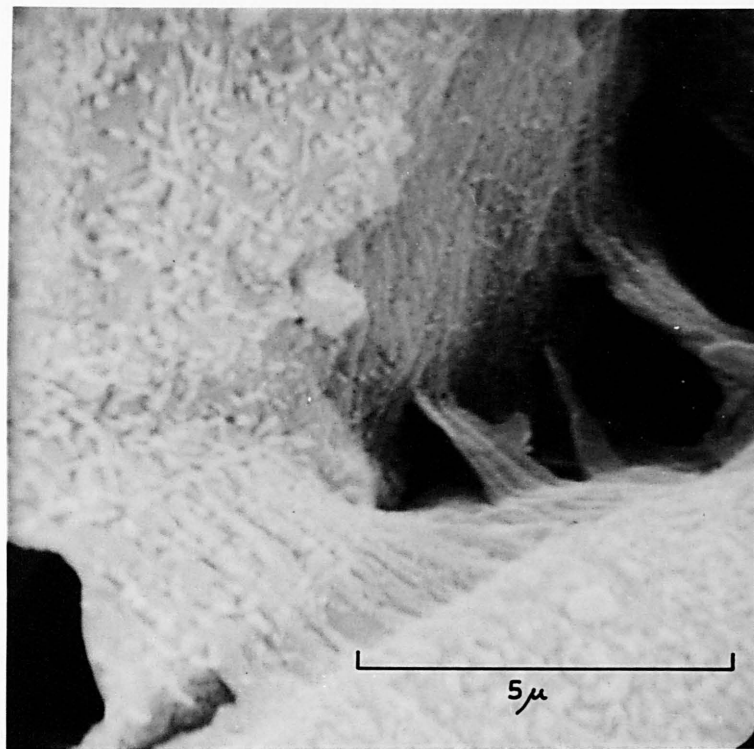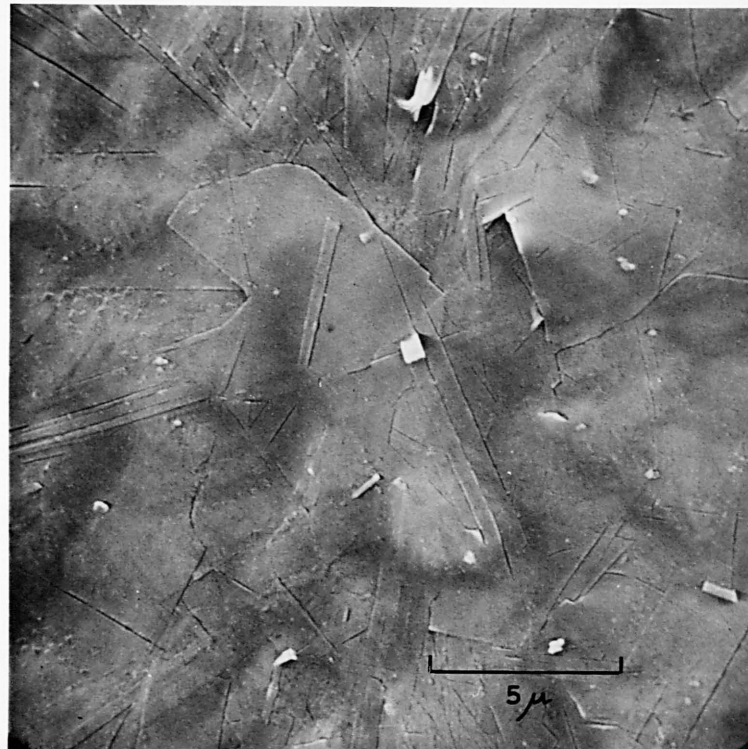
(e)   Shropshire. A thin coating of fibrous clay that completely envelops the sand
        grains and bridges the gap between them around the contact area. This skin
        appears to comprise a network of interlaced pairs of 'fibres'. Note the small
        clay mineral particles on this skin which in appearance are similar to halloysite.

(f)   Vale of Clwyd. Coating on a well rounded aeolian sand grain comprising overlapping
        crystalline laths and plates, typically 4-5 microns long. This type of coating
        was not observed in the cellular form between the grains.

FIG.2 e,f.

minerals is readily identified as tabular colourless kaolinite.
Immediately adjacent is a darker unidentified clay mineral, bright
red/orange in reflected light, that appears to have a sub-crystalline
or cellular habit.   This type of mineral, abundant in many of the
samples studied, lends its colour to the whole rock.

2.b Scanning electron microscopy;   texture of the clay minerals

Scanning electron microscopy enabled greater magnifications and depths
of focus and improved the resolution considerably.   Several samples
from the areas listed above were examined and some of the micrographs
obtained are presented in fig. 2 a to f.   These observations showed
that the quartz and felspar grains are partially or wholly coated with
thin films and networks of material that has crystalline or sub-
crystalline textures.   These coatings occur in several forms but the
cellular network type (fig. 2 a) is ubiquitous.   Subsequent analyses
described below (2.c) identified these coatings as clay minerals,
dominantly illite (hydromica) and montmorillonite.   Kaolinite was also
shown to be present in variable quantities, but this mineral is easily
recognised either in clusters or isolated tabular crystals.

Descriptions of these clay coatings are given with the micrographs but
some pertinent general observations are made here.

(a) With the exception of kaolinite, these clays are interconnected
     by membranes between the sand grains and therefore, in bulk,
     constitute a continuous network throughout the sandstone.
     The membranes have developed directly between the sand grains
     surfaces wherever these are close together e.g. 5 - 10 microns.

(b) In most samples from each area, the clay film (illite -
     montmorillonite) on each sand grain surface has thickened in

- 11 -

a cellular membrane habit, further enveloping the grains
and in some instances wholly occupying the pore spaces.
Typically the thicknesses of the clay films and membranes
are 0.1 - 0.2 microns and the 'cell size' of the cellular
types may vary between 1 and 5 microns.

(c) Undoubtedly these clays are authigenic, the evidence
suggesting a saturated or partially saturated environment
for their development. The membranes between the sand
grain surfaces were possibly influenced by surface
tension effects.

2.c Mineralogical identification of the coating material - x-ray diffraction method

The author is unaware of any comprehensive index giving scanning electron
micrographs of clay minerals, and transmission electron micrographs (e.g.
Beutelspacher and van der Marel 1968) are generally inadequate for
comparisons in this instance. Some analyses were therefore necessary to
establish the mineralogical identity of thin films and networks.

Some samples similar to those in figs. 2 a and f were immersed in hot
hydrochloric acid (5N) until the red colouration had been removed.
Inspection under the S.E.M. showed that whilst some cracking and corrosion
of the coatings and networks had occurred, the structures were still intact.
This precluded iron oxides as the principal component, although x-ray
fluorescence (X.R.F.) analyses on a sample similar to that in fig. 2 f
indicated that the percentage of iron oxides, calculated as Fe_2O_3, had
been reduced from 0.60 to 0.18 by the acid. Hematite in its crystalline
form was not observed in any of the micrographs. The optical reflection
micrographs indicated the red/orange colouration of the untreated
coatings, including the cellular membrane form, and therefore the

FIG 3: X-ray diffraction charts of clays from some Bunter sandstones.

Cu(K_α) source, 40kV ; 20mA

Nickel filter

Collimation 1°:0.5°:1°

Time constant 2s

Speed 1° of 2θ per minute

3° starting line lightly arrowed on the right of each chart.

Dominant responses from clays:-

$2\theta=5.5^\circ$–6.0° (lattice spacing d=16–14.7 Å) Montmorillonite (M).
                    Glycolation of a sample from Cumberland shifted
                    the response from 5.8° to 5.0° (d from 15.2Å to 17.7Å).
                    This characteristic increase of lattice spacing
                    supports the identification as montmorillonite.

8.7°–8.9° (d=10.2 –9.9Å) Illite (I)

17.8° (d=5.00)   "

26.7°–27° (d=3.33–3.30)   "

45.5° (d=1.99)   "

12.4° (d=7.14)   Kaolinite (K)

24.9° (d=3.58)   "

37.8° (d=2.38)   "

The response at $2\theta=26.7^\circ$, particularly for some of the Fylde samples, is due in part to traces of α–quartz (Q).

SAMPLES FROM
FYLDE B/H

T 62

T 37

T 70

T 71

T 69

T 44

T 38

VALE OF CLWYD
B/H E

SHROPSHIRE
Drakeley

CUMBERLAND
St. Bees sst

°2θ
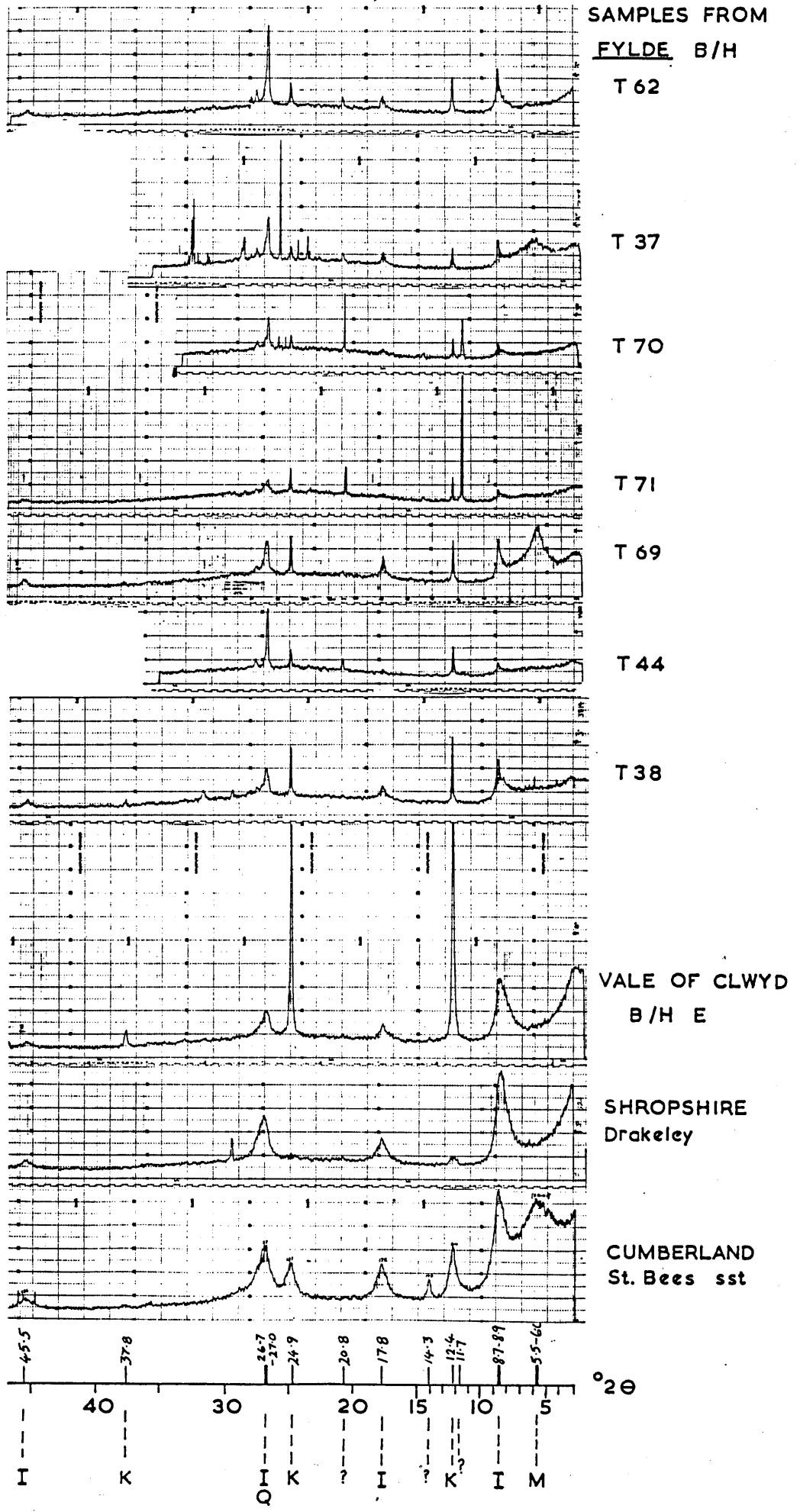
FIG. 3

combined evidence showed that removable iron was present, probably in oxide form.

Several of these mineral coatings, at least two of each type, were analysed by x-ray diffraction to determine their mineralogy. Samples were prepared by gently rubbing the sandstone with a nickel spatula in a small quantity of de-ionised water. A few drops of the obtained coloured suspension were transferred to a suitable glass slide and dried under a lamp. By repeating this process of evaporation several times, a translucent film of red/light brown precipitate was accumulated on the slide although for some weak suspensions the process did require extended repetition. This method was found to be more successful than any other because contamination of the precipitate by minute quartz and felspar fragments was almost wholly avoided and the obtained diffraction charts corresponded to clay minerals only. These analyses therefore established that the films and cellular networks shown in fig. 2 were clay minerals. Some examples of these charts, obtained with copper (K_α) radiation are given in fig. 3 .

The data show that illite is present in all samples, although the response is variable, whilst montmorillonite is apparent only in some of the widespread cellular forms of clay. This does not necessarily preclude montmorillonite from other samples, however, because in many instances the micrographs illustrate the sub-crystalline and tortuous nature of the clays, which would greatly reduce the diffraction response. It is possible that in many cases the clays are inter-layered illite - montmorillonite although a form similar to that in fig. 2 a has been observed in Peruvian Rotliegende sandstones by Stalder (1973) who refers to this type of clay as illite. Hauser (1953) has photographed thin films of sodium bentonite, which is largely montmorillonite, in transmitted light. There is a similarity between the micro-structure of the clay films he illustrates

and the habit of the clay in fig. 2 a, allowing for the added perspective and adjustment of magnification.

Kaolinite, by virtue of its well formed tabular habit, has a strong diffraction response (e.g. fig. 3, Vale of Clwyd) and is also easily identified with either the electron or optical microscopes. This mineral is also widespread amongst the sandstones.

The texture of the clays and their tendency to remain firmly adhered to the disaggregated sand grains, even after treatment with hydrochloric acid, poses problems to the quantitative evaluation of the clay fraction. In this instance x-ray diffraction is wholly unsuitable for this purpose and clearly evaluation by disaggregate size analyses will unavoidably include large errors. Quantitative analyses of percentage clay content of the sandstones have not been made for these reasons although in retrospect, a measure of cation exchange capacity (C.E.C.) would probably have been a suitable substitute and appropriate for the purpose.

CHAPTER 3

APPARATUS AND PROCEDURES

3.a Apparatus for containing the sandstone samples

Sandstone plugs, 35 mm diameter and 50 mm long, were drilled from borehole cores. Each of these samples was firmly contained in a hollow cylinder of soft vinyl, moulded size 46 mm outer diameter, 32 mm inner diameter and 60 mm long, which was then squeezed into a clean wetted glass sleeve 45 mm inner diameter by 130 mm long (fig. 4 a). The soft vinyl was therefore compressed and moulded against the rough surfaces of the sandstone core and errors due to leakage along this boundary were thus avoided. This method of containing the samples was both efficient and economic. It facilitated the flushing of samples, rapid setting up for permeability measurements and convenient attachment of the electrodes (fig. 4 b) in that sequence, without removal of the samples from the glass sleeves. The vinyl cylinders could be re-used many times without deterioration and when necessary could be melted and re-moulded.

3.b Apparatus for changing the pore water

The pore water of each sample was changed by flushing. Each glass sample holder was attached by a rubber stopper to the lower end of a vertical glass tube, 12 mm diameter, and the system was topped up with the required solution which then percolated through the sample. To ensure that the pore water was completely changed a minimum volume of 200 ml of the solution was allowed to flush through each sample, those of exceptionally low permeability requiring several days for the process. A few initial repeatability tests verified that with further flushing the electrical conductivity of the samples remained unchanged.

3.c Apparatus and method of measuring permeability

Permeabilities of the sandstone samples were measured by the falling head technique (Akroyd 1957). A laboratory clock and mercury thermometer were used in addition to the apparatus shown in fig. 5. The scale on the apparatus was calibrated in 5 mm units and the descending water level could be monitored against it with an accuracy better than 0.5 mm.

The sandstone samples were initially saturated with de-ionised water in high vacuum. Subsequent flushing with de-aerated, de-ionised water removed any traces of dissolved salts, after which permeabilities were measured. Air was excluded from the permeability apparatus by emplacing the rubber stopper downwards into the vertical, water filled sample holder, which was then inverted and clamped against the stop (fig. 5). Heads of water were limited to 500 mm maximum and the amount of fall was in each case conveniently decided according to the rate of flow. Temperature was monitored throughout the programme of measurements.

Permeabilities K(mms^{-1}) were calculated from the expression:

$$K = \frac{\mu}{\mu_{10}} \ \frac{r_t^2}{r_s^2} \frac{L}{t} \ \log_e \left(\frac{h_o}{h_1} \right) \qquad \ldots\ldots\ldots \ 3.1$$

where μ, μ_{10} = dynamic viscosity of water at test temperature and $10^{\circ}C$ respectively

  r_t = radius of the tube (mm)

  r_s = radius of the sample (mm)

  h_o = initial head of water (mm)

  h_1 = final head of water (mm)

  L = length of the sample (mm)

  t = time for the height of water in the tube to fall from h_o to h_1 (s).

a.

SOFT VINYL — SANDSTONE SAMPLE — GLASS TUBE

C_1 — C_2 — Ag CURRENT ELECTRODE

Na Cl SOLUTION

CALOMEL ELECTRODE

P_1 — P_2

b.
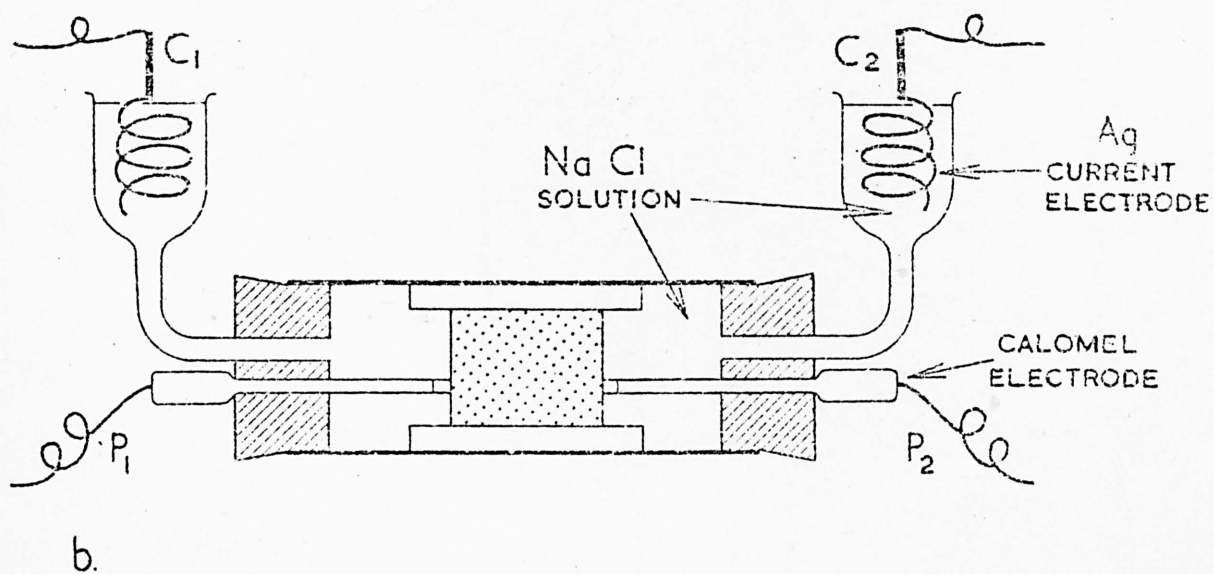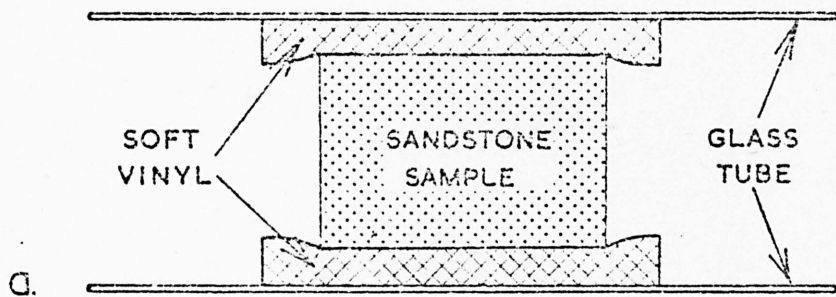
(a) Apparatus for containing the sandstone samples.

(b) Method of attaching electrodes to the apparatus.

FIG.4

moveable scale

stand

rigid stop

head of water

fixed glass tubing

sandstone sample

rubber bung

splash tray

clear flexible neoprene tubing
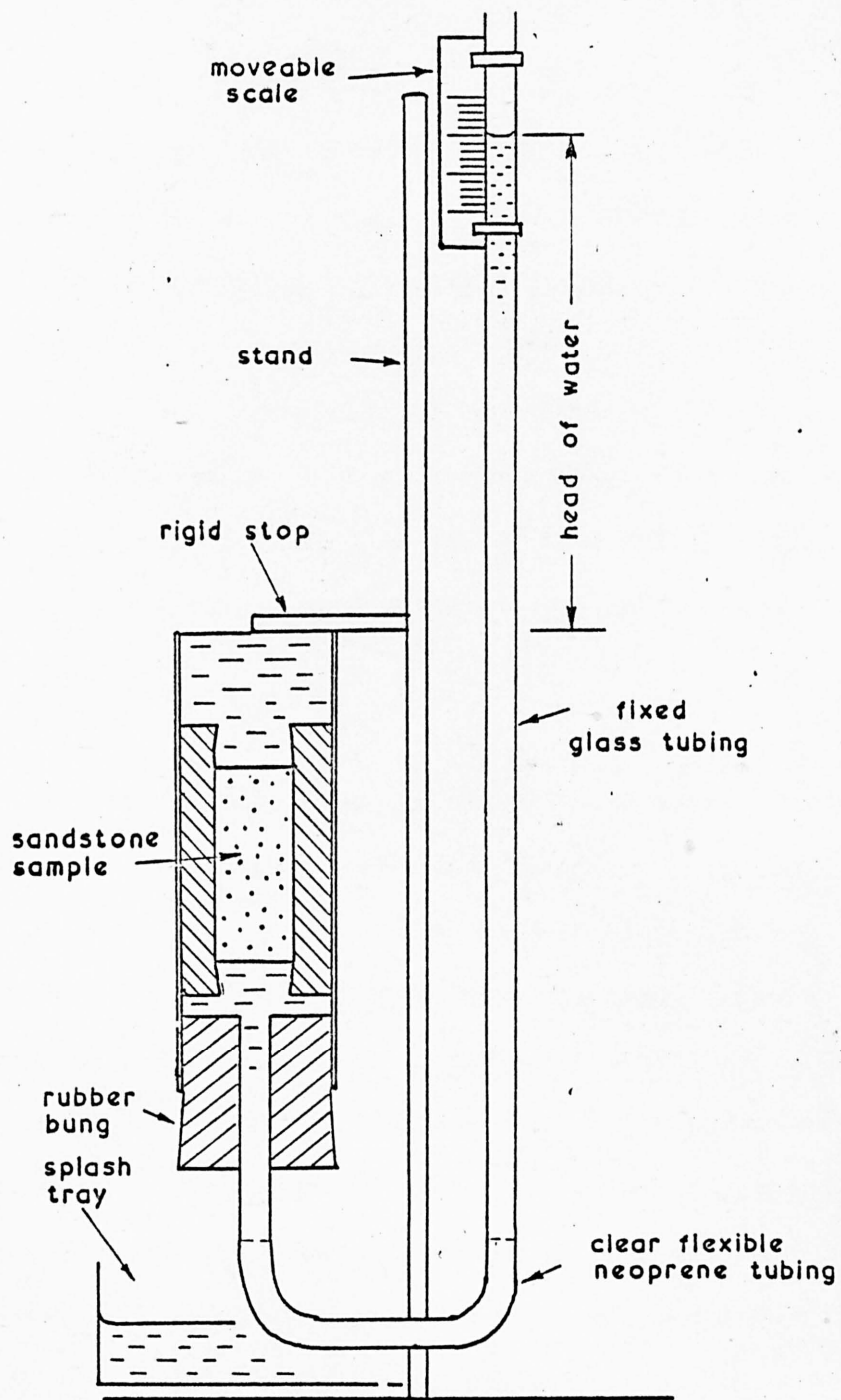
Apparatus used for measuring permeability by the falling head method.

FIG.5

The value of t was taken as the average of three repeated measurements upon each sample, unless t was extremely large, in which case a single value was accepted.

3.d Electrodes

Current electrodes (fig. 4b) were made from 18 swg pure silver wire, coiled to increase the emissive surface area. These electrodes were initially prepared by washing in dilute nitric acid to remove surface impurities then anodically plated in sodium chloride solution. Thereafter they were not handled throughout the experiments. They were capable of passing the normal maximum required current, 2mA, in cyclic sequence with very little polarisation and without deterioration. As a safety measure, these electrodes were permanently fixed to the apparatus with insulation blocks.

Calomel electrodes were used for potential measurements and were connected directly across each sample as shown in fig. 4b. The operating conditions imposed i.e., univalent (NaCl) solution; equal ionic concentration either side of the sample; high impedance circuit (recorder input greater than 1 M ohm), were ideal for this type of electrode (Ives and Janz 1961). The net polarisation of the potential electrodes did not exceed 1.0 mV throughout the experiments. Spurious polarisations were occasionally encountered and were attributed largely to a frictional interaction between the rubber stoppers and the inserted glass potential electrodes. This type of polarisation was steady throughout any cycle of measurement and therefore could be backed off. This effect was only noticeable with low conductivity waters.

3.e Electrical Apparatus

The transmitting and recording devices comprised the following items -

SIMTECH 500	Time domain IP transmitter
	output 50 - 250 V dc; 12 mA - 2A
RIKADENKY	High impedance pen recorder
	Scale ranges 1mV fsd. to 2V fsd.
SOLARTRON	High impedance digital voltmeter
AVOMETER	Calibrated 0 - 50 μA; 0 - 1mA; 0 - 10mA
RHEOSTAT	900 ohms
RELAY	12V 2 pole 1 way

The Simtech 500 is essentially an output voltage controlling device employing manually triggered thyristor switching in the power circuit. It also switches the input line to the recorder, through a single relay which is triggered simultaneously with the power circuit. This input line to the recorder incorporates a self potential balancing facility which is used to nullify extraneous polarisation. The normal sequence of switching is arranged so that the recorder input line is broken (recorder input short circuited, potential electrodes open circuited) during the current output period. This sequence can be overridden by push button controls. Further details of this instrument are given in the maker's specification literature.

The circuit was arranged as shown in fig. 6. Although current was switched electronically, an external relay was required to isolate the current electrodes during the recording period, to prevent small leakage currents (microamps) that otherwise passed back through the transmitter. The minimum output current that could be triggered and sustained was 12mA and therefore the rheostat was required on the output of the transmitter to meet this condition and supply much lower currents to the sample cell. The pen recorder was initially calibrated against the digital voltmeter and thereafter periodically checked. The paper speed was set at 10 mm s^{-1} and the step response time of the recorder did not exceed 0.5 s.
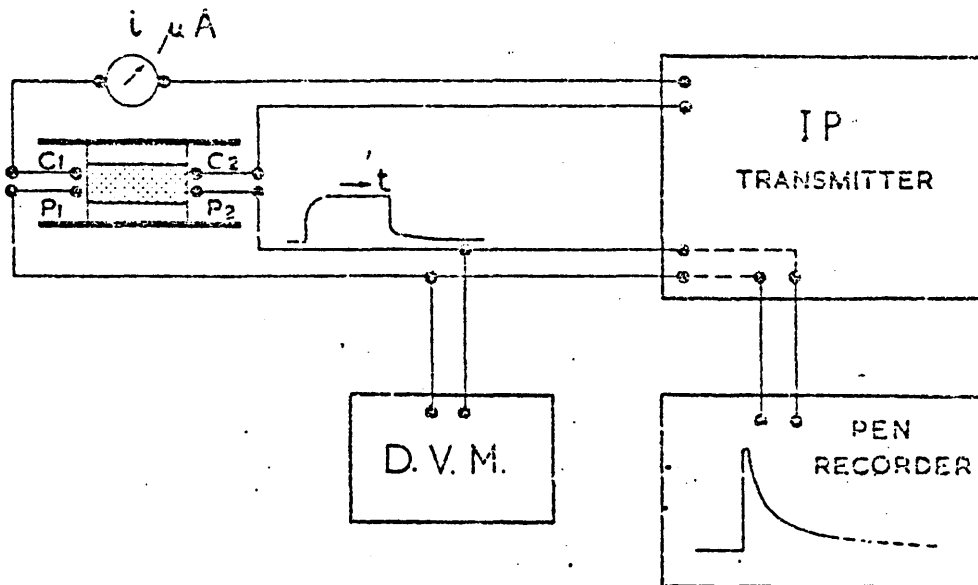
Schematic circuit arrangement. The waveform shown
in the potential circuit depicts the IP effect
obtained with a rheostat output on the constant
voltage transmitter.

FIG.6

Switching intervals were controlled manually, timed against a laboratory clock.

3.f Preparation of the water

The water used for flushing the samples and topping up the sample cell was bulk prepared by adding small quantities of sodium chloride (NaCl) solution to 100 litres of de-ionised tap water until the required conductivity was obtained. This conductivity was measured with the electrical apparatus using a suitably adapted cell. This water was not de-aerated because of the long delays and difficulties of preparing adequately large volumes under high vacuum to a uniformly high standard of purity. Mayper (1959), describing some measurements of IP in the laboratory, laid emphasis upon high vacuum de-aeration of the copper sulphate pore fluid he used for saturating his samples. He reported that a trace of dissolved air in the pore fluid of a 9 micron glass filter produced spurious and erratic IP responses and attributed the effect to bubbles. The actual levels of IP he recorded for this effect were very small though, less than the levels of experimental error obtained in the work described here. In this case no measureable IP was obtained for 50 micron glass beads and clean sands saturated with untreated tap water, and in a later test on three sandstone samples, IP measured before and after high vacuum treatment was found to be unaltered within the limits of other errors.

Water temperatures were monitored throughout the experiments and did not exceed the range 16.0^{o} to 21.0^{o}C.

3.g Testing the apparatus

In preliminary electrical measurements on saturated sandstone cores, polarisation decay curves were obtained which, if attributed to sandstone

IP, meant that chargeabilities (V_s/V_p at $t = 1s$) could be greater than 10%. A series of simple tests was therefore carried out to ascertain whether or not part of this polarisation was due to capacitor effects in the apparatus or electrode polarisation.

A glass cell was suitably modified so that the potential electrodes could be admitted to the sandstone sample or removed during the measuring cycle without loss of water. For the first test, the potential electrodes were included in the apparatus for the charging period. During the subsequent recording period, these electrodes were temporarily removed from the cell for a few seconds, in which time they were immersed together in a beaker of weak NaCl solution. The obtained recorder trace (fig. 7) showed that the observed potential decay was independent of the recording circuit and that furthermore the potential electrodes had not polarised transiently. Polarisation was also shown to be independent of the current electrodes by removing these from the apparatus during a recording sequence. The decay trace was unaffected.

A final test was made to investigate whether the polarisation was due to a transient NaCl concentration difference, induced between the cell solutions either end of the sandstone sample. Polarisation was measured on two long sandstone samples. Each sample was then cut transversely to give a pair with length ratio 2:1. The four samples obtained were re-measured electrically at the same current. The results, plotted as primary voltage V_p (V), polarisation potential V_s (mV) at $t = 1s$ and V_s/V_p against length (cm) (fig. 8) show that although there are some zero length errors by extrapolation, the magnitude of the polarisation is closely proportional to the sample length and the chargeability V_s/V_p is almost constant for each sandstone.

From these tests it was concluded that the apparatus did not contribute significantly to the observed polarisation and that this phenomenon
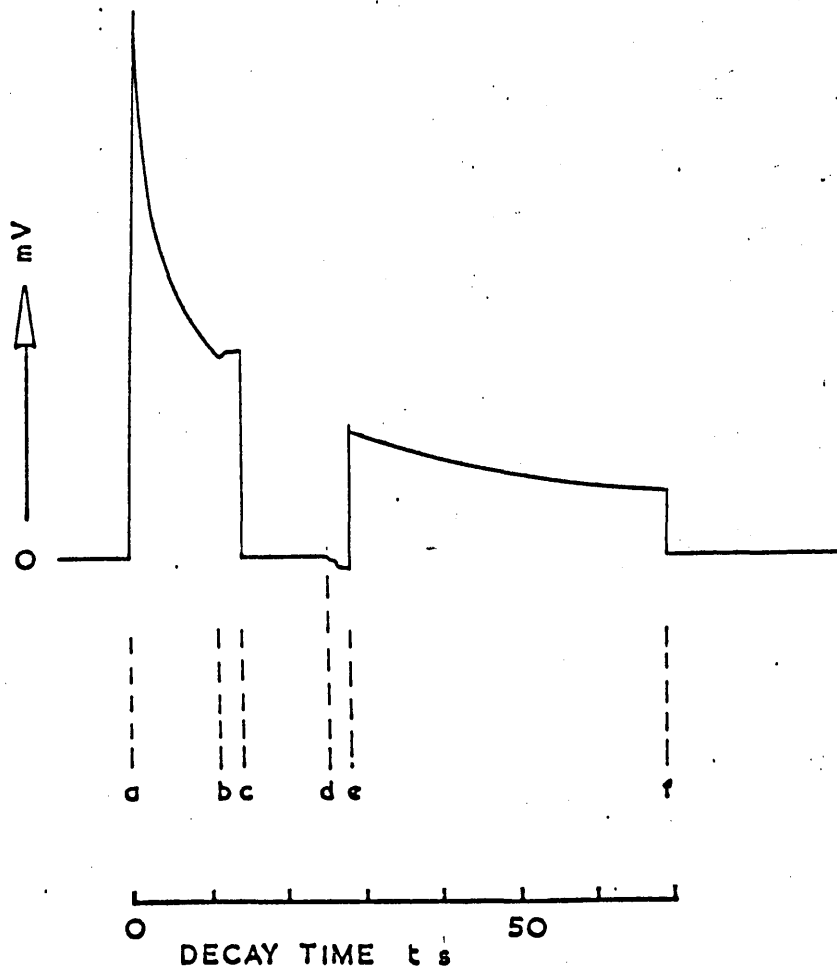
Electrode test recording trace

a. Current switched off, recorder switched on.

b. Potential electrodes removed from apparatus and -

c. placed in a beaker of NaCl solution.

d. Potential electrodes removed from beaker and -

e. re-inserted in apparatus.

f. Paper drive switched off for 290 s.

FIG.7
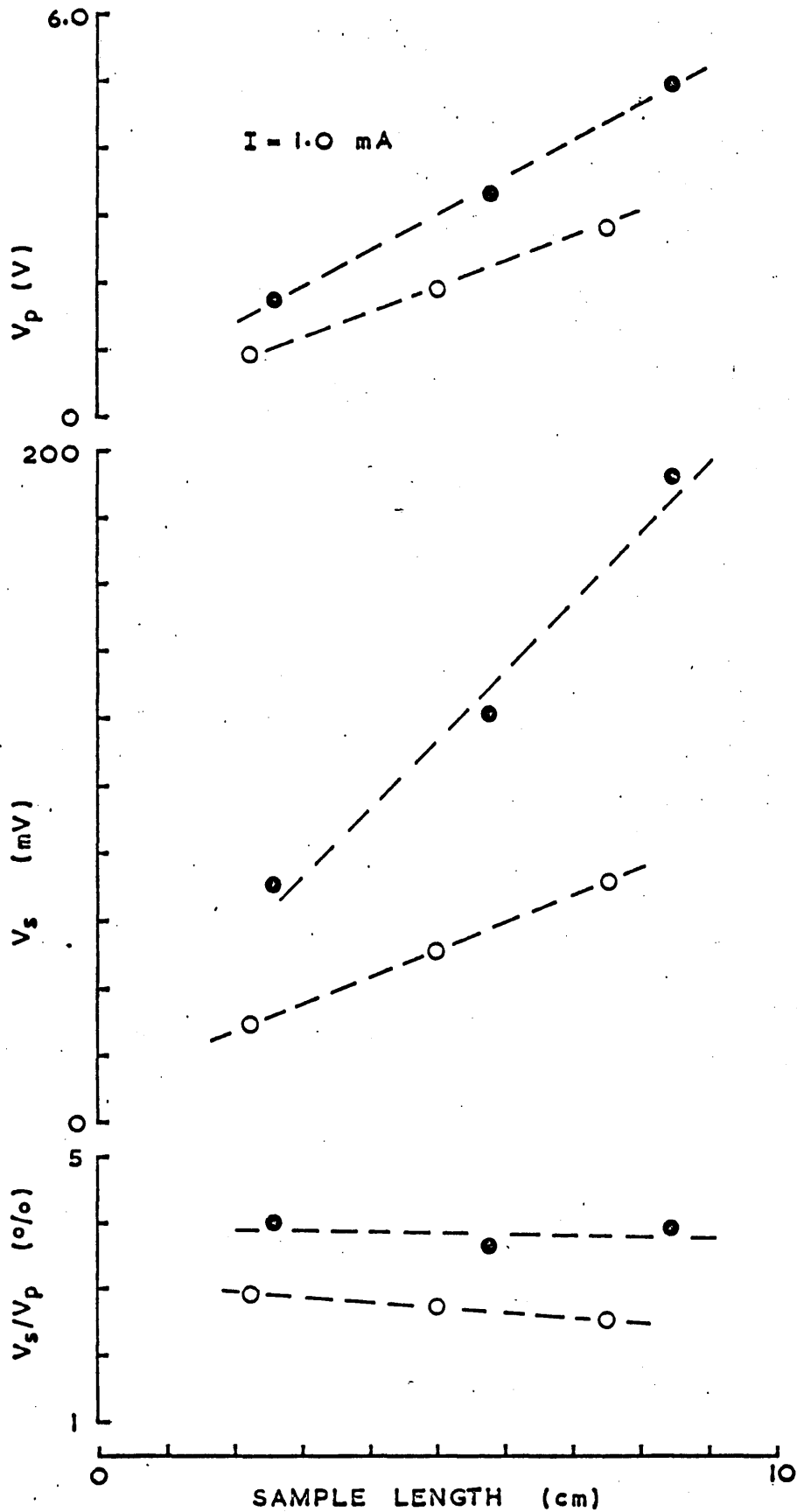
Measurements of primary voltage Vp, secondary voltage Vs
and IP (Vs/Vp%t = 1s) for two sandstone samples from the
Vale of Clwyd.

FIG.8
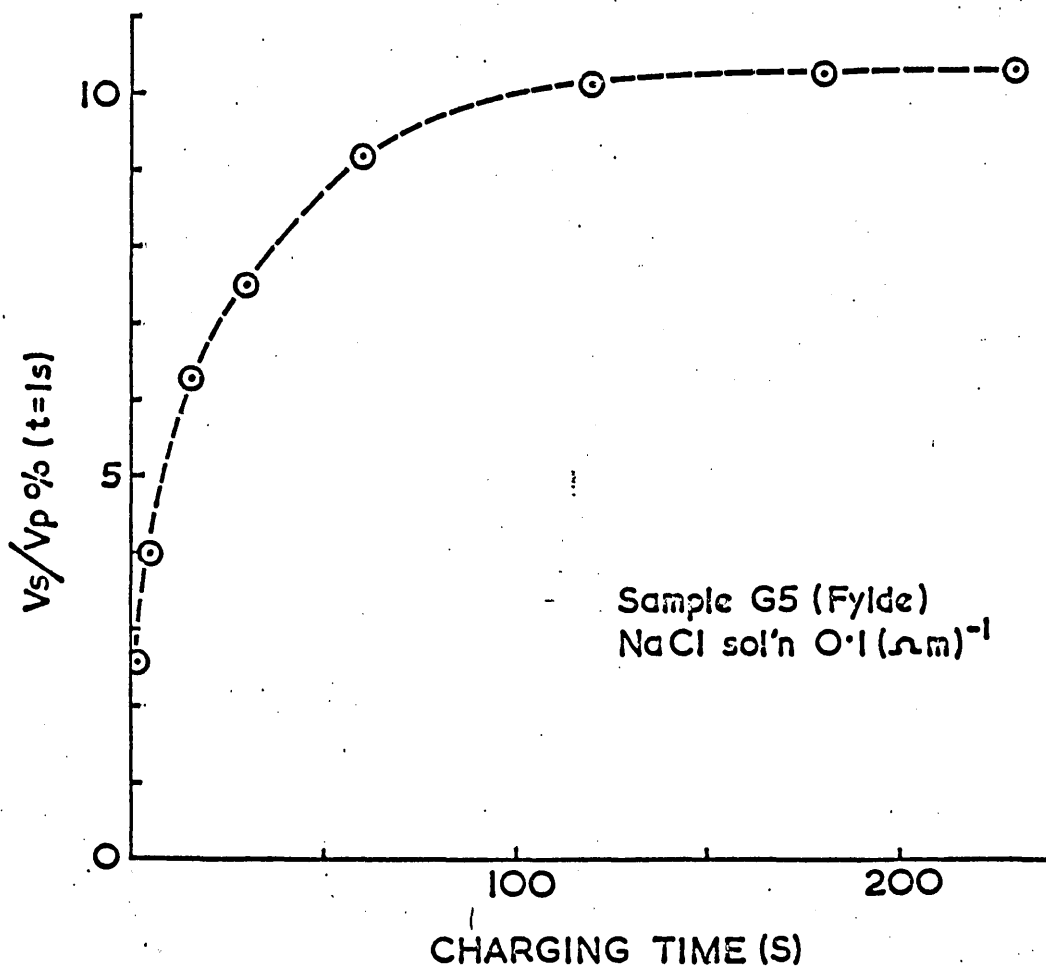
Fig.9a : Variation of IP (Vs/Vp%t = 1s) with charging time.
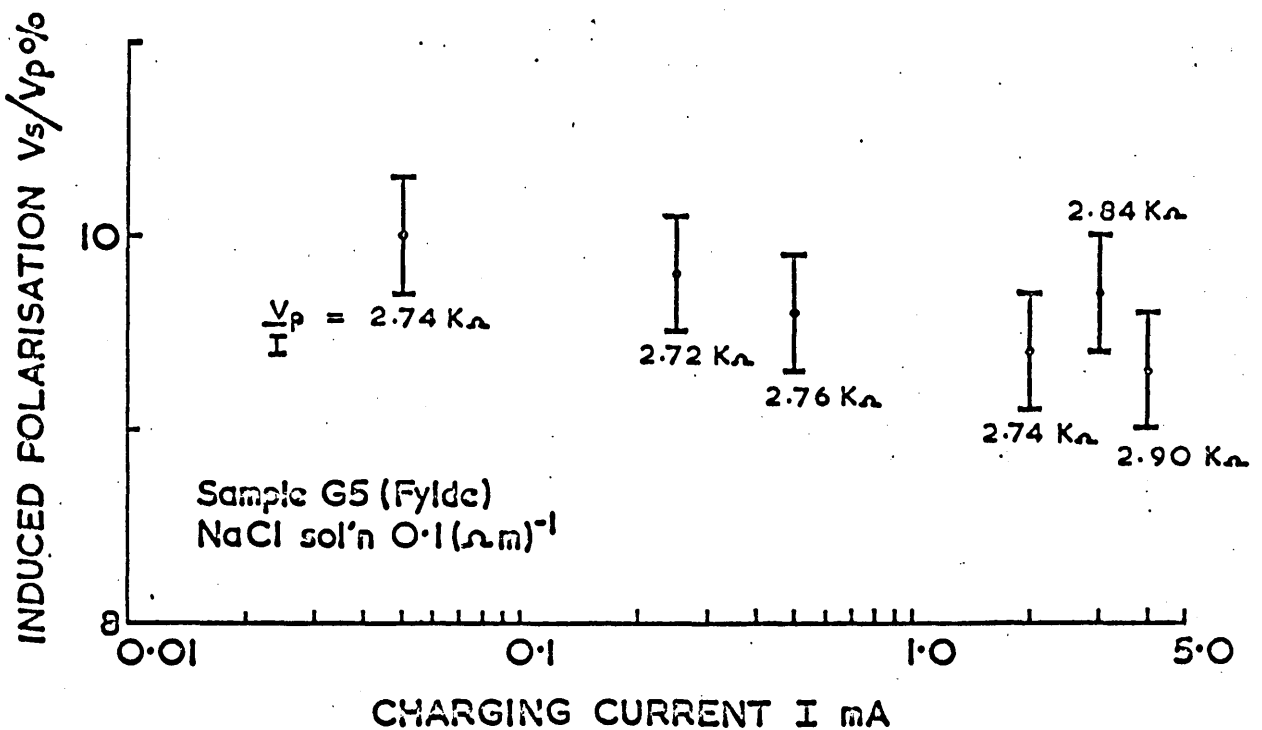
Fig.9b : Variation of IP with charging current. Current densities (Am^{-2}) numerically equal to current in mA.

FIG.9

must be a bulk property of the saturated sandstone sample i.e. Induced Polarisation (IP).

Preliminary experiments were carried out to determine the dependence of IP on the duration and magnitude of the charging current. IP of a saturated sandstone sample was recorded corresponding to charging periods varying between 2 and 240 s. The results (fig. 9a) show that IP, expressed as chargeability Vs/Vp ($t = 1s$), is very sensitive to charging duration for values up to 60 s, but above 120 s approaches a maximum value. 180 s was therefore adopted as the standard for all subsequent measurements because at this value any small timing errors would have no effect upon the measured IP. This duration allowed all samples to reach an equilibrium chargeability.

To investigate the effect of current density, IP was measured over the range of currents 0.05 - 4.0 mA which, for these sandstone samples, corresponded to the current densities 0.05 - 4.0 Am^{-2}. The results, plotted as a graph of $Vs/Vp\%$ ($t = 1s$) against I (mA) (fig. 9b), indicate that over this wide range of current densities the sample chargeability can be considered to be constant within the levels of errors.

Summarising, the sequence for measuring IP was standardised to the following procedure. To induce polarisation a measured current was passed through the sample for a period of 180 s, toward the end of which the steady potential difference Vp was measured on the digital voltmeter. The polarisation decay was monitored by the pen recorder during the subsequent 180 s although paper feed was stopped after 15 s. The cycle was then repeated with reversed electrical polarity and the measurements were averaged. For all samples, 180 s was adequate to allow the polarisation to decay completely.

3.h Choice of parameter for measuring IP

There are several ways of expressing chargeability as a measure of IP. The most commonly used in prospection work is an integration of the transient V_s over a specified time interval, normalised against V_p, the units for this measure being millivolts second per volt or milliseconds. The advantages of this measure are that some account is taken of decay rate, and the effects of spurious noise and EM coupling are minimised. Other ways include an expression of decay rate as a normalised ratio of V_s corresponding to different times t, for example $V_{s_5}/V_{s_{20}}$ used by Vacquier et al (1957), and a simple expression of Vs normalised against Vp at a specified time t. The latter measure is referred to as polarisability by some authors (Bertin and Loeb 1976).

Decay curves obtained for seven samples over a range of pore water conductivities (4.a) have been superimposed on bi-logarithmic axes, normalised for t = 6s so that the decay rates may be compared. Some typical examples, corresponding to σ_w = 0.013 and 1.2 mhos m^{-1} are presented in fig. 10. Generally the contrast amongst these rates of decay is not very great. However comparisons of chargeabilities expressed as Vs/Vp at t = 1s gave a strong contrast and therefore this convenient measure was adopted throughout the laboratory experiments. The sampling time t = 1s was outside the recorder response time.

3.i Sandstone samples

Fine traces of close spaced bedding planes may be observed in many of the sandstones. These are small scale inhomogeneities which being parallel may be expected to cause anisotropy in the permeation and electrical properties, the latter having been demonstrated by Barker and Worthington (1973b).

To minimise the effects of these anisotropies, samples have been

drilled axially horizontal which for most of the sandstones is approximately parallel to the mean bedding plane. Wherever the depths of borehole cores were indicated, the sample plugs were drilled at regular depth intervals, otherwise they were taken randomly. Core recovery of very friable sandstones was low and therefore some bias in the sample distribution may be expected. However, by collecting a large number of samples, some friable types have been included and therefore a wide range of sandstone textures has been represented.

Analyses of the following experimental data are based upon the initial assumption that each sample is texturally homogeneous.
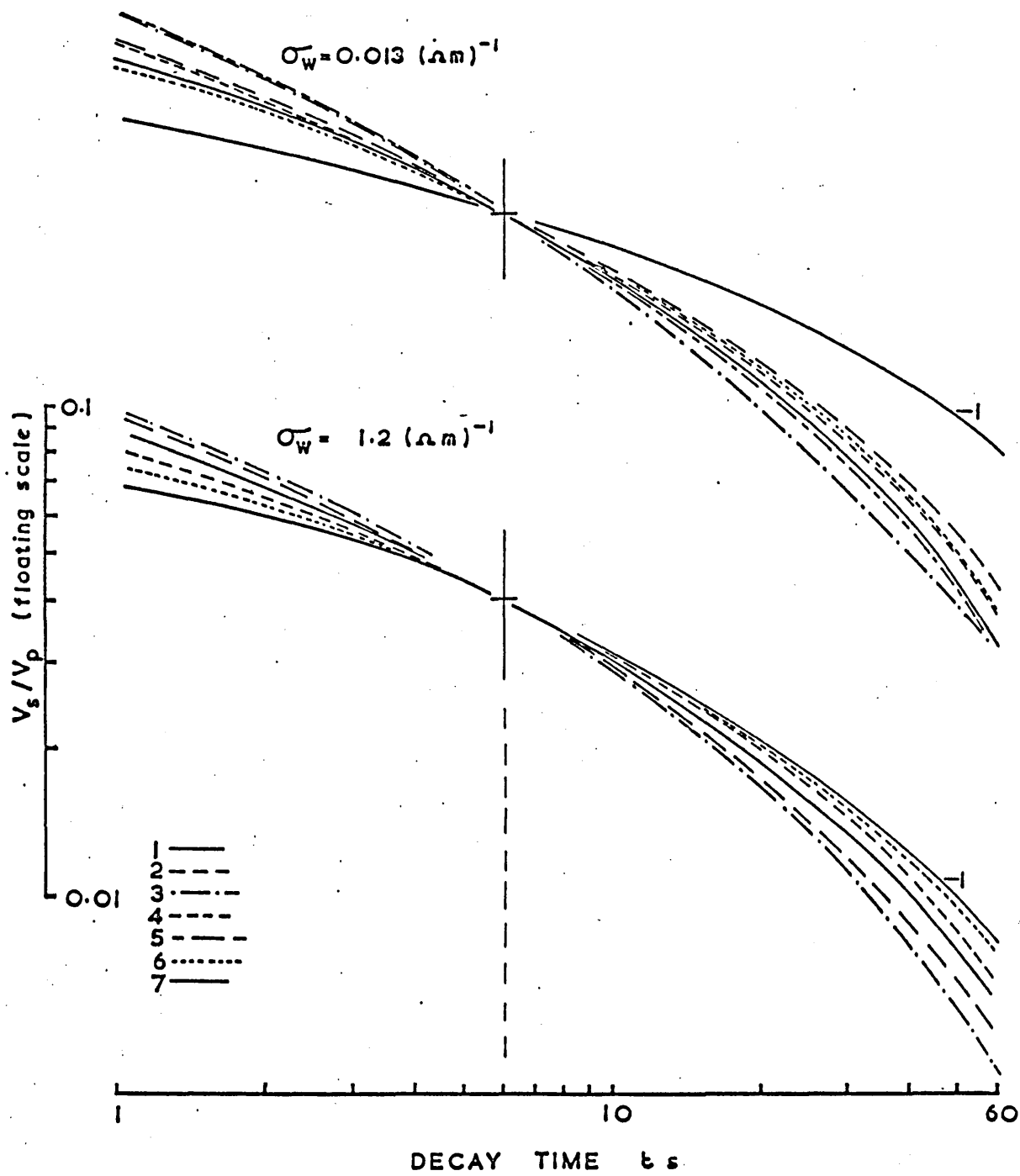
Comparison of seven IP decay curves on bi-logarithmic scales for σ_w = 0.013 mhos m^{-1} and 1.2 mhos m^{-1}

FIG.10

CHAPTER 4

THE VARIATION OF SAMPLE CONDUCTIVITY AND IP WITH PORE WATER CONDUCTIVITY

Prior to the experiments, data relating the IP of Bunter sandstones to pore water conductivity (σ_w) were not available and although other workers (e.g. Henkel and Van Nostrand 1957, Keevil and Ward 1962, Henkel and Collins 1961) have presented some data of this type for other rocks no consistent pattern has emerged.   This information was required to establish adequate control in later experiments and therefore preliminary detailed measurements of IP with variable σ_w were necessary.

4.a Experimental procedure

Seven samples from five boreholes (Fylde) covering a wide range of permeability were selected for this purpose.   Sample conductivities σ_s mhos m^{-1} and IP were recorded against σ_w, this variable being progressively increased by logarithmic increments to cover the range $\sigma_w = 0.00013$ to 5.60 mhos m^{-1}.   Thirteen sets of measurements were thus obtained.   The value of $\sigma_w = 0.00013$ mhos m^{-1} was obtained with de-ionised water and from repeated measurements was found to be the lowest consistent value that could be practically achieved.   For all low values of σ_w, careful preparation of the apparatus and handling precautions were necessary to avoid contamination.

It was assumed that the de-ionised water contained no NaCl.   The maximum current density for each sample that the apparatus could achieve with this water was 0.003 Am^{-2}, the limiting factors being the output voltage of the transmitter and the emissive surface area of the current electrodes.   Current density was maintained constant for all samples at each value of σ_w, but throughout the range of the experiment, in order to maintain adequate recording levels, it was necessary to increase the current density from 0.003 to 2.1 Am^{-2}, this being done in steps small enough to allow some overlaps.

4.b Conductivity results

The data for each sample are presented as graphs of dc. conductivity σ_s against pore water conductivity σ_w, figs. 11 a and b covering the ranges $\sigma_w = 0.00$ to 0.03 mhos m^{-1} and 0.0 to 6.0 mhos m^{-1} respectively. A sharp depression of σ_s at very low values of σ_w (fig. 11 a) is a feature which is common to these conductivity curves although it is improbable that the increased σ_s at the lowest σ_w is a true physical property of the sandstones. In the inset of fig. 11a, the broken line represents the expected correct form of these curves, although as far as the author is aware, this reduction of sandstone conductivity has not been described elsewhere. This high σ_s value at the lowest σ_w is attributed to experimental limitations, these being either water ionisation due to necessarily high voltages (approx. 250 V.) on the current electrodes or the contamination of the pore water due to removal of sorbed ions from the clay matrix of the sample. In either case, some electrodialysis of the clays probably occurred whereby the counter ions, e.g. Na$^+$ K$^+$ and Ca$^+$ were replaced by H$^+$. In turn H$^+$ would later have been replaced by Na$^+$ upon the addition of NaCl to the pore water, which to some extent must have standardised the counter ions within the clays.

For values of σ_w between 0.01 and 1.0 mhos m^{-1} (figs. 11 a and b) the variation of sample conductivity is almost linear, although over wider ranges of σ_w (fig. 11b) a characteristic departure from linearity is evident amongst all the curves. The significance of the shape of these curves is discussed in Chapter 5.

4.c IP results

The IP data for each sample have been plotted as percentage chargeability (Vs/Vp) x 100 at t = 1s against σ_w mhos.m^{-1} (fig. 12), the latter being
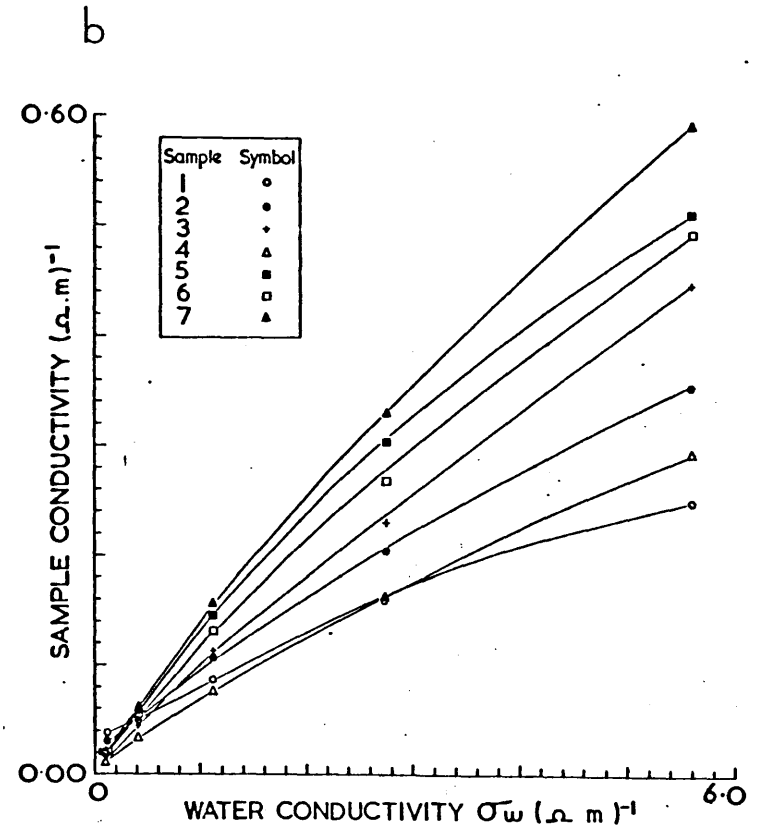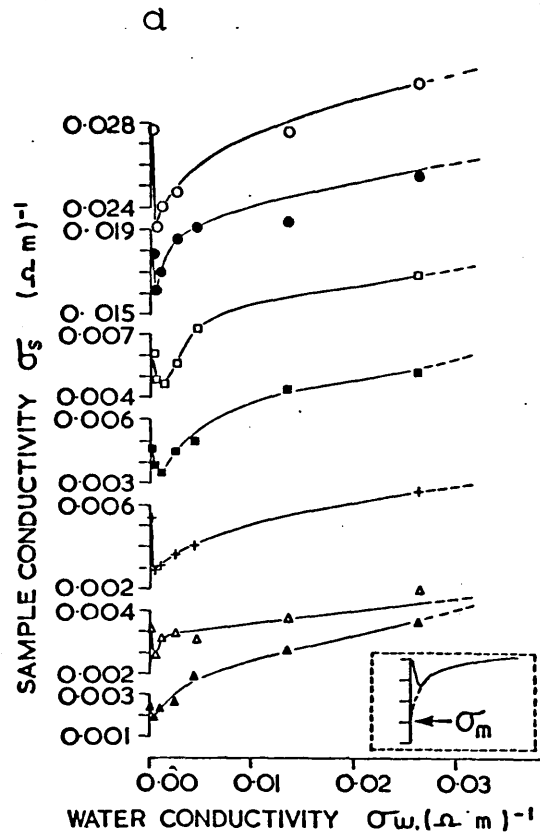
Variation of sandstone conductivity σ_s against pore water conductivity σ_w for seven samples from the Fylde.

(a) σ_w from 0.00 to 0.03 mhos m^{-1}

(b) σ_w up to 6.0 mhos m^{-1}

FIG.11
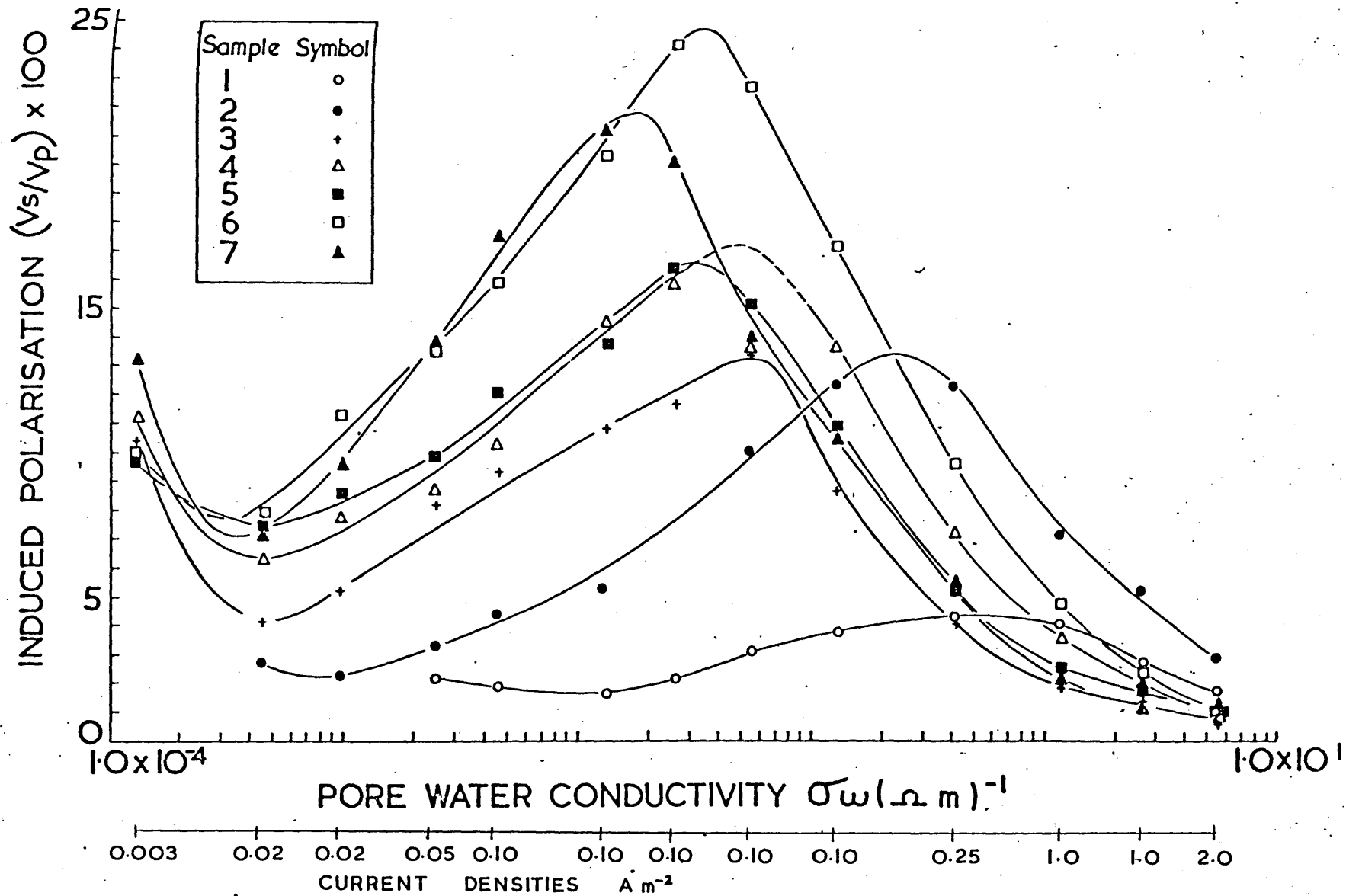
Variation of IP against pore water conductivity (NaCl solution) for seven sandstone samples. Corresponding primary current densities indicated beneath.

FIG. 12

represented on a logarithmic scale to accommodate the wide range of values. The overall shapes of the seven curves are markedly similar and include some notable common features.

The increased IP at the lowest water conductivity (σ_w = 0.00013 mhos m^{-1}) is attributed to the same factors that were discussed with reference to the corresponding conductivity data (4.b), and other than this departure the IP of each sample tends to zero together with σ_w. In each case, for σ_w increasing, IP rises to a maximum and thereafter decreases asymptotically to zero. The rates of increase of IP and the amplitudes of the maxima differ amongst the samples but the rates of decrease apparently are similar. These maxima do not coincide about a single value of σ_w, but generally are progressively displaced to greater values for decreasing amplitudes.

CHAPTER 5

ANALYSES OF THE CONDUCTIVITY DATA: A DISCUSSION OF IP

5.a Application of equations 1.2 and 1.3 to the conductivity data

The parallel conductor model used by Patnode and Wyllie (1950), expressed

by the straight line equation 1.2 is inadequate to account for the

observed non-linear variations between sandstone conductivity σ_s and

pore water conductivity σ_w (fig. 11). Moreover these data are more

consistent with the general conclusions of Winsauer and McCardell (1953)

and Hill and Milburn 1956) inasmuch that the curvature can be explained

if matrix conductivity is not constant but varies according to the pore

water salinity.

The empirical expression (1.3) which Hill and Milburn used to describe

their data has been examined to determine whether it might fit the

conductivity data in figs. 11a and b. The logarithm of equation 1.3

can be written in the form:-

$$\log F_a = b\left[\log (100/\sigma_w)\right]^2 + \log F._{ol}$$

from which a graph of $\log F_a$ against $\left[\log (100/\sigma_w)\right]^2$ has a slope b

and intercept $F._{ol}$. The conductivity data for the seven samples (figs.

11a and b) have been plotted in this form and the obtained curves (fig.13)

are very similar to those given by Barker (1971), although in this case,

the range of σ_w extends to a much lower value. Over the range of σ_w

between 0.001 and 0.05 mhos m^{-1} these curves are approximately linear

and therefore an expression having the general form of equation 1.3

could be fitted to the corresponding part of the conductivity curves

(fig.11). However, fig. 13 also shows that in most cases the negative

slope b decreases progressively for σ_w greater than 0.05 mhos m^{-1}, in

some cases by as much as a factor of 10 between σ_w = 0.05 to 1.0 mhos m^{-1}.

Therefore an expression of the form 1.3 , requiring constant b and $F._{ol}$

values, is inadequate to fit the whole data. This is consistent with

Barker's (1971) conclusion.
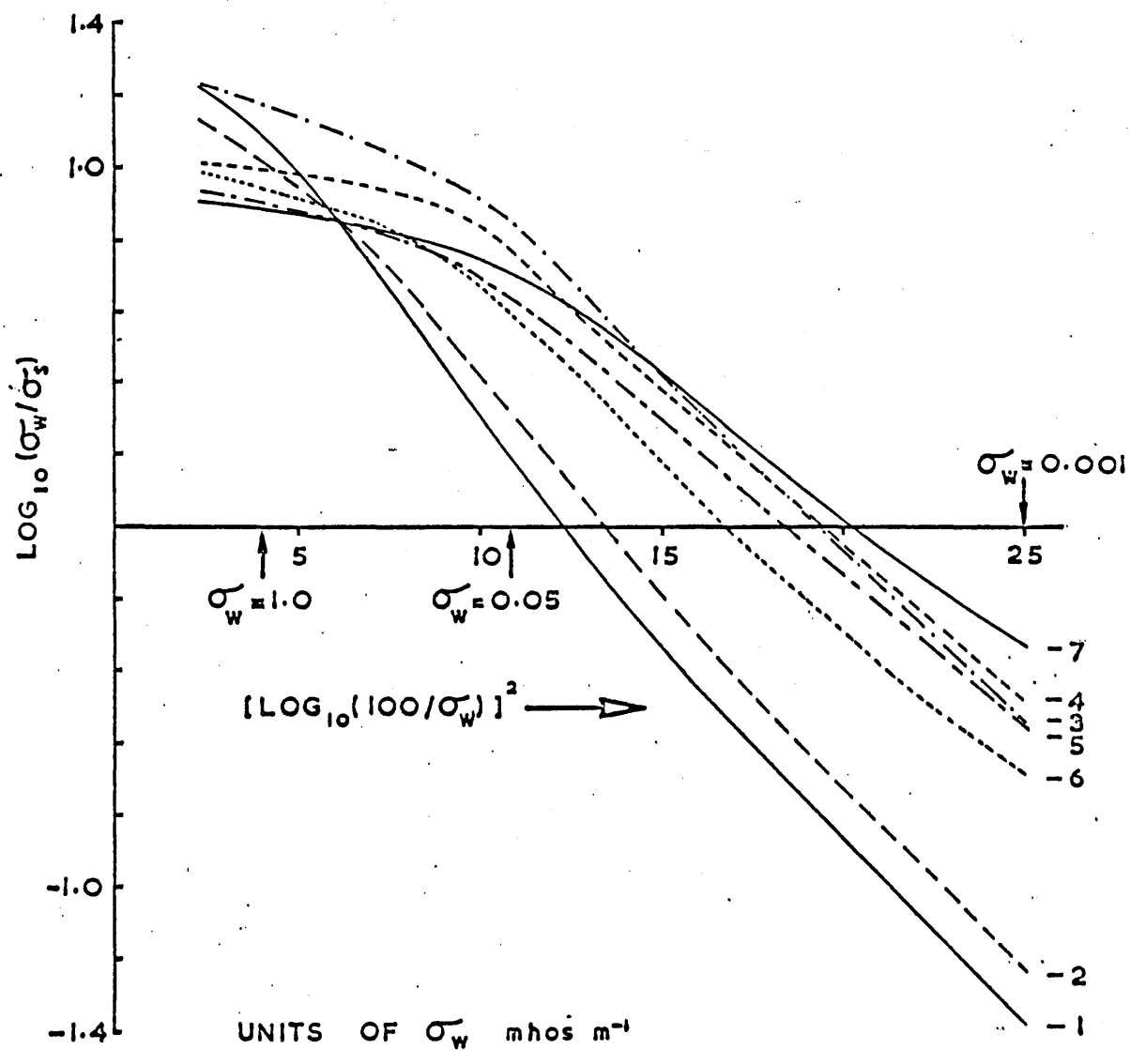
Curves obtained by plotting the conductivity data of figs 11a and b
as $Log_{10}F_a$ ($F_a = \sigma_w/\sigma_s$) against $[\log_{10}(100/\sigma_w)]^2$.

Corresponding sample numbers on the right.

FIG.13
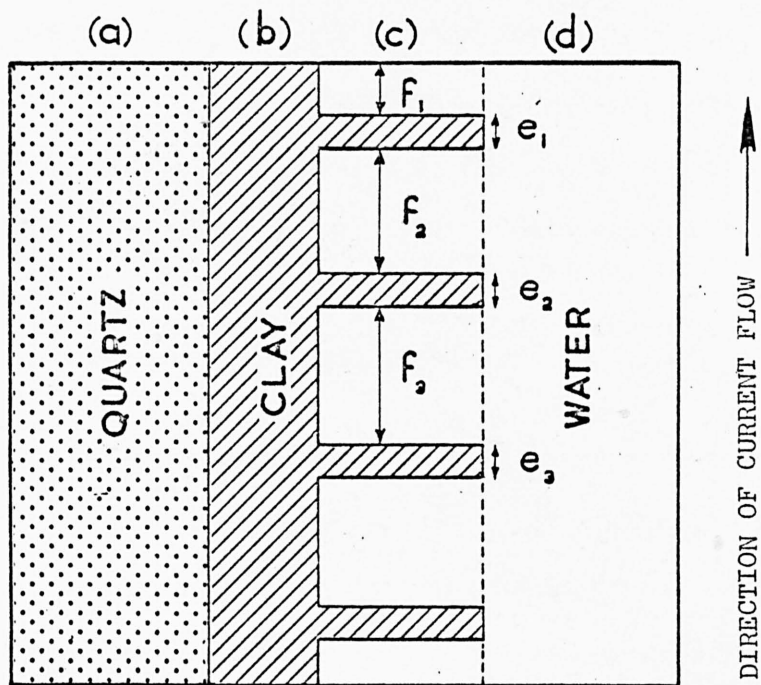
Simple conductivity model to represent
the sandstones.

FIG. 14

It is clear from the above discussions that neither of the expressions 1.2 and 1.3 describes the whole data accurately, moreover the departures can be considerable.

5.b A conductivity model for the sandstone

A simple model has been invoked to represent the sandstone and can account for the characteristic shape of the conductivity curves over low σ_w (fig.11a). It has been suitably adapted from the one that Spiegler, Yoest and Wyllie (1956) used to account for the similarly shaped conductivity curves of ion exchange bead beds. The model used here consists of the three components quartz, clay and water (electrolyte solution) arranged in four columns (fig. 14). These columns are:-

(a) Quartz
(b) Continuous clay film
(c) Clay membranes separated by water
(d) Water

The scanning electron micrographs (figs. 2a to f) suggest that this model is structurally consistent with the sandstones. It differs essentially from the Patnode and Wyllie (1950) model by the addition of column (c). Columns (b), (c) and (d) are ionically conductive and therefore, using the notation of fig. 14, an expression for the total conductivity of the model can be obtained. For unit area and length:-

$$a + b + c + d \quad = 1$$

$$e_1 + e_2 + e_3 + \ldots = e$$

$$f_1 + f_2 + f_3 + \ldots = f$$

$$e + f = 1$$

Conductance of column (a) $= a.\sigma_a$

" " " (b) $= b\,\sigma_b$

" " " (c) $= \dfrac{c\,\sigma_b\,\sigma_d}{(e\,\sigma_d + f\,\sigma_b)}$

" " " (d) $= d\,\sigma_d$.

where σ_a = conductivity of quartz

σ_b = " " the clay mineral

σ_d = " " " water

The conductivity of quartz, σ_a, is effectively zero, therefore:-

$$\text{Total conductance of the model} = \frac{c\,\sigma_b\,\sigma_d}{(e\,\sigma_d + f\,\sigma_b)} + b\,\sigma_b + d\,\sigma_d.$$

σ_T, the conductivity of the whole model, is given by:-

$$\sigma_T = \frac{\text{Total conductance} \times 1}{a + b + c + d}$$

$$\therefore \quad \sigma_T = \frac{c\,\sigma_b\,\sigma_d}{(e\,\sigma_d + f\,\sigma_b)} + b\,\sigma_b + d\,\sigma_d \quad \ldots 5.1$$

A graph of σ_T against variable σ_d has a form which is similar to the conductivity curves in figs. 11a and b, underlining the parallel between some of the model notations and those used for the sandstone. These are:-

Model notation	Sandstone notation	Description
σ_d	σ_w	Conductivity of pore water
d	F^{-1}	Slope of conductivity curve = Reciprocal of formation factor
$b\,\sigma_b$	σ_m (fig.11a)	Intercept of conductivity curve
σ_T	σ_s	Total conductivity of sandstone

Differentiating σ_T w.r.t. σ_d in equation 5.1

$$\frac{d\,\sigma_T}{d\,\sigma_d} = \frac{cf\,\sigma_b^2}{(e\,\sigma_d + f\,\sigma_b)^2} + d \quad \ldots 5.2$$

From equations 5.1 and 5.2 -

when $\sigma_d = 0$, $\sigma_T = b\,\sigma_b$

" " , $\dfrac{d\,\sigma_T}{d\,\sigma_d} = \dfrac{c}{f} + d$

$$\lim_{\sigma_d \to \infty} \frac{d\,\sigma_T}{d\,\sigma_d} = d$$

when $\sigma_d = \sigma_b$ $\qquad \dfrac{d\,\sigma_T}{d\,\sigma_d} = cf + d$

For a complete set of data that are known to conform to equation 5.1 the above relationships can be used to determine accurately most of the corresponding model parameters. However, the data available (figs. 11a and b) fall short of these ideals and therefore analyses have been made by an alternative approach.

The model contains too many unknown parameters for solution but by assuming the values of two of these, e and f, and calculating an appropriate slope d from the data, the corresponding values of σ_b, a, b and c can be determined to match the model to each sandstone sample. This has been done for illustration by applying equation 5.1 to interpolated data for the values $\sigma_d (\cong \sigma_w) = 0.001, 0.01,$ 0.03 mhos m^{-1} and solving the obtained simultaneous equations. The parameters e = 0.9, f = 0.1 were kept constant for all samples. These values were assigned after a number of trial and error calculations in which it was found that for ratios e : f much less than 9, the values of a, b and c became unrealistic and exceeded the unit constraint. Trial and error fitting also showed that equation 5.1 fitted the data over the range of σ_w less than 0.1, but for values significantly beyond this level, diverged progressively. This divergence was attributed to a non-linear increase of the clay conductivity as σ_w increased and therefore the best estimate for the slope d ($\cong F^{-1}$) was obtained at large values of σ_w.

In the first instance, equation 5.1 was solved for the conductivity data (figs. 11a and b) and three examples of this, samples 1, 5 and 7 which include the range of matrix conductivities σ_m and formation factor F, are shown in figs. 15 to 17. In each example the solution of equation 5.1 for the slope d ($\cong 1/F$) defined over the highest range of σ_w is

shown by the continuous line (i), and that corresponding to d from a lower range of σ_w by the dashed line (ii).   In both instances the equation describes the data adequately over the lowest range of σ_w (figs. 14a to 16a), but thereafter diverges according to the choice of d.   The values obtained for the parameters a, b and c (table 1) are partly controlled by those assigned to e and f but the proportions appear to be reasonable.   These diagrams verify that the column of clay membranes (c) included in the model (fig. 14) can adequately account for the curvature of the conductivity data over lower ranges of pore water conductivity (fig. 11a).

5.c Modifications to the model

In a following section (5.d), IP in saturated sandstones is attributed to ionic concentration gradients across the clay membranes, induced by the applied electric field.   The development of these ionic gradients effectively reduces the conductivity of the sandstone.   Therefore in the model (fig.14), IP would be represented by a reduction in the total conductivity of column (c).   Because this model is based upon elements with fixed properties, no allowance has been made in equation 5.1 for this change in properties of column (c).   Therefore the solutions of this expression (table 1) for the conductivity data (figs. 11a and b) are strictly incorrect.   Re-calculating the sandstone conductivity data as:-

$$\sigma_s = G.\frac{I}{(Vp - Vs)} \qquad \text{for Vs at t = 1s}$$

where Vp and Vs are the primary and secondary voltages and $\dot{G}$ the geometric factor, partially corrects for the IP effect.   Re-cast in this form of course, the data would resemble conductivities measured with alternating current.

Using sample 5 as an example, equation 5.1 has been solved for the

Table 1

Sample	d	a	b	c	σ_b mhos m^{-1}	$b\,\sigma_b$ mhos m^{-1}
1	(i) 0.031	0.491	0.371	0.107	0.0613	0.0227
	(ii) 0.045	0.477	0.371	0.107	"	"
5	(i) 0.08	0.693	0.079	0.148	0.029	0.00228
	(ii) 0.11	0.663	0.079	0.148	"	"
7	(i) 0.101	0.733	0.052	0.114	0.0244	.00128
	(ii) 0.117	0.717	0.052	0.114	"	"

(i) examples of solution to equation 5.1 for samples 1, 5 and 7 assigning e = 0.9, f = 0.1.

In examples (ii), d and a have been adjusted, b c and σ_b being constrained from (i), for comparisons in figs. 15 - 17.

Figs. 15 to 17:

Comparisons of equation 5.1 with conductivity data for samples 1, 5 and 7, (a) low range of σ_w (b) high range of σ_w, where

(i) d is defined at highest values of σ_w and

(ii) d is defined for the intermediate range of σ_w.   Parameters a, b, c and d as in Table 1.
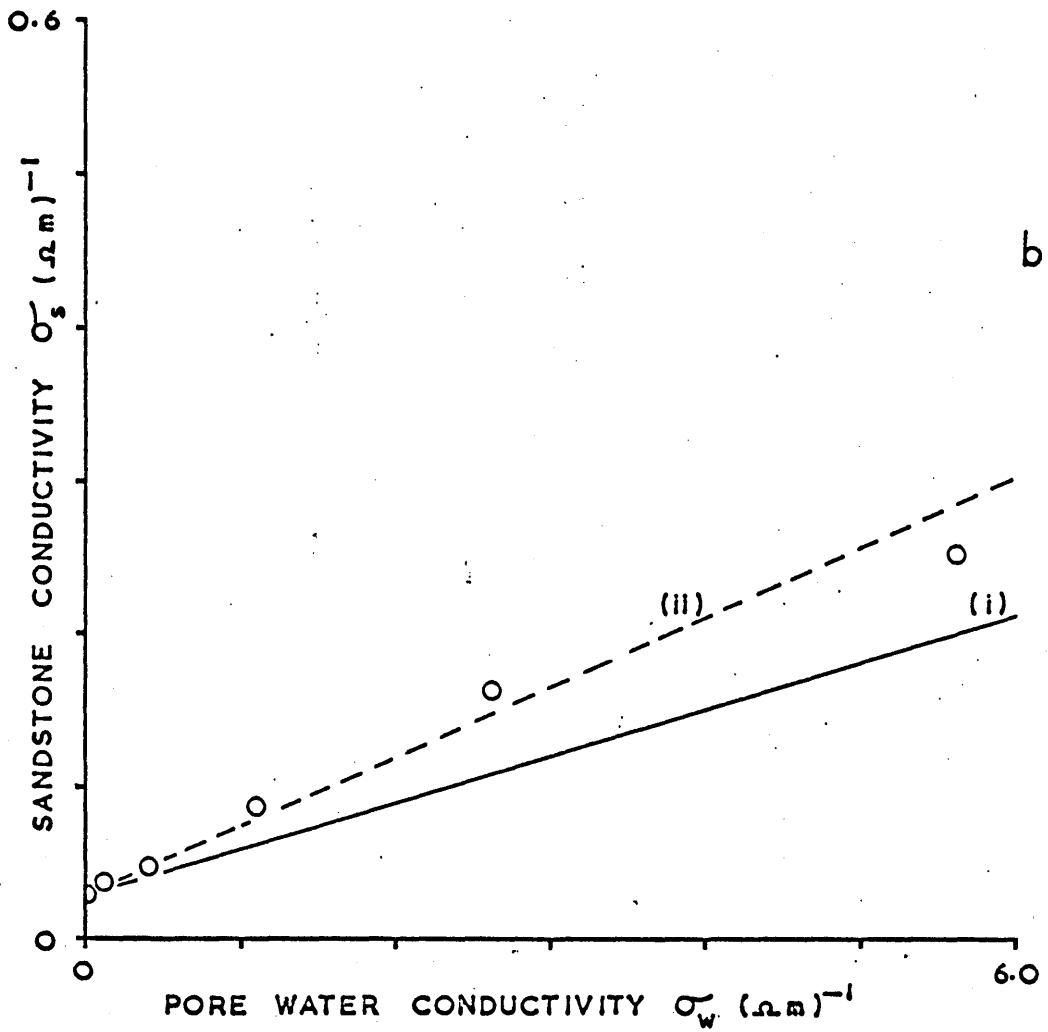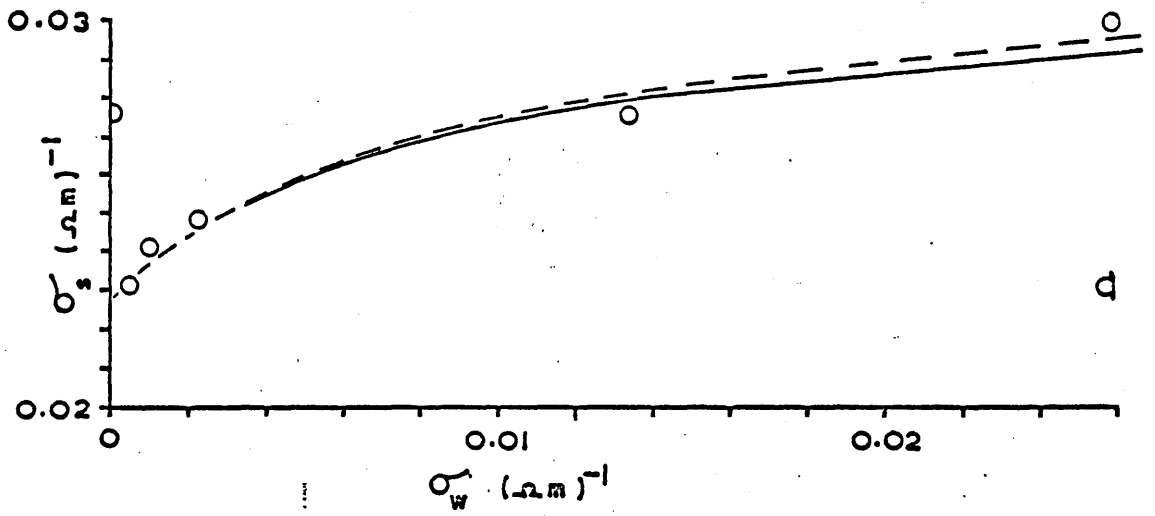
SAMPLE 1: See Table 1 for explanation

FIG.15
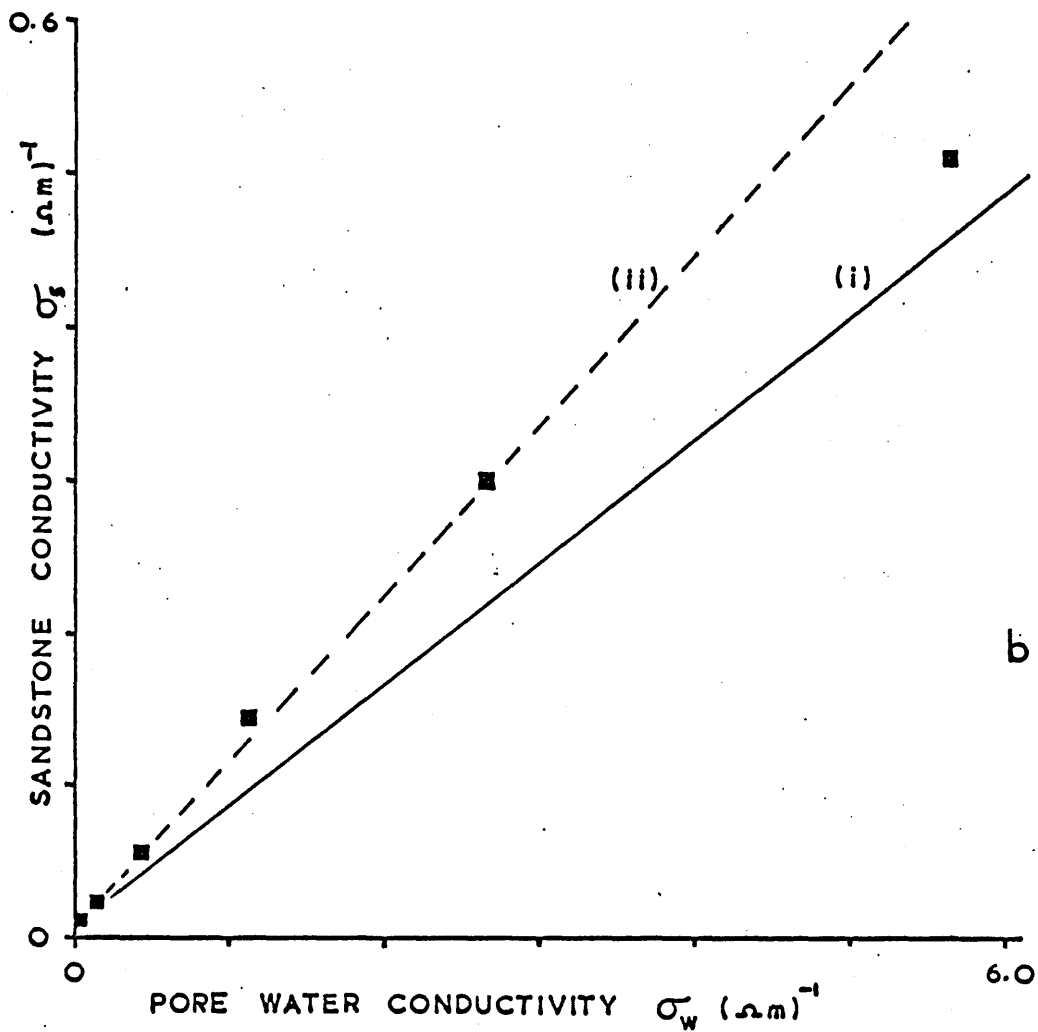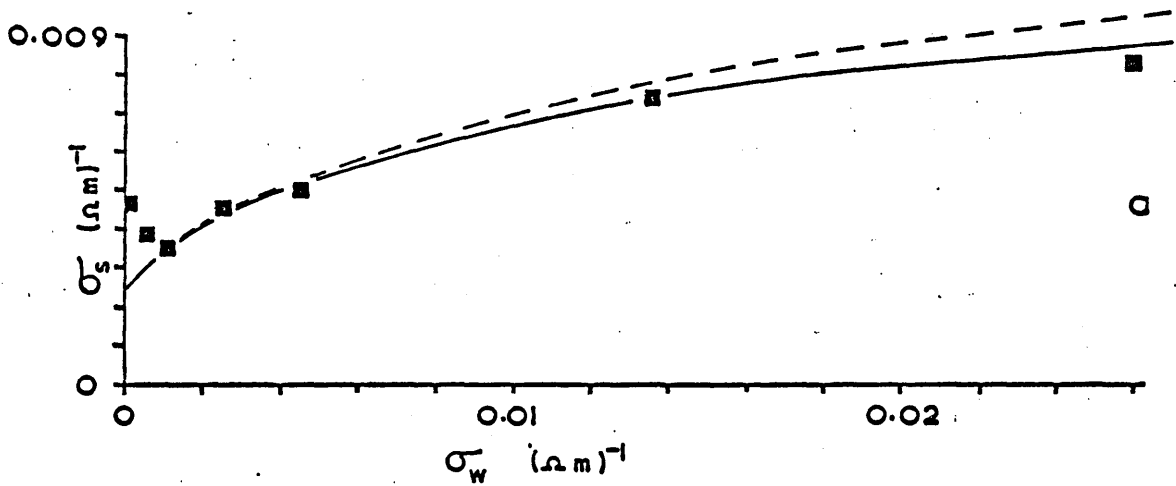
SAMPLE 5: See table 1 for explanation

FIG.16
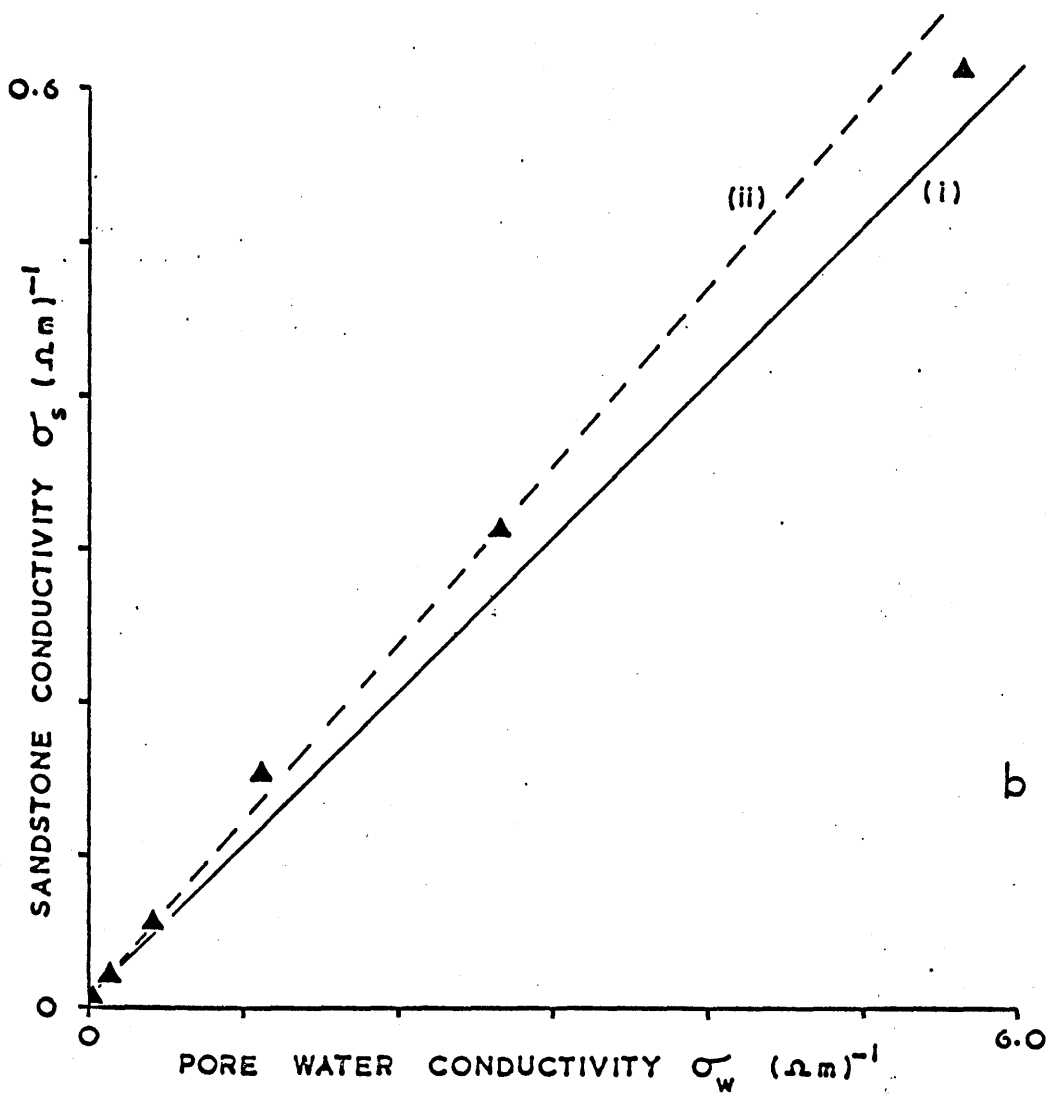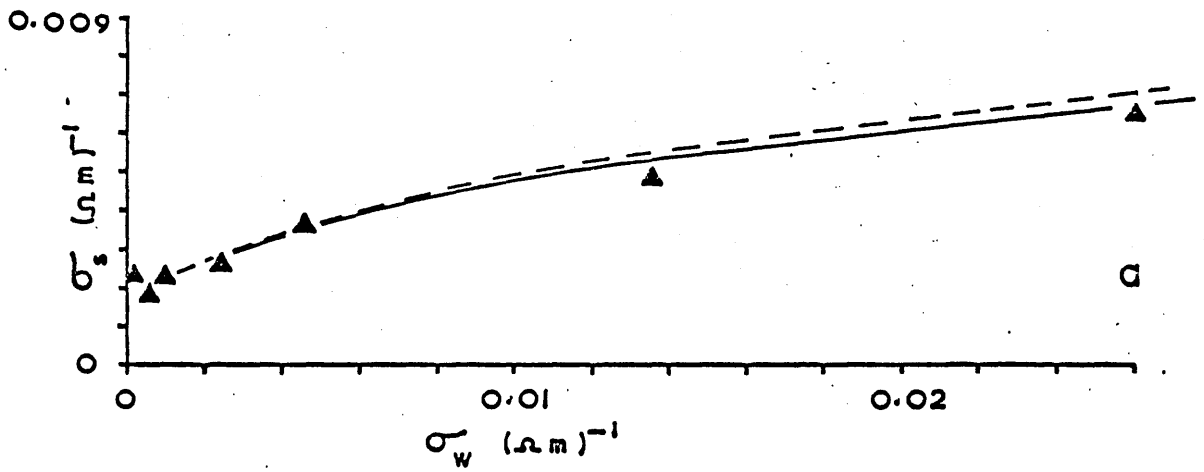
SAMPLE 7 : See table 1 for explanation

FIG.17

corrected conductivity data, obtaining the corrected values of $\widetilde{\sigma_b}$, a, b and c. These are compared with the uncorrected values in the table (2) below:-

	Corrected	Uncorrected
b $\widetilde{\sigma_b}$	0.0025	0.0023
$\widetilde{\sigma_b}$	0.0531	0.029
a	0.757	0.693
b	0.048	0.079
c	0.115	0.148

Table (2)   Parameters calculated for sample 5 (fig. 11)

for which d = 0.08; e = 0.9; f = 0.1

This table shows that whilst the values b and σ_b have incurred the largest corrections the value b $\widetilde{\sigma_b}$ ($\triangleq \sigma_m$) has remained almost constant.

Having obtained these corrected parameters, the effect of IP upon the conductivity σ_T over the lower values of σ_d e.g. $0 < \sigma_d < 0.1$, may be incorporated into the model by assigning a new term σ_b'' for the conductivity of the clay membranes.

Equation 5.1 becomes:-

$$\sigma_T = \frac{c\ \sigma_b''\ \sigma_d}{e\ \sigma_d + f \sigma_b'} + b\,\widetilde{\sigma_b} + d\,\sigma_d \quad \dots 5.3$$

from which σ_b'' may be calculated by assigning the corrected values of $\widetilde{\sigma_b}$, a, b and c and solving for the uncorrected data (fig. 11). For the example of sample 5 the value obtained was $\sigma_b'' = 0.0384$ mhos m^{-1}.

Summarising, the conductivity model (fig. 14) is structurally acceptable as a simulation of the sandstone. Over a wide range of pore water conductivities it can account for the non-linear variations of the conductivity data (fig. 11) with some improvement over the Hill and Milburn (eqn. 1.3) and Patnode and Wyllie (eqn. 1.2) expressions. This has been

illustrated in a general way in fig. 18, where the different expressions 1.2, 1.3, 5.1 have been fitted to the conductivity data (fig. 11) for sample 5. The Hill and Milburn equation (1.3) describes the data well over the higher ranges of pore water conductivity (fig. 18b, curves iii and iv) but at the lower range (fig. 18a) deviates from the data considerably and passes through the origin, although the true sandstone conductivity σ_s for zero pore water conductivity ($\sigma_w = 0$) is indeterminate. The linear Patnode and Wyllie equation (1.2), curve i, describes the data well except at both extremes of pore water conductivity, whereas the equation 5.1 offers further improvement at the lowest end of the range (fig. 18a).

5.d Discussion of membrane IP

Most authors attribute membrane IP to the ion exchange properties of clays (e.g. Schoeppel and Thrasher 1966, Keller and Frischknecht 1966). This view is not shared by all workers however, some claiming that clays only play a secondary role (e.g. Sami Soliman Mohamed 1970). Factors other than clay have been discounted here because during these experiments IP was measured on clean sand and again on a variety of sizes of glass beads but it was found that in the absence of clays the polarisation was too small to be measured with an acceptable degree of accuracy (Vs/Vp $\ll$ 0.015%) and totally negligible compared with IP in the presence of clays. Possible causes of membrane IP have therefore been carefully considered and that thought to be most probable is outlined below.

Fig. 19 schematically depicts several permselective clay membranes contained within a saturated porous rock. The mean activity of the electrolyte in aqueous solution is $a^{\pm}$.

In the absence of an applied electric field, the pore water on both

Fig 18:

A comparison of the form of the equations - (i) 1.2, Patnode and Wyllie, (ii) 5.1, sandstone conductivity model, (iii) and (iv) 1.3, Hill and Milburn, and the conductivity data for sample 5. The following parameters have been used:-

(i) $\frac{1}{F}$ ($\hat{=}$ d) = 0.112 $\qquad$ σ_m = 0.006 mhos m^{-1}

$\quad$ (From linear regression of data between σ_w = .013 and 2.7 mhos m^{-1})

(ii) d = 0.112 $\quad$ a = 0.682 $\quad$ b = 0.073 $\quad$ c = 0.133
$\quad$ (Retaining d from (i))

(iii) $F_{.01}$ = 10.67 $\quad$ b =-0.0287
$\quad$ Direct solution from interpolated data points between
$\quad$ σ_w =0.06 and 2.68 mhos m^{-1}

(iv) $F_{.01}$ = 13.68 $\quad$ b =-0.0510
$\quad$ From linear regression analysis of logarithmic data
$\quad$ (fig 13) corresponding to the range σ_w = 0.014 to 2.68 mhos m^{-1}
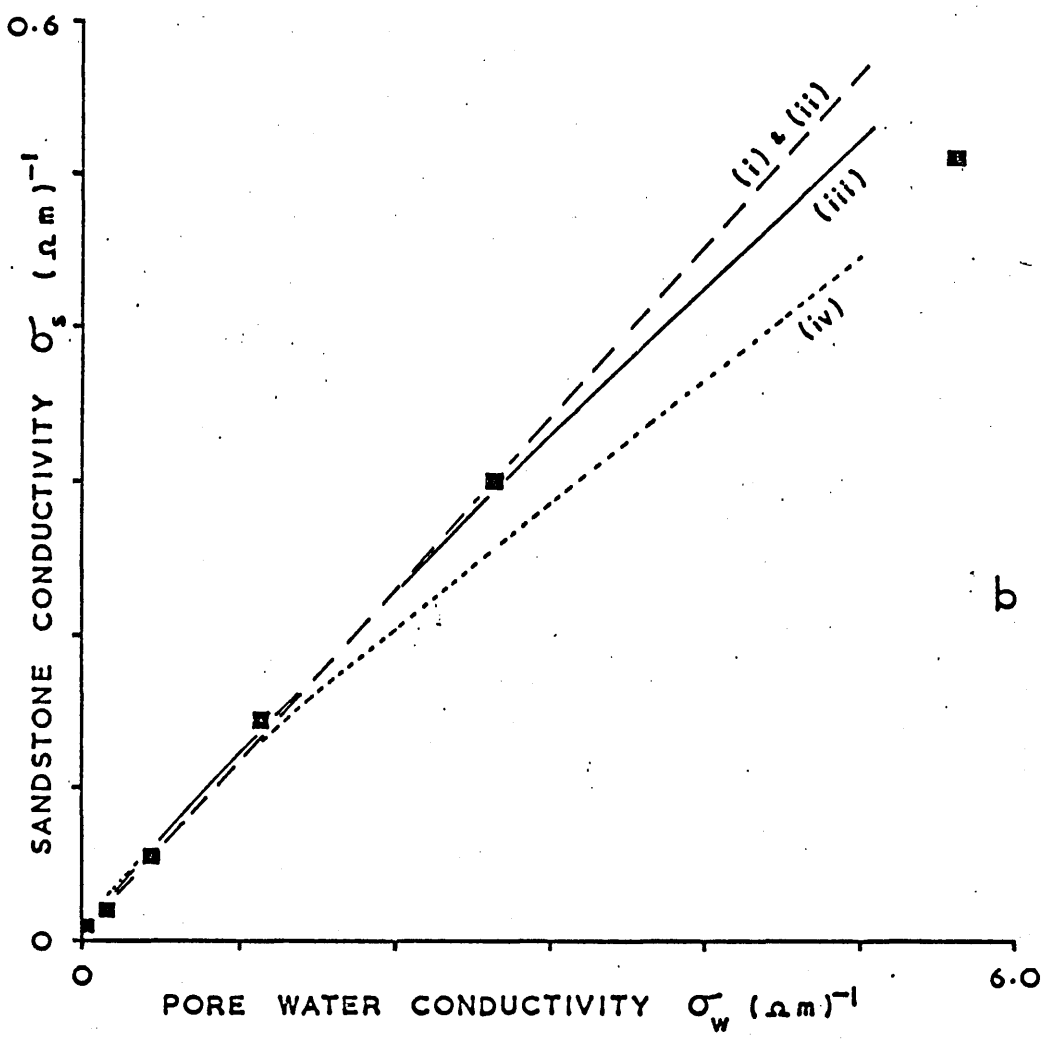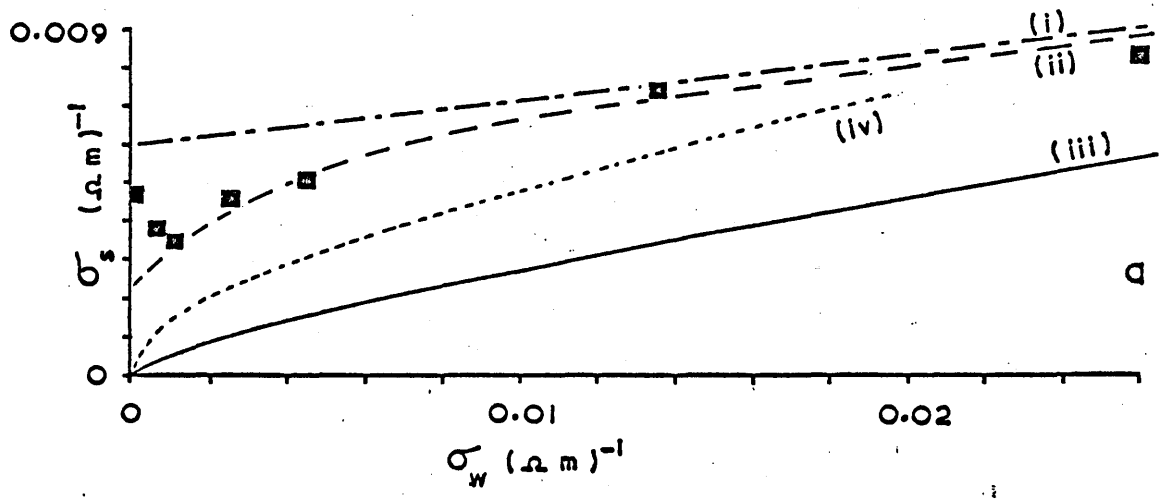
FIG.18
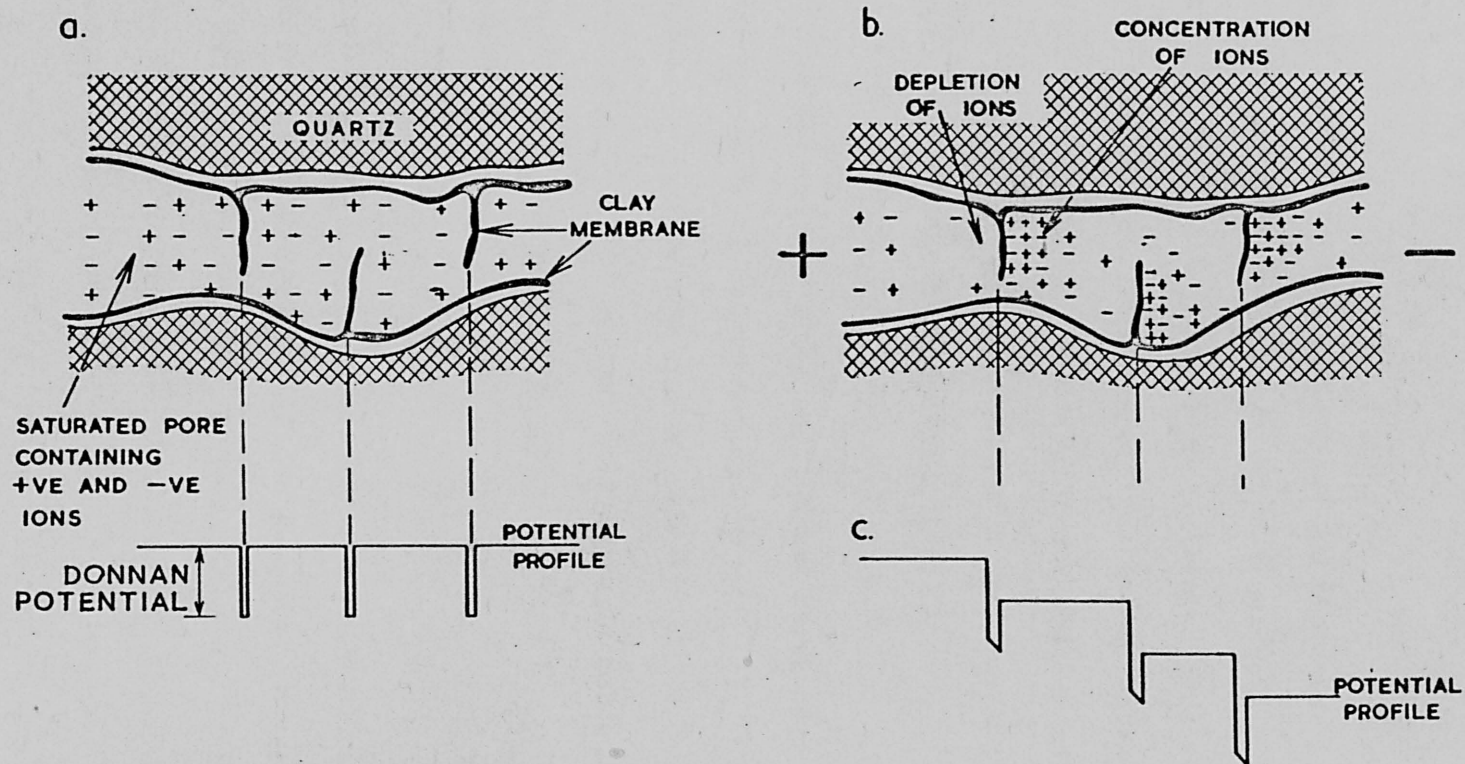
Schematic representation of a saturated sandstone.
(a) No external field, sum of the Donnan potentials is zero.
(b) Applied e.m.f. induces ionic concentration differences across the clay membranes.
(c) After removal of the external e.m.f., the sum of the Donnan potentials gives
     a net potential gradient.

FIG. 19

sides of any one membrane contains equal concentrations of ions (fig.19a). The respective electrolyte mean activities a_1 and a_2 are equal and $a_1 = a_2 = a^{\pm}$; therefore the net potential E_m across the membrane is zero.

The application of an e.m.f. perpendicular to the membranes induces movement of ions, anions toward the anode and cations toward the cathode. However, the cation selectivity of the clay restricts transference of anions and consequently the distribution of ions in the water is altered in the vicinity of each membrane, depletion of cations and anions being induced on the anodic side of the membrane and a concentration of these ions being induced on the cathodic side (fig. 19b).

Whilst the e.m.f. is maintained, a new equilibrium state develops, the concentration difference being mainly determined by:-

    a)   the permselectivity of the clay membrane

    b)   the average activity $a^{\pm}$ of the electrolyte in solution

    c)   the magnitude of the applied e.m.f.

    d)   the rate of diffusion of ions.

A permselective membrane that separates dilute electrolyte solutions of different concentrations develops an electric potential between its boundaries, the Nernst potential, which is mainly the sum of the Donnan potentials. For an ideal membrane that separates solutions with activities a_1 and a_2 the magnitude of this potential is given by

$$E_m = \frac{RT}{F} \log \frac{a_2}{a_1} ,$$

where R is the gas constant, T the absolute temperature and F Faraday's constant. This type of potential difference, already familiarly known in well logging as a self potential (Mounce and Rust 1944, McCardell, Winsauer and Williams 1953, Wyllie and Southwick 1954, Hill and Milburn 1956) occurs in the case of

cation selective membranes with the positive on the side of lowest electrolyte concentration (fig. 19c).   This subject is treated in detail by texts such as Marshall (1949) and Helferrich (1962).

When an e.m.f. is applied to a wet porous rock containing a network of clay membranes, this potential is induced about each membrane.   Summed over the whole rock, this induced potential may be observed to rise to an equilibrium whilst a constant current flows and return to zero when the e.m.f. is removed.   This explanation for membrane IP is similar to, although less formal than, the one given by Marshall and Madden (1959).

The scanning electron micrographs (figs. 2a to f) show that the clay membranes often occur on the grain surfaces and across the intergranular spaces.   In these cases therefore, polarisation potentials might be expected to develop across any membrane regardless of its location within the porous framework, and not be confined to constrictions between the grains.   Applying the Nernst equation to the IP potentials (from figures 11 and 12) and assuming membrane separations of 5 microns (2.b), the observed polarisations for current densities of 0.1 Am^{-2} would be obtained with induced activity ratios as low as 1.0004.   However the clays are unlikely to behave as perfect ion exchange membranes and therefore ratios greater than this might be expected.

A formal account for the observed variations of IP with pore water conductivity (fig. 12) has not been found but, with reference to the above discussion, a few important points can be considered.   For the condition when the pore water is almost free of contamination, the mean electrolyte activity $a^{\pm}$ is nearly zero and therefore ionic concentration differences will not be induced across the membranes.   Then the IP, being proportional to log a_1/a_2, should be zero also.   As $a^{\pm}$ increases from zero, the ratio a_1/a_2 can assume rapidly increasing values which

would result in corresponding increases of IP. For the mean activity increasing further, the permselectivity of the membrane eventually will be impaired by sorption (Spiegler et al 1956) and consequently the induced activity ratios will be decreased and the membrane potentials will progressively depart from the proportionality log a_1/a_2. Therefore IP would be expected to reach a maximum and thereafter decrease as the salinity of the water is increased from zero.

It is well known that clays attract cations to their surfaces, forming electric clouds or layers. This is recognised to have important bearing upon the ionic conduction within wet sandstones (Winsauer and McCardell 1953). The ions present within a saturated pore may therefore be considered in two categories:-

    (a)   those which are remote from surface influences and are

           free to diffuse randomly;

    (b)   ions which are linked by the surface charges but may

           still participate in electrical conduction.

If those ions of category (a) only are involved in the selective process about a clay membrane in an applied electric field, then a saturated sandstone with a large specific surface area of clay might be expected to have a low proportion of type (a) ions and therefore also to have a low chargeability.

In discussion of membrane IP in saturated porous rocks, Keller and Frischknecht(1966) assumed that 'polarisation is approximately proportional to the number of anions in solution which are free to accumulate at the potential (clay) barriers, $(a-a_0)/a$', where a is the pore water salinity and a_0 a measure of the rock cation exchange capacity, and also proportional to the number of potential barriers (a_0/a) formed by the active clay. The total proportionality:-

$$\text{polarisation} \propto a_0 (a - a_0)/a^2$$

they term the anion trap number. It is interesting to note that for the salinity a steadily increasing above a_o, the polarisation would be expected to reach a maximum and thereafter decrease asymptotically to zero, which is consistent with the data in fig. 12.

CHAPTER 6

EXPERIMENTALLY SHOWN RELATIONSHIPS BETWEEN IP, K AND σ_w FOR A WIDE
RANGE OF BUNTER SANDSTONES

6.a Relationships between IP and K: $\sigma_w = 0.025$ mhos m^{-1}

Permeabilities have been measured for the seven samples described in
Chapter 4 and the results compared with the IP data given in fig. 12.
A marked correlation may be observed between log K and IP at values of
σ_w up to 0.025 mhos m^{-1} (fig. 20).   For σ_w increasing beyond 0.025,
the IP of the permeable samples decreases (fig. 12) and therefore the
correlation with log K may be expected to deteriorate.

IP and permeability K were measured on a further 350 samples, drilled
from Fylde, Shropshire, Vale of Clwyd and Cumberland borehole cores,
to determine whether this correlation extended to a wider range of
Bunter sandstones.   The samples were saturated with a NaCl solution of
approximately 150 ppm the conductivity of which, σ_w, was 0.025 mhos m^{-1}
and the obtained IP data have been plotted against log K.

6.b Discussion of results

The extensive data for the Fylde samples are initially presented as a
whole (fig. 21).   There is a broad distribution of data, the envelope
of which describes a general increase of IP with log K, but the
correlation coefficient $r_c = 0.75$ is poor.   These data do not clearly
define a unique relationship that would be widely applicable to the
Fylde sandstones.

The data have also been subdivided into groups (figs. 22a to i), each
of which comprises the samples from a single borehole.   Data for the
Cumberland, Shropshire and Vale of Clwyd sandstones are presented in

n = 7
r_c = 0.93
s = 5.27

y-axis: Vs/Vp%(t=ls)

x-axis: Log K mms^{-1}

n   =   number of samples

r_c =   correlation coefficient

s   =   slope of linear regression

IP at σ_w = 0.025 mhos m^{-1} plotted against log permeability for the seven sandstone samples described in chapter 4.

FIG.20

$n = 217$
$r_c = 0.75$
$s = 2.70$

FYLDE

$Vs/Vp \% (t=1s)$

$Log K \ mms^{-1}$
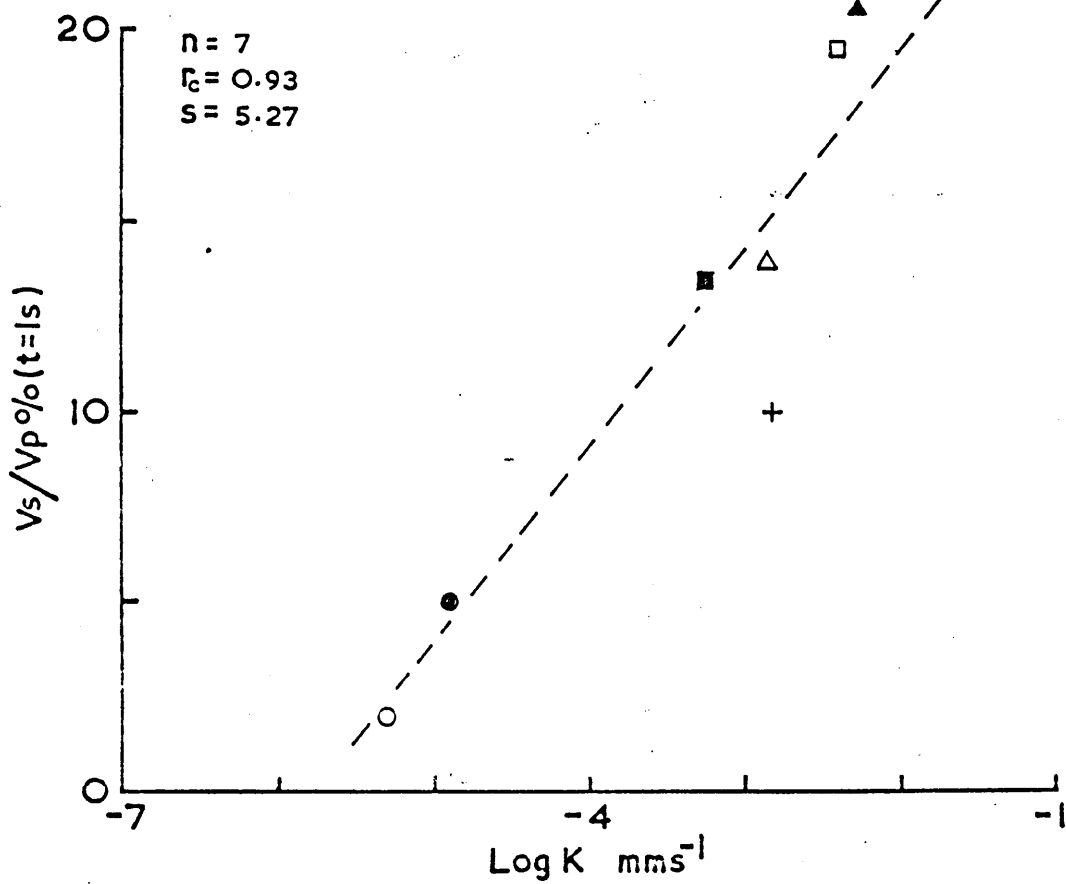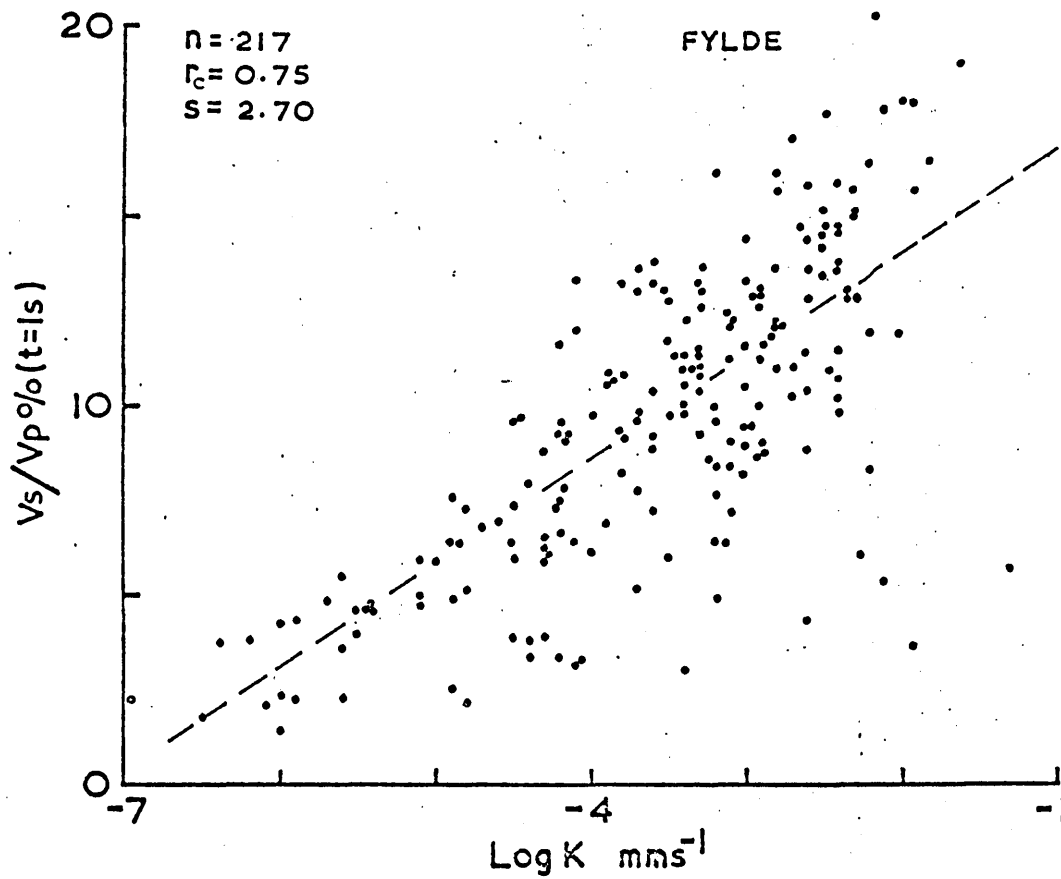
n   =   number of samples

r_c =   correlation of coefficient

s   =   slope of linear regression

IP at $\sigma_w = 0.025$ mhos m^{-1} plotted against log K
for a large group of sandstone samples from the Fylde.

FIG.21
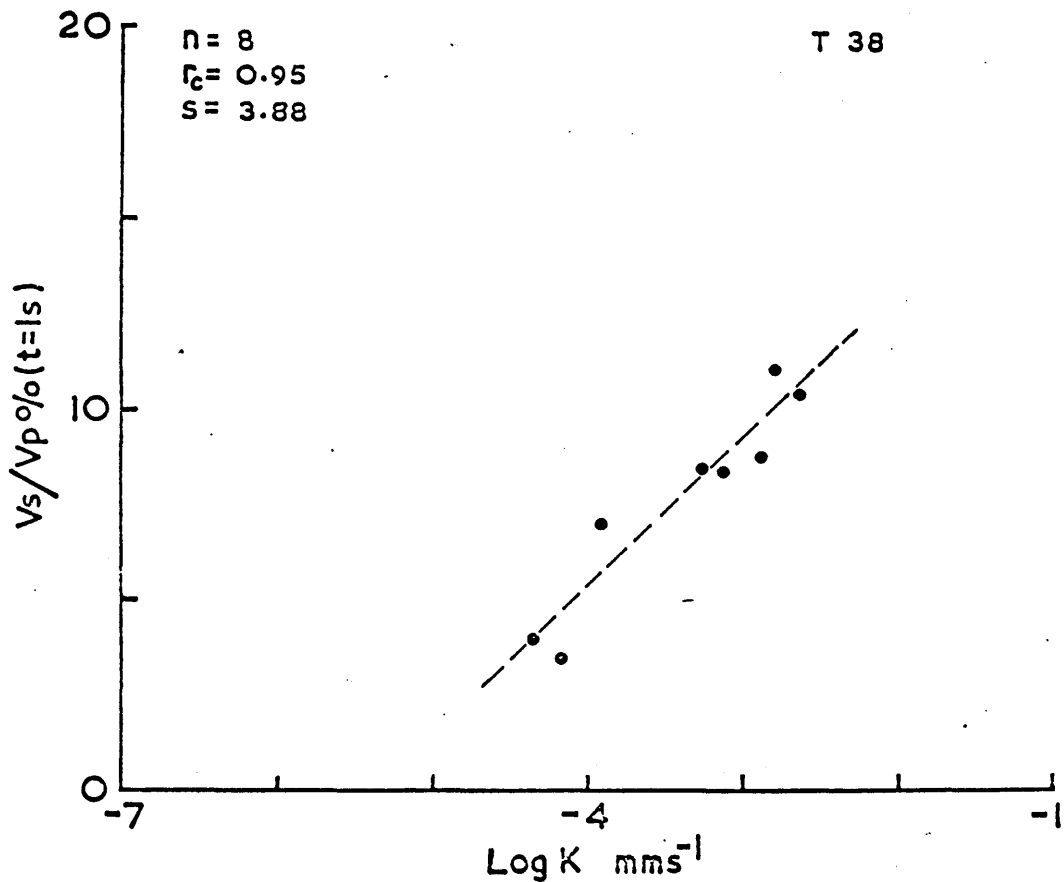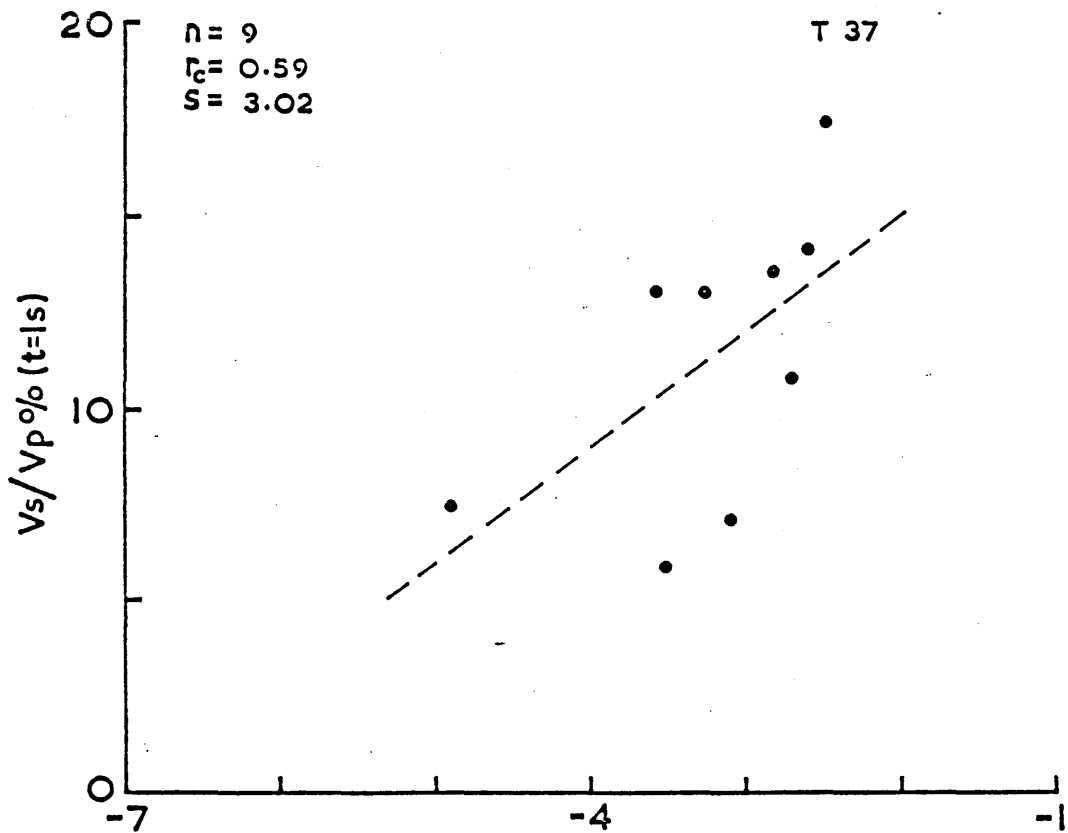
Fig 22a : IP at σ_w = 0.025 mhos m^{-1} plotted against Log K

for samples from boreholes T37 and T38 (Fylde).

n = number of samples: r_c= correlation coefficient

s = slope of linear regression
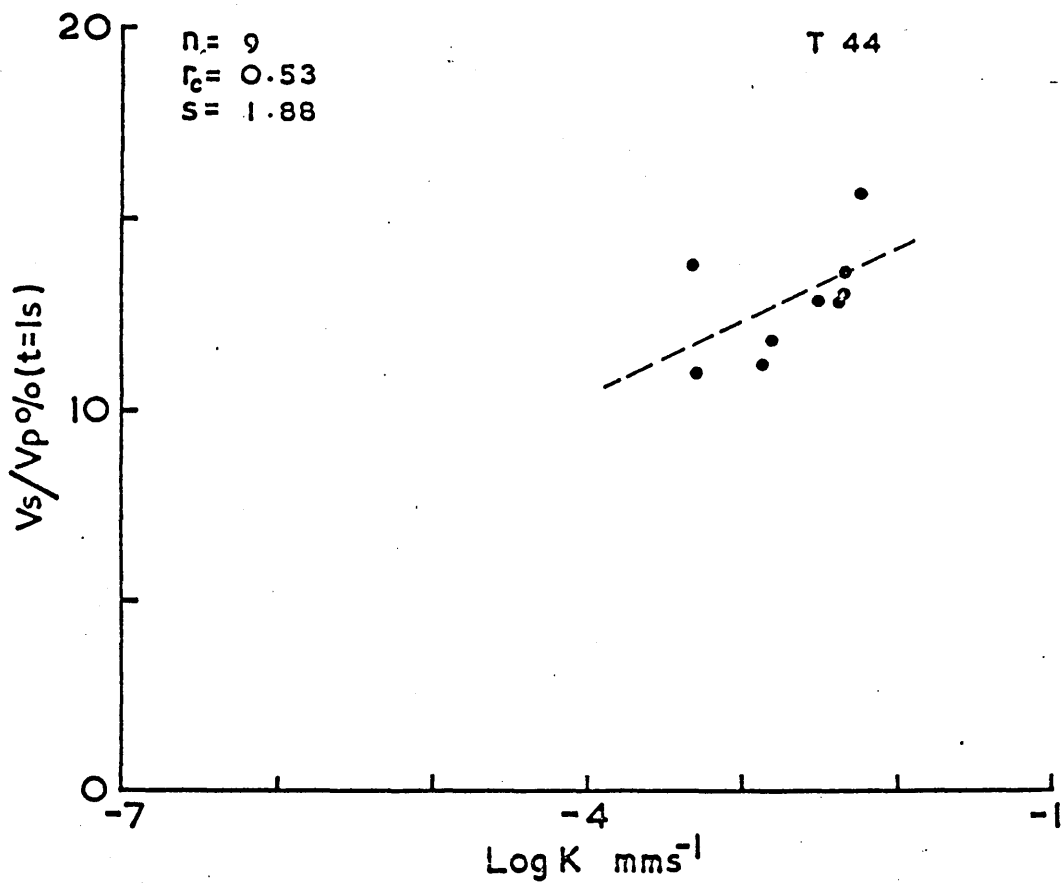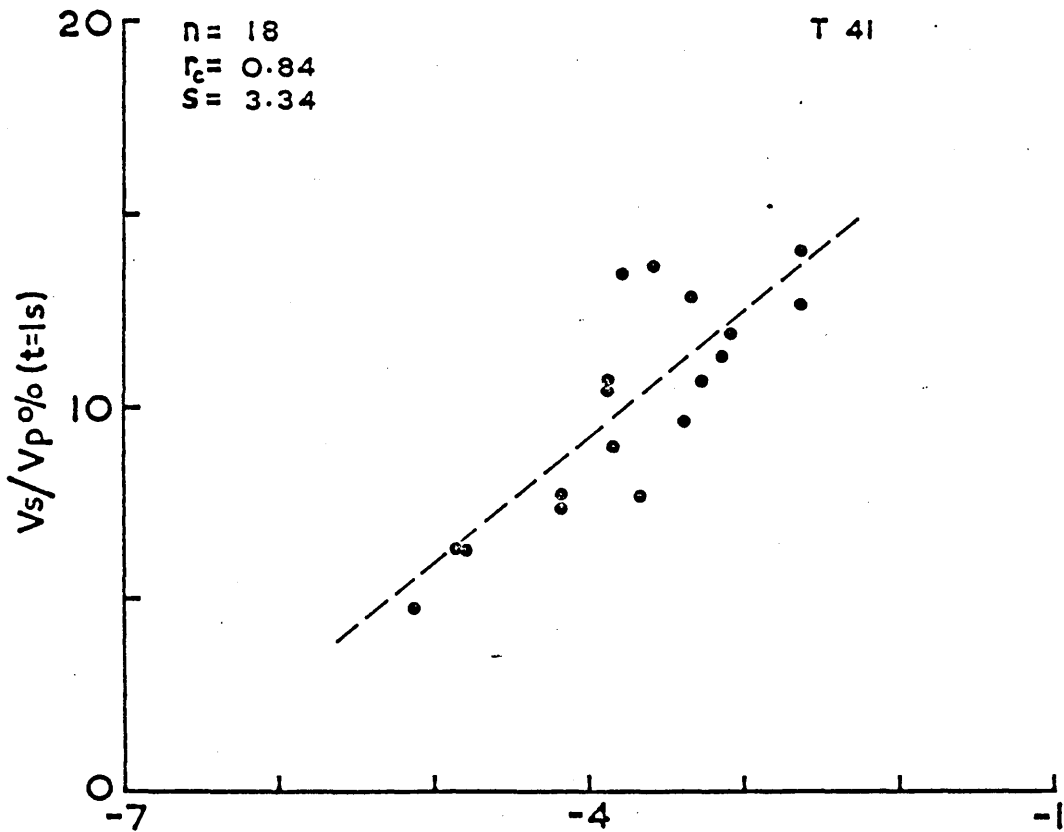
Fig 22b : IP at σ_w = 0.025 mhos m^{-1} plotted against Log K for samples from boreholes T41 and T44 (Fylde)
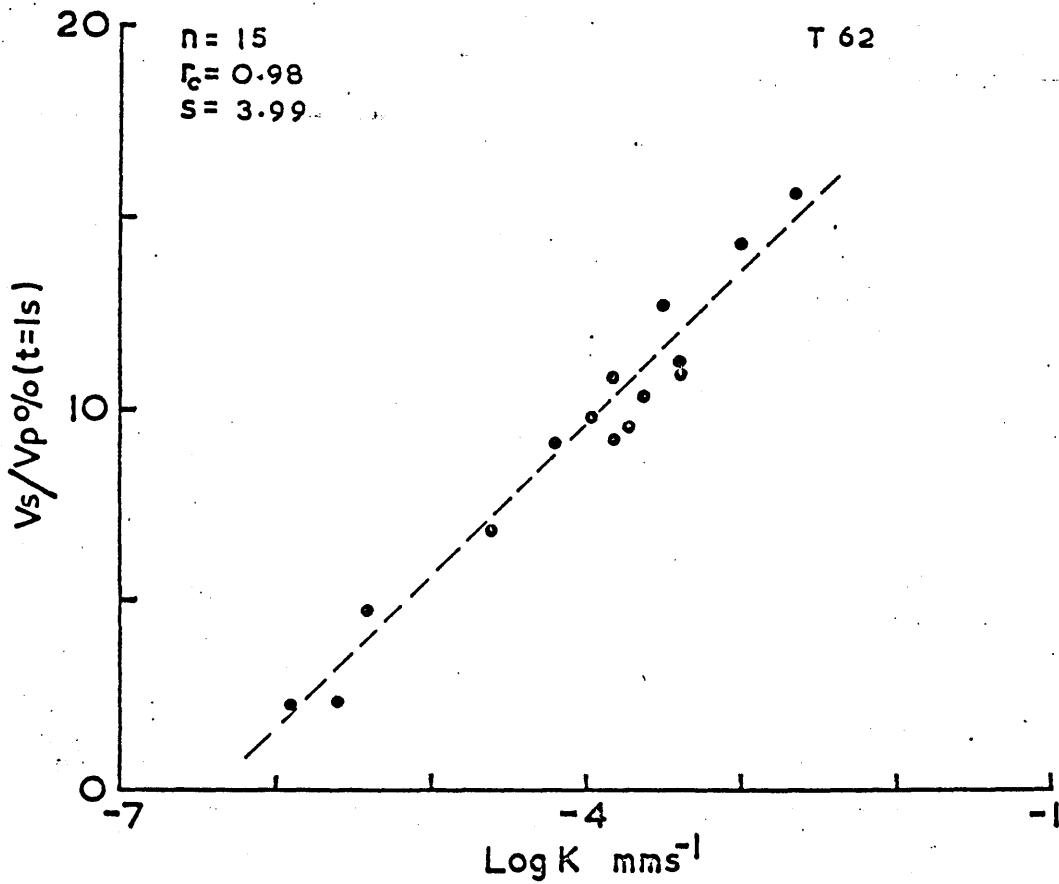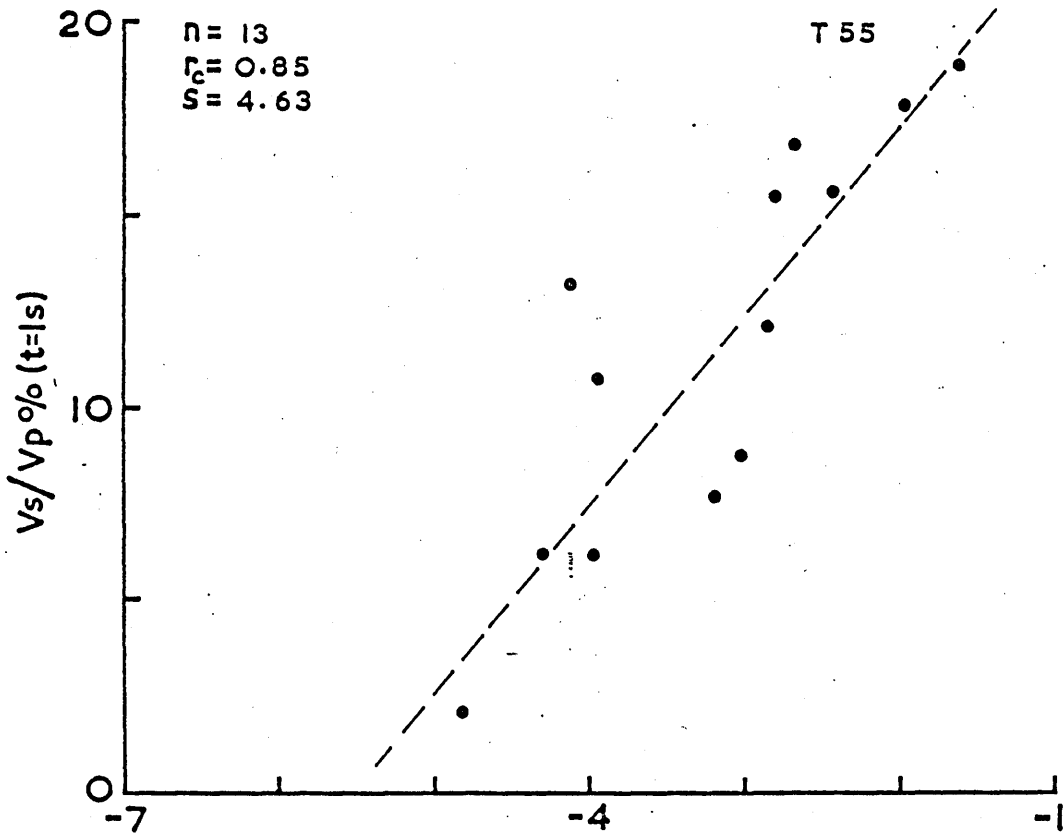
Fig 22c : IP at σ_w = 0.025 mhos m^{-1} plotted against Log K for samples from boreholes T55 and T62 (Fylde).
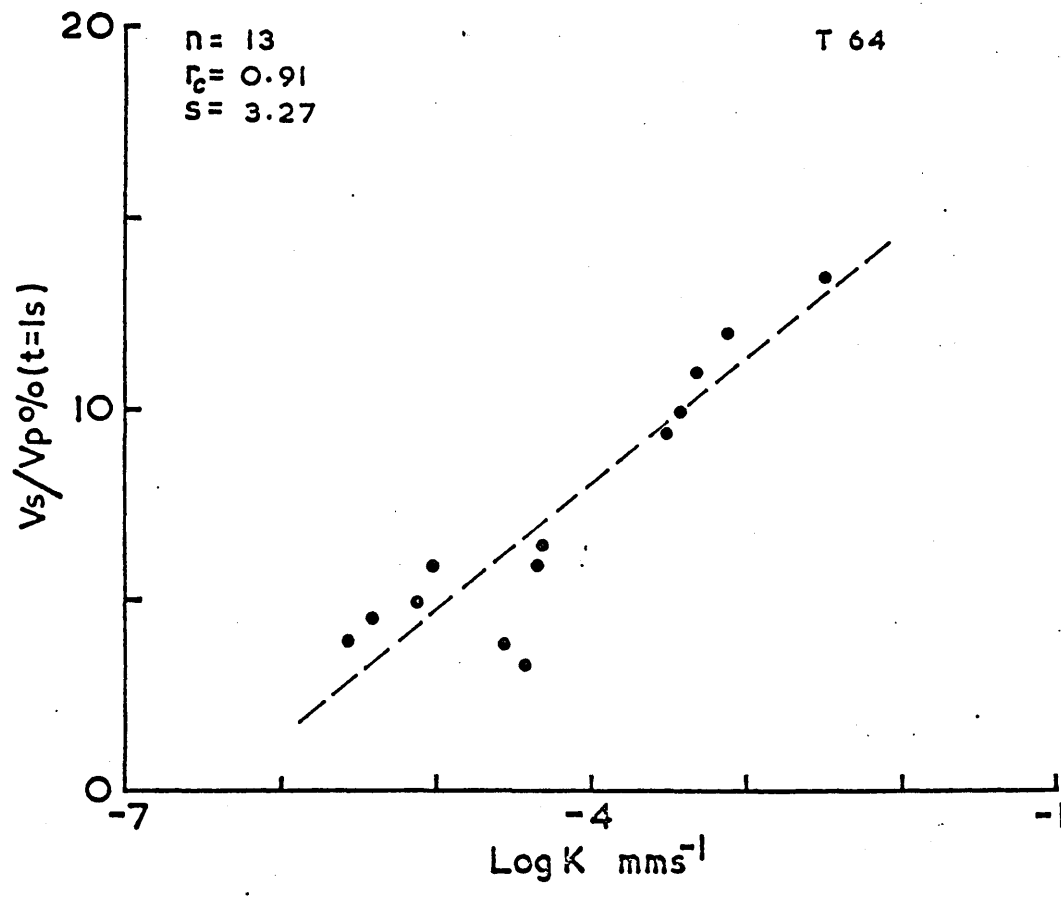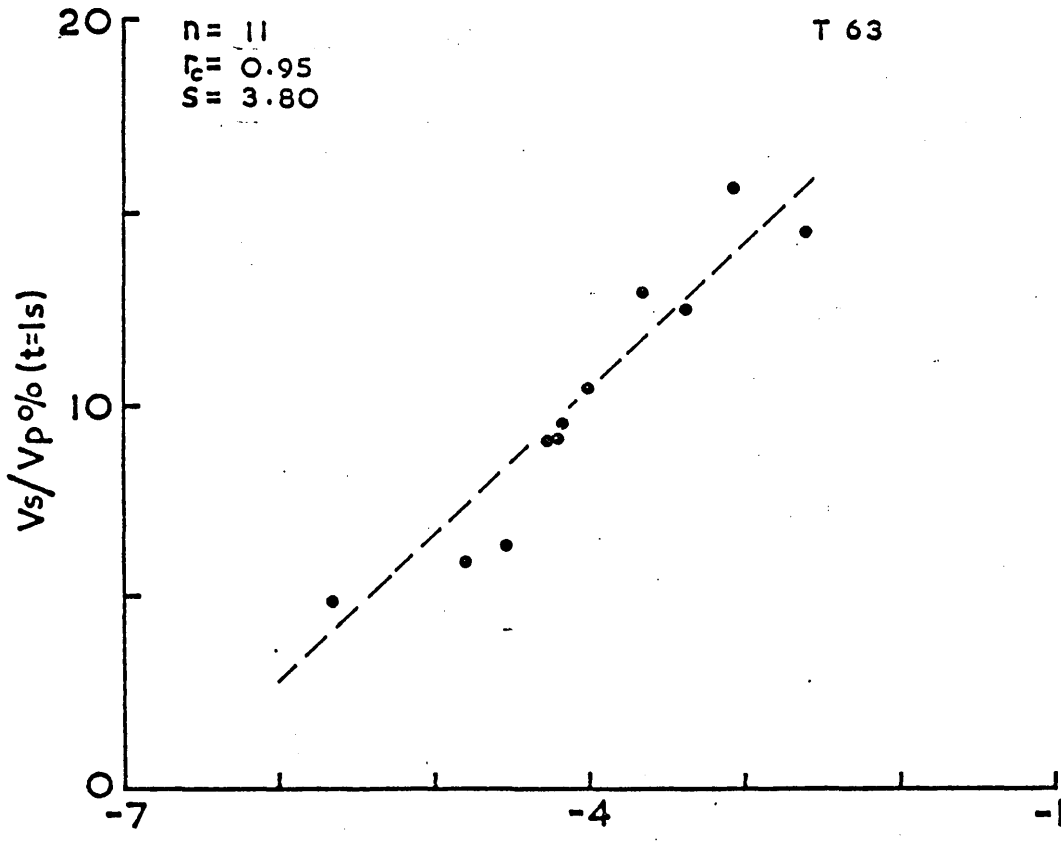
Fig 22d : IP at σ_w = 0.025 mhos m^{-1} plotted against Log K for samples from boreholes T63 and T64 (Fylde)
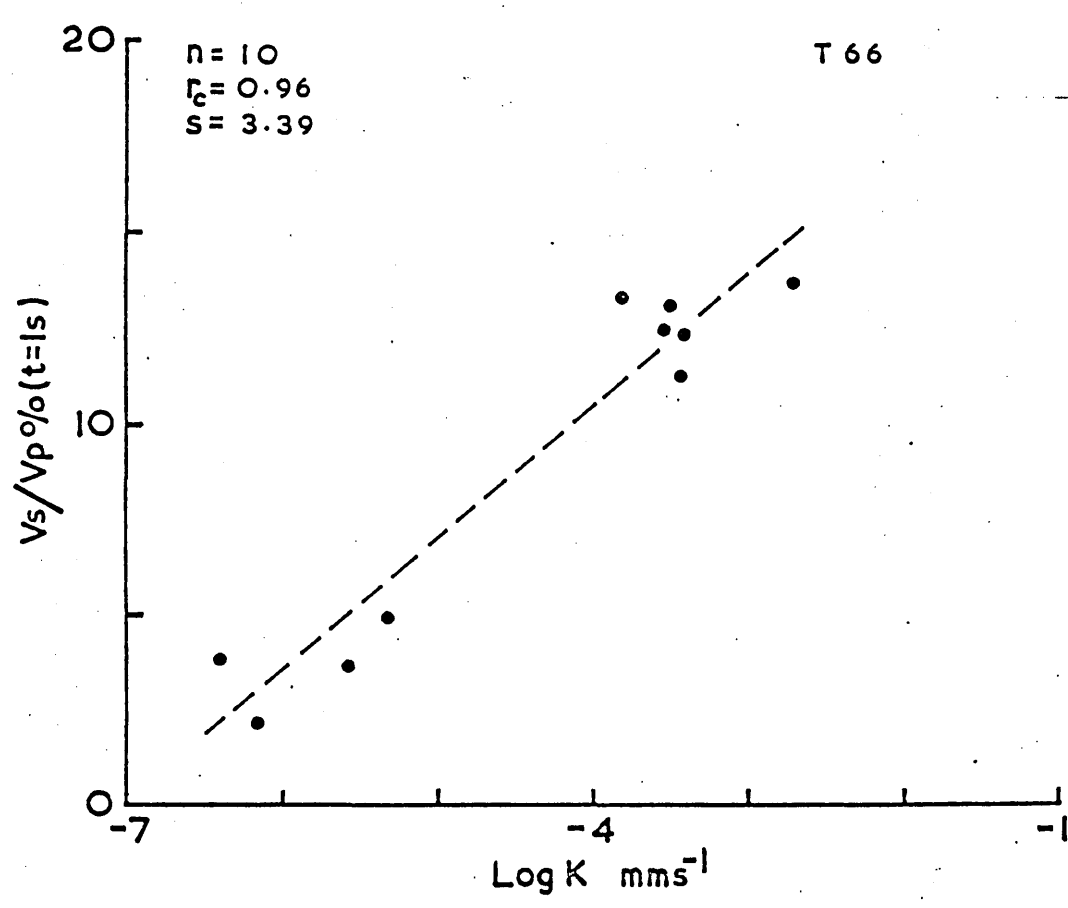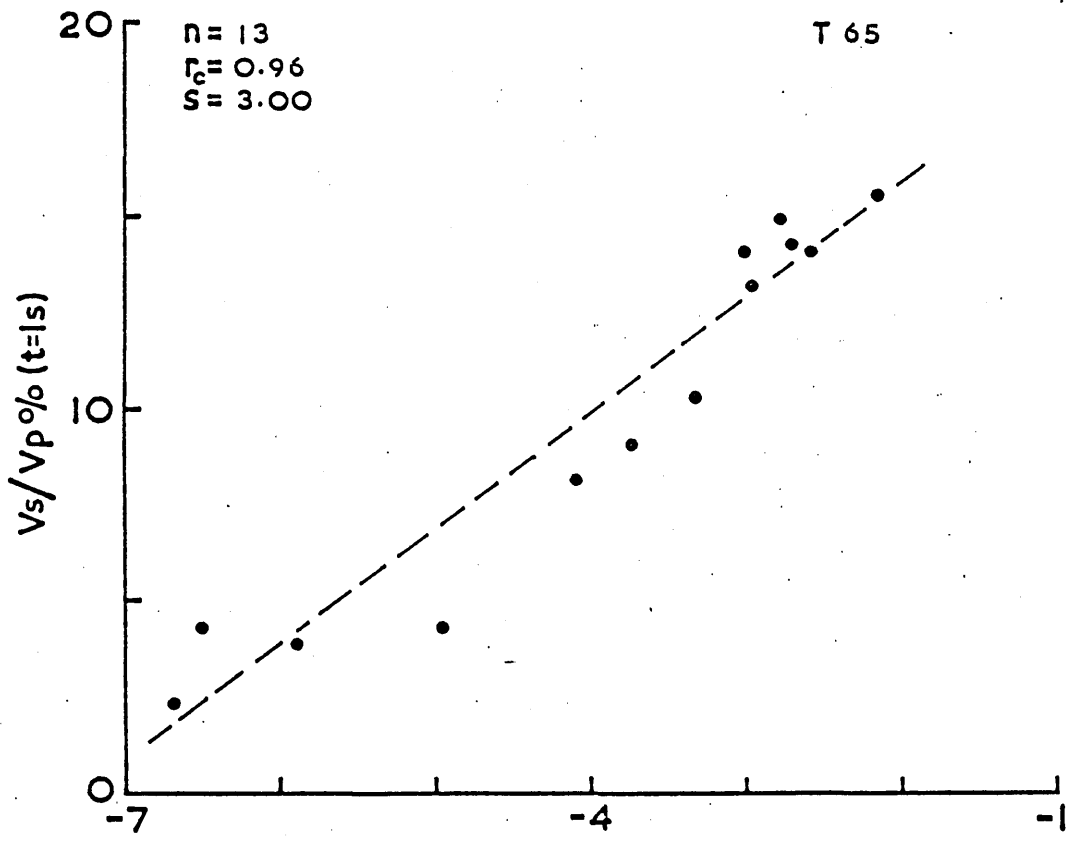
Fig 22e : IP at σ_w = 0.025 mhos m^{-1} plotted against Log K for samples from boreholes T65 and T66 (Fylde).
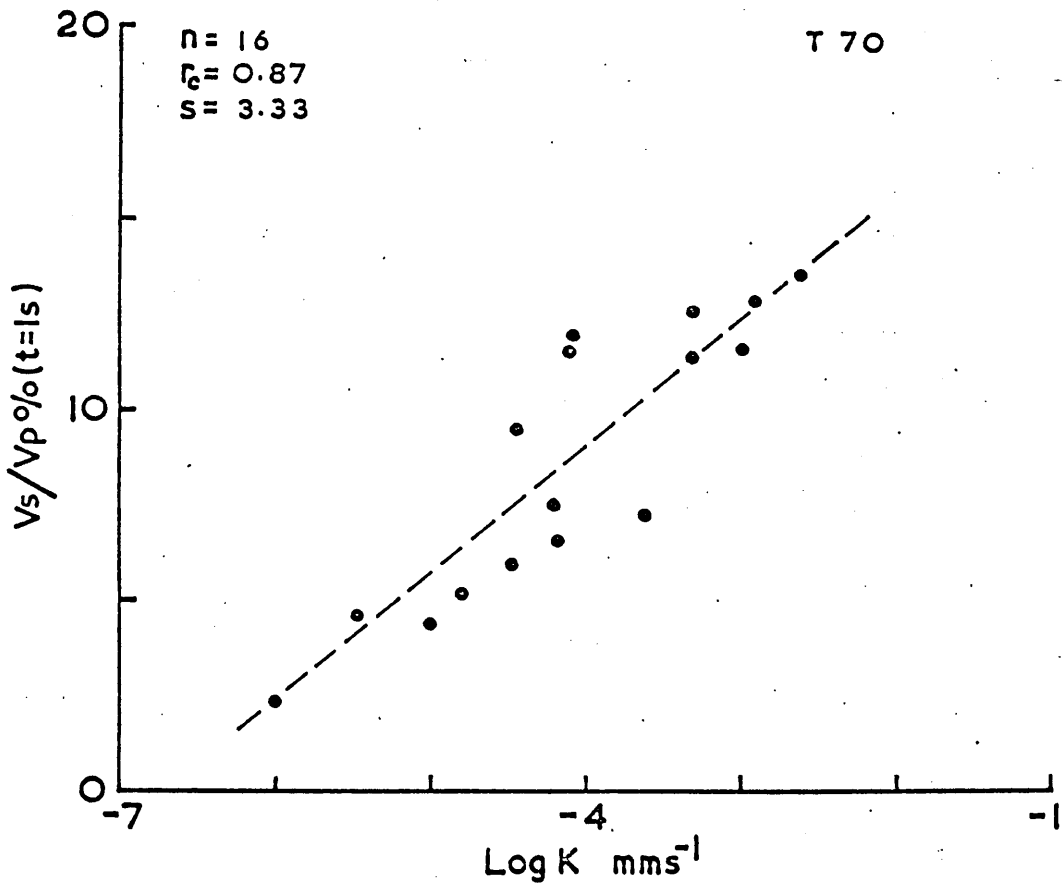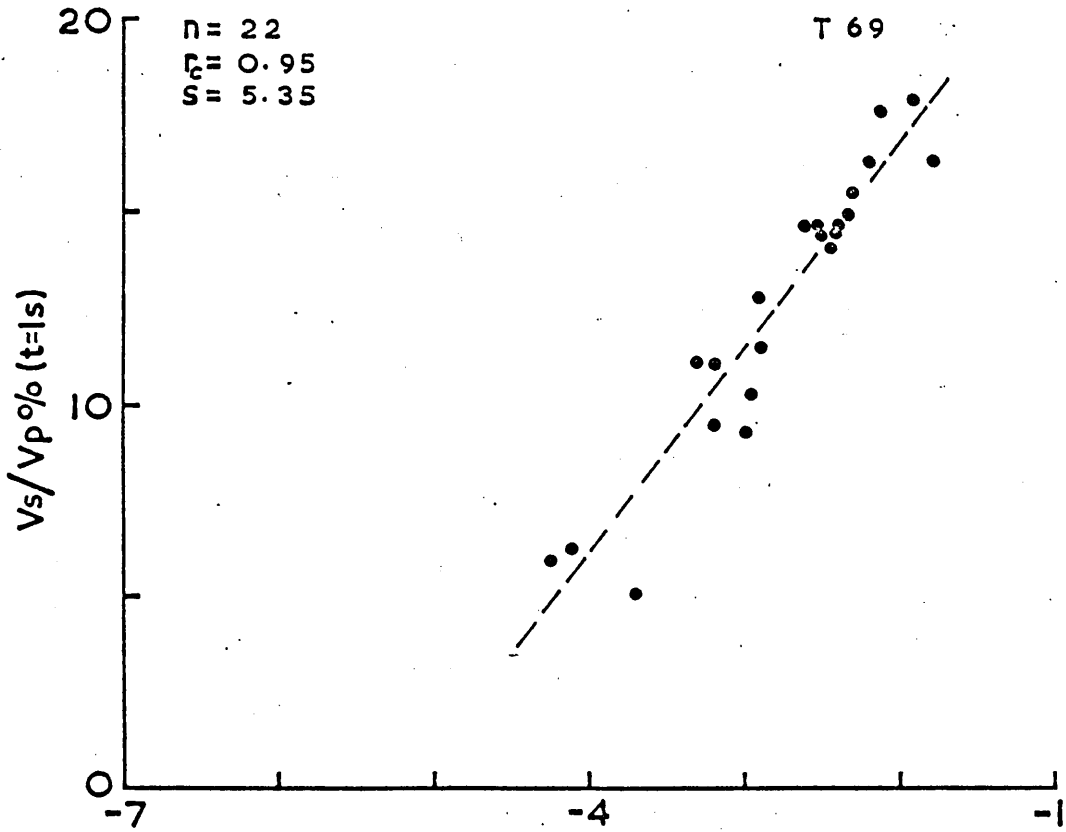
Fig 22f : IP at σ_w = 0.025 mhos m^{-1} plotted against Log K for samples from boreholes T69 and T70 (Fylde).
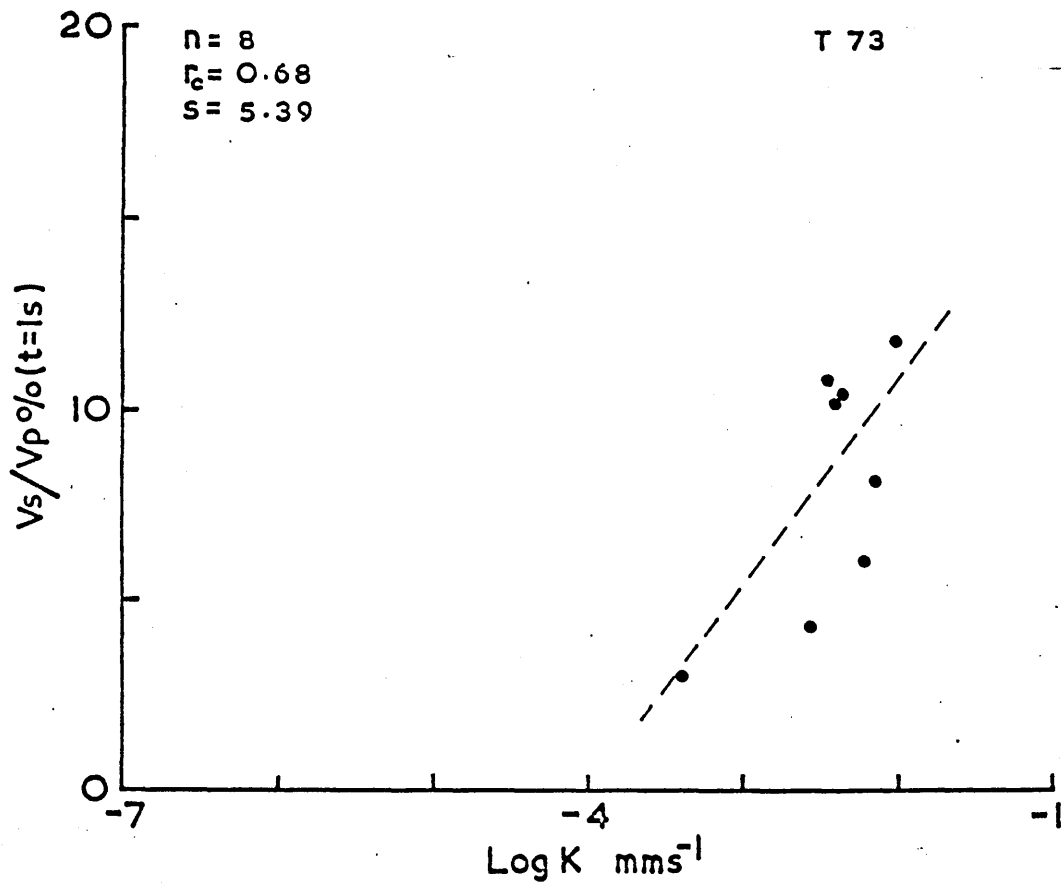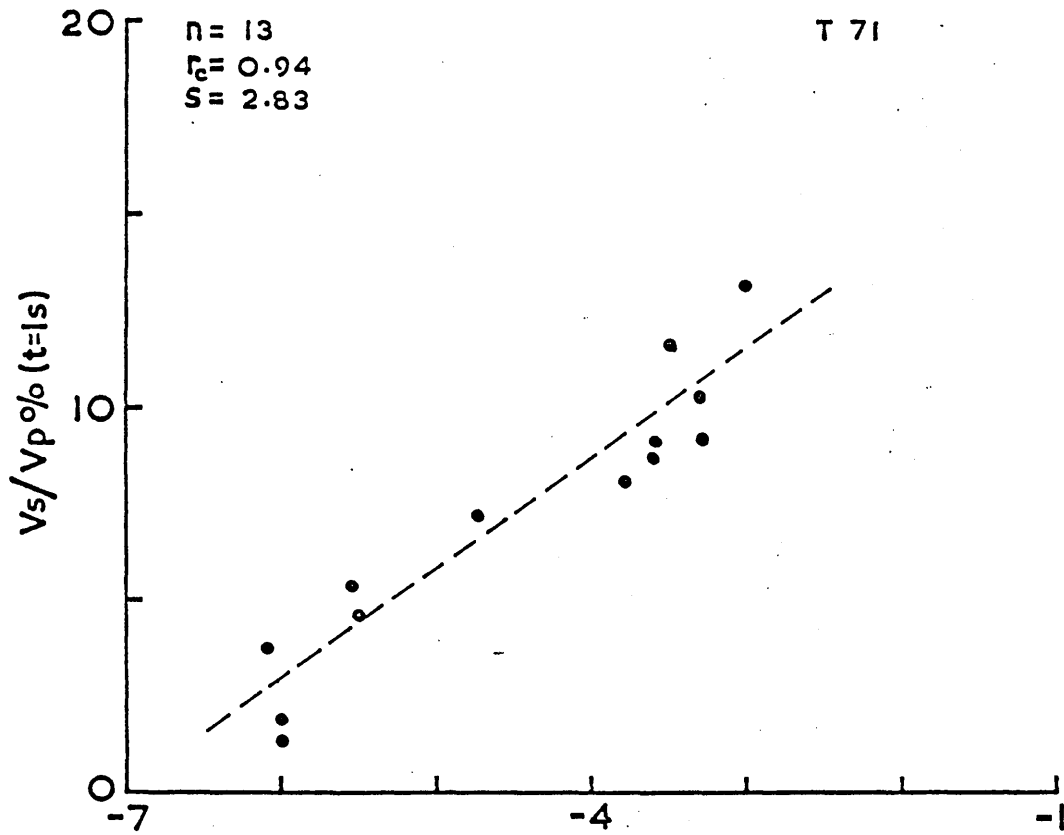
FIG.22f

Fig 22g : IP at σ_w = 0.025 mhos m^{-1} plotted against Log K for samples from boreholes T71 and T73 (Fylde)
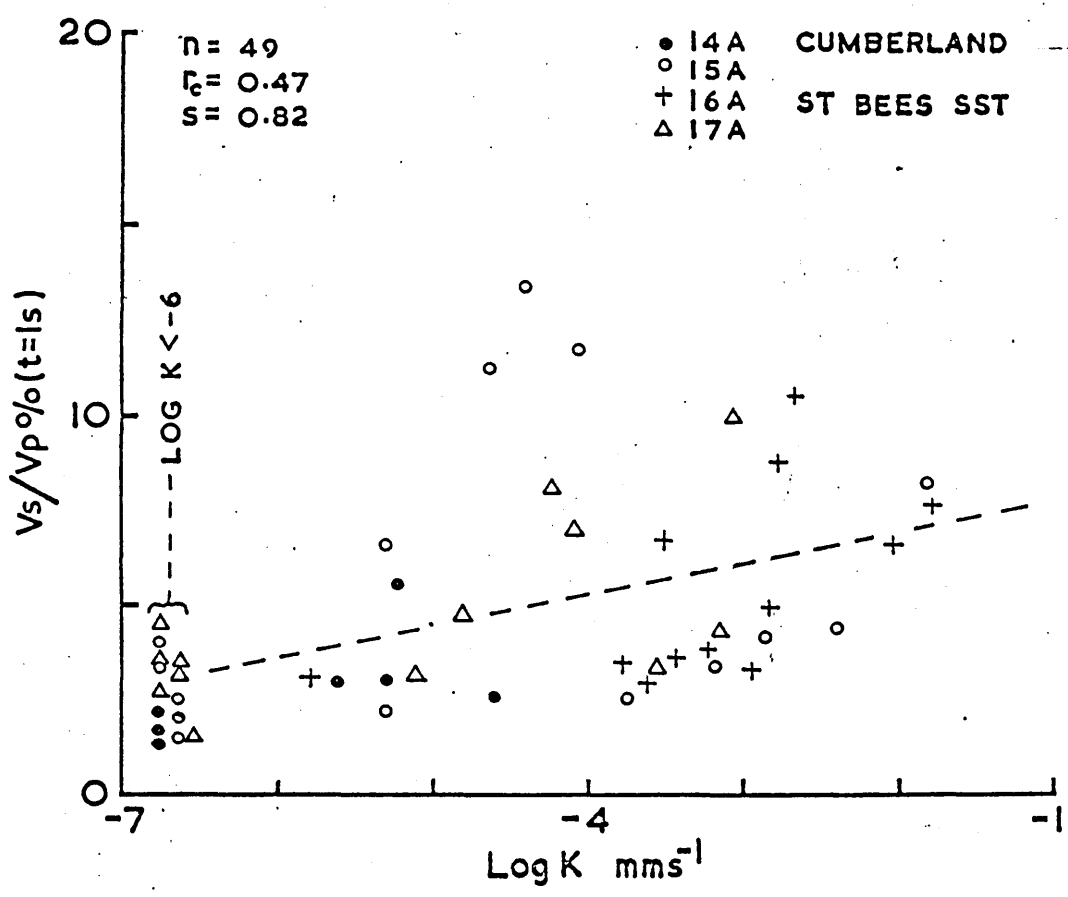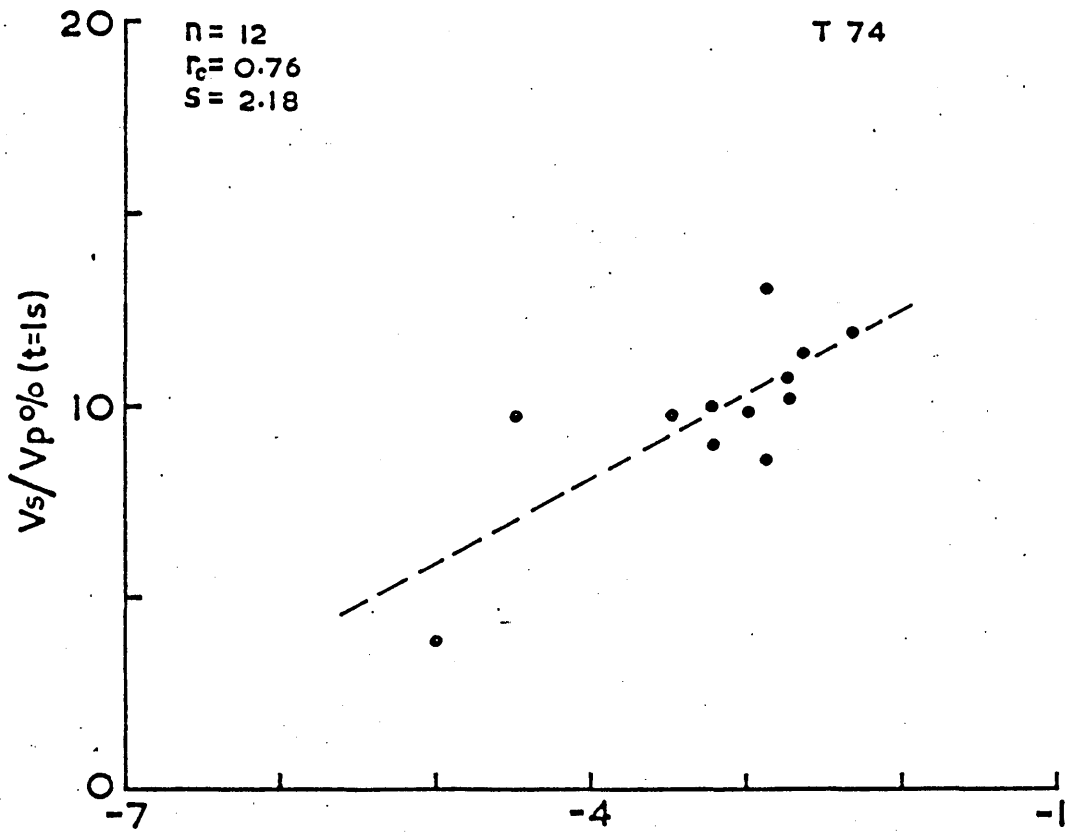
Fig 22h : IP at σ_w = 0.025 mhos m^{-1} plotted against Log K for samples from boreholes T74 (Fylde) and 14A – 17A (Cumberland).
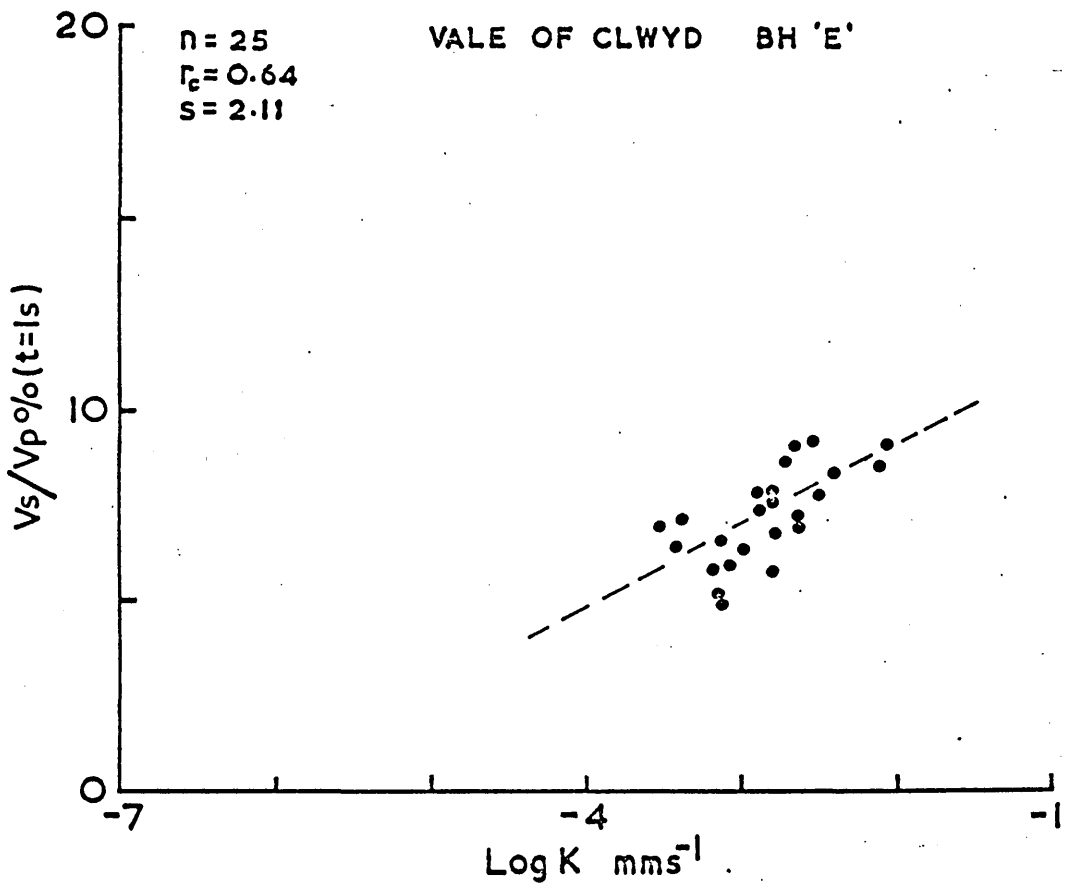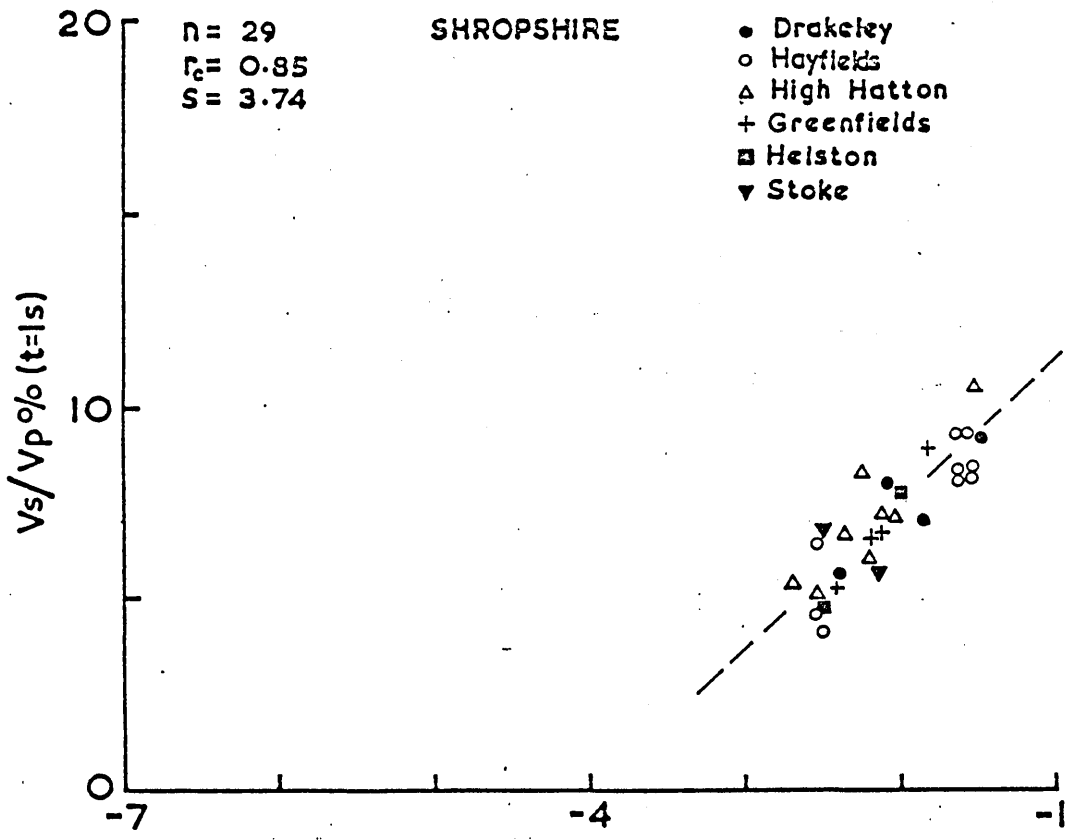
Fig 22i : IP at σ_w = 0.025 mhos m^{-1} plotted against Log K for samples from Shropshire boreholes and Vale of Clwyd borehole E.
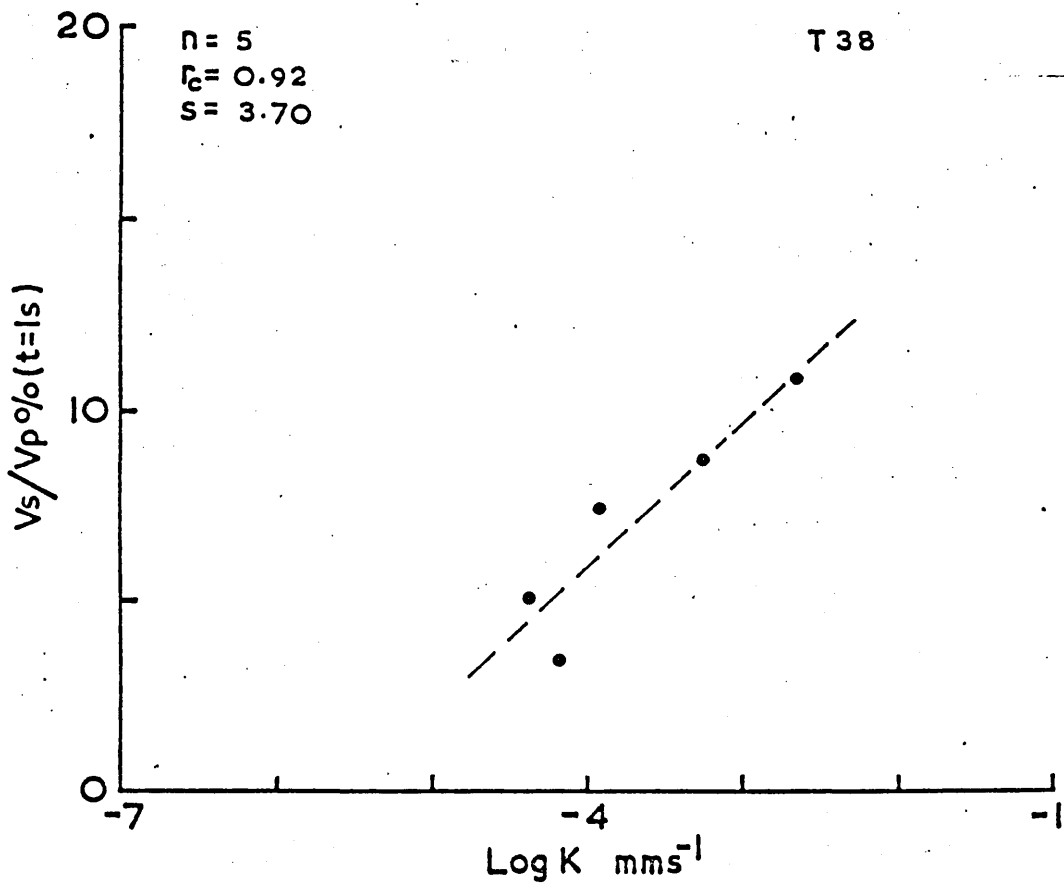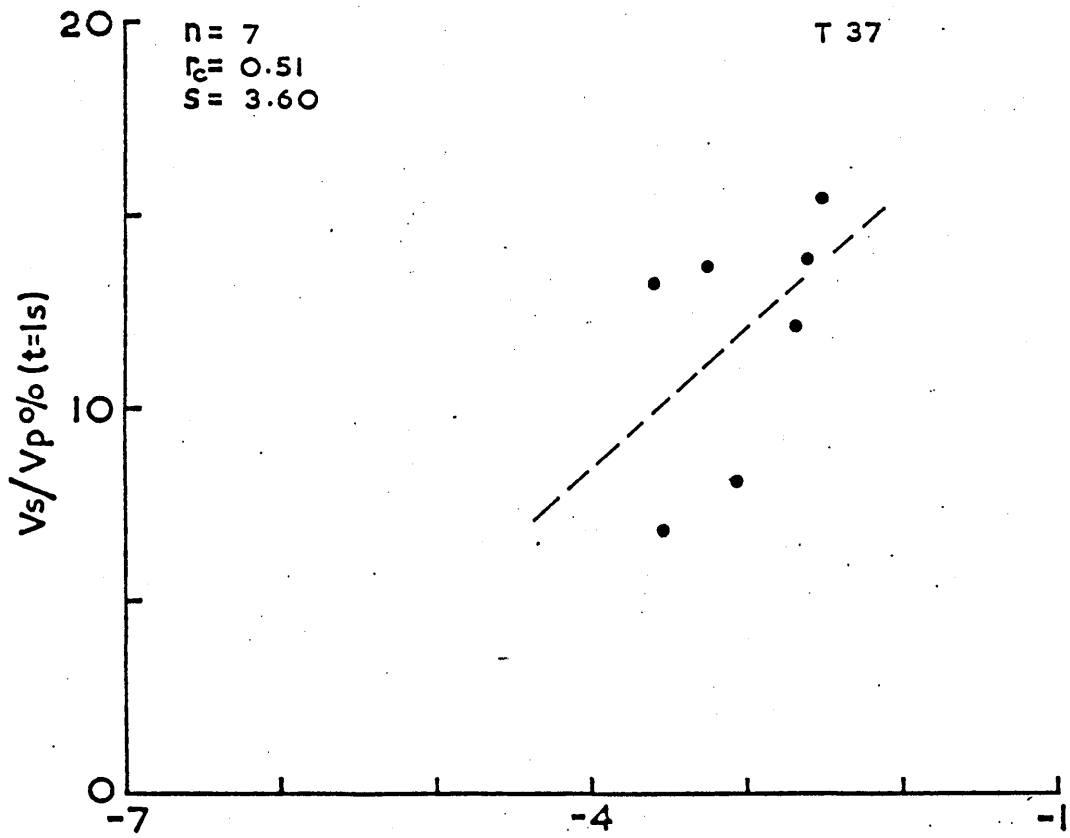
Fig 23a : IP at σ_w = 0.05 mhos m^{-1} plotted against Log K for samples from boreholes T37 and T38 (Fylde)

n = number of samples r_c = correlation coefficient

s = slope of linear regression.
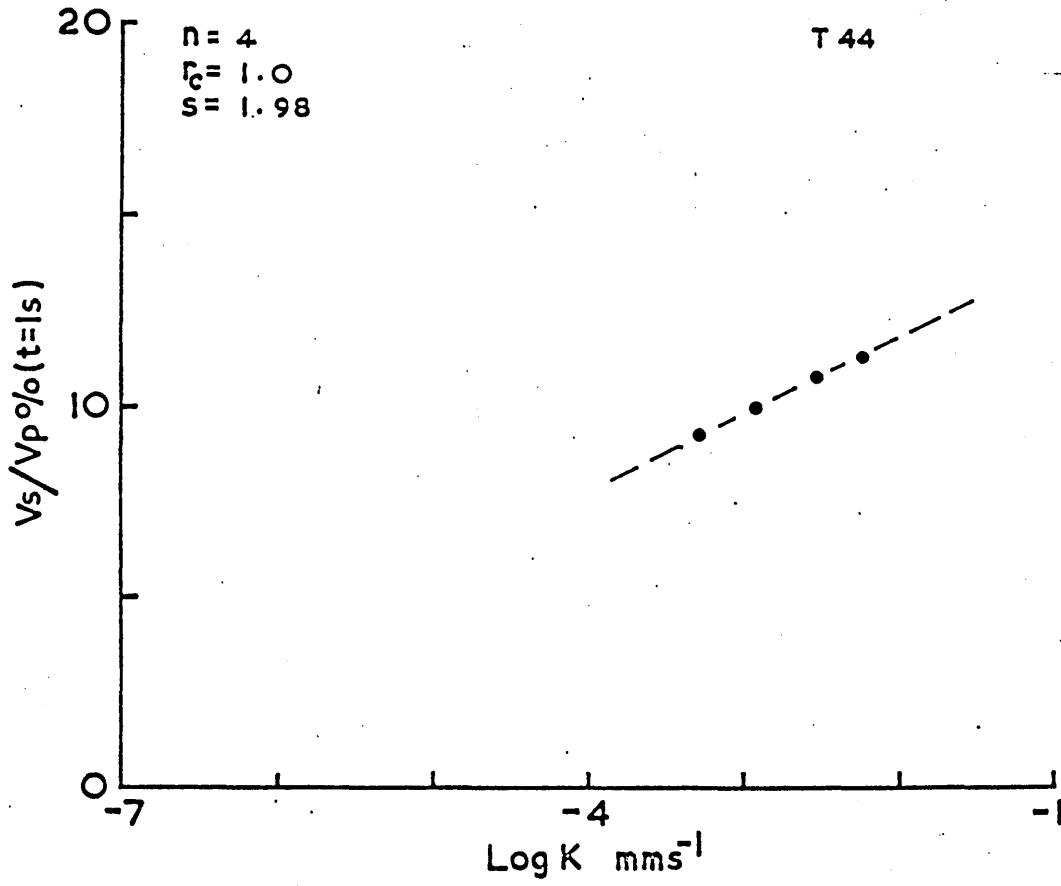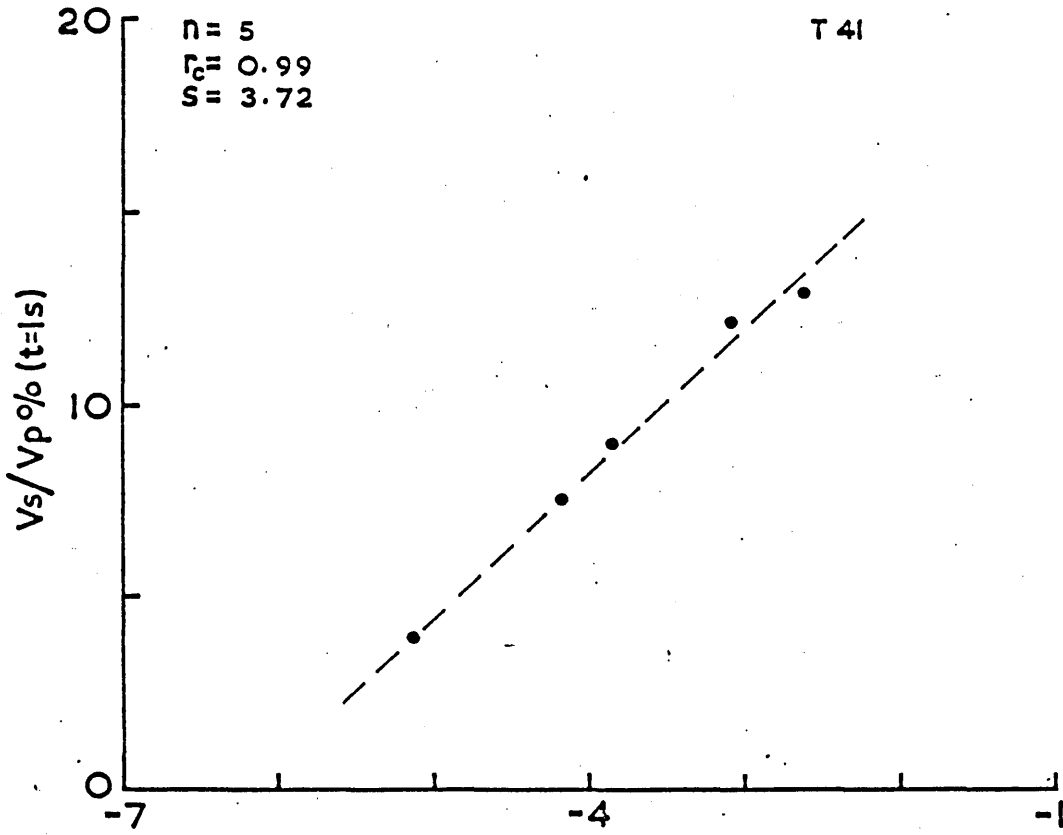
FIG,23a

Fig 23b : IP at σ_w = 0.05 mhos m^{-1} plotted against Log K for samples from boreholes T41 and T44 (Fylde)
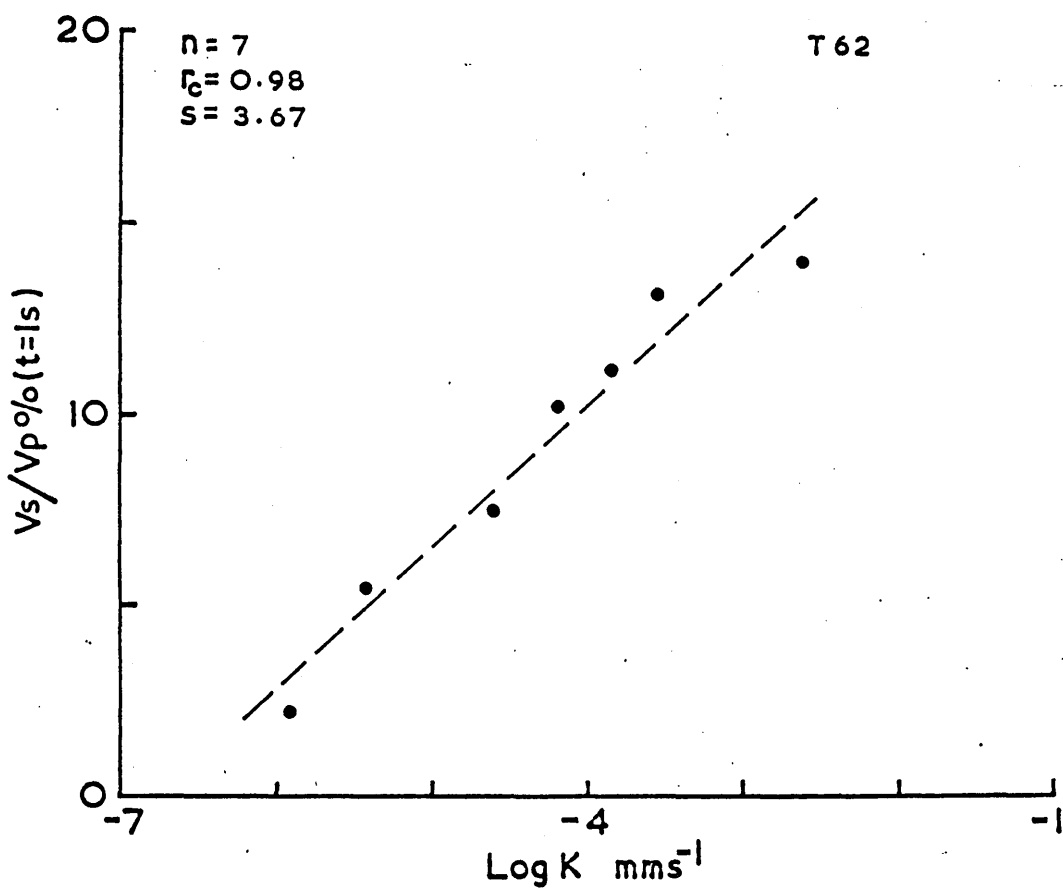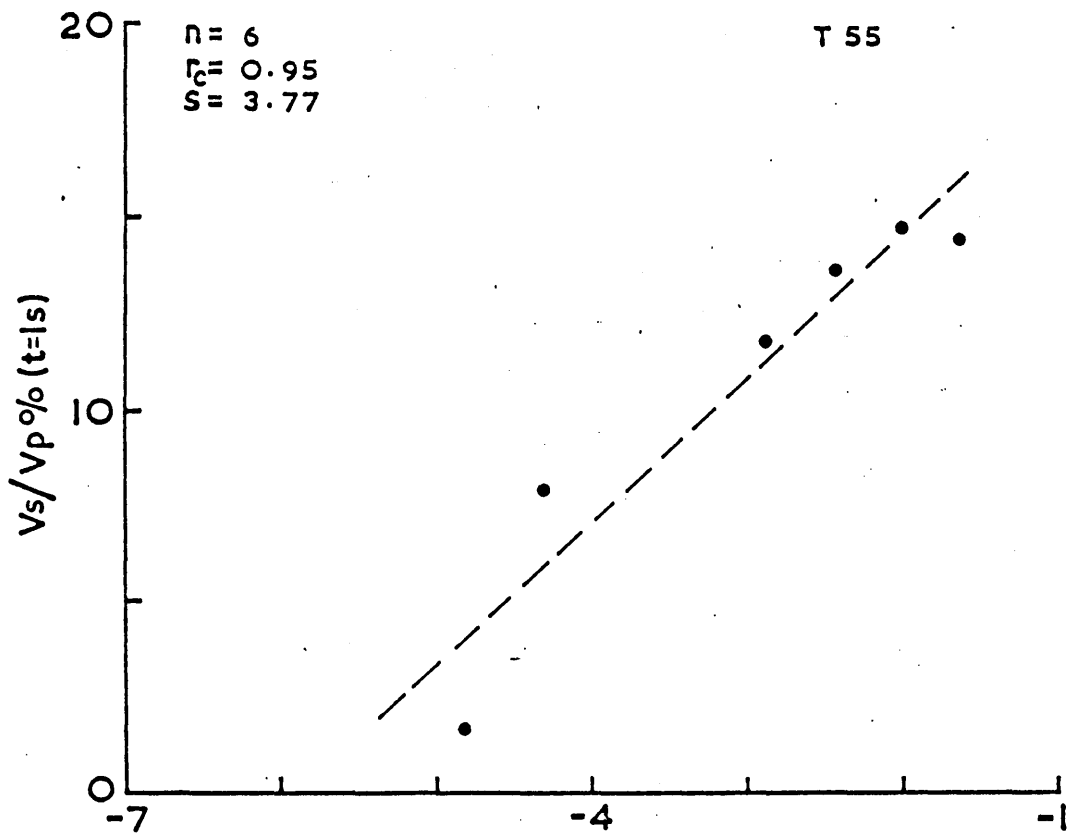
Fig 23c : IP at σ_w = 0.05 mhos m^{-1} plotted against Log K for samples from boreholes T55 and T62 (Fylde).
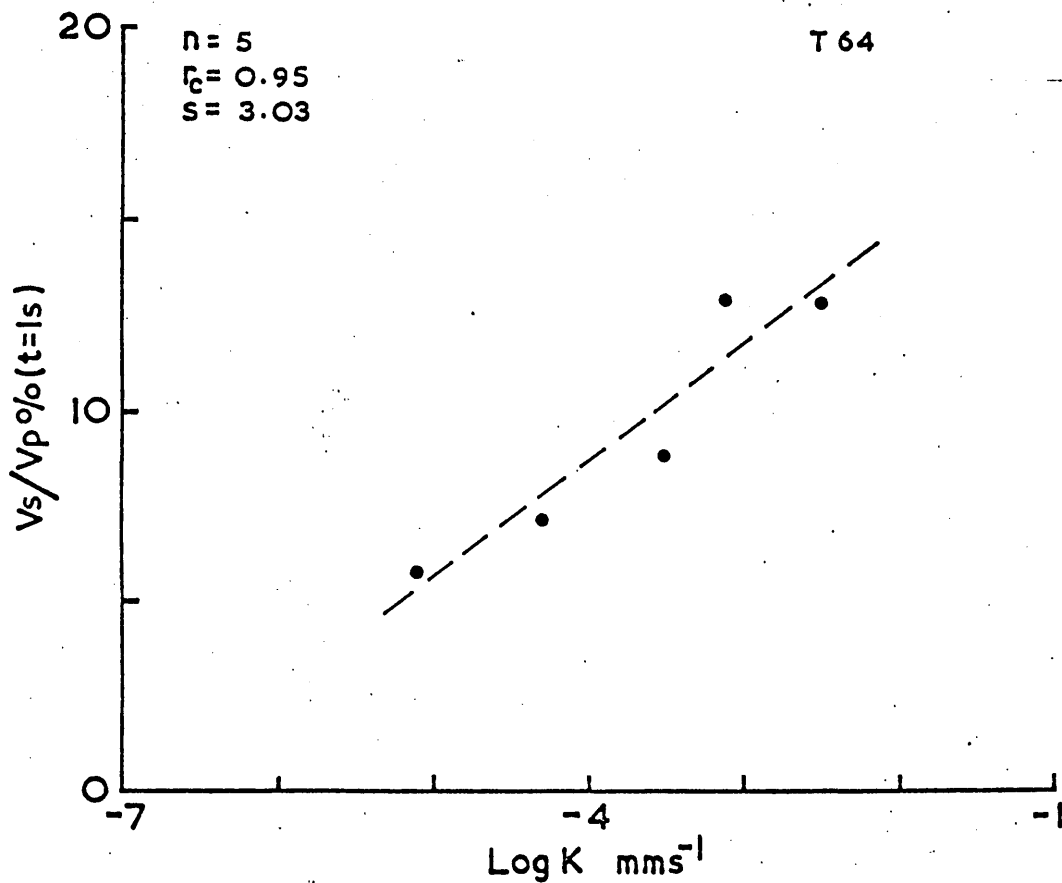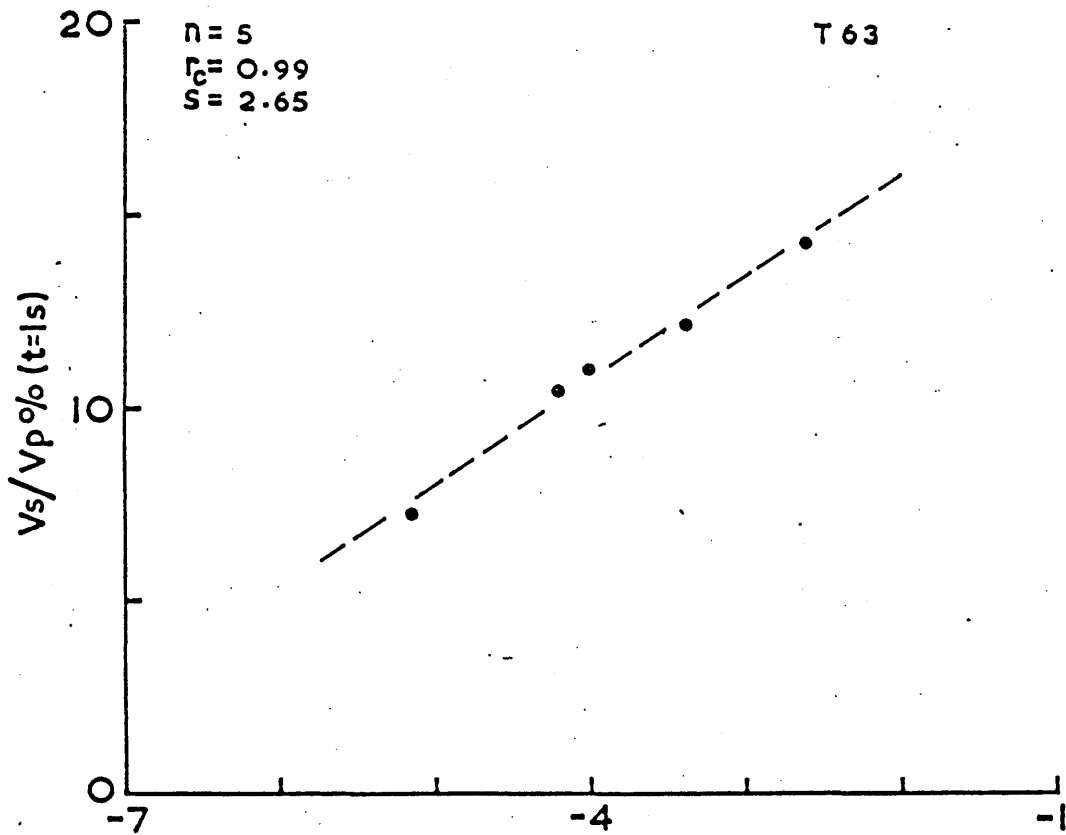
FIG.23c

Fig 23d : IP at σ_w = 0.05 mhos m^{-1} plotted against Log K for samples from boreholes T63 and T64 (Fylde).
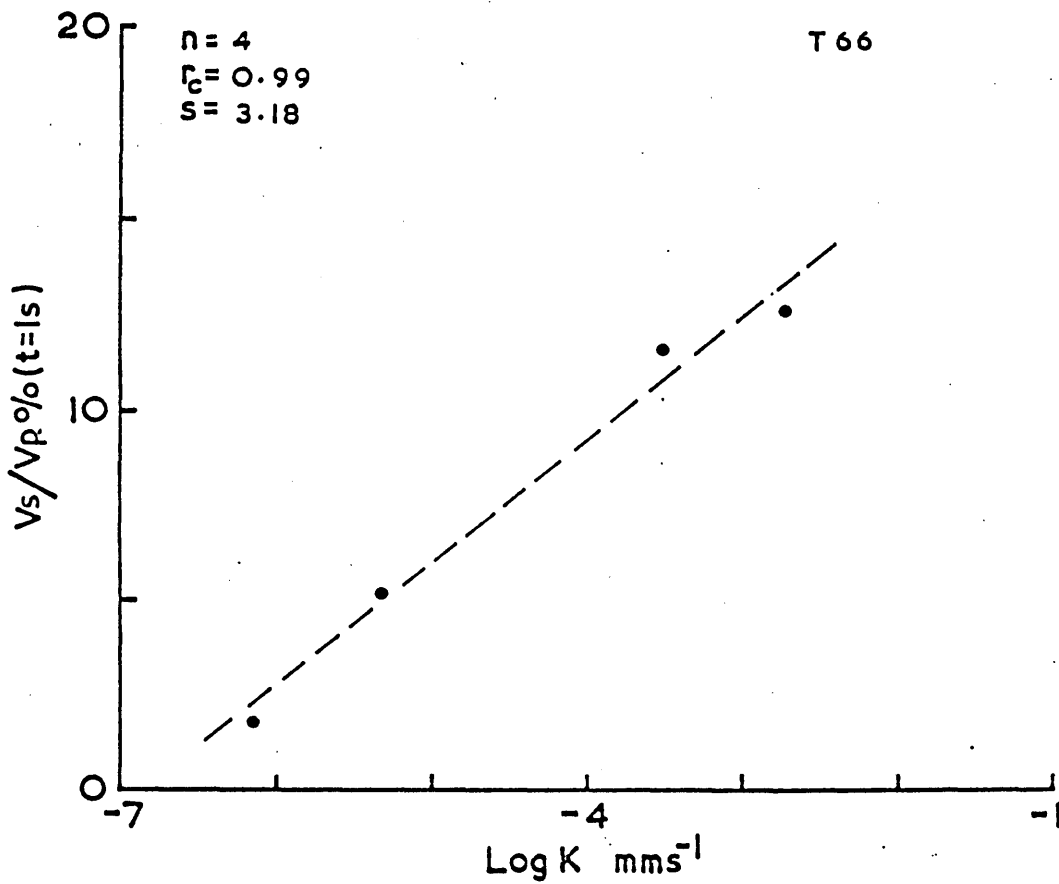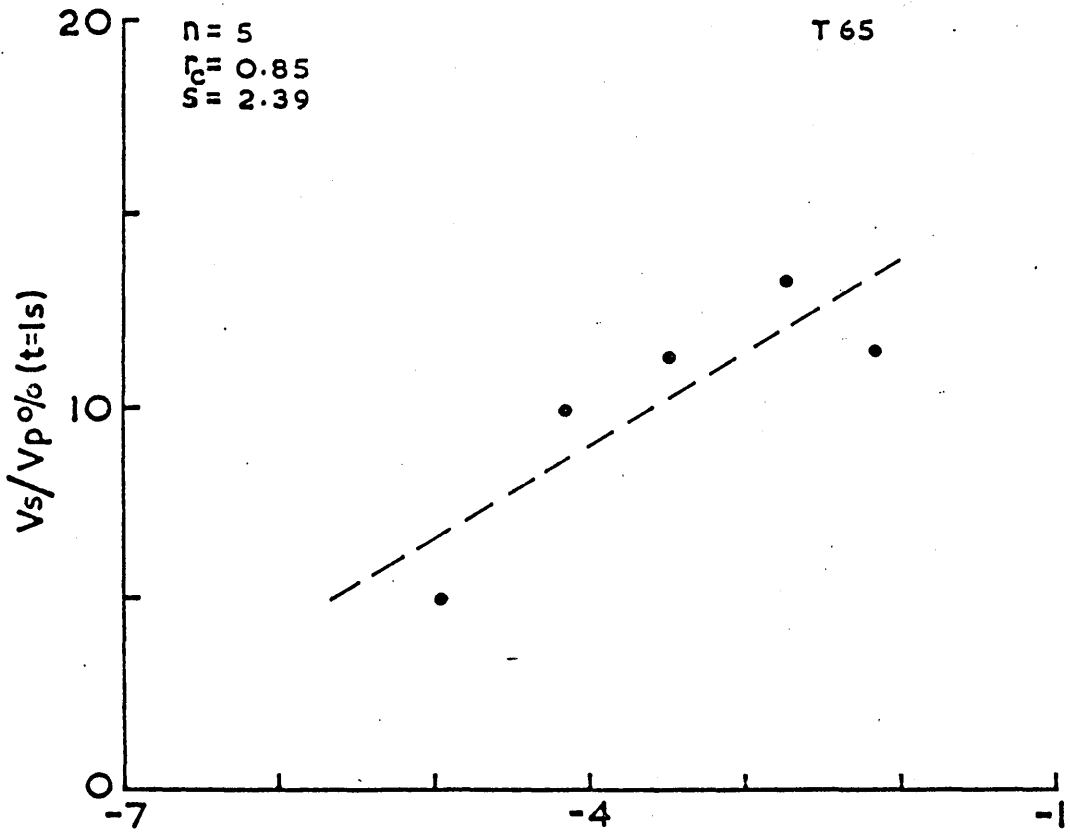
Fig 23e : IP at σ_w = 0.05 mhos m^{-1} plotted against Log K for samples from boreholes T65^w and T66 (Fylde).
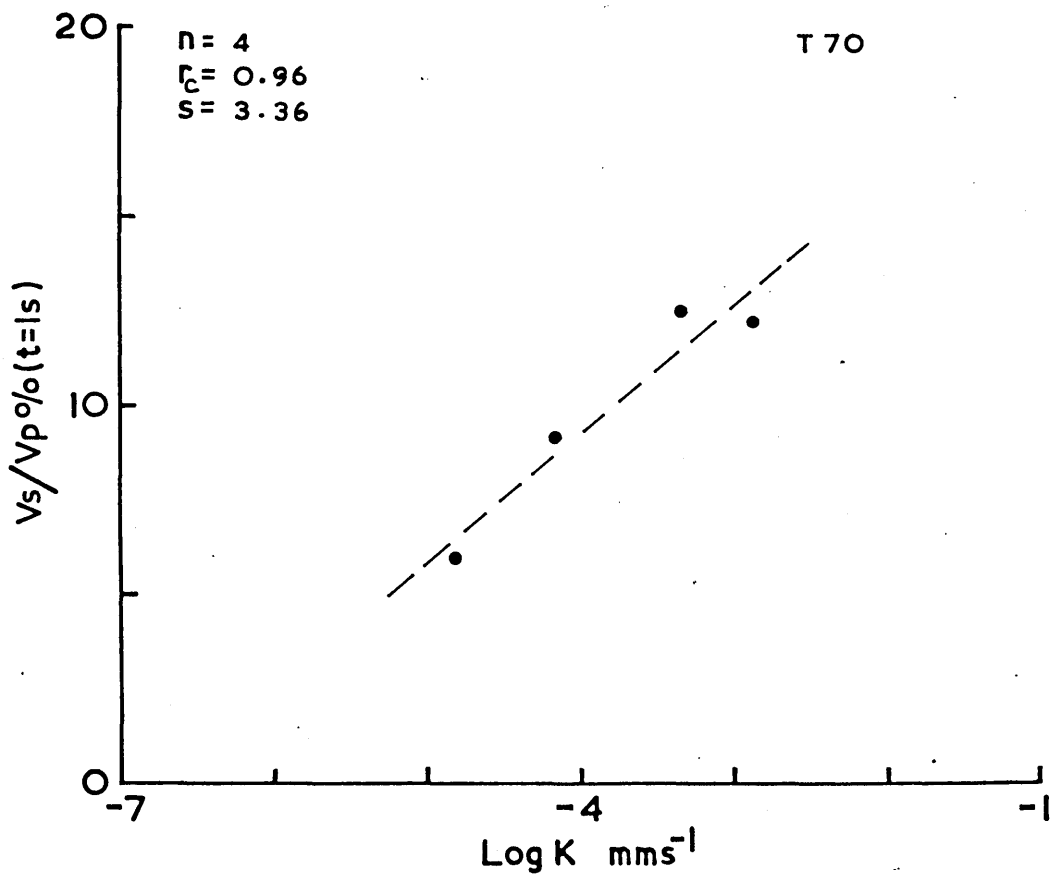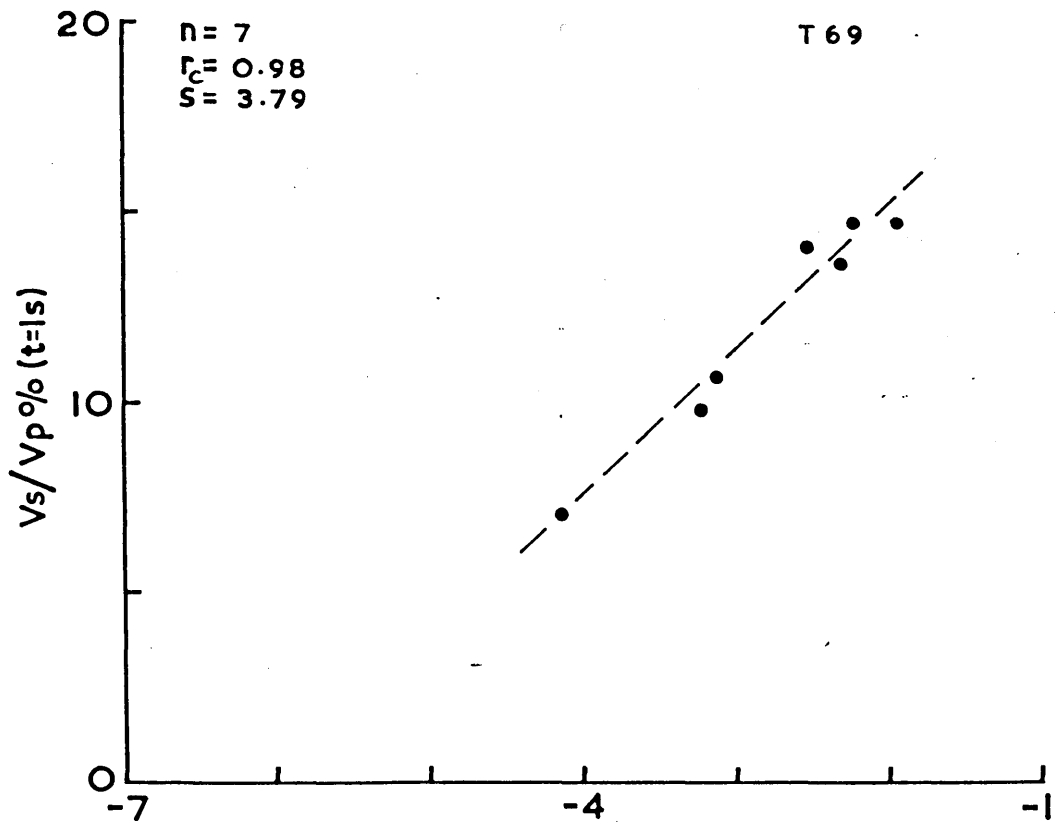
Fig 23f : IP at σ_w = 0.05 mhos m^{-1} plotted against Log K for samples from boreholes T69 and T70 (Fylde).
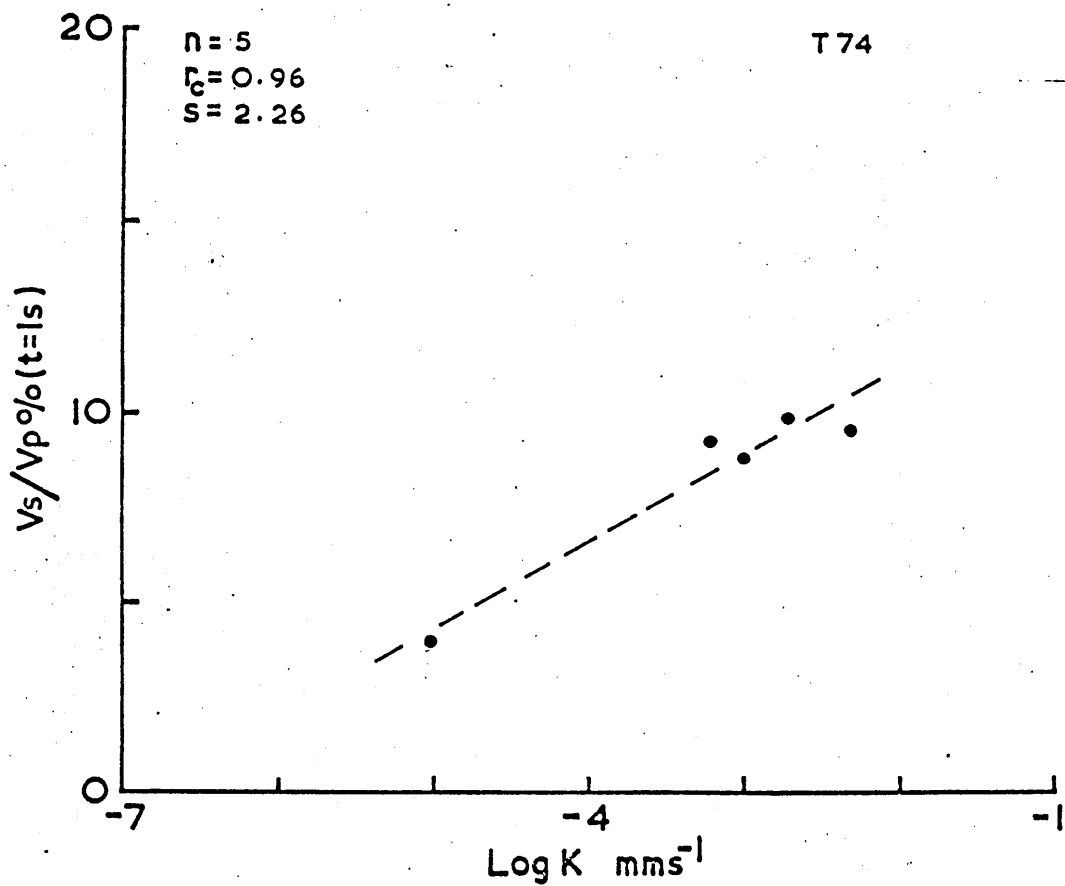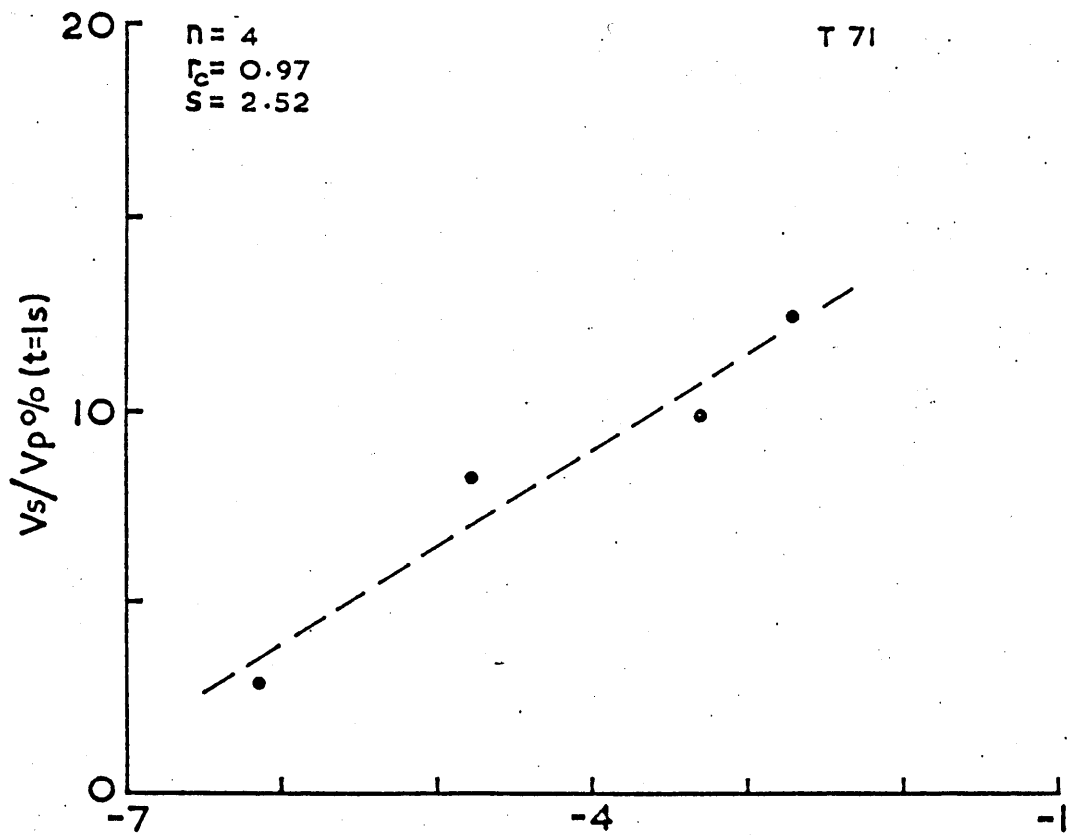
FIG.23f

Fig 23g : IP at σ_w = 0.05 mhos m^{-1} plotted against Log K for samples from boreholes T71 and T74 (Fylde).

FIG.23g

figs. 22h and i, where those from individual boreholes may be distinguished by the appropriate symbol. Grouped in this way the data describe relationships between IP and log K which in many cases are well defined, although some scatter is still evident and this may be partly attributed to textural inhomogeneities in the sandstone samples. In each group the data have been simply described by linear regressions of IP dependent upon log K and the results are included in the diagrams where n is the number of data, r_c is the coefficient of correlation and s the slope. All of the slopes are positive and in the case of the Fylde data occur in the range 1.9 to 5.4 although most are within 3.0 to 4.0. The correlation coefficients vary but a large proportion are significant, exceeding 0.9. Data from the Shropshire boreholes (fig. 22i) are closely grouped with a correlation coefficient of 0.85 which, considering the limited range of log K, is high. Those from the Vale of Clwyd (b/h E) are also grouped although the coefficient is lower at 0.64. These two groups of data differ from most of those of the Fylde by their low range of IP for high permeability K. The data from four Cumberland boreholes are scattered, $r_c = 0.47$, although it appears that the group of data at log K less than -4.0 is coincident with those from Shropshire (fig. 22i).

6.c <u>Further measurements of IP for $\sigma_w = 0.05$ mhos m^{-1}</u>

The groundwater in the Bunter sandstone of the Fylde has a conductivity typically about 0.05 mhos m^{-1}. According to fig. 12 this conductivity is marginally outside the range in which the maximum correlation between IP and log K may be expected. Therefore further IP measurements were made corresponding to a water conductivity of $\sigma_w = 0.052$ mhos m^{-1} to investigate the new levels of correlation. The measurements were made on Fylde samples, selected through figs. 22a to h, to represent the range of the IP - log K distribution along each regression line. The obtained data, grouped in figs. 23a to g, show that the correlations 'r_c' are with one exception still within the range 0.85 - 1.0 at this higher conductivity level.

6.d **A systematic experimental error of permeability data**

Although permeabilities had been measured with water which nominally was de-aerated, later tests indicated that water which had been subjected to high vacuum for many hours gave consistently shorter permeation times. The resulting increases in calculated permeability were found to be small or negligible for samples with higher orders of permeability and greater for those of low permeability. This is shown in fig. 24 where the different permeabilities are compared. By the time this error had been found many of the sandstone samples had been subjected to other experiments outside this work in which they were rendered unsuitable for further permeability measurements. Therefore for purposes of comparison amongst figs. 22a - i, all these data include the initial permeability values. However corrected permeabilities for samples from boreholes T38, T41, T62 and T69 are used in fig. 23, some of these data being used in later analyses.

6.e <u>Further measurements of IP for variable water conductivity</u>

The results in figs. 22 and 23 indicate that the sandstones may be classified into a wide range of types, each of which is distinguished by its characteristic IP - log K properties. The seven sandstone samples used for the preliminary measurements of IP with variable σ_w (fig.12) represented a limited part of this range and therefore further IP data covering a range of σ_w were required on the other sandstone types. 24 of the samples were chosen for this purpose, representing boreholes in the Fylde (T38, T41, T62 and T69), Shropshire (Mayfields) and Vale of Clwyd (B/h E). They were selected through figs. 22 and 23 to include most of the permeability ranges whilst appearing to conform reasonably to the respective IP - K relationship. IP was measured for seven salinities at approximately logarithmic intervals over the range $\sigma_w = 0.0043$ to 0.256 mhos m^{-1}. The experimental details are otherwise similar to those in section 4.a.

6.f Discussion of results

The data, plotted in figs. 25 to 29 as IP against log σ_w, are characteristically similar to those of fig. 12 described in section 4.c. Although for the whole data, the magnitudes of IP differ considerably amongst samples of similar permeability (i.e. the original basis for selection), the amplitudes of the corresponding IP maxima also vary proportionately because these occur about similar values of σ_w.

Some of the IP - log σ_w data for individual samples depart from a smooth curve but generally for a set of samples there is an overall systematic variation. This is best illustrated by the example of T62 (fig. 27) in which for log σ_w increasing, the rates of increase of IP vary with the permeabilities of the samples. Beyond the individual IP maxima, the rates of decrease are similar, the data are closely spaced and, particularly noticeable in this example, the order of sequence at higher σ_w is progressively inverted. In chapter 7 an empirical equation (7.3) has been obtained to describe these data. In figs. 25 to 29 the dashed line represents this equation fitted to the data through least squared errors analyses.

6.g An experimental error of IP data

The IP data corresponding to σ_w = 0.025 and σ_w = 0.05 mhos m^{-1} were abstracted from the previous measurements (6.b, 6.c) and in figs. 25 to 29 those corresponding to σ_w = 0.025 mhos m^{-1} are consistently high. This implies a change in the properties of the sandstones had occurred in the interval prior to the measurements at σ_w = 0.05 mhos m^{-1}, causing a reduction of IP. During that period, up to five weeks, the samples were kept saturated in tap water. In the absence of an alternative explanation for this anomalous behaviour, ionic substitutions within the clay lattices is suggested and whilst this should be borne in mind

throughout the following analyses, it is regarded as an 'error' of

magnitude rather than of form.   Comparative analyses of the data of

6.b and 6.c have not been attempted for this reason.

n = 122
r_c = 0.95
s = 1.11

Log K mm s^{-1} (De-aerated water)

Log K mm s^{-1} (High vacuum water)
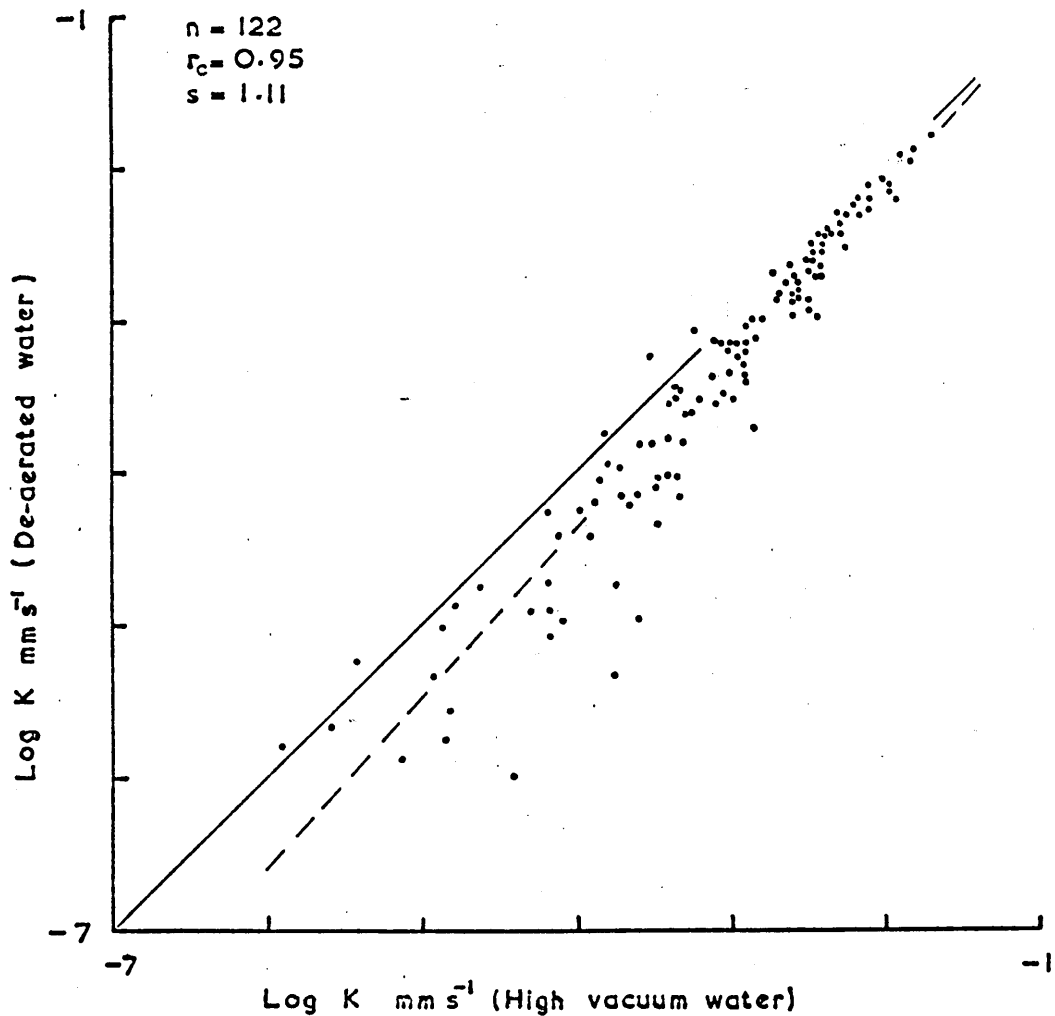
n = number of samples
r_c = correlation coefficient
s^c = Slope of linear regression

Comparison of permeability measured with nominally
de-aerated water and water subjected to high vacuum.

FIG.24
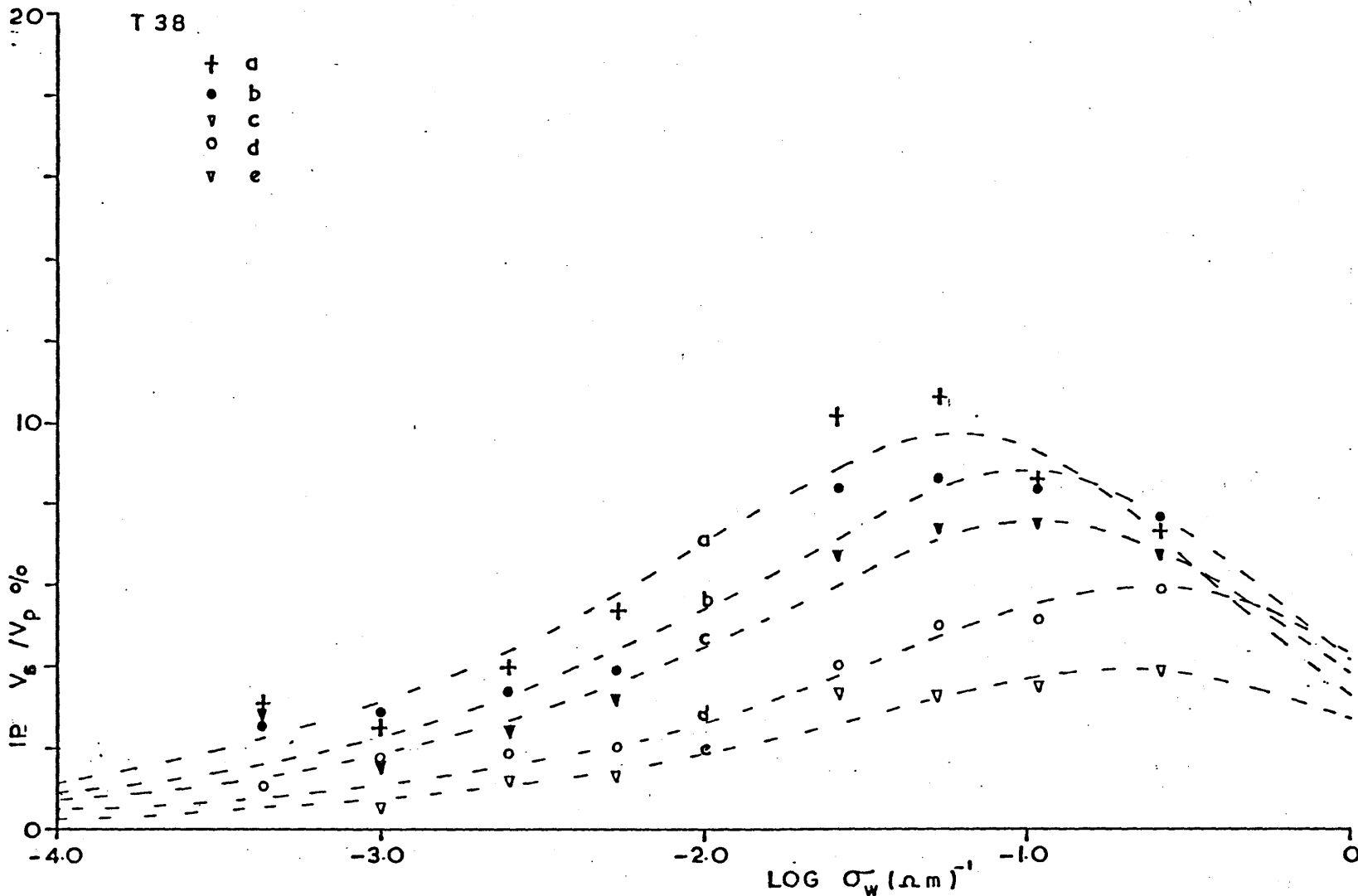
IP plotted against Log σ_w for 5 samples from T38 (Fylde). Dashed lines are least squared errors analyses of the data through equation 7.3 . Values of k and k' obtained for z = 0.445. Letters a - e identify these lines with the samples.

FIG. 25
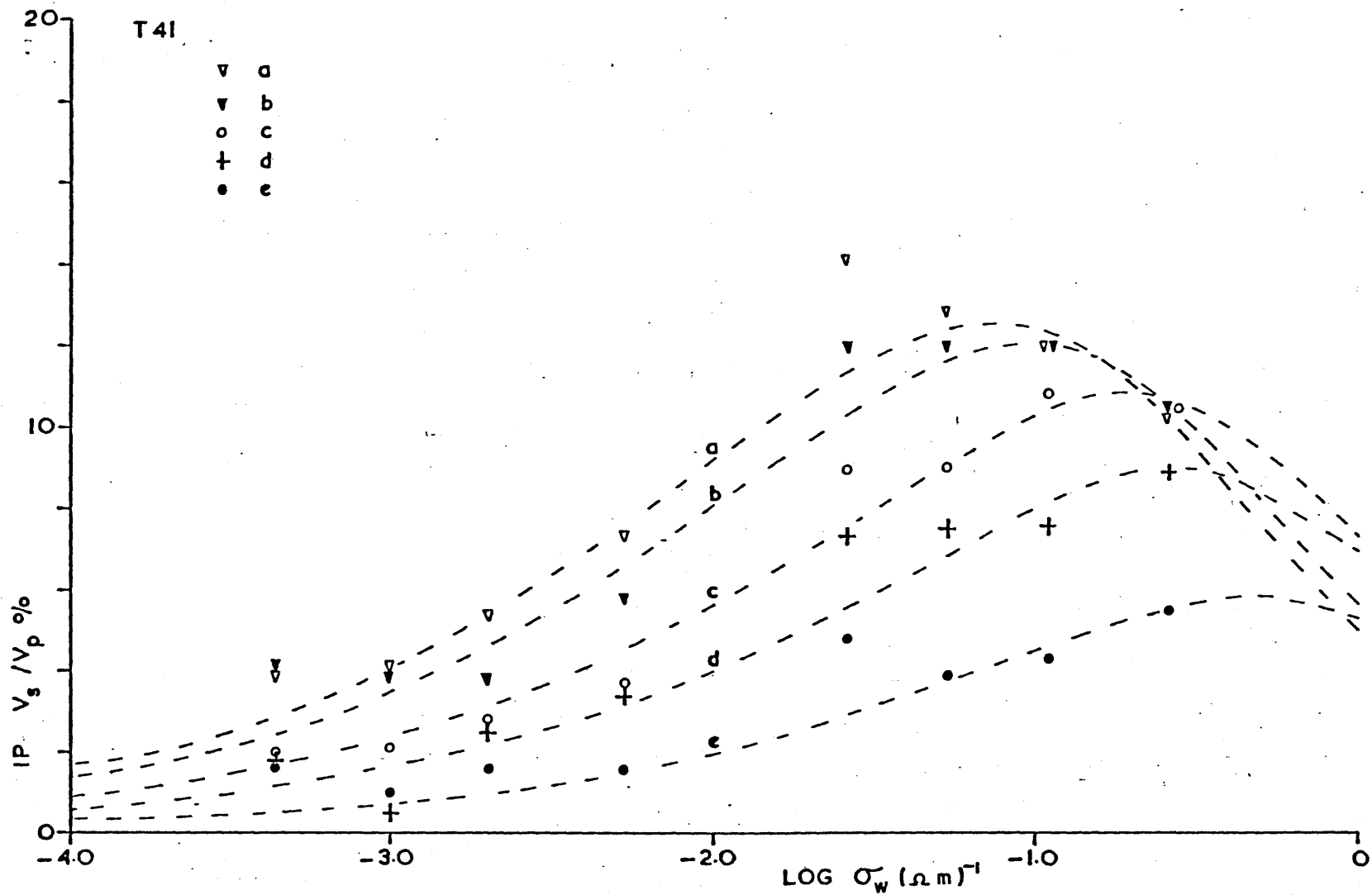
IP plotted against log σ_w for 5 samples from T41 (Fylde). Dashed lines are least squared errors analyses of the data through equation 7.3 . Values of k and k' obtained for z = 0.445. Letters a - e identify these lines with the samples.

FIG. 26

FIG.27
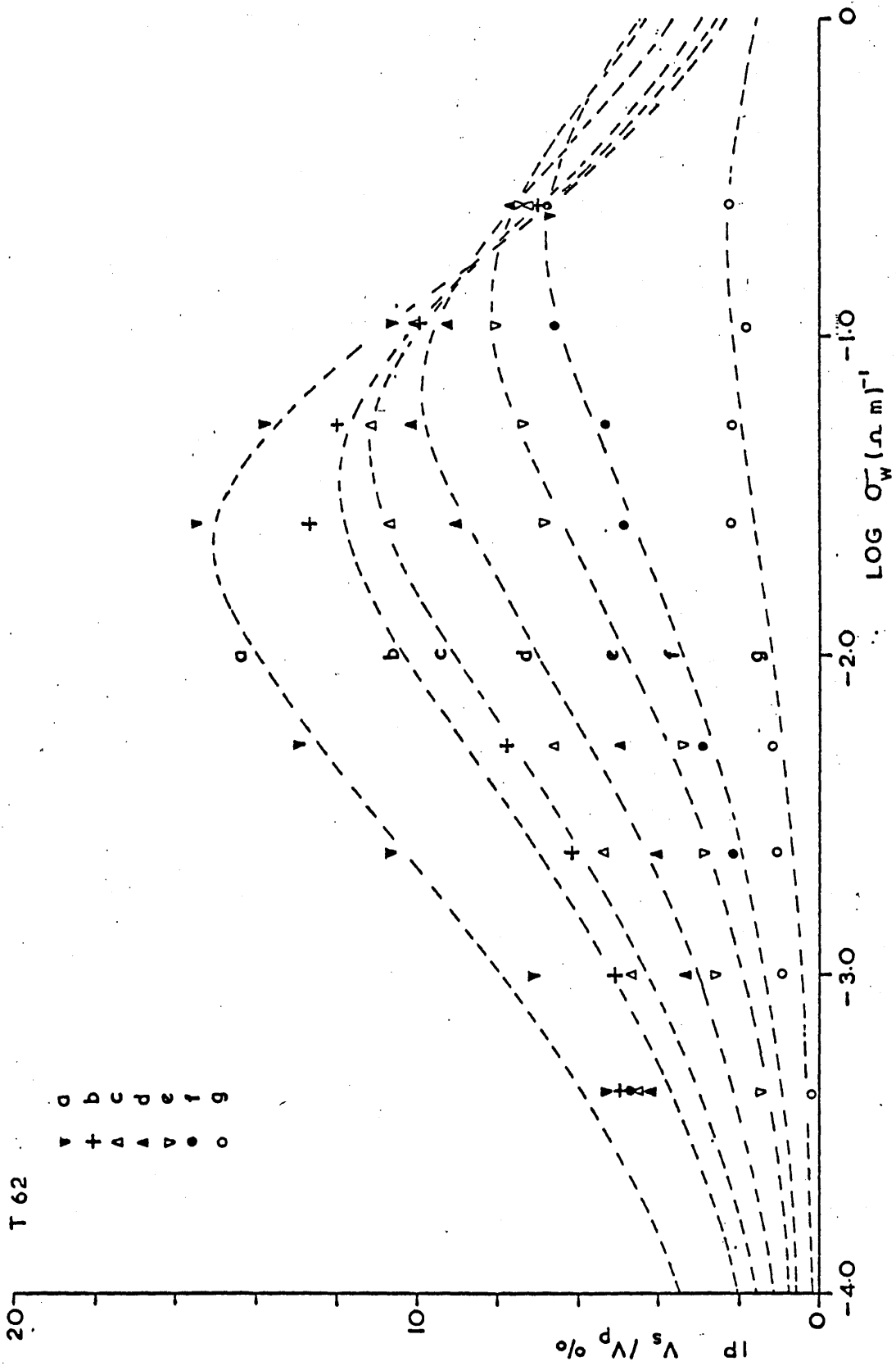
IP plotted against log σ_w for 7 samples from T62 (Fylde). Dashed lines are least squared errors analyses of the data through equation 7.3 . Values of k and k' obtained for z = 0.445. Letters a – g identify these lines with the samples.
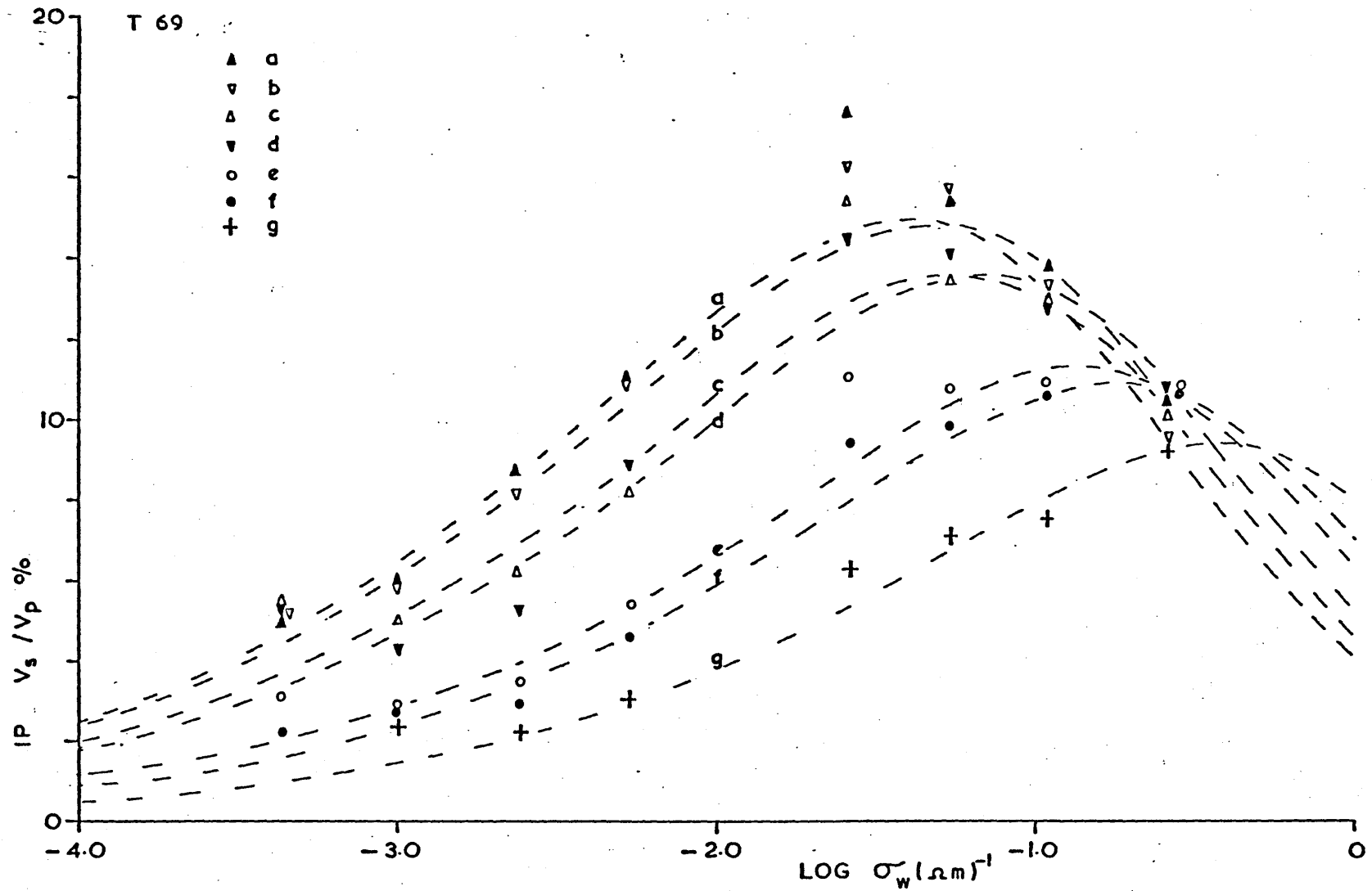
IP plotted against log σ_w for seven samples from T69 (Fylde). Dashed lines are
least squared errors analyses of the data through equation 7.3. Values of k and k'
obtained for z = 0.445. Letters a - g identify these lines with the samples.

FIG. 28
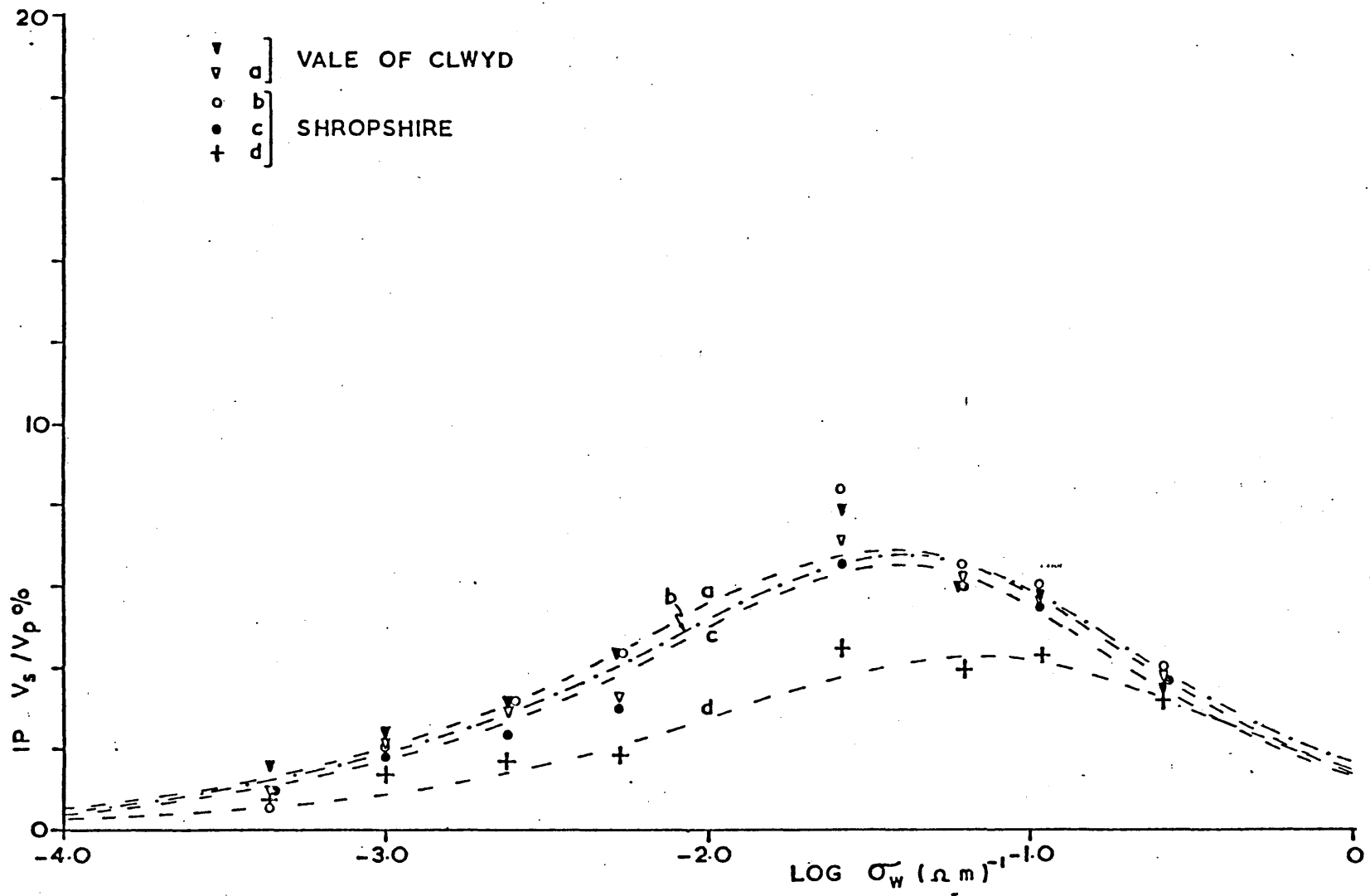
IP plotted against log σ_w for 2 samples from the Vale of Clwyd and 3 from Shropshire. Dashed lines are least squared errors analyses of the data through equation 7.3. Values of k and k' obtained for z = 0.58. Letters a (2 samples) to d identify these lines with the samples.

FIG.29

CHAPTER 7

AN EMPIRICAL RELATIONSHIP BETWEEN IP AND PERMEABILITY

7.a Application of the theoretical model (5.b) to the IP data

A systematic variation between IP and σ_w may be observed within each

group of data in figs. 25 to 29, and the sandstone model (5.b) has been

considered further to account for this.   The potential difference V_M

across the clay membranes of column (c)(fig. 14) expressed as a fraction

of a total applied potential difference V_T across the model is:

$$\frac{V_M}{V_T} = \frac{S_W}{S_W + S_M}$$

where S_W is the total conductance for the water in column (c) and S_M the

total conductance of the membranes.   Similarly

$$\frac{V_W}{V_T} = \frac{S_M}{S_W + S_M}$$

where V_W/V_T is the fractional potential difference across the water

in column (c) and by definition

$$\frac{V_W}{V_T} + \frac{V_M}{V_T} = 1$$

Expressed in terms of conductivities σ_w, σ_M ($\equiv \sigma_d, \sigma_b$ p.29)

$$\frac{V_M}{V_T} = \frac{\sigma_w}{\sigma_w + \sigma_M\left(\frac{f}{e}\right)}$$

and

$$\frac{V_W}{V_T} = \frac{\sigma_M}{\sigma_w\left(\frac{e}{f}\right) + \sigma_M}$$

Assuming the conductivity of the clay σ_M to be constant for all values

of water conductivity σ_w, then:

$$\frac{V_M}{V_T} = \frac{\sigma_w}{\sigma_w + k_1} \qquad \ldots 7.1$$

and

$$\frac{V_W}{V_T} = \frac{1}{k_2\,\sigma_w + 1} \qquad \dots \; 7.2$$

where k_1 and k_2 are constants for a given sandstone. If IP is directly proportional to the potential difference across the clay membranes then equation 7.1 would be expected to fit the data in figs. 25 to 29, assigning appropriate values of k_1. However this is not the case because, although for all positive values of k_1 and over a limited range of σ_w, V_M/V_T increases with σ_w in the same way as the IP data, the maximum value of V_M/V_T is reached asymptotically when σ_w approaches infinity. Furthermore in all cases the maximum slope of this theoretical curve is much greater than that of the data.

On the other hand, the curve of V_W/V_T from equation 7.2 is a mirror reversal of that obtained through 7.1 but the maximum negative slope is similar to that shown by the data. Therefore by selecting appropriate values of k_2, equation 7.2 can be fitted to the data reasonably well over a limited upper range of σ_w. But over the whole range of σ_w, neither of these equations can describe the data adequately.

Henkel and Collins (1961) measured IP on 'earth plugs' saturated with NaCl solutions over the range $\sigma_w = 0.04$ to 2.5 mhos m^{-1} and they found that IP decreased against increasing σ_w, similar to many of the corresponding data in section 6.e. To describe this variation of IP with σ_w they derived an equation from a model which, in effect similar to the columns (d) and (c) of fig. 14, represented conduction paths through water and water plus clay. From Henkel and Van Nostrand (1957) they assumed that polarisation induced at the water - clay conduction boundary was inversely proportional to the effective electrolyte concentration and proportional to the current density, and obtained the equation:

$$\frac{V_{Op}}{V_{1p}} = \frac{H \rho_s}{\rho_s + B}$$

where V_{Op} and V_{1p} are the secondary and primary voltages respectively, H is a constant, B is a factor which depends upon the dimensions of the model and the clay conductivity, and ρ_s is the resistivity of the water. This equation, which is essentially identical to equation 7.2 (a result which stems from the two initial assumptions these authors adopted), described the decrease of IP against increasing pore water conductivity that they had observed experimentally. Previously Collett (1959) and Hunter (1959) independently had noted that, for σ_w increasing, the IP of some rock samples increased at low values of σ_w but reached a maximum and thereafter decreased. Henkel and Collins considered this point against their own results but, claiming that at low values of σ_w their own experimental IP data were unreliable, dismissed the phenomena in their analyses.

Neither equation 7.2 nor the Henkel and Collins equation can account for the whole variation of IP against σ_w observed here and therefore resort has been made to an empirical equation developed from a combination of equations 7.1 and 7.2.

7.b <u>An empirical equation to fit the IP data</u>

The equation comprises two functions:

(a) $$\frac{\sigma_w^z}{\sigma_w^z + k}$$

(b) $$\frac{1}{1 + \sigma_w k'}$$

Fig. 30 a shows the variation of these functions against log σ_w together with the product (c).

It is shown that:

when $\sigma_w \longrightarrow 0$: (a) $\longrightarrow 0$, (b) $\longrightarrow 1$, (c) $\longrightarrow 0$

and when $\sigma_w \longrightarrow \infty$: (a) $\longrightarrow 1$, (b) $\longrightarrow 0$, (c) $\longrightarrow 0$

By changing the values of k and k' , the functions (a) and (b) respectively are displaced along the log σ_w axis but retain their shapes and therefore both amplitude and position of (c) can be modified through these constants.

Initially IP has been empirically related to σ_w using (c) as:

$$IP = \frac{c^z}{c^z + k} \cdot \frac{N}{1 + k'C} \quad \dots \ 7.3$$

where N is a scaling factor (< 1) and C has been arbitrarily assigned the value $100 \times \sigma_w$.

After many attempts to match this equation to the IP - σ_w data (figs. 25 to 29) by trial and error, it was found that, assigning constant values to z and N, all of the data could be described by varying only the parameters k and k'. (In the following section it is shown that the factor N can be eliminated.) The constants adopted were:

$$z = 0.5 \quad : \quad N = 0.33$$

Inserting these in equation 7.3

$$IP = \frac{c^{0.5}}{(c^{0.5} + k)} \cdot \frac{0.33}{(1 + k'C)}$$

k and k' have been evaluated for the data by visual trial and error fitting of this expression and their mutual variation amongst the sandstone samples from each borehole is shown in fig. 30 b. These two parameters k and k' appear to have a reciprocal type of relationship. In those cases where the maximum IP occurs at large values of σ_w , the incomplete variation of IP shown by the data within the limited range of σ_w prevents accurate determination of k and k'. Consequently for large values of k in fig. 30 b, the errors in k and k' may be large. Further errors in these values of k

and k' may be expected from the large percentage experimental errors incurred by the lower values of IP data.

This trial and error method formed the basis of the analyses described by Collar and Griffiths (1976). Subsequently, equation 7.3 has been solved for these data by least squared errors analyses.

7.c Least squared errors analyses of equation 7.3

Although a direct determination of the most probable value of z for the whole data (figs. 25 to 29) would be preferable, for mathematical simplicity individual solutions for the sets of data have been found, from which an average value of z has been calculated.

Because the values of water conductivity σ_w are common to each group of data, errors have been considered in IP only. In this case, writing equation 7.3 as

$$P = \frac{c^z N}{(c^z + k)(1 + k'c)}$$

where P is the induced polarisation, the total squared error E in P is given by:

$$E = \sum \left(P - \frac{c^z N}{(c^z + k)(1 + k'c)} \right)^2$$

from which

$$\frac{\partial E}{\partial z} = \sum \frac{2(c^z N - P(c^z + k)(1 + k'c))kc^z N \ln c}{(c^z + k)^3 (1 + k'c)^2}$$

$$\frac{\partial E}{\partial k} = \sum \frac{2(P(c^z + k)(1 + k'c) - c^z N)c^z N}{(c^z + k)^3 (1 + k'c)^2}$$

$$\frac{\partial E}{\partial k'} = \sum \frac{2(P(c^z + k)(1 + k'c) - c^z N)c^{z+1} N}{(c^z + k)^2 (1 + k'c)^3}$$

$$\frac{\partial E}{\partial N} = \sum \frac{2(c^z N - P(c^z + k)(1 + k'c))c^z}{(c^z + k)^2 (1 + k'c)^2}$$

Minimising E against z,k,k' and N

$$\frac{\partial E}{\partial z} = \frac{\partial E}{\partial k} = \frac{\partial E}{\partial k'} = \frac{\partial E}{\partial N} = 0$$

from which it is evident that the normal equations given by $\frac{\partial E}{\partial k}$ and $\frac{\partial E}{\partial N}$ are effectively identical and therefore either k or N is redundant and equal to 1.

Equation 7.3 could therefore conveniently be written:

$$IP = \frac{1}{(1 + kC^{-z})(1 + k'C)}$$

although in the following treatment the term N = 0.33 has been retained to enable comparisons to be made with Collar and Griffiths (1976) results. The three normal equations obtained are:

$$[PC^{2z} \ln C] + [PC^{2z + 1} \ln C] k' + [PC^z \ln C] k + [PC^{z + 1} \ln C] kk' - [C^{2z} \ln C] N = 0 \qquad \ldots 7.4$$

$$[PC^{2z}] + [PC^{2z + 1}] k' + [PC^z] k + [PC^{z + 1}] kk' - [C^{2z}] N = 0 \quad \ldots 7.5$$

$$[PC^{2z + 1}] + [PC^{2z + 2}] k' + [PC^{z + 1}] k + [PC^{z + 2}] kk' - [C^{2z + 1}] N = 0$$
$$\qquad \ldots 7.6$$

where $[\quad]$ indicates $\sum_1^n$, for n data points.

From equations 7.5 and 7.6:

$$k'^2 ([PC^{z + 1}][PC^{2z + 2}] - [PC^{z + 2}][PC^{2z + 1}]) + k' ([PC^z]$$
$$[PC^{2z + 2}] - [PC^{z + 2}][PC^{2z}] + N[PC^{z + 2}][C^{2z}] -$$
$$N[PC^{z + 1}][C^{2z + 1}]) - N ([PC^z][C^{2z + 1}] - [PC^{z + 1}]$$
$$[C^{2z}]) - [PC^{z + 1}][PC^{2z}] + [PC^{2z + 1}][PC^z] = 0 \quad \ldots 7.7$$

and

$$k = \frac{[C^{2z}] N - [PC^{2z}] - [PC^{2z + 1}] k'}{[PC^{z + 1}] k' + [PC^z]} \qquad \ldots 7.8$$

Solution for z, k and k' is achieved by assigning an arbitrary value to z, solving for k' then k through equations 7.7 and 7.8, and returning these values to 7.4 to determine the inequality. The value of z can be progressively adjusted and the process repeated until the equality of equation 7.4 is achieved. For data which include a limited range of pore

water conductivity σ_w (= C /100), such as those in 6.e, these computations can be accommodated in stages by a modern programmable calculator, e.g. 12 significant figures capability, but for a very wide range of σ_w, for example as in fig. 12, a precision of about 20 significant figures is essential (see footnote).

Some of the data (figs. 25 to 29) were selectively excluded from these analyses: all those for $\sigma_w = 0.00043$ mhos m^{-1} are considered atypical for the reasons outlined in 4.b, and those corresponding to $\sigma_w = 0.025$ mhos m^{-1} as discussed in 6.g. From the remainder, which includes six values of σ_w, the most probable values for z,k and k' have been evaluated for N = 0.33 and are given in table 3.

Expectedly, there is some fluctuation amongst these values of z, but in general those from the Fylde (i.e. T38, T41, T62 and T69) occur in the range 0.4 - 0.5, the exception being those where the data are inadequate to describe the IP - σ_w variation, whilst those from Shropshire and the Vale of Clwyd are marginally higher. It is reasonable therefore to assign a different but single value of z to each area, although the previous work (Collar and Griffiths 1976) suggested that one value may even be applied ubiquitously.

Footnote   A FORTRAN programme, written to give a double precision least squared errors solution to equation 7.3 by the method outlined above (adopting N = 1), is included in the appendix. This programme has been used to solve the equation for the data in fig. 12, between $\sigma_w = 0.00098$ to 2.68 mhos m^{-1} inclusive, on a machine capable of 16 significant figures in double precision. The results are also presented in the appendix.

Table 3   Most probable values of z k and k'

	z	k	k'	$K \, mm \, s^{-1}$
T38	0.455	3.457	0.061	0.00242
	0.427	4.776	0.036	0.00058
	0.502	6.306	0.046	0.000224
	0.362	10.416	0.013	0.0001
	0.446	16.591	0.030	0.000069
T41	0.468	2.507	0.043	0.0024
	0.517	3.130	0.039	0.00085
	0.550	5.329	0.025	0.00014
	0.445	7.169	0.015	0.000065
	0.334	13.970	0.002	0.0000076
T62	0.428	1.102	0.112	0.0024
	0.507	1.979	0.099	0.00029
	0.495	2.448	0.083	0.00015
	0.464	3.550	0.055	0.000067
	0.425	5.709	0.032	0.000025
	0.341	8.184	0.013	0.0000039
	0.211	23.962	0.0053	0.0000013
T69	0.425	1.552	0.049	0.0123
	0.480	1.484	0.062	0.00653
	0.486	2.066	0.0497	0.0051
	0.464	2.164	0.042	0.0031
	0.452	3.904	0.024	0.00076
	0.448	4.554	0.0199	0.00063
	0.351	6.964	0.0039	0.000076
Shrops.	0.572	4.311	0.157	0.029
	0.604	9.791	0.129	0.0029
Vale of Clwyd	0.583	4.012	0.177	0.0013

Appropriate values of z have been obtained by calculating a weighted mean $\bar{z}_s$ for each (borehole) set of samples, where

$$\bar{z}_s = \frac{\sum \omega z}{\sum \omega}$$

and taking the arithmetic mean

$$\bar{z} = \frac{\sum \bar{z}_s}{n}$$

A suitable weighting ω is obtained through

$$\omega = \frac{\partial}{\partial z}\left(\frac{\partial E}{\partial z}\right) \qquad \text{for} \qquad \frac{\partial E}{\partial z} = 0$$

which is the rate of change of error E against z, as z departs from its most probable value. This weighting therefore takes some account of the quality and comprehensiveness of the data in each case. ω may be readily evaluated as:

$$\omega = \frac{\partial}{\partial z}\left(\frac{\partial E}{\partial z}\right) = \sum \frac{2kNC^z \ln^2 C \left((1 + k'C)(C^z + k)(C^z - k)P - NC^z(C^z - 2k)\right)}{(1 + k'C)^2 (C^z + k)^4}$$

for each sandstone sample. It is interesting to note that for perfect data the expression reduces to:

$$\sum 2 \left(\frac{P\, k \ln C}{C^z + k}\right)^2$$

which is always positive.

The values of $\bar{z}_s$ obtained for the Fylde boreholes:

    T38 0.434 ;   T41 0.474 ;   T62 0.430 ;   T69 0.439

are similar and give an arithmetic mean $\bar{z} = 0.445$. Returning this value $\bar{z}$ to equation 7.7 and 7.8 the values of k and k' have been recalculated for $\frac{\partial E}{\partial k} = \frac{\partial E}{\partial k'} = 0.$

Inserting these values of k and k' with z = 0.45 and N = 0.33 in equation 7.3, IP has been calculated over a range of σ_w for each sandstone sample and is compared with the corresponding original data in figs. 25 to 29. It is concluded that through the variation of the two parameters k and k' alone, equation 7.3 satisfactorily describes these data.

The reciprocal relationship shown between these two parameters (fig. 31) is almost identical to the earlier results (fig. 30 b) although two obvious departures from the general variation occur at large values of k , the reasons having been discussed previously (7.b). Consequently, these two data, which refer to samples from T62 and T38, have been included in subsequent diagrams (where they may be identified by an enclosing dashed circle) but have been excluded from further numerical analyses.

7.d Relationship between IP and permeability K

The variations between k and k' (fig. 31) is a significant result, indicative of a petrophysical property which is common to the broad range of Bunter sandstones. But although these empirical parameters relate to each sandstone specimen they cannot be determined directly by physical measurement. However, by considering the sandstone samples collectively, useful relationships can be shown between these parameters and at least two petrophysical properties, both of which can be measured in the laboratory. For example, in figs. 32, 33 and 34 where on logarithmic axes the values of k and k' are plotted against corresponding sample permeabilities K, the data from the Fylde may reasonably be described by the equations:

$$\log k = m \log K + \log p \qquad \ldots \quad 7.9$$

$$\log k' = m' \log K + \log q \qquad \ldots \quad 7.10$$

$$\text{or} \qquad k = p K^{m}$$

$$k' = q K^{m'}$$

where m, m', p and q are constants.

The data from Shropshire and the Vale of Clwyd (fig. 34) do not show convincing linear relationships here although there is reason to expect them. Obviously further numerical analyses upon these data would be inconclusive and therefore have not been attempted here but are considered at a later stage.

- 51 -
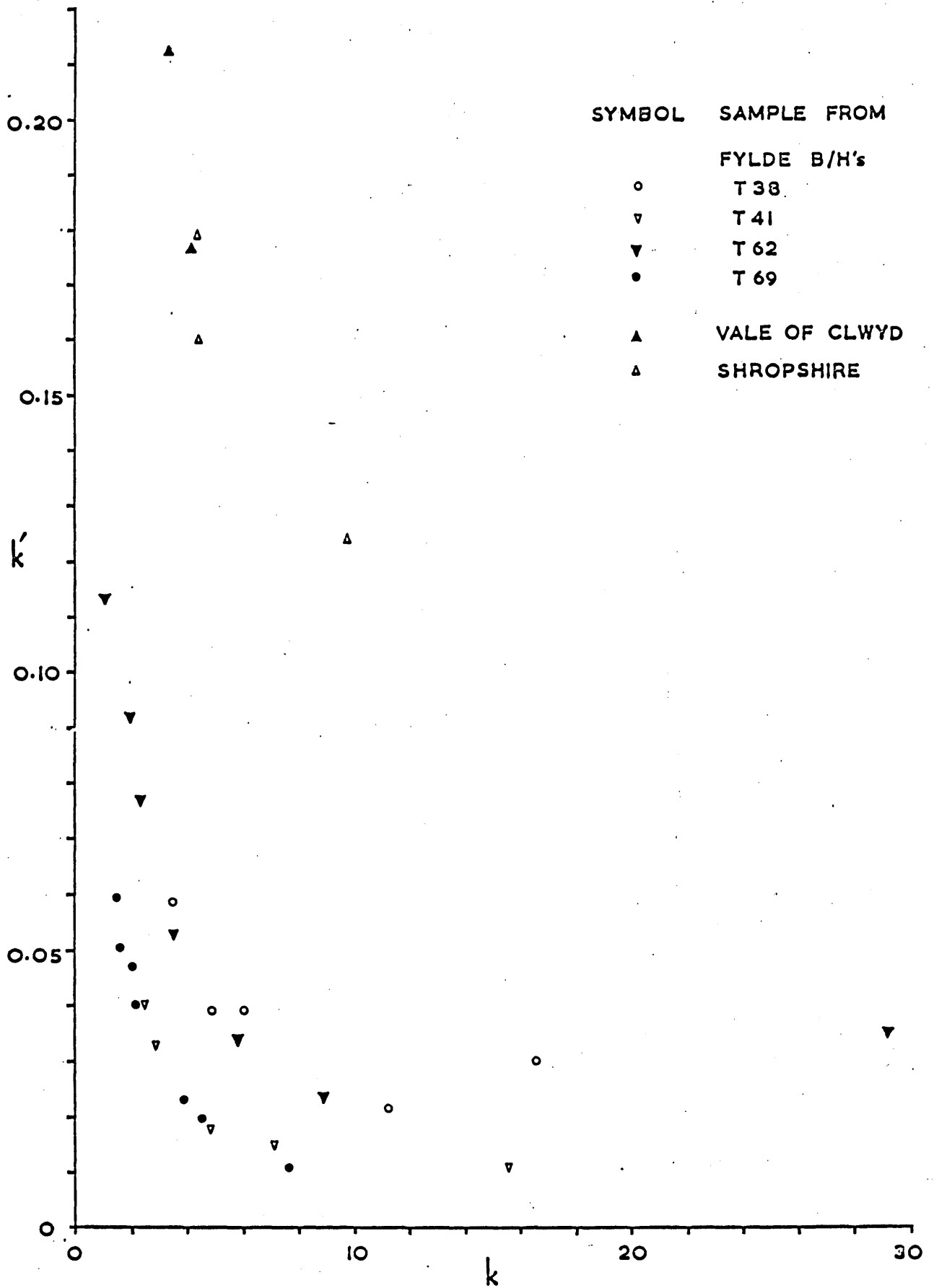
Values of k' plotted against k, evaluated through least squared errors analyses from data in figs 25 to 29.

FIG.31
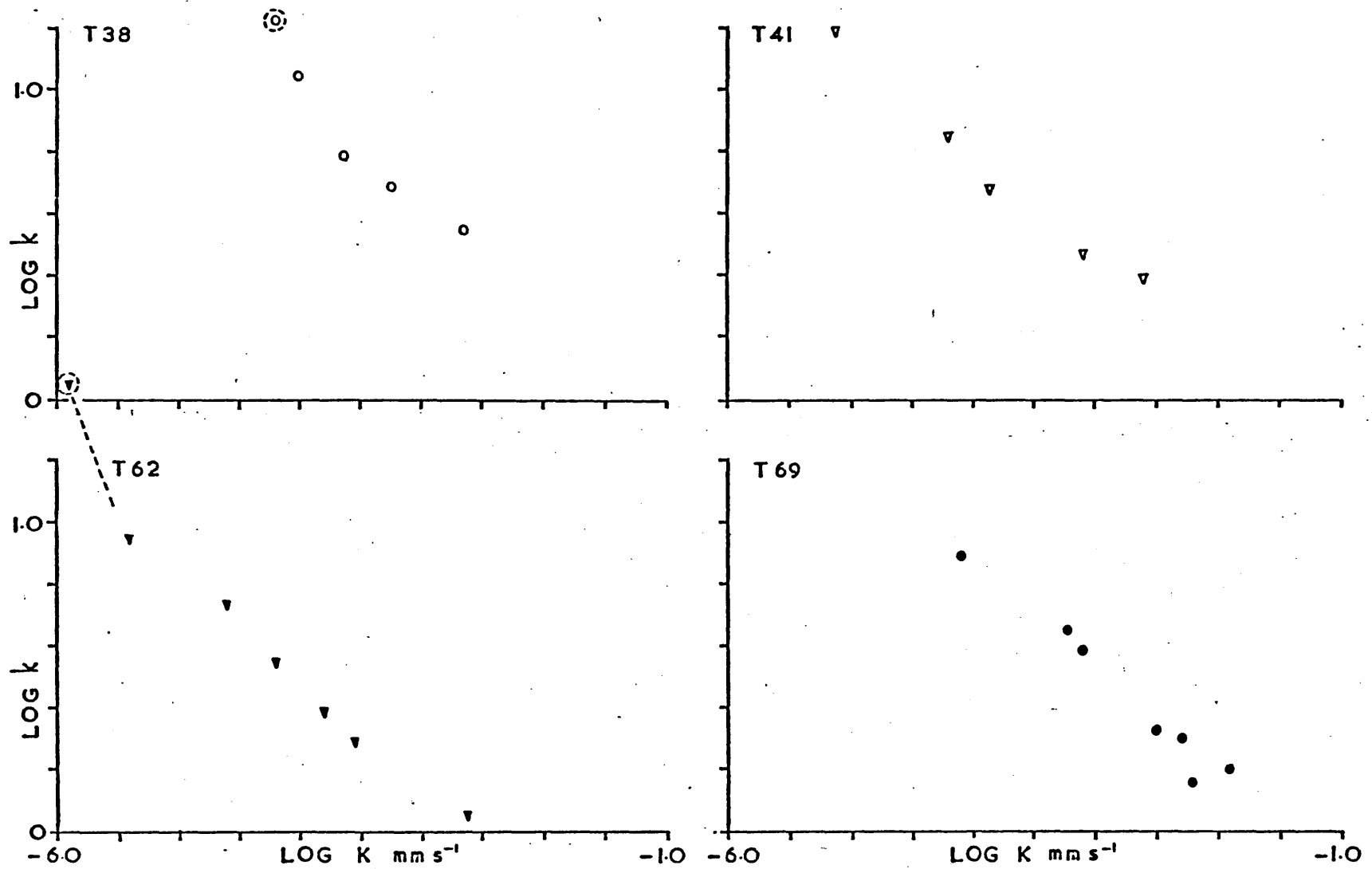
Logarithmic variation of the parameter k against permeability K for the samples
from Fylde boreholes T38, T41, T62, and T69.

FIG.32
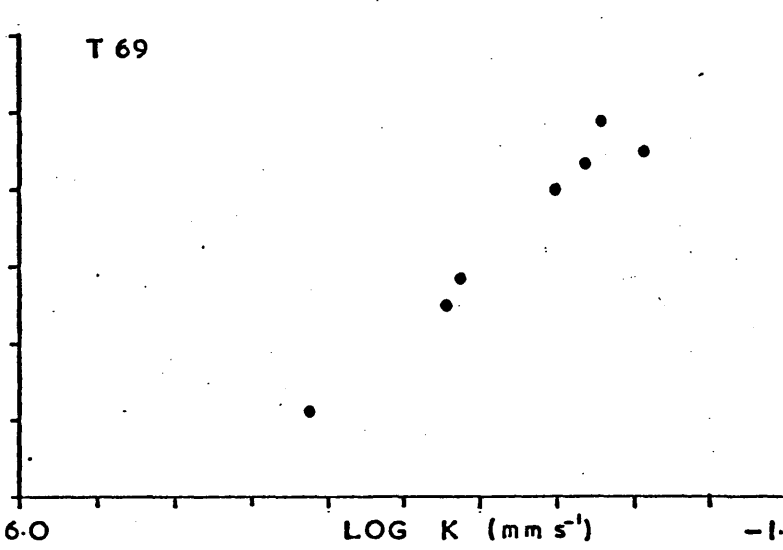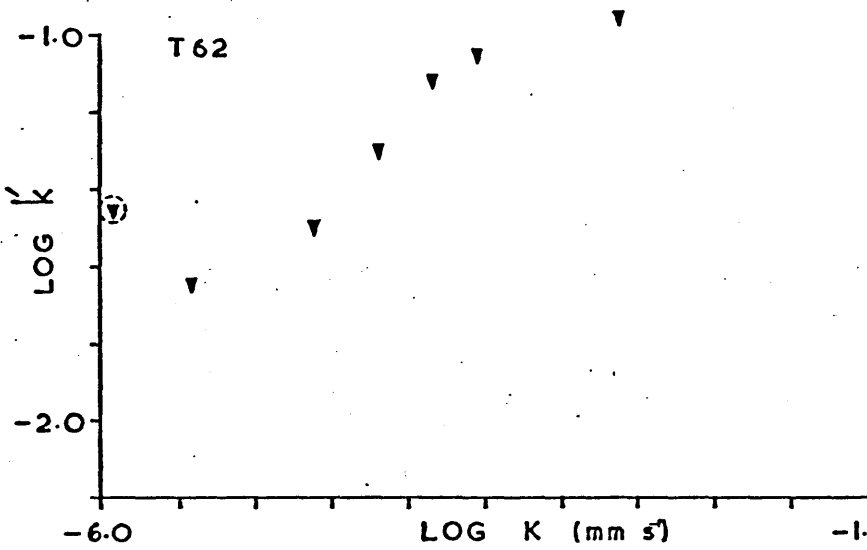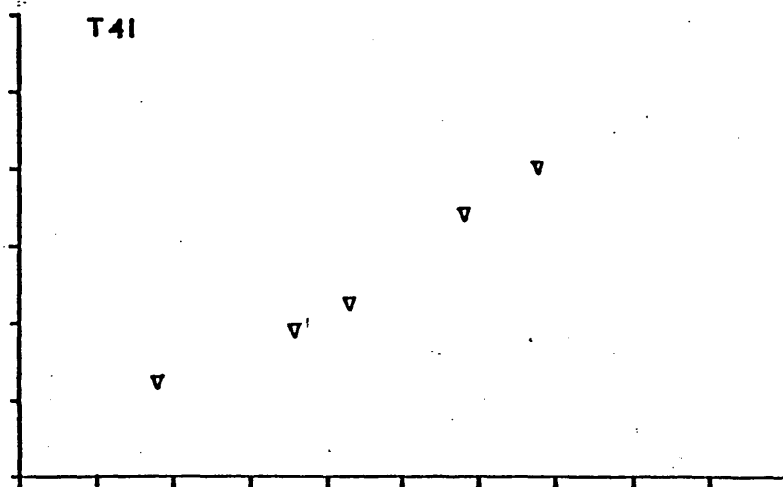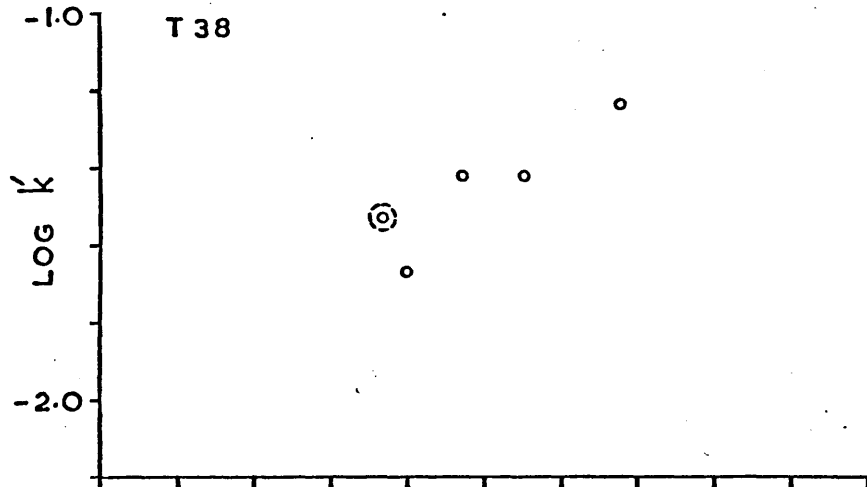
FIG. 33

Logarithmic variation of the parameter k' against permeability K for samples from the Fylde boreholes T38, T41, T62, and T69.
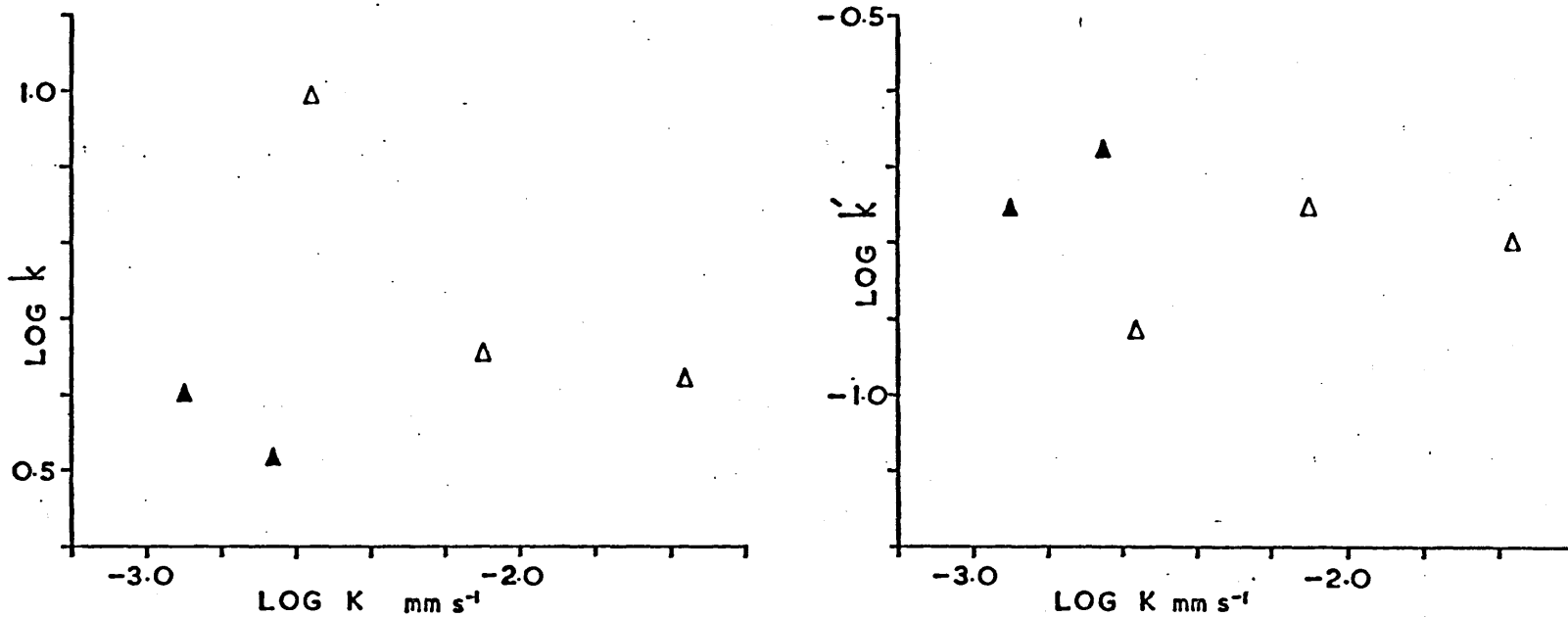
Logarithmic variation of the parameters k and k' against permeability K for samples from the Vale of Clwyd (solid triangles) and Shropshire (open triangles).

FIG. 34

The most probable values of m, p, m' and q for the Fylde data (figs. 32, 33) have been determined by the least squared errors method applied to equations 7.9 and 7.10, errors being considered in k, k' and K. Using equation 7.9 as the example, the total squared error E is given by:

$$E = \sum \frac{(\log k - m \log K - \log p)^2}{(m^2 + 1)}$$

From the normal equations, obtained through $\dfrac{\partial E}{\partial m} = \dfrac{\partial E}{\partial \log p} = 0$

$$\log p = \frac{[\log k] - m [\log K]}{n}$$

and

$$m^2 \left([\log k \log K] - \frac{[\log K][\log k]}{n} \right) + m\left([\log^2 K] - \frac{[\log K]^2}{n} \right.$$

$$\left. - [\log^2 k] + \frac{[\log k]^2}{n} \right) - [\log K \log k] + \frac{[\log K][\log k]}{n} = 0$$

where n is the number of data points and the symbol $[\ ]$ represents $\sum_1^n$. By this method, m, p, m' and q have been determined for each borehole section (table 4(a)) and the respective standard errors α_m, α_p, $\alpha_{m'}$ and α_q have been determined through

$$\frac{\alpha_m^2}{n} = \frac{\alpha_T^2}{n [\log^2 K] - [\log K]^2} = \frac{\alpha_{\log p}^2}{[\log^2 K]}$$

where $\alpha_T^2 = \dfrac{[(\log k - m \log K - \log p)^2]}{n - 2}$ (Topping 1972)

substituting m' k' and q appropriately.

In this case α_p and α_q are given by

$$p \,(\text{alog}^{-1} \, \alpha_{\log p} - 1) \quad \text{and} \quad q \,(\text{alog}^{-1} \, \alpha_{\log q} - 1)$$

respectively.

Inspection of table 4(a) and fig. 32 shows that the values of m obtained are similar and likewise the values of m' within the standard errors. Therefore if m and m' assume unique values, the parameters k and k' can be related directly to K through p and q, which are constants for each represented borehole section. Mean values $\bar{m}$ and $\bar{m}'$ have been obtained by weighting m and m' with the inverse square of their standard errors (Topping 1972):

$$\bar{m} = \sum \left(\frac{m}{\alpha_m^2}\right) \bigg/ \sum \left(\frac{1}{\alpha_m^2}\right)$$

$$\text{and } \alpha_{\bar{m}} = \left(\frac{\sum \left(\frac{1}{\alpha_n}\right)^2 (m_n - \bar{m})^2}{(n-1) \sum \alpha_n^{-2}} \right)^{\frac{1}{2}}$$

where m_n is the nth value of m and α_n is its standard error.

Returning the values $\bar{m}$ and $\bar{m}'$ to equations 7.9 and 7.10, the new values of p and q have been calculated (table 4(b)) by the least squares method. These values of p and q are generally within the limits of error of the corresponding most probable p and q (table 4(a)) although two exceptions occur in q. This is not surprising as a consequence of the limited number of data available at this stage.

Equations 7.9 and 7.10 can now be written

$$k = p K^{-0.34}$$

$$k' = q K^{0.28} \qquad \qquad \text{(cf.equations (2) and (3)}$$
$$\text{Collar and Griffiths 1976)}$$

and incorporated into equation 7.3:

$$IP = \frac{c^{0.45} \cdot 0.33}{(c^{0.45} + p K^{-0.34})(1 + C q K^{0.28})} \qquad \dots \quad 7.11$$

through which, given p and q, the IP of the sandstone can be predicted for any pore water conductivity σ_w, and permeability K.

The suitability of equation 7.11 has been assessed by assigning values to p and q from table 4(b) and comparing the calculated variation of IP with K for appropriate σ_w, against the corresponding observed data (6.e). From the examples given in figs. 35 and 36, it is concluded that this generalised equation offers a comprehensive description of the data.

For T62, the fit of the equation to the data could be improved by altering p and q within the limits of their standard errors. In the previous work

Table 4(a)   Most probable values of m, p, m', q.   Std errors $\propto$

	m	$\propto_m$	p	$\propto_p$	m'	$\propto_{m'}$	q	$\propto_q$
T38	- 0.350	0.080	0.380	0.180	0.286	0.083	0.347	0.166
T41	- 0.327	0.026	0.306	0.064	0.239	0.028	0.167	0.037
T62	- 0.344	0.024	0.129	0.027	0.270	0.036	0.699	0.202
T69	- 0.347	0.030	0.307	0.054	0.350	0.032	0.286	0.054

Table 4(b)   Weighted means $\bar{m}$ and $\bar{m}'$ with derived p and q

$$\bar{m} = - 0.340 \pm .005$$

$$\bar{m}' = 0.283 \pm .027$$

	p	$\propto_p$	q	$\propto_q$
T38	0.368	0.170	0.372	0.180
T41	0.274	0.057	0.243	0.053
T62	0.134	0.028	0.780	0.226
T69	0.322	0.057	0.187	0.035
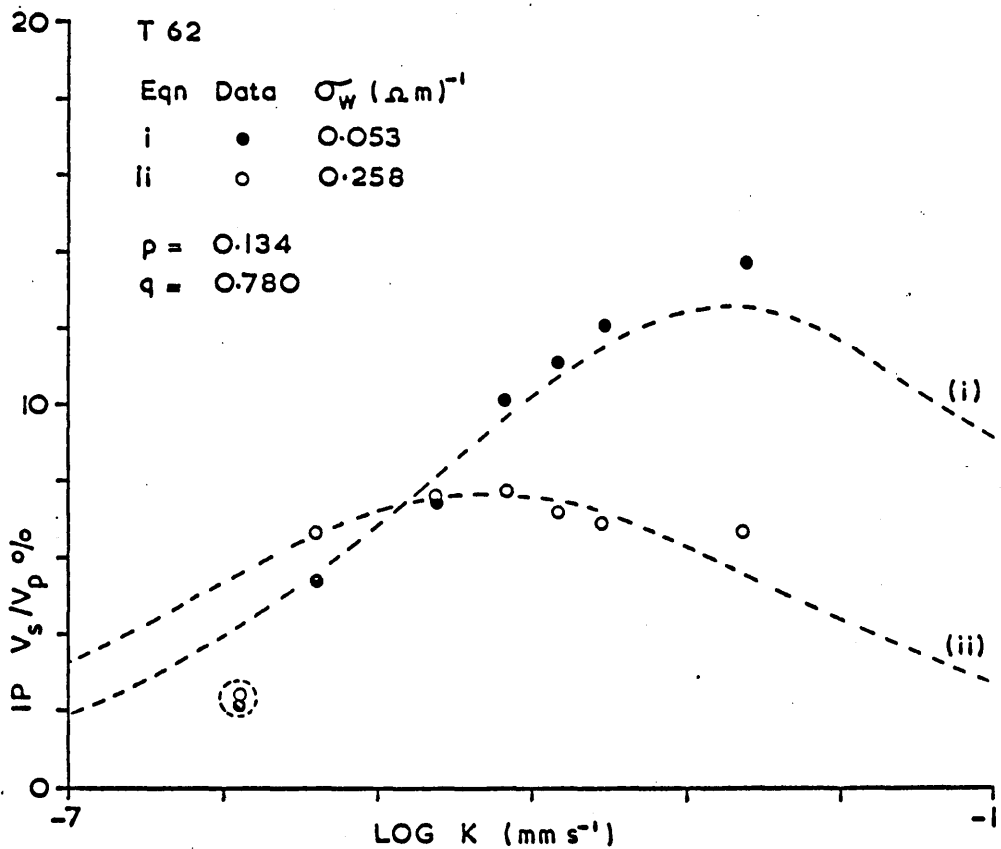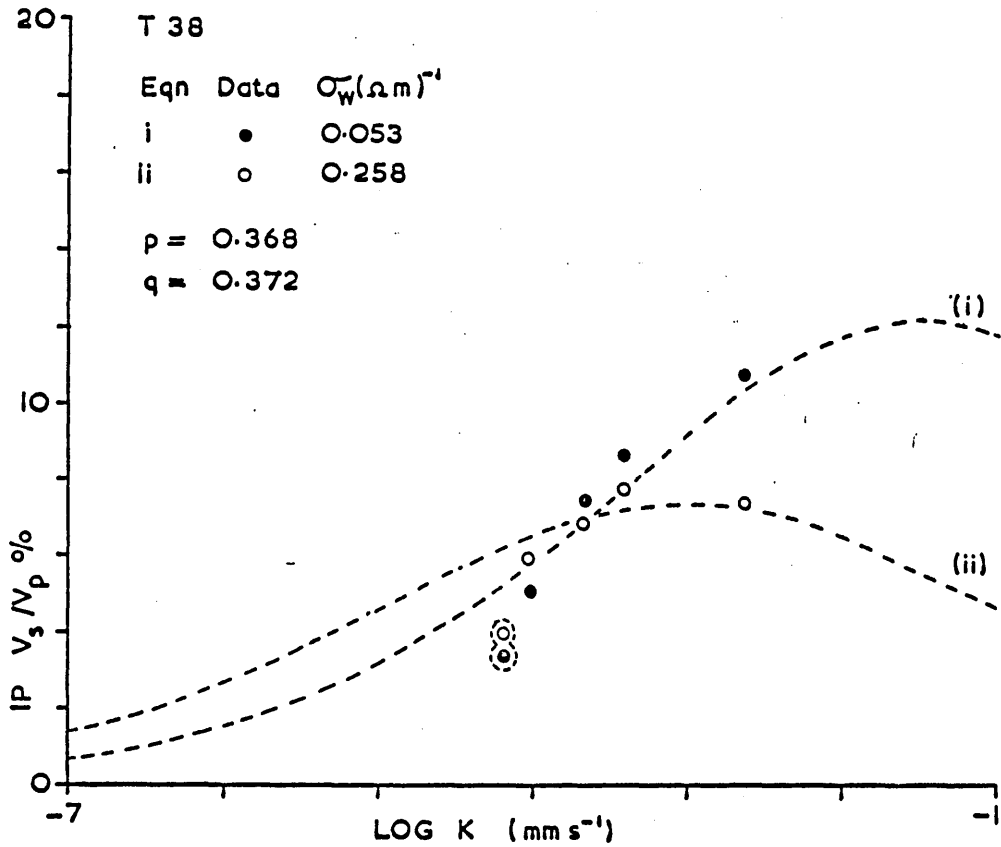
Variation of IP against log permeability for two values
of σ_w. Dashed lines from equation 7.11 (p and q from
table 4(b)) and IP data from fig 25 (T38) and fig 27 (T62)
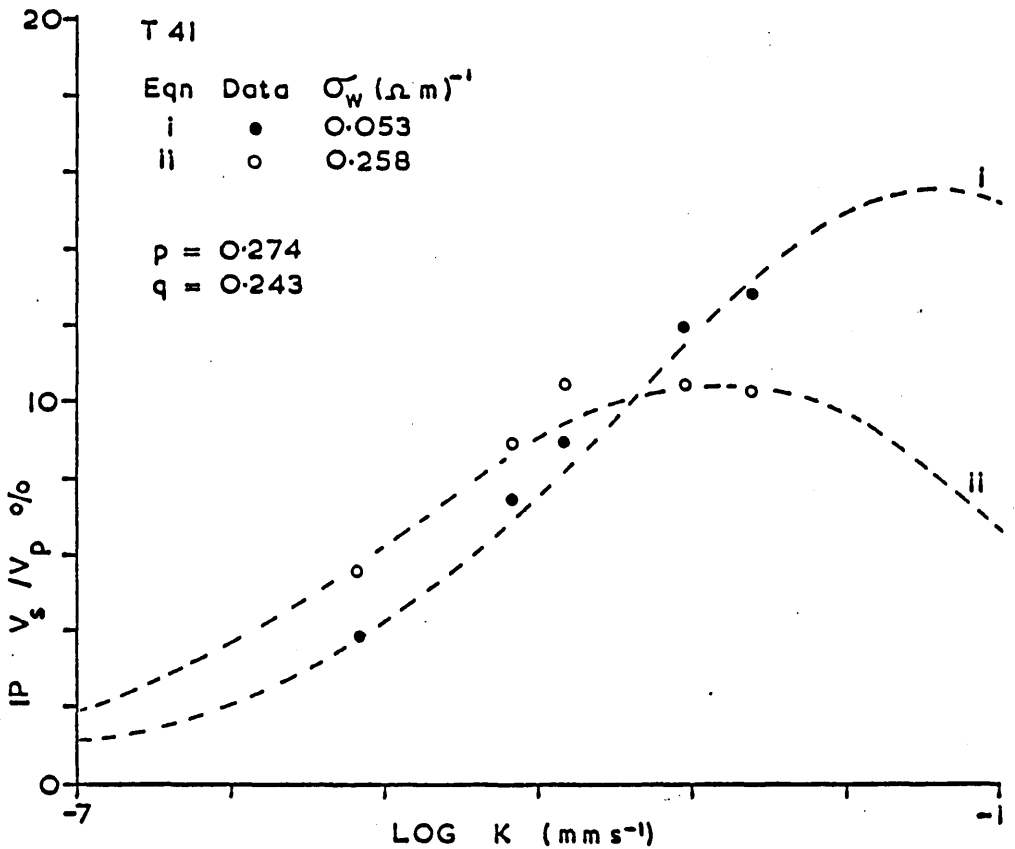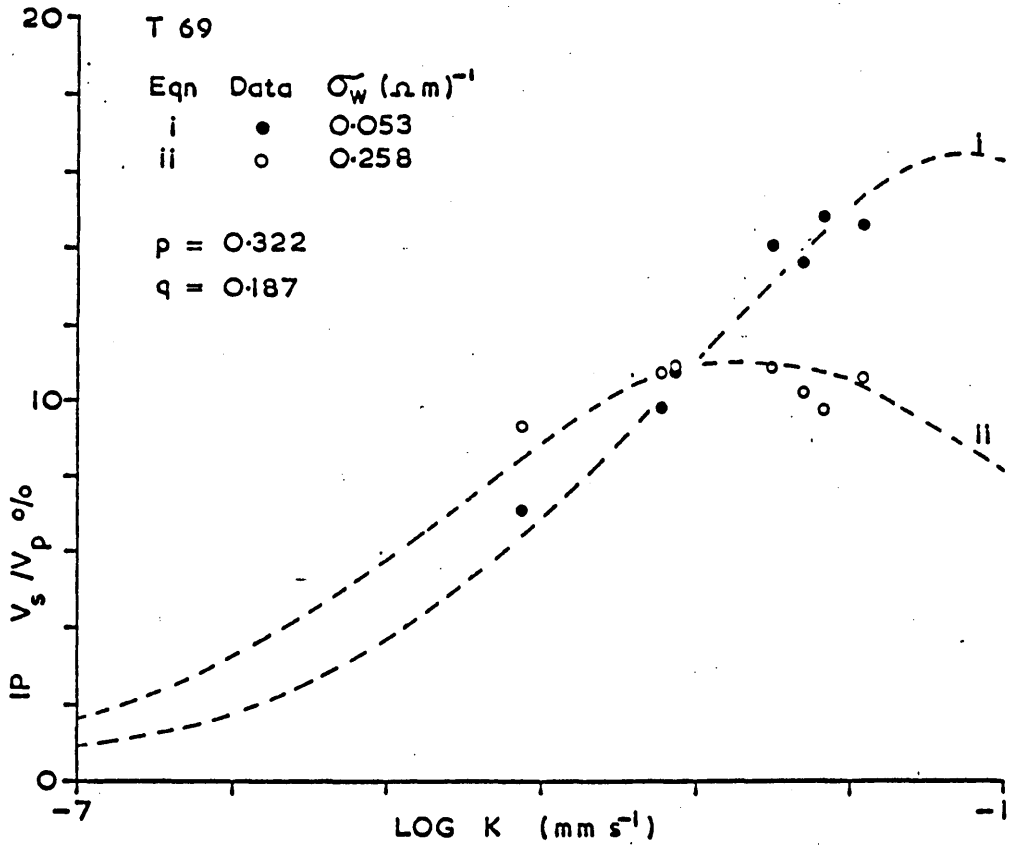
FIG.35

Variation of IP against log permeability for two values of
σ_w. Dashed lines from equation 7.11 (p and q from table 4(b))
and IP data from fig.28 (T69) and fig 26 (T41).

FIG.36
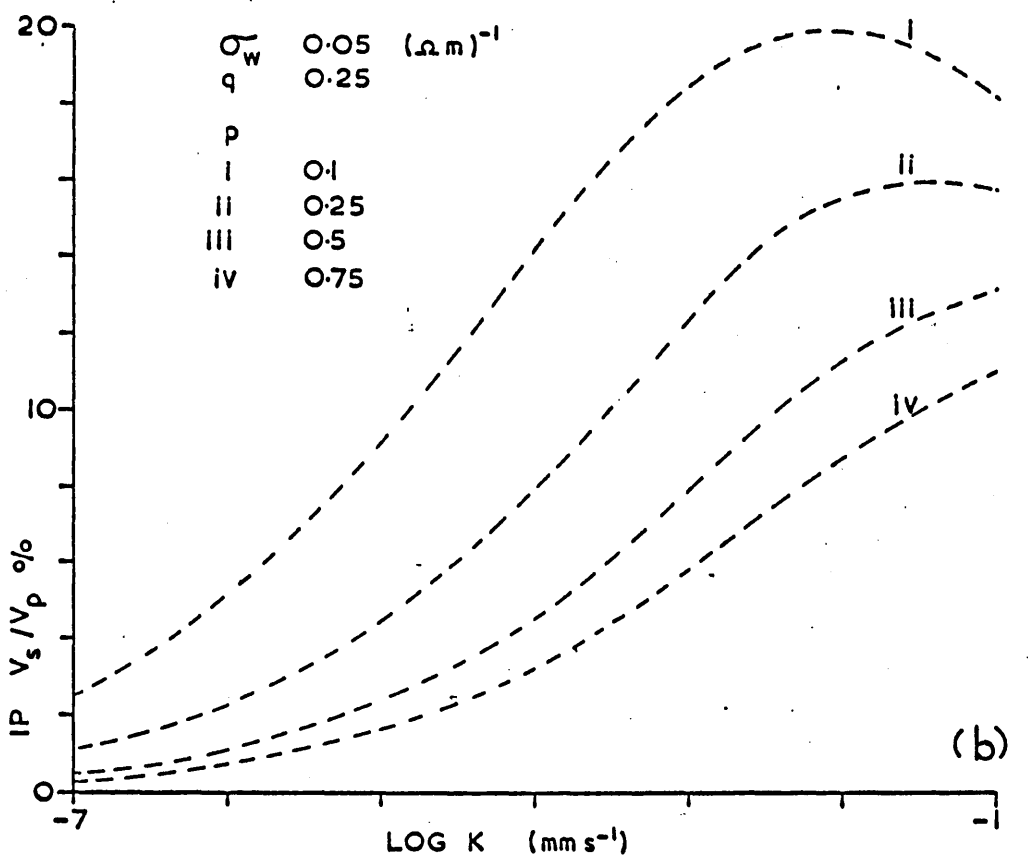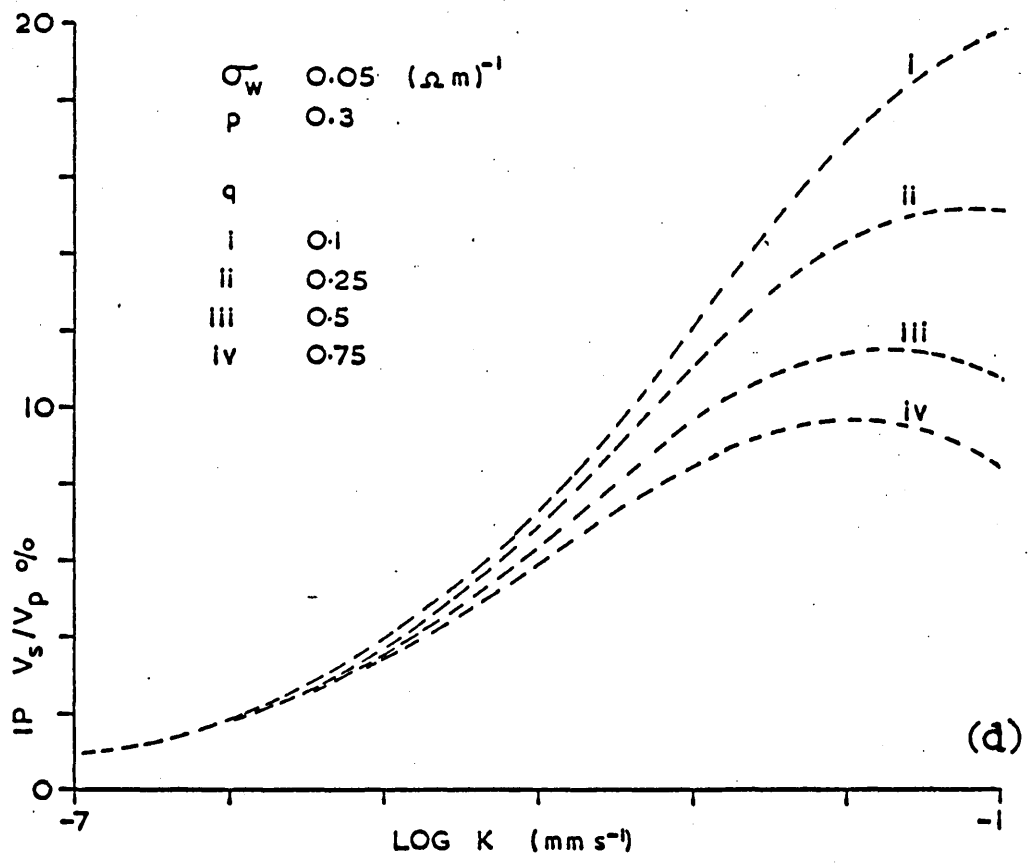
Variations of IP against log K determined through equation 7.11 for σ_w = 0.05 mhos m^{-1}. (a) p constant, 4 values of q; (b) q constant, 4 values of p.

FIG.37
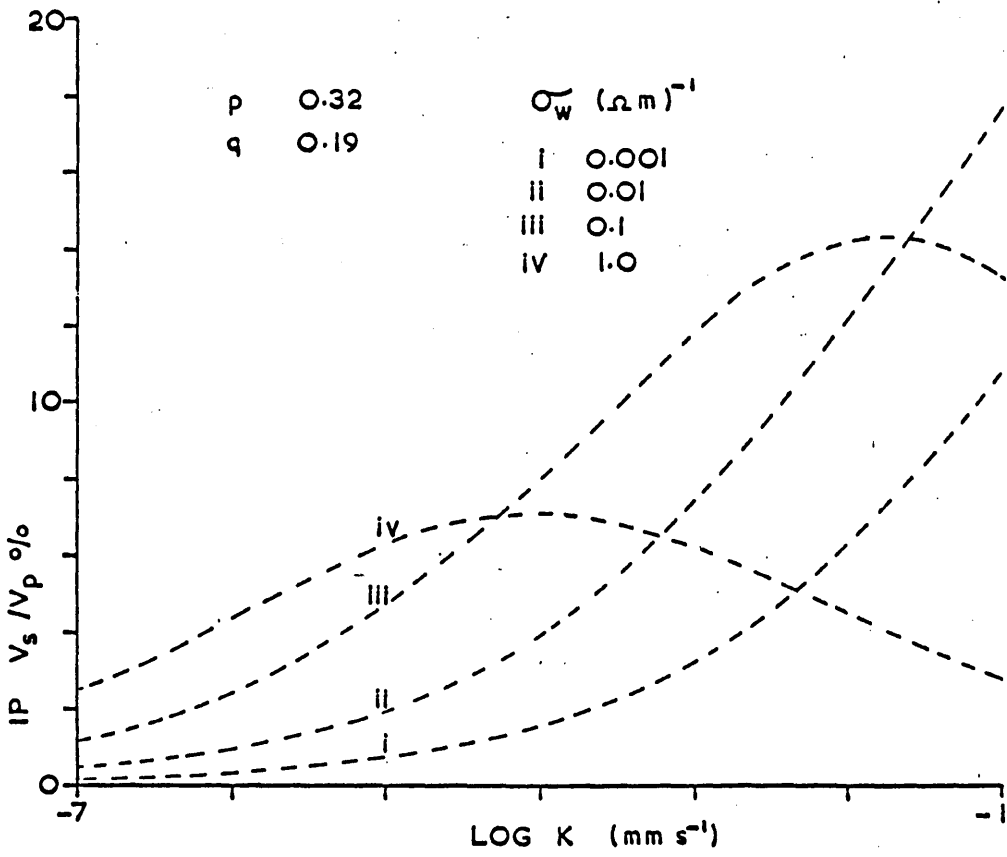
Variations of IP against log K.
p and q fixed; 4 values of σ_w.

FIG.38
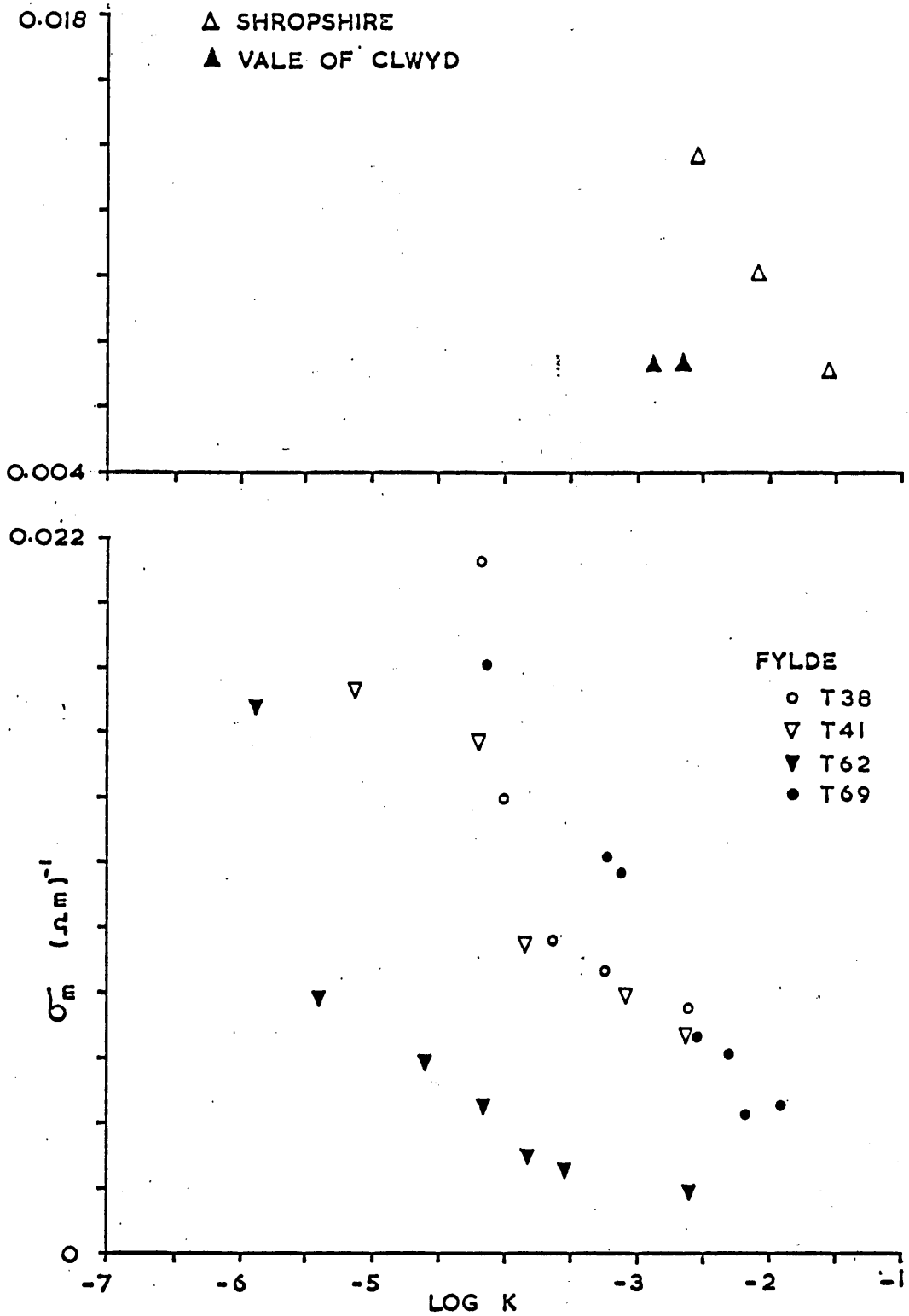
Matrix conduction parameter σ_m plotted against log
permeability K mms^{-1} for the range of samples from
Shropshire, Vale of Clwyd, and the Fylde.

FIG.39

(Collar and Griffiths 1976) where equation 7.11 was written

$$IP = \frac{c^{0.5} \cdot 0.33}{(c^{0.5} + p\, K^{-0.35})(1 + c\, q\, K^{0.23})}$$

a similar comparison for T62 was slightly better.

Owing to the experimental discrepancy discussed in 6.g, comparisons between equation 7.11 and the data for σ_w = 0.025 mhos m^{-1} would not in general be successful (with the exception of T62 for which fig. 28 suggests minimal discrepancy - see Collar and Griffiths fig. 3).

A number of graphs have been constructed from equation 7.11 to illustrate the influence of p and q upon the variation between IP and K, for a value of σ_w that is typical of the groundwater. These are shown in fig. 37 where for σ_w = 0.05 mhos m^{-1}, (a) q is varied and p = 0.3, (b) p is varied and q = 0.25. In fig. 38 another set of curves have been plotted from equation 7.11 to demonstrate the influence of pore water conductivity σ_w upon the IP-log K relationship for constant p and q. In this case the values for these parameters have been adopted from T69.

Although the log k, log k', and log K data for Shropshire and the Vale of Clwyd (fig. 34) are not conclusively linear (possibly for the Shropshire data because of the effect upon k and k' of normal experimental errors incorporated in the closely grouped IP data of fig. 29) the marked apparent linearity of the IP and permeability K data of fig. 22 i and also of the K - matrix conductivity σ_m data (fig. 39) indicates that relationships, similar to those which have been analysed from the Fylde data, may be expected here. For comparative purposes, values of p and q have therefore been estimated for these data through equations 7.9 and 7.10 by adopting the values of $\bar{m}$ and $\bar{m}'$ from the analyses of the Fylde data. The values obtained by this method were:

Shropshire　　　　p = 1.15　　q = 0.57

Vale of Clwyd　　p = 0.42　　q = 1.16

These values of p are high, particularly of the Shropshire sandstones, which seems appropriate after inspection of the IP - K data (fig. 22 i).

Summarising, for a wide range of Bunter sandstones, IP can be calculated against K and σ_w through equation 7.11, provided the parameters p and q are known. These are specific constants to each represented sandstone sequence, independent of changes in K. The values obtained for p and q, included in table 4(b), suggest that these parameters may be mutually independent although these values will have been influenced to a small extent by the initial selection of the samples through the IP - permeability data in figures 22 a to i. These samples were chosen because for each group they covered almost the full range of permeability and their data approximated the overall linear IP - permeability (K) distributions at $\sigma_w = 0.025$ mhos m^{-1}. If a different set of samples from each group had been selected for these analyses, the exponents z (equation 7.3) would not necessarily have been different, but some change would be expected in p and q.

In fact it is now known that the IP - K distribution is not linear but because the data cover a wide range the errors that have been introduced by this selection process are thought to be small, particularly in relation to those incurred through natural scatter and incomplete experimental control. Of course some of these errors have been taken into account by the least squared errors analyses but one systematic uncertainty is known to be incorporated in the results, that is the reduction of chargeabilities discussed in chapter 6, and the extent of this is largely unknown. Only further measurements can resolve this, a suitable programme being to measure IP for a large number of sandstone samples from each borehole, initially keeping them saturated with the local groundwater. Electrodialysis in very pure water would be recommended prior to further measurements using other electrolytic solutions, e.g. NaCl, and storage should be in the appropriate saturating fluid.

Some discussion of a possible lithological significance of the parameters p and q is given in chapter 9.

CHAPTER 8

MATRIX CONDUCTIVITY AND IP

8.a <u>Definition of matrix conductivity</u>

Other workers e.g. Patnode and Wyllie (1950) (cf. Worthington and Barker (1972))
have obtained values for matrix conductivities σ_m by the linear extra-
polation of sandstone conductivities σ_s to zero pore water conductivity
($\sigma_w = 0$). Modelling studies (5.b) show that the sandstone conductivity
σ_s for $\sigma_w = 0$ i.e. $\sigma_s = b\,\sigma_b$, is less than this measure of σ_m.

Where a considerable number of matrix conductivity data are required though,
it is impractical to obtain the true values of σ_m , whereas the method
used by Patnode and Wyllie gives an approximate but convenient measure.
Accordingly, in the following discussion, matrix conductivities have been
determined as the parameter σ_m by linear extrapolation of the sandstone
conductivity data between $\sigma_w = 0.001$ and 0.053 mhos m^{-1}, to $\sigma_w = 0$,
using the least squared errors method.

8.b <u>Relationship between matrix conductivity and IP</u>

Values of σ_m determined for the samples used in section 6.e are compared
against the respective permeabilities expressed as log K in fig. 39.
Individual groups of data describe an increase of σ_m for decreasing log K,
a result which appears to be consistent with Worthington's (1976) regression
analyses of log b (= log σ_m) against log k (= log K) for Bunter sandstone
samples from the Fylde, from which he obtains a negative correlation
coefficient. The importance of the correlation between these two rock
properties is discussed together with some related factors in chapter 9.

Empirical relationships between the logarithms of permeability K and the
IP parameters k and k' have already been derived in section 7.d .
Pronounced linear correlations between log σ_m and log k or log k' are also

evident amongst the Fylde data (figs. 40 and 41) but not amongst the
Shropshire data (fig. 42), suggesting that for the Fylde the data for
individual boreholes can be conveniently described by empirical relationships
of the type:

$$\log k = \log r + s \log \sigma_m \qquad \ldots \; 8.1$$

$$\log k' = \log r' + s' \log \sigma_m \qquad \ldots \; 8.2$$

or

$$k = r \, \sigma_m^{\; s}$$

$$k' = r' \, \sigma_m^{\; s'}$$

where r, r', s and s' are constants for each group.

These constants have been evaluated for each group of data from the Fylde
by the method used for the permeability data in section 7.d and the results
are given in table 5(a) together with the respective standard errors.
There is a noticeable similarity amongst the values of s' within the limits
of their standard errors although the values of s vary rather more.   The
magnitudes of the errors α_r and $\alpha_{r'}$ have been exaggerated by the
process of conversion from logarithmic to linear scales.   .

Combining equations 8.1 and 8.2 with 7.3 gives:

$$IP = \frac{c^{0.45}}{c^{0.45} + r \, \sigma_m^{\; s}} \; . \; \frac{0.33}{1 + Cr' \, \sigma_m^{\; s'}} \qquad \ldots \; 8.3$$

through which the IP of a sandstone sample is related empirically to the
matrix conduction parameter σ_m .   This equation becomes more generally
applicable if unique values of s and s' can be assigned and therefore the
weighted mean values $\bar{s}$ and $\bar{s}'$ have been calculated (by the method used for
$\bar{m}$ and $\bar{m}'$ in 7. d) and used to derive appropriate values $\bar{r}$ and $\bar{r}'$.   The
results, given in table 5(b) show that the value $\bar{s}$ has been heavily
weighted in respect of T62 and T69.   This is illustrated in figs. 43 and
44 where equation 8.3 is compared against each group of data for σ_m and
IP, at σ_w = 0.053 mhos m^{-1}, inserting the appropriate values of s, s', r,
r' and also $\bar{s}$, $\bar{s}'$, $\bar{r}$, $\bar{r}'$.   The change in shape of the curve of equation 8.3

Table 5(a) Most probable values of s r s' and r'

	s	α_s	r	α_r	s'	$\alpha_{s'}$	r'	$\alpha_{r'}$
T38	1.812	0.181	26204	14908	-1.48	0.29	$3.83 \cdot 10^{-5}$	$2.84 \cdot 10^{-5}$
T41	1.691	0.321	11298	8683	-1.23	0.27	$7.77 \cdot 10^{-5}$	$5.45 \cdot 10^{-5}$
T62	1.412	0.111	8006	3692	-1.13	0.07	$10.51 \cdot 10^{-5}$	$3.58 \cdot 10^{-5}$
T69	1.122	0.056	632	151	-1.12	0.10	$13.92 \cdot 10^{-5}$	$5.23 \cdot 10^{-5}$

Table 5(b) Weighted means $\bar{s}$ and $\bar{s}'$ with derived $\bar{r}$ and $\bar{r}'$

$$\bar{s} = 1.24 \pm 0.12$$
$$\bar{s}' = -1.15 \pm 0.04$$

	$\bar{r}$	$\bar{r}'$
T38	1815	$18.36 \cdot 10^{-5}$
T41	1439	$11.53 \cdot 10^{-5}$
T62	3025	$9.78 \cdot 10^{-5}$
T69	1103	$12.21 \cdot 10^{-5}$
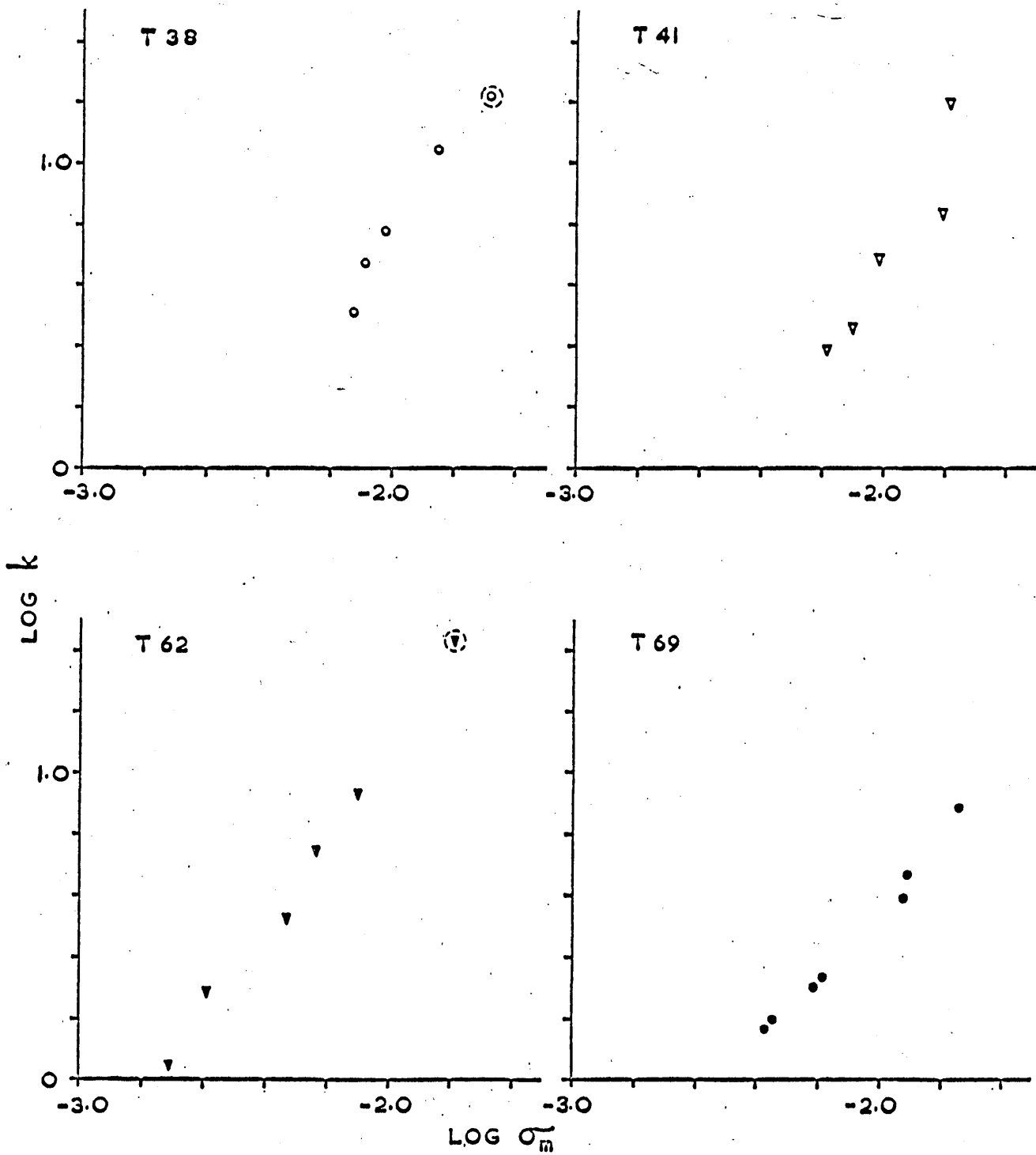
Log k plotted against log σ_m for the samples from Fylde boreholes T38, 41, 62, and 69.
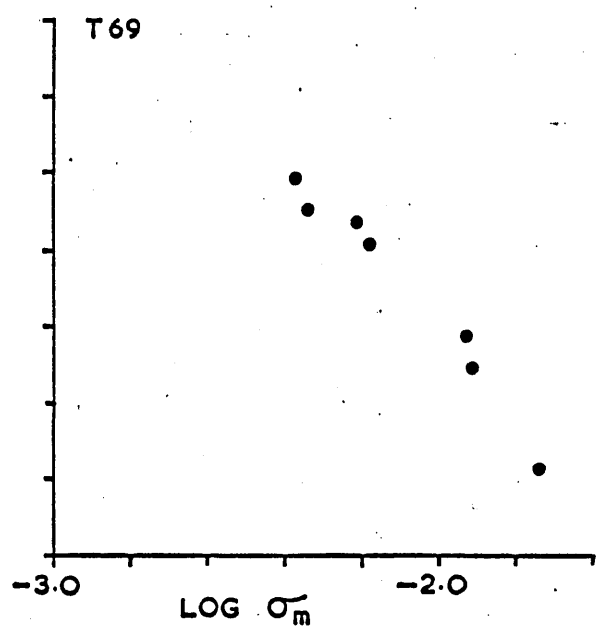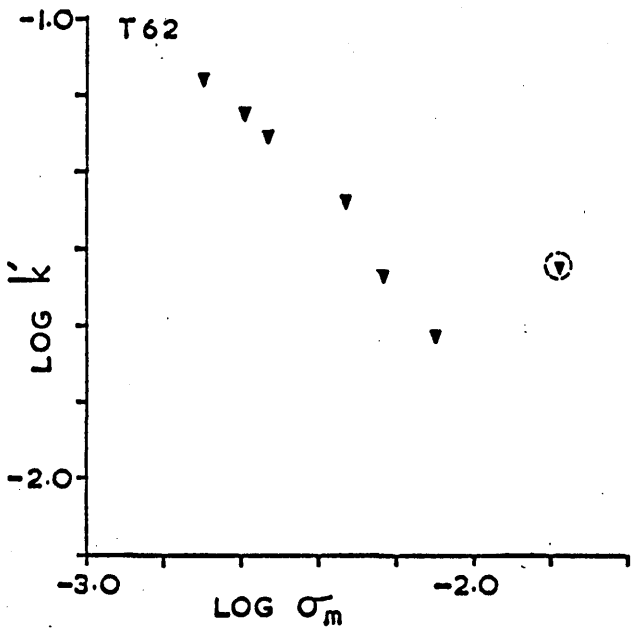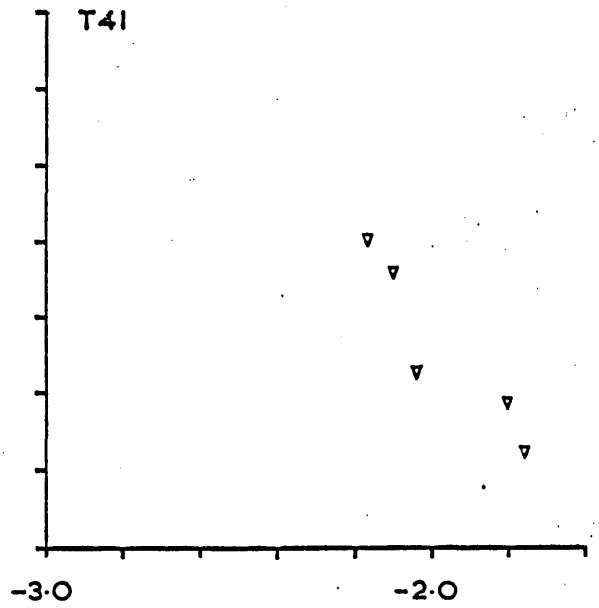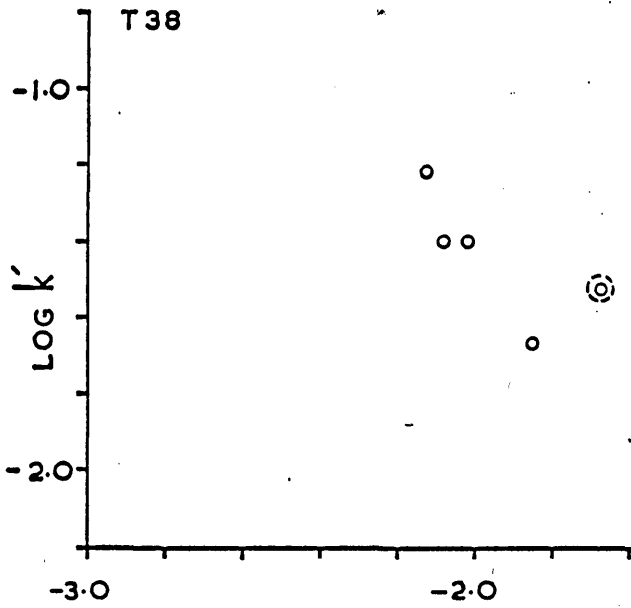
FIG.40

Log k' plotted against log σ_m for the samples from
Fylde boreholes T38, T41, T62, and T69.

FIG.41
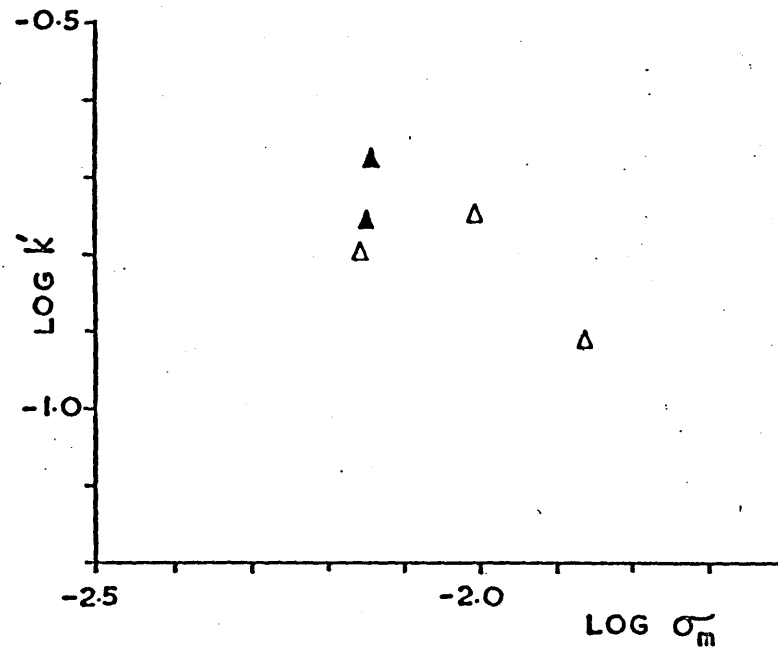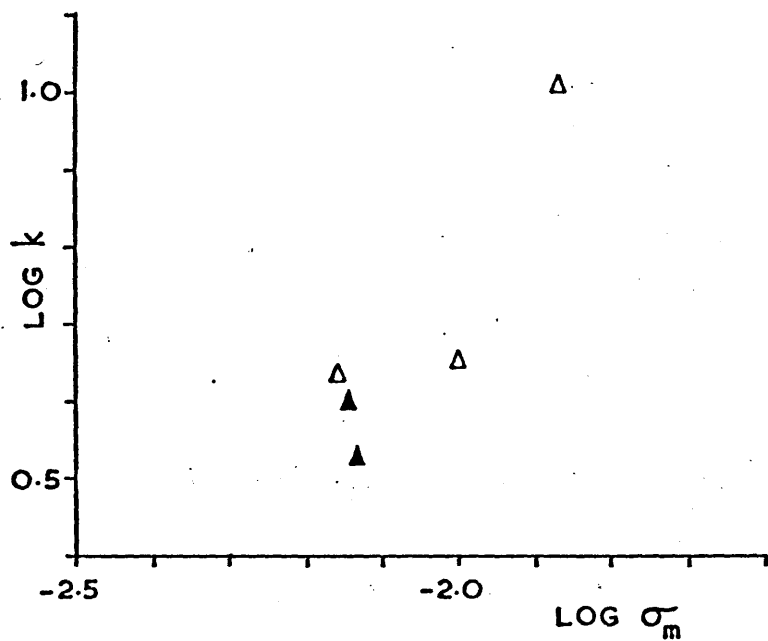
Log k and log k' plotted against log σ_m for the samples from boreholes in Shropshire (open triangles) and Vale of Clwyd (solid triangles).

FIG. 42
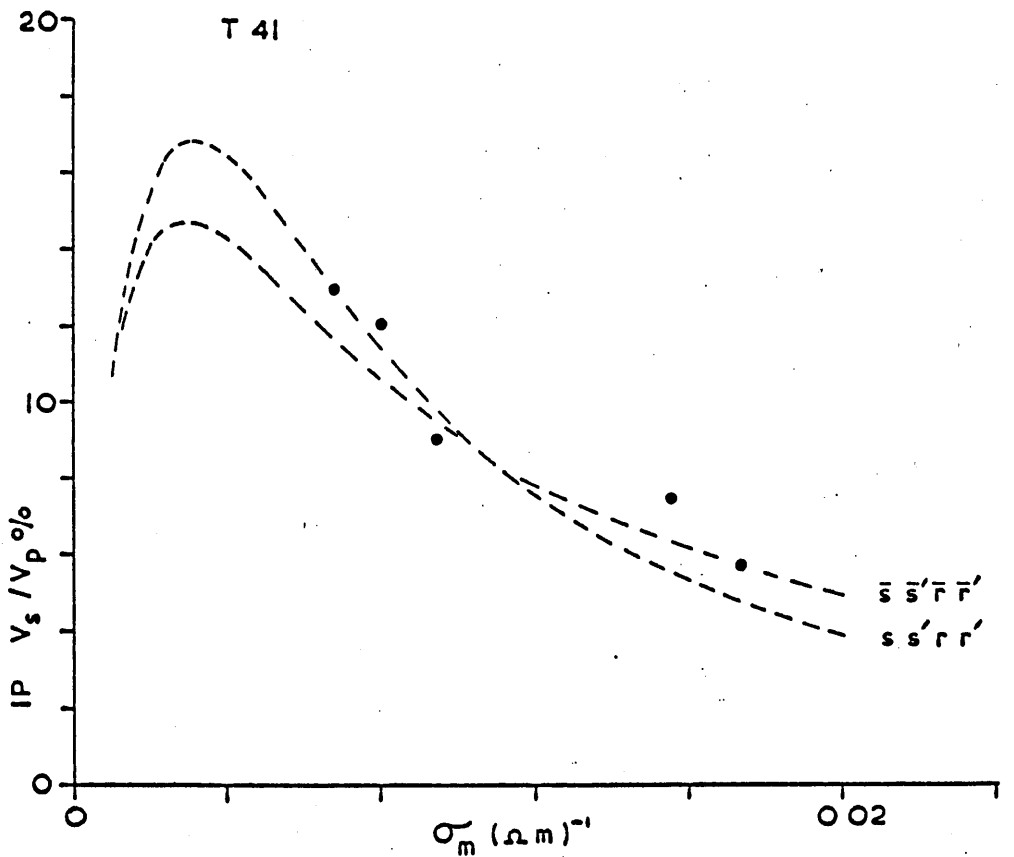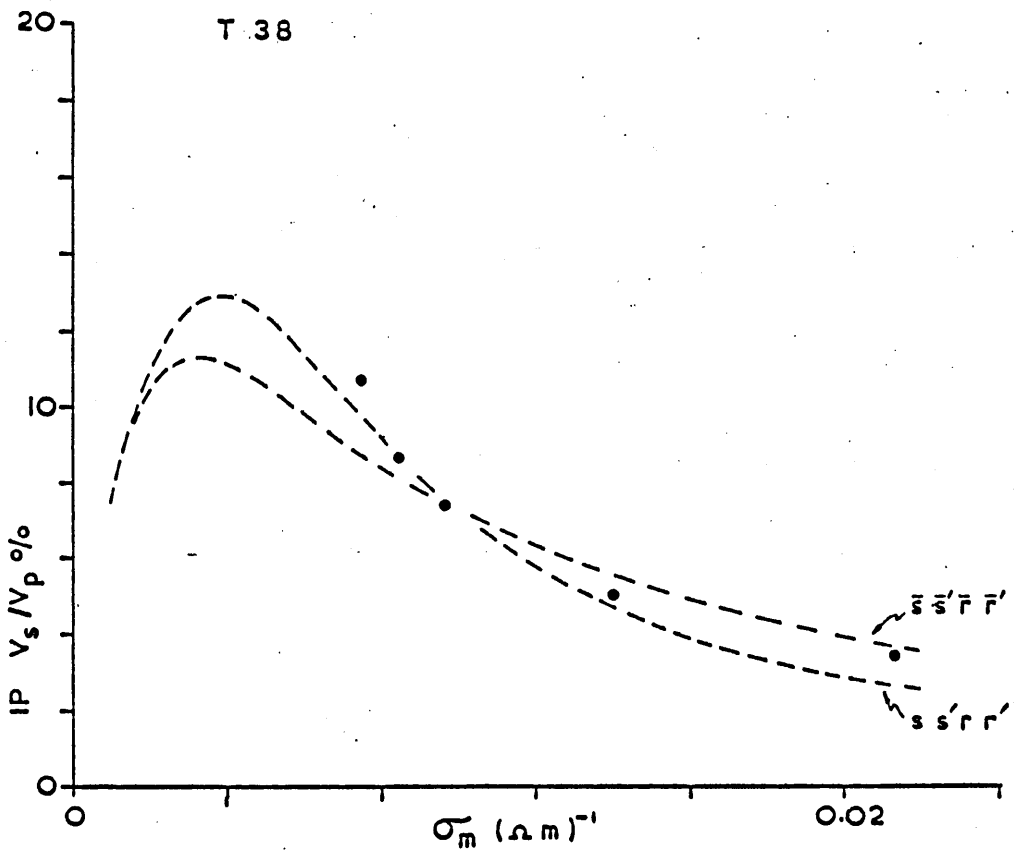
IP plotted against σ_m for samples from T38 and T41.
(σ_w = 0.053 mhos^{-1}). IP data from 6.e, dashed lines
calculated from equation 8.3 with corresponding values of
s s' r r'. and $\bar{s}$ $\bar{s}'\bar{r}$ $\bar{r}'$ from table 5.

FIG.43
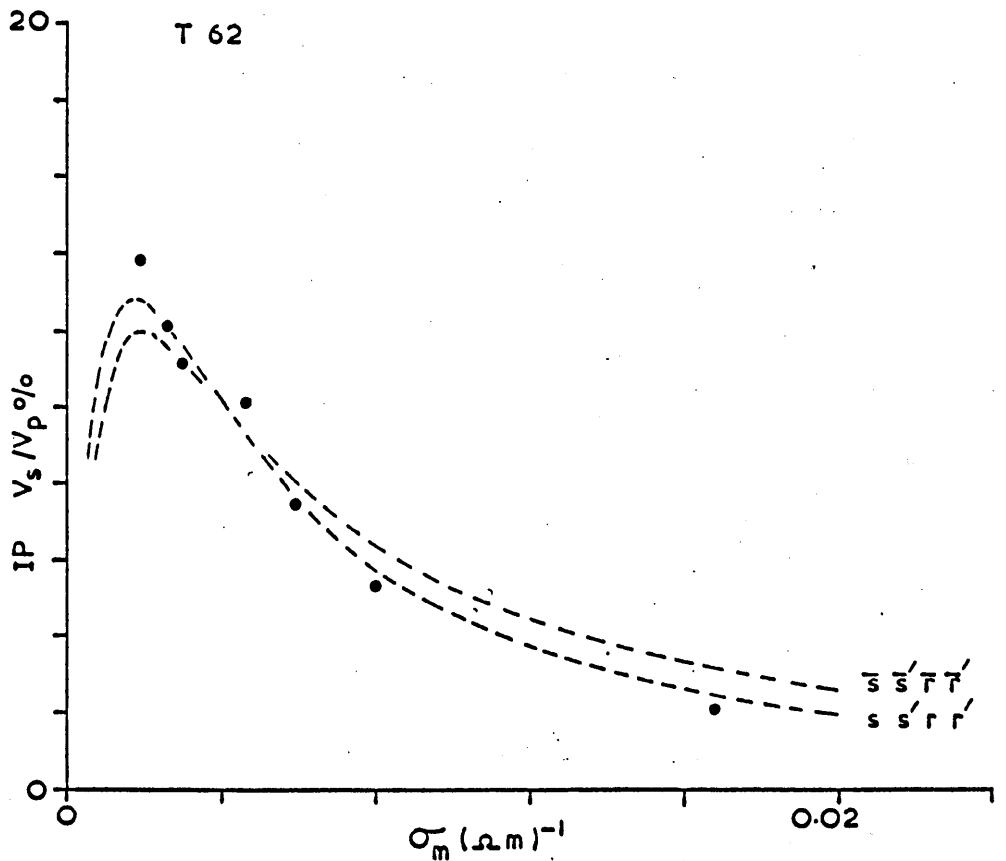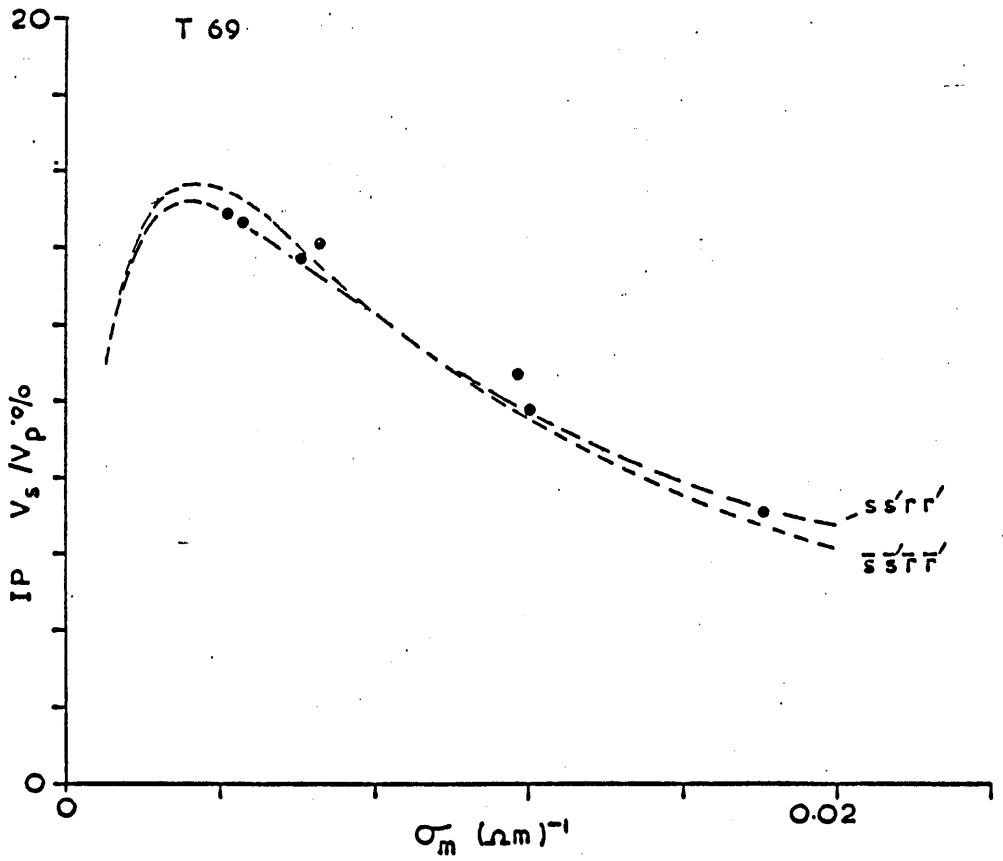
IP plotted against σ_m for samples from T69 and T62
($\sigma_w = 0.053$ mhos m^{-1}). IP data from 6.e, dashed lines
calculated from equation 8.3 with corresponding values of
s s' r r' and $\bar{s}$ $\bar{s}'$ $\bar{r}$ $\bar{r}'$ from table 5.

FIG.44
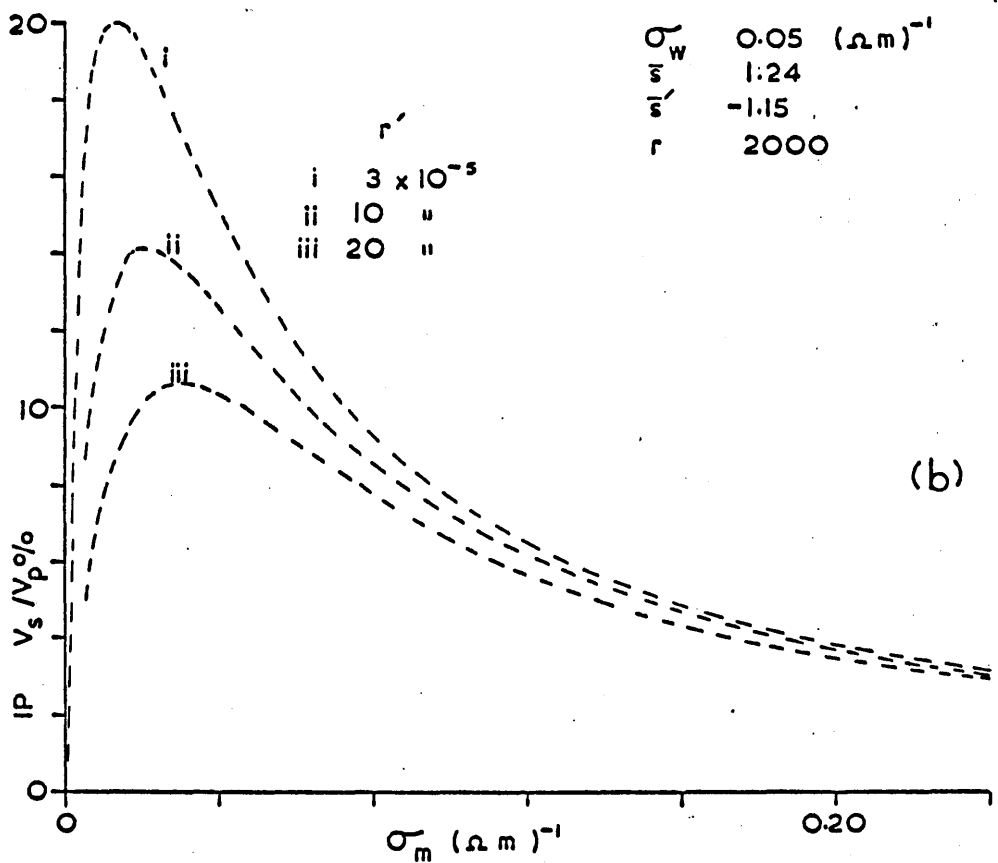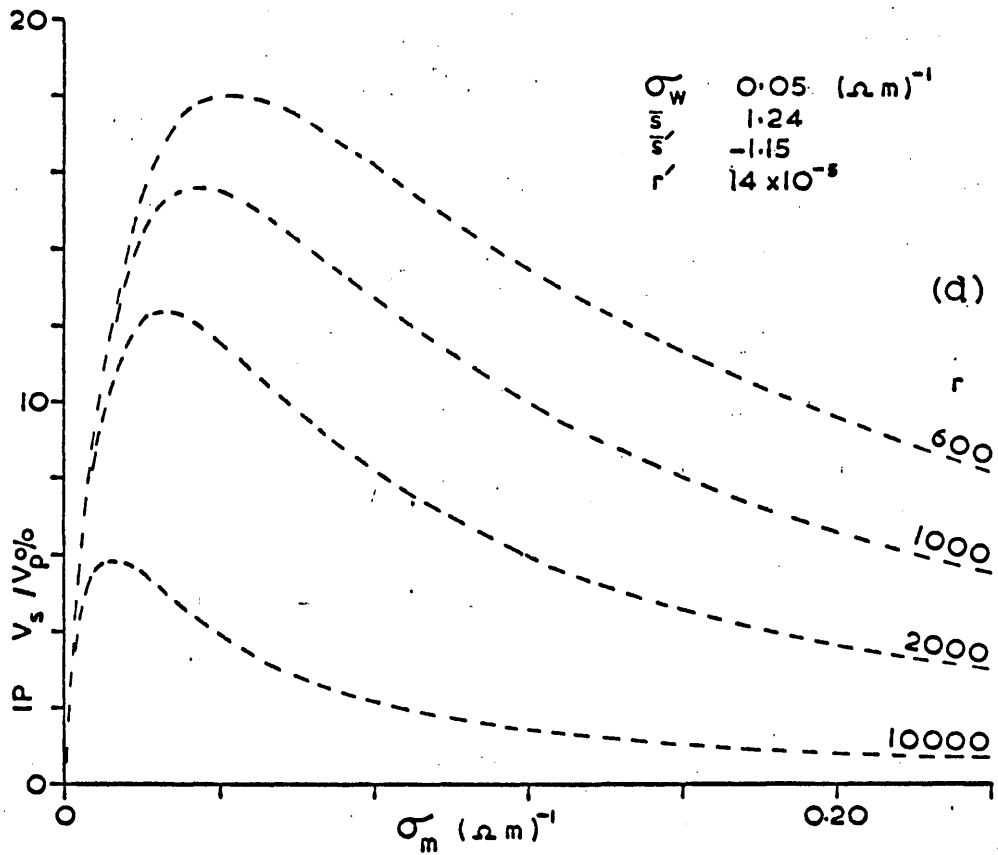
Variations of IP against σ_m determined through equation 8.4 for σ_w = 0.05 mhos m^{-1}. σ_m (a) r' constant, 4 values of r (b) r^w constant, 3 values of r'.

FIG.45
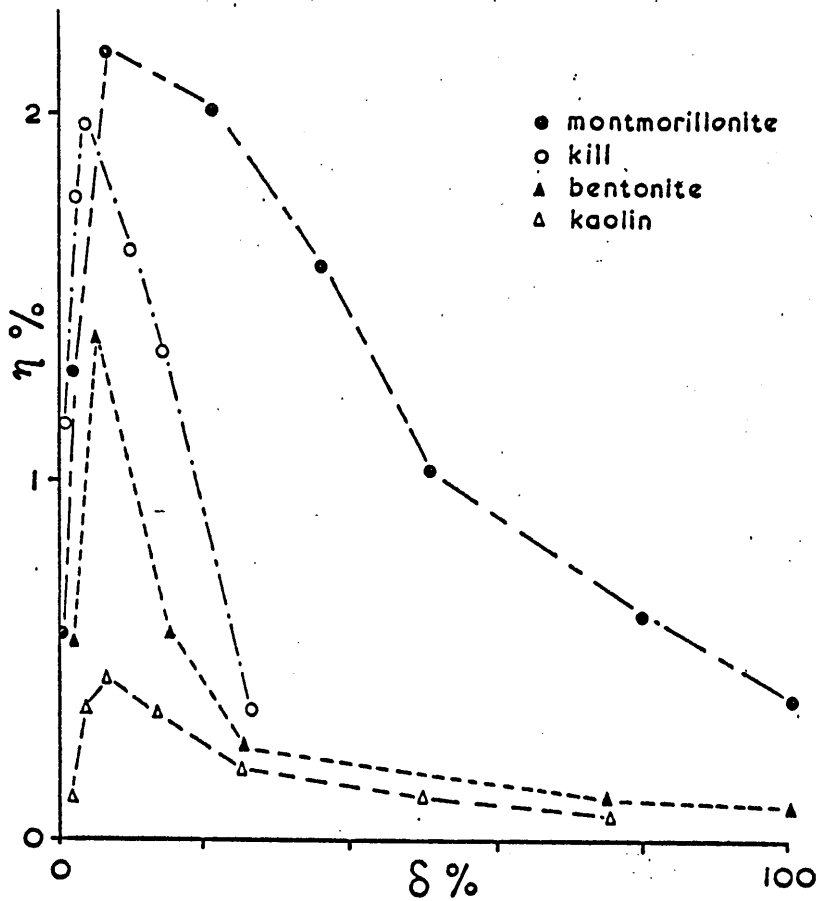
Fig 46a: Variation of chargeability against percentage and
type of clay content in quartz sands (from Ogilvy and Kuzmina
1972 fig 3). σ_w unspecified.
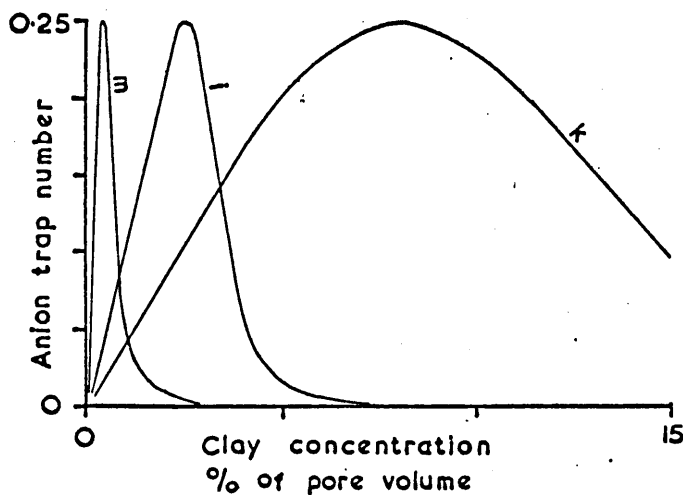
Fig 46b: Anion trap number ($\propto$ polarisation) as a function
of clay concentration for an electrolyte with a salinity
of 100 ppm (from Keller and Frischknecht 1966 fig. 262).
σ_w approx. 0.02 mhos m^{-1} .

k = kaolinite;   i = illite;   m = montmorillonite.

FIG.46

induced by substituting the mean parameters is greatest in the examples of T38 and T41, but nevertheless using these mean parameters the equation still describes the data fairly well. The equation may therefore be written generally for these Fylde sandstones:

$$IP = \frac{c^{0.45}}{(c^{0.45} + r\,\sigma_m^{1.24})} \cdot \frac{0.33}{(1 + r'\,\sigma_m^{-1.15}c)} \quad \ldots \; 8.4$$

Although the true matrix conductivity may change with water conductivity, it appears that this variation (fig. 11 b) is likely to be small within the typical range of groundwater salinities of the Fylde.

Replotting the σ_m data against k and k' (from figs.40,41) on linear axes shows that as σ_m tends to zero, k also tends to zero and k' becomes very large. In general terms this means that as the clay content of a sandstone decreases, the IP maximum for variable σ_w occurs about progressively decreasing values of σ_w. (It is also an interesting extrapolation of equation 7.3 that for k tending to zero and k' very large, or conversely, IP tends to zero for all values of σ_w. These are extreme conditions that would not be expected amongst sandstones although might be closely approached by pure sands and thick clays respectively.)

The form of the variation of IP against matrix conductivity σ_m for constant pore water conductivity σ_w, which is obtained through equation 8.4, is shown in fig. 45. For σ_m increasing steadily from zero, IP rises rapidly from zero to a maximum and thereafter returns asymptotically, the amplitude, width and position of the maximum of the curve being controlled through r and r'. The ranges of values adopted for these two parameters here include those given in table 5 and the value of σ_w, 0.05 mhos m^{-1}, is typical of the groundwater in the Fylde.

There is a notable similarity between this result (fig. 45) and the variation of IP measured against the fractional clay content of sands and sandstones,

which for a selection of clay minerals has been observed by Ogilvy and Kuzmina (1972) and Keller and Frischknecht (1966). Their results have been reproduced in figs. 46a and b for comparison.

In figs. 43 and 44, IP has been plotted against σ_m for $\sigma_w = 0.053$ mhos m^{-1} using data from 6.e.

Although the ranges of the σ_m data are wide, unfortunately none of the values is low enough to confirm the predicted maxima of the IP - σ_m curves.

CHAPTER 9

GEOLOGICAL ASPECTS OF p AND q

For each group of sandstone samples which represent sandstone successions

not less than 20 m thick, relationships have been found between

permeability K, matrix conductivity σ_m and IP (equations 7.11, 8.3).

It is improbable that IP is directly dependent upon the permeability;

moreover a fundamental textural factor is implied which is constant

throughout each group.   This is the factor to which the parameters p and

q refer and which, from general observations, is probably associated with

the clay matrix.   This matrix has been shown to comprise interconnected

clay films and networks of membranes coating the sand grains (2.b), which

suggests that the constant values of p and q in a borehole section may be

due to a uniform clay mineralogy and a constant clay film thickness.   It

is easy to envisage how these two properties might account for the observed

relationships between K, σ_m and IP.   An increase of the (sand grain)

specific surface area due to a decrease of the modal grain size would be

accompanied by similar increases of both the specific surface area and

volume of the clay matrix.   It follows that the matrix conductivity would

increase correspondingly.   Measurements made with columns of sorted glass

beads have shown that permeability K is inversely related to the specific

surface area, which in fig. 47 has been plotted as an inverse proportionality

to the bead diameters.   Therefore consistent with the previous data (fig. 39)

an inverse relationship would be expected between K and matrix conductivity

σ_m.

X-ray diffraction analyses have been made of the clay matrices from sandstones

which cover a wide range of p and q to determine whether either of these two

parameters depends in any way upon clay mineralogy.   Quantitative analyses

of the results have not been attempted because of the inherent difficulties,

but it is noticeable that clays corresponding to samples of high p show a

strong response for Illite.   This may be seen in fig. 3 where, in general, the lower traces correspond to samples with higher p values.

As far as possible the clay residues for these x-ray analyses were prepared (2.c)to similar thicknesses, but it was very noticeable in the process that the sandstones with highest p values would release the greatest quantities of clay.   This also reflects their tendency to crumble readily, a property by which sandstones characterised by high p values could invariably be distinguished.   In contrast, those sandstones with low p values were always hard and contained visible authigenic quartz and usually considerably less clay.   Some examples of these different types of sandstone may be seen in the scanning electron micrographs (figs. 2a - f) where 2a is characterised by high p and 2c and e by low p.

The nature of p to adopt a specific value for a particular stratigraphical unit is particularly notable where p changes abruptly within an individual borehole section.   A good example of this has been noted in a borehole section of East Shropshire.   In fig. 48, where IP is plotted against log K for samples from this borehole, the data occur in two groups, the lower one of which is identical to the central Shropshire data (fig. 22i) for which p is estimated to be 1.15 and q 0.57.   For the upper group, p is estimated to be in the range 0.3 to 0.4 but q is undetermined.   Fig. 48 also refers to the borehole section on which are shown the individual sample depths, the solid circles corresponding to samples for which p = 1.15 and the open circles to those of the lower p value.   The former samples are typically soft, crumbling easily with abundant clay, whilst the latter are hard with much less clay.   p changes within one sampling interval at a depth between 390 ft and 400 ft corresponding to this major textural change of the sandstone.

Reinspection of the IP - log K data of fig. 22 reveals other possible examples of abrupt changes of p with depth within borehole sections, which of course in these cases would account for some of the observed scatter.   This is
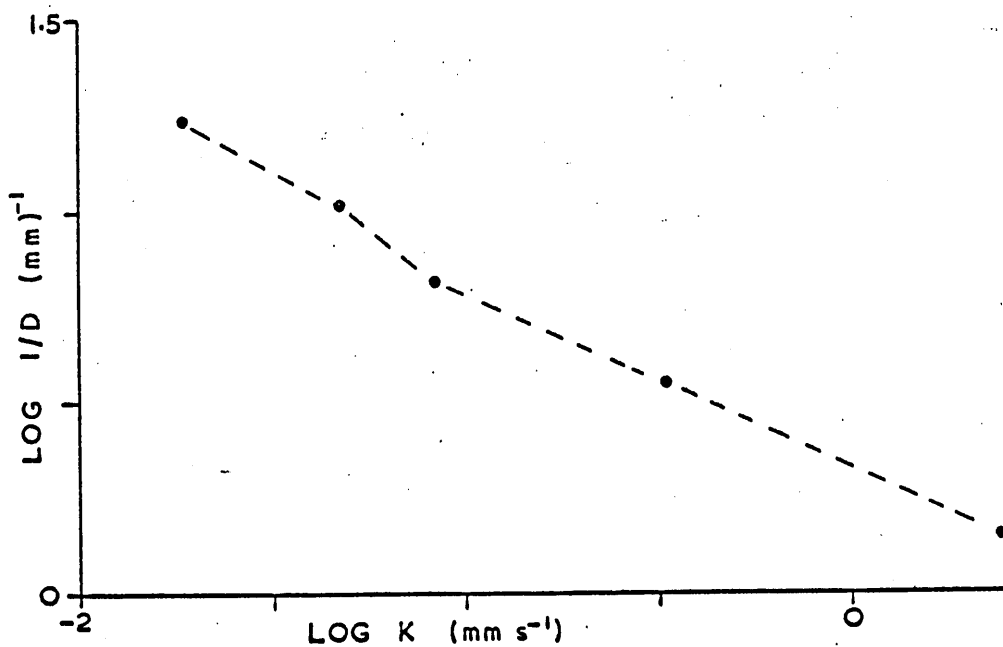
Variation of measured permeability (K) against specific surface
area of sorted glass beads. The specific surface area has been
calculated as an inverse proportionality to bead diameter, for
uniformly close packed beads.

FIG.47
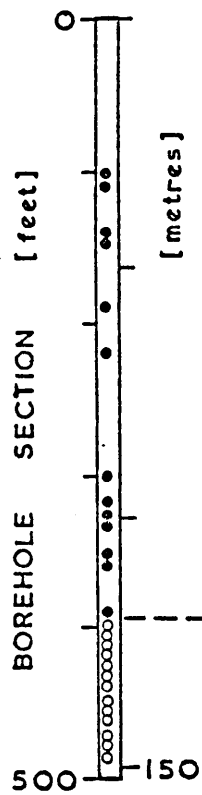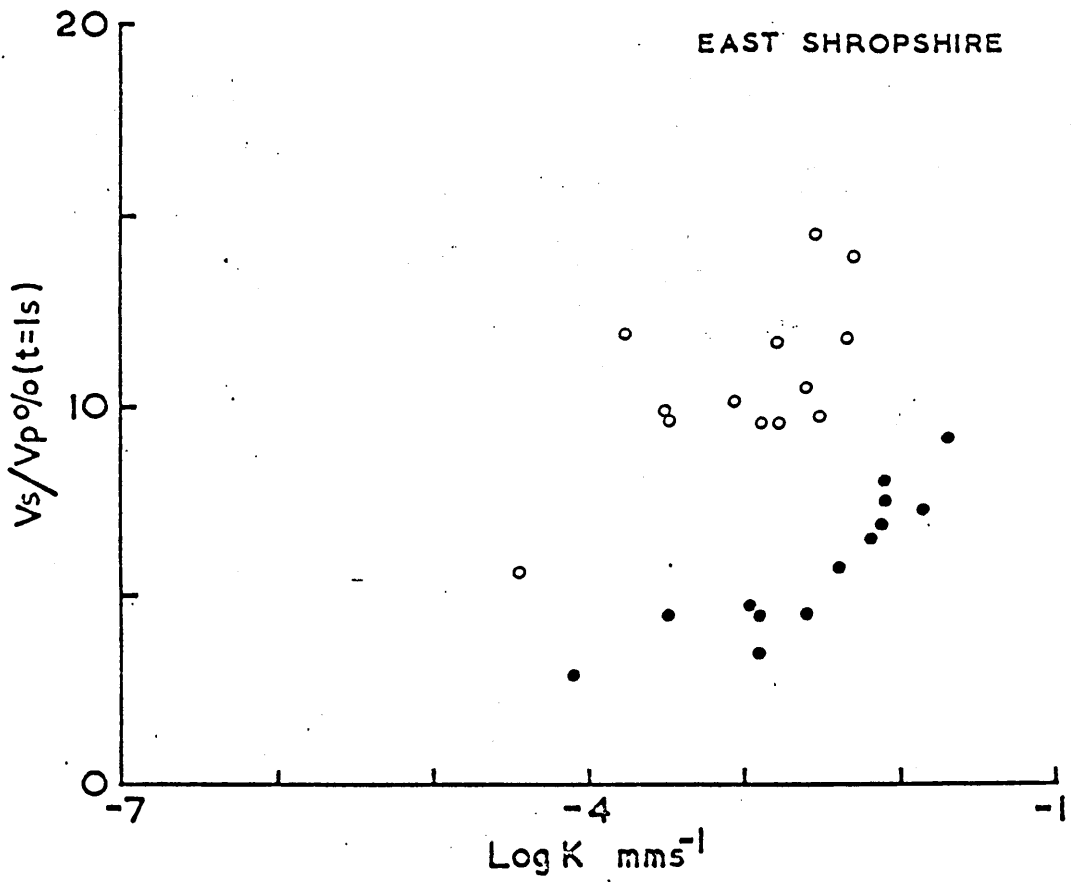
EAST SHROPSHIRE

Implied stratigraphic variation of
p and q in a borehole section in
East Shropshire. Estimated values are:

solid circles   p = 1.15   q = 0.57
open circles   p = 0.3 – 0.4   q undetermined

___ Level of textural change

FIG.48

almost certainly the case for the Cumberland data (fig. 22h) amongst which
there is a group of data which is distributed along a trend similar to that
of the Shropshire examples (fig. 22i), indicating a very high value for p.
Amongst the Fylde data, those for T37 and T73 (figs. 22a and g) might also
be divided, with the latter again including this very high value of p.
In fact the soft sandstones which are characterised by this high value of p
seem to be geographically widespread.

The values of p obtained in chapter 7 have been plotted on a map together
with those estimated from figs. 23a to g, and a general indication of the
lateral variation of this parameter within the Fylde has been obtained.
For convenience this has been incorporated in fig. 52 in the following
chapter.   These data refer to the top 30 m of sandstone and although more
than half are estimated, they indicate a general northerly increase of p.
These lateral variations may be transitional rather than abrupt as in the
vertical sections (e.g. fig. 48), although some sharp lateral fluctuations
may be expected across outcrops of contrasting dipping strata.

CHAPTER 10

FIELD MEASUREMENTS

The relationship (equation 7.11) between IP and permeability (K) would be particularly useful for determining the local average permeability of a sandstone aquifer from surface IP measurements, assuming prior knowledge of σ_w, p and q. Therefore some preliminary IP measurements have been made in the field to test whether this relationship can be applied.

The Fylde area was selected for these field tests because, having been studied previously in considerable detail, necessary information about the groundwater electrical conductivity and hydraulic conductivity was already available (Worthington 1971, Forshaw 1975).

10.a Survey details

48 time domain soundings in expanding Wenner configuration have been made over the drift covered sandstone aquifer. The electrode separation 'a' followed the sequence 1, 2, 4, 8, 16, 32, 64, 128, 192, 256 ft, occasionally extending to 384 ft. The stations were generally distributed in a narrow north - south band which extended approximately 12 km from Garstang to Broughton (north of Preston), to investigate regional variations of IP. At St. Michaels on Wyre, seven of these soundings were arranged in a close spaced traverse 2 km long to investigate the sensitivity of the IP to the rapid changes in aquifer conditions which are known to occur here.

The Wenner configuration was adopted to obtain large signal to noise ratios, the background noise levels being generally high in this area. This electrode arrangement is particularly prone to mutual induction between the transmitter (current) and receiver (potential) field wires and therefore these were laid well apart. The effect of this induction was assessed in

a simple test by twice measuring IP at an electrode separation of a = 256 ft,
on the second occasion having widely separated the wires. In this instance
the chargeability (Vs/Vp per cent) decreased by less than 0.1 in 3, which was
within the error of repeatability due to noise. Mutual induction for
separations less than 256 ft was therefore insignificant. Electrical noise,
usually 50 Hz, was greatest near power lines although spurious noise was
sometimes observed near to farm buildings. Furthermore it was noticed that
buried iron pipes or steel fencing gave local abnormally high IP anomalies
and therefore all these locations were avoided as far as possible. Negative
polarisations were rarely observed and then only near to buried pipe lines.

10.b Apparatus

The instruments used for the field survey were Huntec Mk.III time domain
transmitter and receiver. The 250 watts power of this constant current
transmitter was adequate for this survey when used with the Wenner electrode
configuration. It supplies a square wave current of which alternate pulses
have reversed polarity. The receiver synchronises remotely to this output
through the potential circuit and records the IP decay during the zero current
time (t off). In this instrument the polarisation Vs is integrated over four
consecutive periods tp, 2tp, 4tp and 8tp where tp is manually preselected.

The four time integrals of Vs are each divided by the corresponding duration
and presented as chargeabilities M_1 to M_4 by normalising against Vp as a
percentage. The chargeabilities can then be referred to a mid-time of each
period relative to the interruption of the primary·current, and by
preselecting an initial recording delay time, td, these chargeability times
can be varied to include most of the 'current off' time. The receiver also
records Vp, the primary voltage, whereas the current is measured and controlled
on the transmitter. Comprehensive descriptions of the instruments are given
in the manufacturer's manuals and by Hutchins (1971).

The cycle time of the instruments, (t on + t off) x 2, was set to the maximum of 16s with the duty ratio, t on/t off, at 1 to enable the optimum IP signal to noise ratio, although of course this also reduced the speed of the survey. For each electrode separation, IP was measured at two settings:

$$tp = 20 \text{ ms} \qquad td = 30 \text{ ms}$$
$$\text{and} \quad tp = 70 \text{ ms} \qquad td = 480 \times 5 \text{ ms}$$

The first setting measured the early part of the decay curve, whereas the second, for which M_4 corresponded to 3170 ms, enabled an SP correction to be calculated.

Copper sulphate porous pot electrodes were used for both the potential and current circuits and were capable of passing more than 400 mA, which was the maximum current used in the survey, without introducing spurious polarisation effects (Phillips and Richards 1974). The survey normally required a current of 100 mA.

10.c Preparation of field data

Although the Huntec Mk.III receiver automatically cancels the residual IP and SP input at the end of each zero current period, a correction to the chargeabilities M_1 to M_4 was required to obtain absolute values (Richards - personal communication). This correction was $- M_{t_s} /2$ where M is the chargeability at time t_s. t_s is given by $t_s = t_c \left(\dfrac{15}{32} - \dfrac{R}{2(R + 1)} \right)$ where t_c is the cycle time and R the duty ratio. (cf. Hutchins 1971 p.17). M_4 at t = 3170 ms has been taken as a close approximation to M at 3500 ms. The corrected values of M_1 to M_4 for tp = 20 ms have been weighted and averaged as

$$m_{(a)} = (M_1 + 2M_2 + 4M_3 + 8M_4) / 15$$

where $m_{(a)}$ is the apparent chargeability. The apparent resistivity $\rho_{(a)}$ has been calculated through the normal expression for the Wenner configuration:

$$\rho_{(a)} = \frac{Vp. \, 2\pi a}{I}$$

where 'a' is the electrode separation and I is the current.

Families of type curves for interpretation of time domain IP soundings are
not commonly available although various workers have proposed methods of
calculating these (e.g. Siegel 1959, Patella 1972, Elliot and Lauritsen 1977).
Calculation of a large number of theoretical curves for this work was not
convenient and therefore the method proposed by Patella (1973) was tried.
This method requires calculation of an apparent fictitious resistivity,
$\rho_{(a)'}$, as the product of the measured apparent resistivity and
chargeability i.e.

$$\rho_{(a)'} = m_{(a)} \rho_{(a)}$$

Interpretation of $\rho_{(a)'}$ as a function of the electrode separation 'a'
utilises the standard resistivity master curves from which the horizontal
layered sequences of resistivity $\rho_1 \ldots \rho_n$ and fictitious resistivity
$\rho_1' \ldots \rho_N'$ can be combined as

$$\rho_n / \rho_N' = m_n$$

where ρ_n and ρ_N' refer to the same layer and m_n is its chargeability.
Although the method is supported by rigorous theoretical treatment it was
found to be unsatisfactory for these data. Often where $m_{(a)}$ increased
with $\rho_{(a)}$ for a increasing, the product $m_{(a)} \cdot \rho_{(a)}$ exceeded the
theoretical limit k = +1.0 where in this case k is the 'reflection
coefficient' given by

$$k = \frac{\rho_2 m_2 - \rho_1 m_1}{\rho_2 m_2 + \rho_1 m_1}$$

An alternative simple method has therefore been devised.   Unlike Patella's
approach in which, for a homogeneous ground, resistivity ρ and forward
current density $\overrightarrow{Jss}$ are assumed constant and IP is represented as a time
variant reversed current of density - $\overrightarrow{J'}(t)$, this method treats IP as the
change of field produced by a constant current flowing through a time
variant resistivity.
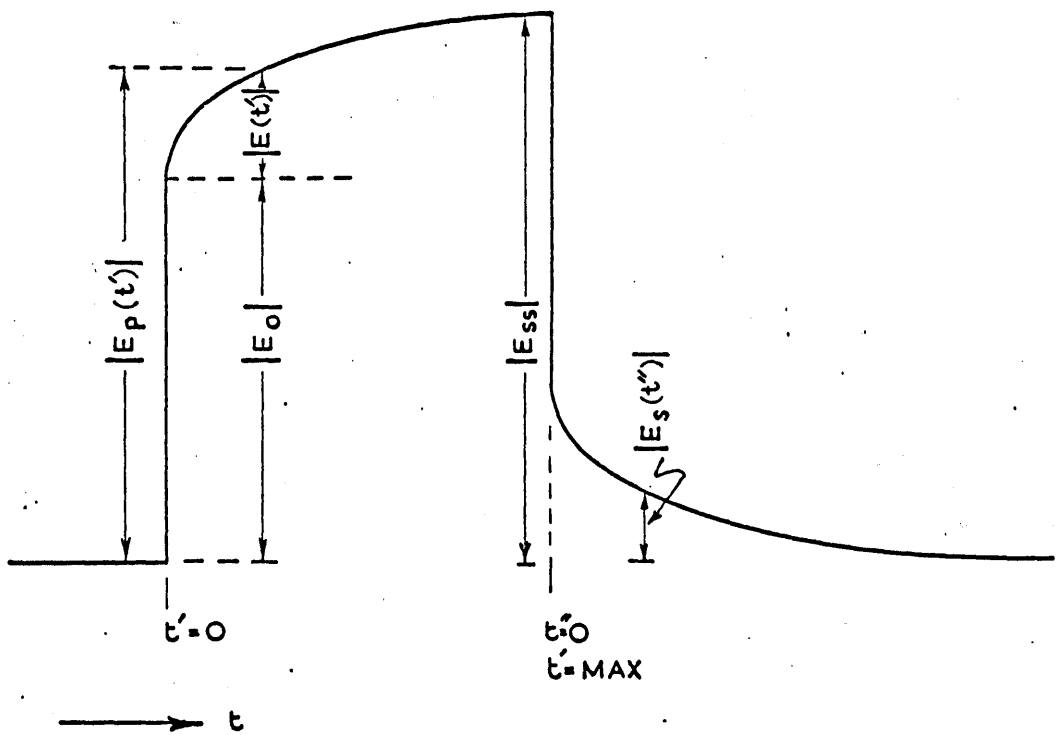
SYMBOLS USED TO DESCRIBE I.P. PULSE

FIG. 49

Using the notations given in fig. 49 the primary electric field $\overrightarrow{Ep}$ can be written

$$\overrightarrow{Ep}\,(t') \;=\; \overrightarrow{Eo} \;+\; \overrightarrow{E}\,(t') \qquad\qquad \dots \quad 10.1$$

where $\overrightarrow{Eo}$ is the instantaneous primary field ($t' = o$) and $\overrightarrow{E}\,(t')$ the time dependent component due to increasing resistivity. Linearity between charge and discharge of the rock is assumed such that

$$\overrightarrow{Es}\,(t'') \;=\; \overrightarrow{Ess} \;-\; \overrightarrow{Ep}\,(t') \qquad\qquad \dots \quad 10.2$$

where $\overrightarrow{Es}\,(t'')$ is the de-polarisation field, $\overrightarrow{Ess}$ the primary steady state field and t' and t'' refer to equal polarisation and de-polarisation times respectively. This assumption has also been implied by other workers (e.g. Keller and Frischknecht 1966, Patella 1972). Therefore the chargeability, m, of a rock is defined as:

$$m \;=\; \overrightarrow{Es}\,(t'' = o) \,/\, \overrightarrow{Ess} \qquad\qquad \dots \quad 10.3$$

but is measured as $\quad m = \overrightarrow{Es}(t'' = t) \,/\, \overrightarrow{Ep}\,(t')$

where usually t is less than t'.

For $t' = 0$ the ground is considered to comprise two superimposed resistivities ρ_A and ρ_B such that the constant current, density $\overrightarrow{J}$, may be written

$$\overrightarrow{J} \;=\; \overrightarrow{JA} + \overrightarrow{JB} \qquad\qquad \dots \quad 10.4$$

and $\qquad \overrightarrow{JA}\cdot\rho_A \;=\; \overrightarrow{JB}\cdot\rho_B \;=\; \overrightarrow{Eo} \qquad\qquad \dots \quad 10.5$

As t' increases, polarisation is represented by an increase of ρ_B such that when the steady state is approached, ρ_B tends to infinity. In this condition

$$\overrightarrow{Ep} \;=\; \overrightarrow{Ess}$$

and $\qquad \overrightarrow{J}\cdot\rho_A \;=\; \overrightarrow{Ess} \;=\; \overrightarrow{Eo} + \overrightarrow{E}\,(t' = \text{max}) \qquad \dots \quad 10.6$

Combining equations 10.5 and 10.6

$$\rho_A\,(\overrightarrow{J} - \overrightarrow{JA}) \;=\; \overrightarrow{E}\,(t' = \text{max})$$

which with 10.4 gives

$$\frac{\rho_A\,\overrightarrow{Eo}}{\rho_B} \;=\; \overrightarrow{E}\,(t' = \text{max})$$

Writing $\vec{Eo}$ as $(\vec{Ess} - \vec{E}(t' = max))$

$$\rho_B = \rho_A \frac{(\vec{Ess} - \vec{E}(t' = max))}{\vec{E}(t' = max)}$$

Therefore through equation 10.3 which, from equations 10.2 and 10.6, can be written $m = \vec{E}(t' = max) / \vec{Ess}$

$$\rho_B = \rho_A \frac{(1 - m)}{m} \qquad \ldots \quad 10.7$$

Substituting 10.7 in 10.6

$$\vec{J} = \vec{Ess} \frac{(1 - m)}{m} \cdot \frac{1}{\rho_B} \qquad \ldots \quad 10.8$$

If m and ρ_B are isotropic, $\vec{J}$ is continuous and the field may be written $\vec{Ess}(1 - m) / m$, equation 10.8 can be solved for a theoretical ground of homogeneous horizontal layers with contrasting resistivities ρ_B, through Stefanescu's equation (e.g. Keller and Frischknecht 1966). In this case, because linearity of charge and discharge has already been assumed, if it is also assumed that all layers reach the steady state simultaneously, then the surface apparent resistivity $\rho_{B(a)}$ can be written from equation 10.7:

$$\rho_{B(a)} = \rho_{A(a)} \frac{(1 - m_{(a)})}{m_{(a)}}$$

where $m_{(a)}$ is the measured chargeability at $t'' = 0$

and $$\rho_{A(a)} = V_p 2\pi a / I$$

for a Wenner configuration of spacing a on which V_p is the measured potential difference at $t' = max$, and I is the current.

The vertical sequences of ρ_A and ρ_B can be interpreted with the aid of standard resistivity curves and therefore the chargeability of any layer is obtained through:

$$m = \frac{\rho_A}{\rho_A + \rho_B}$$

Clearly the method is approximate in practice because it assumes that the de-polarisation field decays to zero at the same time in all layers and that steady state conditions are reached.

The $\rho_{A(a)}$ and $\rho_{B(a)}$ data (see appendix) have been interpreted using two layer master curves in conjunction with a generalised set of auxiliary curves (Koefoed 1960). The $\rho_{B(a)}$ data, plotted as log $\rho_{B(a)}$ against log 'a' varied smoothly and for spacings up to 192 ft were all contained well within the unity limits of the reflection coefficient. Two typical examples are shown in fig. 50a and b. In a few cases only for spacings of 192 ft or greater, unacceptably sharp increases of $\rho_{B(a)}$ resulted from corresponding decreases of $m_{(a)}$, the most likely explanation for which is inductive coupling. However, data at these large spacings were not essential to the interpretation, especially as most soundings were limited to a maximum separation of 256 or 384 ft. The effect would probably be avoided by rearranging the field layout. An example of this behaviour of $\rho_{B(a)}$ is given in fig. 50c.

10.e Discussion of results

In almost all of the interpreted sections, the top sandstone layer has been distinguished from the overlying drift through its greater chargeability associated with a resistivity in the range 60 to 120 ohm m. The thicknesses of drift defined in this way have not been dealt with in detail here but were reasonably compatible with borehole sections and Worthington's (1972) isopachyte map.

The chargeabilities of the sandstone, although usually higher than those of the drift, were much lower than those recorded in the laboratory. There are probably three factors that may account for this. Firstly the charging times are different, 4s and 180s for the field and laboratory respectively although these are largely offset by the corresponding delay times, 30 ms and 1000 ms. Undoubtedly two principal causes are that the field measurements do not resolve the small scale variations in rock properties but record averaged IP values for the whole bulk, and that these values will be further modified by the pore water chemistry and the partly dependent clay lattice chemistry, according to the types and concentrations of anions and cations present.

(a)

No 11 JUNE 74   SD 5000 3920

LOG $\rho_{A(a)}$ LOG $\rho_{B(a)}$

3.0 — 5.0

2.0 — 4.0

10   a   100

$$\frac{\rho_A}{\begin{array}{c}120\\\hline320\end{array}}\quad\begin{array}{c}d\\0\\18\end{array}$$

$$IP_{sst} = \frac{320}{11320} = 2.8\%$$

$$\frac{\rho_B}{\begin{array}{c}57000\\\hline11000\end{array}}\quad\begin{array}{c}0\\12\end{array}$$

(b)

No 30 JUNE 74   SD 5034 4121

LOG $\rho_{A(a)}$ LOG $\rho_{B(a)}$

3.0 — 5.0

2.0 — 4.0

10   a   100

$$\frac{\rho_A}{\begin{array}{c}450\\\hline2100\\\hline250\end{array}}\quad\begin{array}{c}d\\0\\4.5\\45\end{array}$$

$$IP_{sst} = \frac{250}{8450} = 3.0\%$$

$$\frac{\rho_B}{\begin{array}{c}32000\\\hline130000\\\hline8200\end{array}}\quad\begin{array}{c}0\\5.5\\50\end{array}$$

(C)

No 9 NOV 73   SD 5047 4527

LOG $\rho_{A(a)}$ LOG $\rho_{B(a)}$

3.0 — 5.0

2.0 — 4.0

10   a   100

$$\frac{\rho_A}{\begin{array}{c}250\\\hline1400\\\hline250\end{array}}\quad\begin{array}{c}d\\0\\6.5\\30\end{array}$$

$$IP_{sst} = \frac{250}{6250} = 4.0\%$$

$$\frac{\rho_B}{\begin{array}{c}34000\\\hline6000\end{array}}\quad\begin{array}{c}0\\34\end{array}$$

EXAMPLES OF WENNER SOUNDING CURVES OF $\rho_{A(a)}$ AND $\rho_{B(a)}$ (Ω ft) AT SPACING a (ft). INTERPRETATIONS GIVE ρ_A, ρ_B, DEPTH d (ft) AND CHARGEABILITY (IP) = $\rho_A / \rho_A + \rho_B$. $\bullet \rho_{A(a)}$ data   o $\rho_{B(a)}$ data.

FIG. 50

The areal distribution of sandstone chargeabilities (fig. 51) varies notably. Around Broughton, in the southern end of the area, the values are particularly low, about 1%, whereas north of grid line 3600 they rise rapidly to the lower 3% level and remain fairly constant through Barton to Myerscough where around northings 4000 and 4100 the highest levels are reached at 4% or more.

Beyond here the values decrease again gradually. These chargeabilities have to be considered against the distributions of p, q and σ_w to investigate the average permeability K.

10.f Comparisons of permeabilities calculated through equation 7.11 with aquifer permeabilities

At this stage of the work there are several difficulties which preclude direct comparison between permeabilities predicted through equation 7.11 and the actual permeabilities of the aquifer. One of these difficulties is the large discrepancy, noted above, between the magnitudes of laboratory and field measured chargeabilities. As yet this discrepancy is unresolved and therefore if equation 7.11 is applied to field chargeability data (fig. 51), the calculated permeabilities may be unrealistically low.

The areal distribution of values of the parameters p and q is largely unknown at present, although a further programme of sampling and measuring would furnish this information. However the five values of p that were determined in chapter 7 have been used to estimate p for other borehole sections, mostly by comparing IP - permeability data at $\sigma_w = 0.05$ mhos m^{-1} from 6.c, and all the values have been included in fig. 52, although the extra errors on the estimated values may be at least 0.05. Values of q are difficult to estimate from data at $\sigma_w = 0.05$ mhos m^{-1} and for convenience have been omitted. In fact in fig. 37 it is evident that the parameter q has little effect upon the IP for most of the sandstone permeability range unless groundwater conductivities greatly exceed this level.

A contour map of groundwater conductivities of the area has been taken from Worthington (1971) and, represented as conductivities σ_w, is included in fig. 52. Over the survey area σ_w generally occurs within the range 0.04 to 0.067 mhos m^{-1} which, for sodium chloride solution, is the range for the largest IP maxima. The effects upon IP of variable groundwater chemistry have not been considered.

Through equation 7.11 permeabilities have been calculated from the field chargeabilities (fig. 51) using the values of p and σ_w from fig. 52 and adopting values of q from the four boreholes T37, T41, T62 and T69 (table 4b and fig. 51). Predictably the calculated permeabilities are very low but cover a range of up to four orders of magnitude. However using the sparse p and q data available, it was found that over quite large areas the calculated permeabilities do not vary greatly and therefore it has been convenient to present the results (fig. 53) as shaded areas in each of which permeabilities are generally similar within one order of magnitude. Between adjacent areas there may be as much as two orders of magnitude difference. It is very noticeable that there is a marked decrease of permeabilities shown from Garstang and St. Michaels on Wyre in the north to Broughton in the south.

For comparative purposes an appropriate measure of actual aquifer permeabilities would be obtained by calculating hydraulic conductivities from well pump tests. Unfortunately in those cases where flow of water may be partly along fissures, these hydraulic conductivities cannot be taken to represent average intergranular permeabilities but only the maximum possible values. Consequently direct comparisons between the average permeabilities calculated from IP data and the hydraulic conductivities indicated by pump tests will be unreliable where, as in the Fylde (Crook, Howell, Woodhead and Worthington 1973, Brereton and Skinner 1974, Worthington 1977), the degree of fissuring is largely unknown but thought to be areally variable.
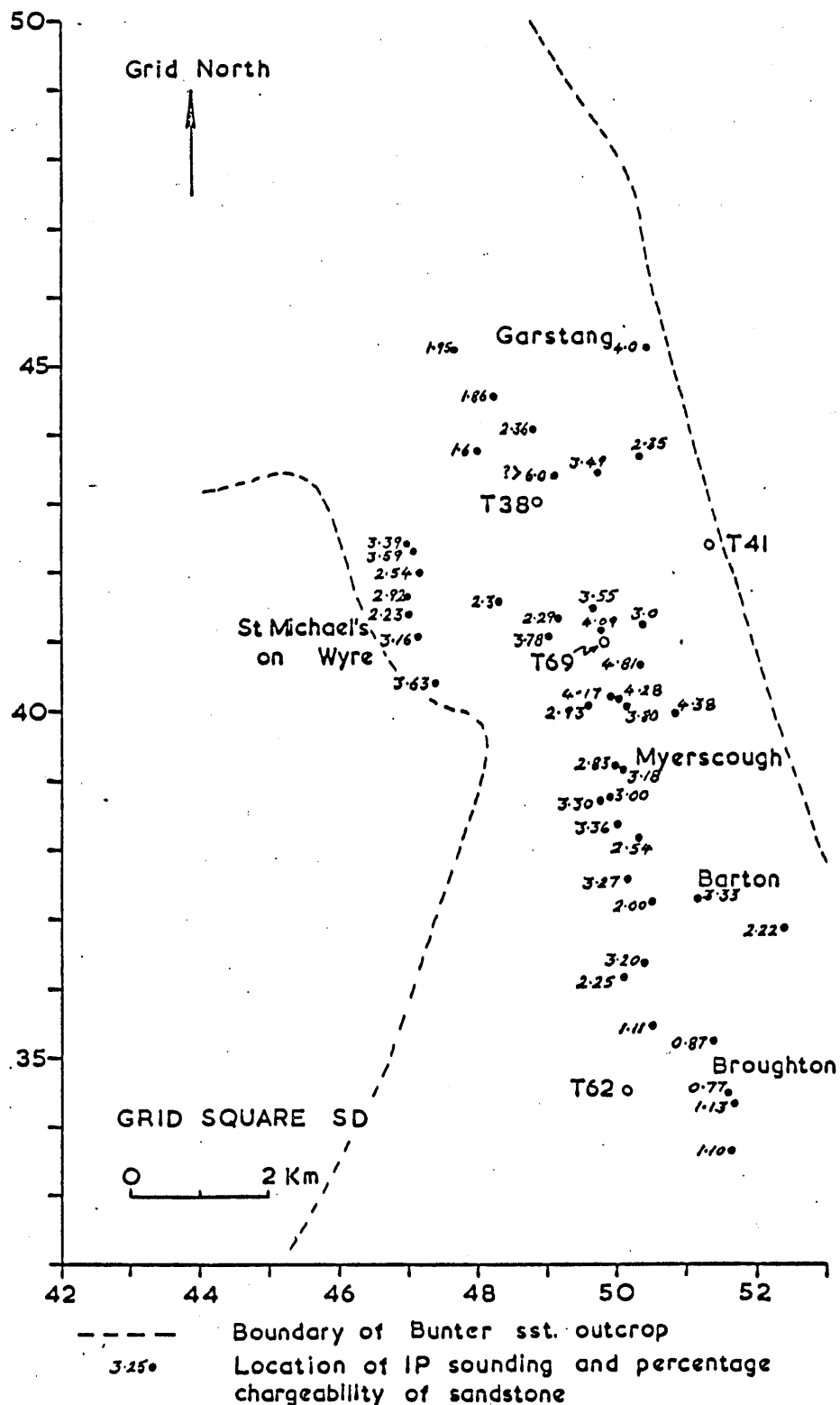
Distribution of sandstone percentage chargeabilities in the Fylde.
Measurement parameters described in 10.b and c.

FIG.51

Distribution of the analysed (7.d) and estimated values of p,
with contours of groundwater conductivity (after Worthington 1971)

FIG.52
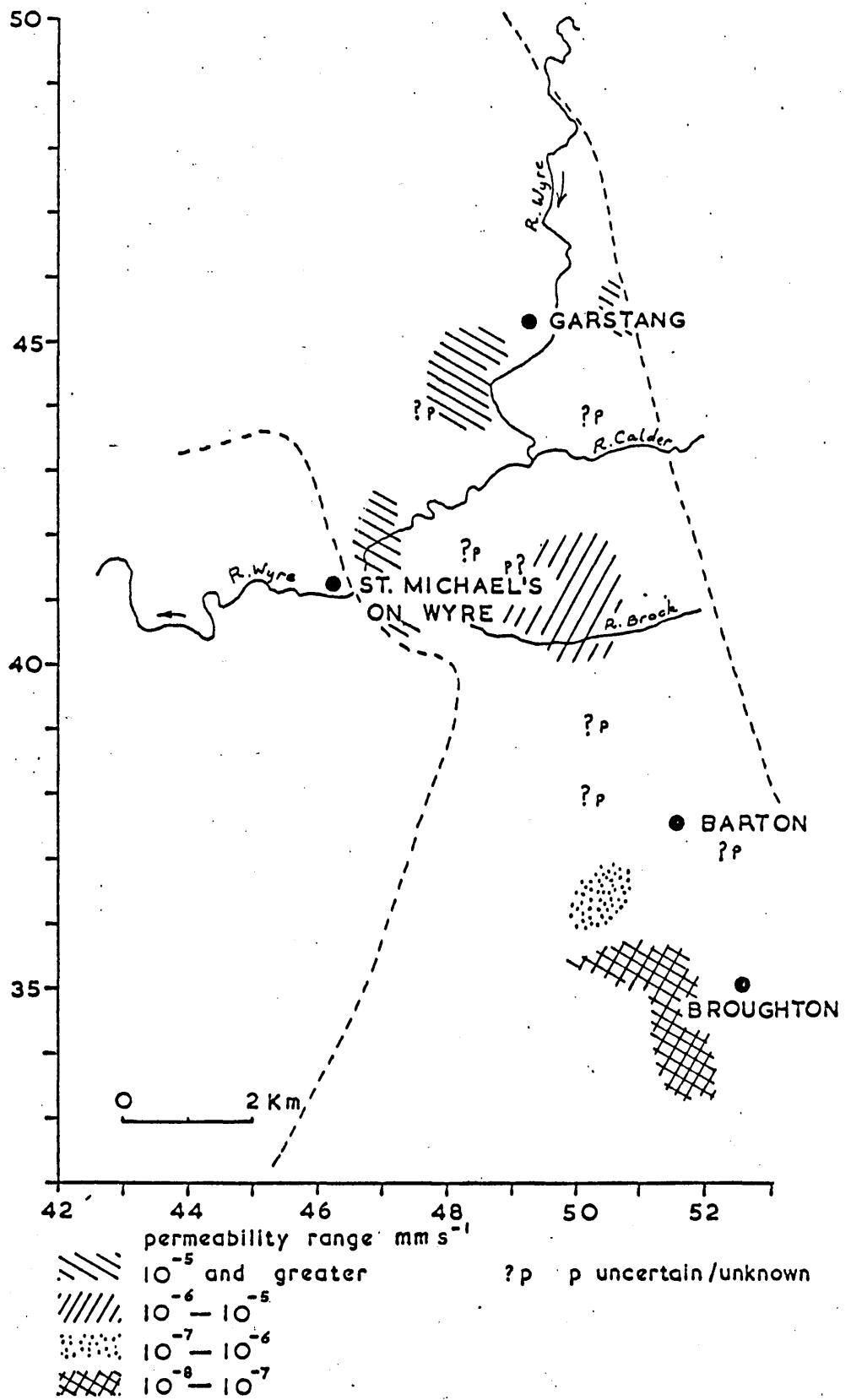
Distribution of average sandstone permeabilities (top 30 m) in the Fylde calculated through equation 7.11, using the data in figs. 51 and 52.
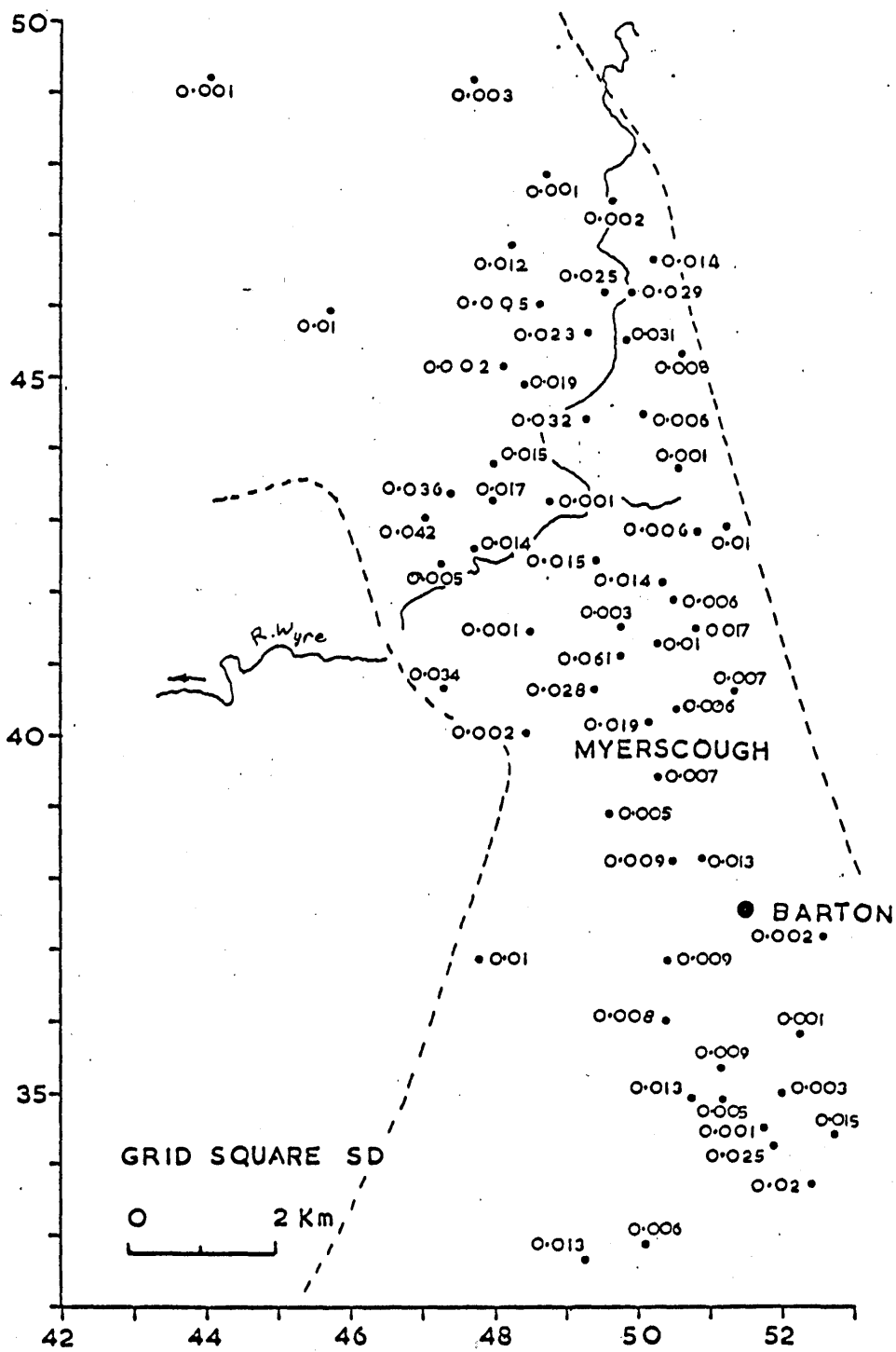
FIG.53

HYDRAULIC CONDUCTIVITIES (mm s⁻¹) IN THE FYLDE
CALCULATED FROM PUMP TEST DATA. (FORSHAW 1975 Fig 5.3)

FIG. 54

K mm s⁻¹

1	—	0·0012
2	—	0·0017
3	—	0·0024
4	—	0·0029
5	—	0·0058
6	—	0·0087
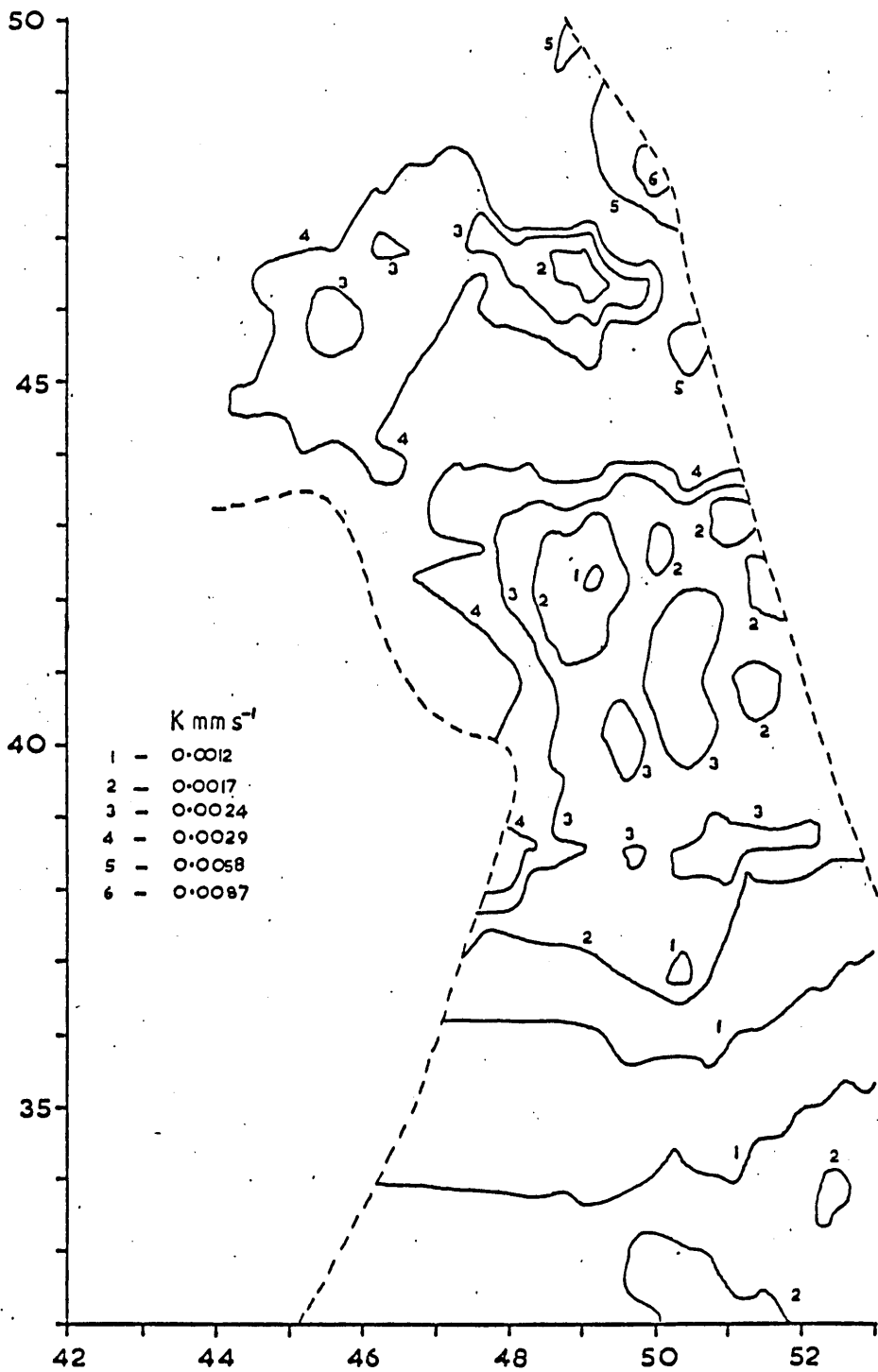
AVERAGED   INTERGRANULAR   PERMEABILITY   USING   FOUR
NEAREST   NEIGHBOURS   (FORSHAW 1975 Fig A 3·5)

FIG.55

Hydraulic conductivities calculated by Forshaw (1975) are shown in fig. 54. These data exceed the permeability values calculated through equation 7.11 (fig. 53) by factors varying between two orders of magnitude in the north and five orders in the south. Comparing the areal variations, in both cases the greatest magnitudes are indicated in the north, otherwise there is no obvious similarity between them.

In discussion of the Fylde aquifer, Brereton and Skinner (1974) have expressed their opinion that the average sandstone permeability is fairly uniform throughout the area and that the flow of water is controlled locally almost entirely by the degree of fissuring. In that case the areal variation of permeability shown in fig. 53 and the method of calculation from field chargeabilities should be rejected. On the other hand Worthington (1977) presents data to show that the contribution of intergranular flow in this aquifer is areally very variable and in many places more significant than the flow from fissuring.

Forshaw (1975) and Worthington (1977) independently have indicated a zone of the aquifer, up to 3 km wide and following approximately the course of the river Wyre, where they describe the groundwater flow as being dominantly intergranular. Therefore the consistently high hydraulic conductivities in this area (fig. 54) imply highest average sandstone permeabilities here, with which observation the tentative results in fig. 53 are generally consistent.

For the region immediately to the south, between Myerscough and Barton, Worthington (1977) considers that '... comparatively strong intergranular flow is enhanced by localised fissuring.' and in fact the scatter of values amongst the hydraulic conductivity data (fig. 54) for this area is compatible with his view. Furthermore he cites one example of very high hydraulic conductivity here which probably has been exaggerated by flow from the overlying drift. So despite some high hydraulic conductivities (fig. 54), the permeabilities

calculated from the IP data here (fig. 53) possibly reflect the field conditions inasmuch as they are slightly lower than those permeabilities immediately to the north.

Further south around Broughton, the consistently low field chargeabilities (fig. 51) have led to very low permeabilities (fig. 53) in the calculations whereas hydraulic conductivities again are variable. For this district, where additional information on the degree of fissuring is not available, it is not possible to comment on the data further, although from borehole seismic velocity analyses, Forshaw (personal communication 1978) anticipates that sandstone permeabilities might be very low over much of this area.

Forshaw (1975 fig. A3.5) has produced a computer contoured map of averaged sandstone permeabilities, based upon extensive sample permeability measurements in the laboratory. This map, reproduced in fig. 55, emphasises that the actual average values could be several orders greater than those calculated through equation 7.11 but shows a distribution of permeabilities with which that shown in fig. 53 is encouragingly compatible.

It is disappointing that at this stage of the work, for the several reasons discussed, the results cannot be rigorously tested. But there appears to be some qualitative evidence that this method of estimating the average sandstone permeabilities from field chargeabilities may yet be feasible.

CONCLUSIONS

This research has achieved the original objectives insofar that, in the laboratory, IP has been found to vary smoothly with the permeability K and matrix conductivity σ_m of Bunter sandstones and the form of these variations have been described, albeit empirically. In fact although attempts failed to quantify the lab results on a sound theoretical basis, so far the empirical approach appears to be fairly successful. Some inadequacies of these empirical equations can be seen, for example the sharpest maxima of IP against water conductivity are not described completely but generally the equations can accommodate a wide range of data and, incorporating a minimum number of variables, are sufficiently simple to be practical for field applications.

It is felt that before the evaluated constants can be reliably accepted, particularly that of z (equation 7.3), many more analyses should be completed. This is largely because the number of available data was eventually reduced to an absolute minimum through the sequence of analyses and therefore the accumulated errors increased. The form of the empirical equations adopted to describe the data also needs to be fully tested.

The electron microscope and x-ray analyses of the clay matrices have not been very useful although several interesting features were noted. Despite these studies, the mineralogical significances of the parameters p and q are still unknown. This is a topic which may be worthwhile pursuing, particularly if rock types other than Bunter sandstone are to be considered. Schoeppel and Thrasher (1966) have observed that IP varies with the cation exchange capacities of sandstones and Keller and Frischknecht (1966) have shown a linear proportionality between observed IP and their qualitative anion trap number, the calculation of which incorporates the cation exchange capacity. Intuitively it seems that a study of the cation exchange capacities of the Bunter sandstones, measured by the method outlined by Keller and Frischknecht

and in conjunction with further x-ray analyses, ought to reveal the mineralogical significances of the parameters p and q.

Disappointingly, the efforts to extend the work to field applications have not given positive results, the problems being the obvious discrepancy between laboratory and field chargeability values and the lack of adequate knowledge of field permeabilities. The first of these difficulties can be eliminated by repeating the laboratory measurements, controlling conditions to be as practically close as possible to those of the aquifer. For example, it is suggested that dehydration of the samples should be avoided at all stages and initially they should be stored in their own groundwater to prevent chemical contamination. A programme of work could include IP logging of several boreholes, using a large diameter short lateral sonde. The results would be compared with laboratory IP data from a corresponding sequence of samples initially saturated with the local groundwater and subsequently with different electrolyte solutions, to determine the relative effects. It is important that measurement parameters e.g. cycle period t, duty ratio (t on/t off), delay time t_d and integration period t_p be standardised for the field and laboratory.

The problem of finding a reliable guide to field permeabilities for comparative purposes is more difficult and for the time being in the case of partly fissured aquifers such as the Fylde, semi-quantitative comparisons may have to be accepted.

Further research should investigate the effects of variable groundwater chemistry, particularly upon the parameters z (equation 7.3), m and m' (equations 7.9,7.10) because the whole approach to the field analyses relies on the stability of these values. The complications of electrical and hydraulic anisotropy must also be considered at some stage.

The procedure described so far for determining aquifer permeabilities from IP data has involved lengthy laboratory analyses to evaluate p and q over the area of interest. Provided that the parameters z, m and m' are known, in future p and q may be determined rapidly by measuring the groundwater conductivity, σ_w, the chargeabilities and permeabilities K of each borehole sequence, then solving equation 7.3 by least squared errors analyses. This approach avoids the process of repeating IP measurements on each sample at different pore water conductivities, but may induce large errors in the obtained values of q. However, in practice these errors may not be important. In fact there is room for further practical improvement, by developing techniques of measuring IP and permeability K directly upon fresh borehole cores.

At this stage it is difficult to estimate the sort of accuracy that might be achieved when estimating intergranular permeability, although from the laboratory data in figures 22a to i, an error of half an order of magnitude seems possible. For a reconnaissance method however this is not greatly important.

REFERENCES

AKROYD, T.N.W., 1957. Laboratory Testing in Soil Engineering. Soil Mechanics Ltd. London.

ARCHIE, G.E., 1942. The electrical resistivity log as an aid in determining some reservoir characteristics. Trans.Am.Inst. Min. metall.Engrs. 146 54-62.

BARKER, R.D., 1971. An Induced Polarization Investigation of a Bunter Sandstone Aquifer. Ph.D. thesis unpublished, University of Birmingham.

_____ and WORTHINGTON, P.F. 1973a. Some hydrogeophysical properties of the Bunter sandstone of northwest England. Geoexploration 11 151-170.

_____ and WORTHINGTON, P.F. 1973b. The hydrological and electrical anisotropy of the Bunter sandstone of northwest Lancashire. Q.J.Eng.Geol 6 169 - 175.

BERTIN, J., 1976. In J. BERTIN and J. LOEB. Experimental and Theoretical Aspects of Induced Polarization. Vol.1. Presentation and Application of the IP Method - Case Histories. Geoexploration Monograph Series 1 No.7 Gebruder Borntraeger. Berlin.

BEUTELSPACHER, H. and VAN DER MAREL, H.W.,1968. Atlas of Electron Microscopy of Clay Minerals and their Admixtures. Elsevier Publishing Co. Amsterdam.

BODMER, R., WARD, S.H., and MORRISON, H.F.,1968. On induced electrical polarization and groundwater. Geophysics 33 No.5 805 - 821.

BRERETON, N.R. and SKINNER, A.C. 1974. Groundwater flow characteristics in the Triassic sandstone in the Fylde area of Lancashire. Water Services (August) 275 - 279.

COLLAR, F.A., and GRIFFITHS, D.H., 1976. A laboratory study of the relationships between induced polarization, permeability and matrix electrical conductivity in Bunter sandstones. Q.J.Eng.Geol.9 57-63.

COLLETT, L.S., 1959. Laboratory Investigation of Overvoltage. In - Overvoltage Research and Geophysical Application. (ed) J.R. WAIT. Pergamon Press London.

CROOK, J.M., DAW, G.P., HOWELL, F.T. and MORGAN, F.R., 1971. Permeation properties of unfissured Bunter sandstones of Lancashire and Yorkshire. Geotechnique 21 No.3 256-259.

CROOK, J.M., HOWELL, F.T., WOODHEAD, F.A. and WORTHINGTON, P.F., 1973. Permeation properties of Bunter sandstones from the Cheshire and Fylde basins. Geotechnique 23 262-265.

ELLIOT, C.L. and LAURITSEN, E., 1977. Induced polarization response of a horizontally multilayered earth with no resistivity contrast. Geophys. Prospect. 25 No. 1 76-95.

FORSHAW, J.R. 1975. Seismic wave velocities and their application to the prediction of water well yield. Ph.D. thesis unpublished, University of Birmingham.

GREENSMITH, J.T., 1978. Petrology of the sedimentary rocks. Allen and Unwin. London.

HAUSER, E.A.,1953. Colloid science of montmorillonite and bentonite. Proc.2nd.Nat.Conf. Clays and Clay Minerals University of Missouri. p.439.

HENKEL, J.H. and COLLINS, T.C., 1961. Induced polarization in electrolyte saturated earth plugs. Geophysics 26 No. 2 205-210.

_____ and VAN NOSTRAND, R.G., 1957. Experiments in induced polarization. Trans. Am.Inst.Min.metall.Engrs.(Mining Eng.) 9 355-357.

HELFFERICH, F. 1962. Ion Exchange. McGraw Hill. New York.

HILL, H.J. and MILBURN, J.D. 1956. Effect of clay and water salinity on electrochemical behaviour of reservoir rocks. Trans.Am.Inst. Min.metall.Engrs. 207 65-72.

HUNTER, R.A., 1959. Electrical polarization of soil samples; M.S. thesis, University of Georgia. Cited in HENKEL and COLLINS (1961).

HUTCHINS, R.W., 1971. A new induced polarization instrument, Huntec Ltd.,1450, O'Connor Drive, Toronto.

IVES, D.J.G. and JANZ, G.J. (eds), 1961. Reference Electrodes, Theory and Practice. Academic Press. London.

JOHNSON DIV. U.O.P. Co.,1966. Groundwater and Wells. Saint Paul, Minnesota 55165.

KEEVIL, N.B.,Jr. and WARD, S.H.,1962 Electrolyte activity; its effect on induced polarization. Geophysics 27 No.5 677-690.

KELLER, G.V. and FRISCHKNECHT, F.C.,1966. Electrical Methods in Geophysical Prospecting. Pergamon Press. Oxford.

KOEFOED, O.,1960. A generalised Cagniard graph for the interpretation of geo-electrical sounding data. Geophys.Prospect.8 No.3 459-469.

LOEB, J.,1976. In J. BERTIN and J. LOEB. Experimental and Theoretical Aspects of Induced Polarization Vol.2. Macroscopic and Microscopic Theories. Geoexploration Monograph Series 1 No.7 Gebruder Borntraeger. Berlin.

LYNCH, E.J.,1962. Formation Evaluation. Harper and Row New York.

MARSHALL, C.E., 1949. The Colloid Chemistry of the Silicate Minerals Academic Press. New York.

MARSHALL, D.J. and MADDEN, T.R., 1959. Induced polarization, a study of its causes. Geophysics 24 No.4 790-816.

MAYPER, V. Jr. 1959. The Normal Effect - Part 1. In - Overvoltage Research and Geophysical Application.(ed) J.R.WAIT. Pergamon Press. London.

McCARDELL, W.M., WINSAUER, W.O. and WILLIAM, M., 1953. Origin of the electric potential observed in wells. Trans.Am.Inst.Min.metall. Engrs. 198 41-48.

MOUNCE, W.D. and RUST. W.M.,1944. Natural potentials in well logging. Trans.Am.Inst.Min.metall.Engrs.155 49-55.

OGILVY, A.A. and KUZMINA, E.N.,1972. Hydrogeologic and engineering-geologic possibilities for employing the method of induced potentials. Geophysics 37 No.5 839-861.

PATELLA, D.,1972. An interpretation theory for induced polarization - vertical soundings (time-domain). Geophys. Prospect. 20 No.3 561-579.

_____ 1973. A new parameter for the interpretation of induced polarization field prospecting (time-domain). Geophys. Prospect. 21 No.2 315-329.

PATNODE, H.W. and WYLLIE, M.R.J.,1950. The presence of conductive solids in reservoir rocks as a factor in electric log interpretation. Trans.Am.Inst.Min.metall.Engrs.189 47-52.

PHILLIPS, W.J. and RICHARDS, W.E., 1974. A comparison of transient
Voltage decay curves obtained with different electrode arrays
and configurations over a mineralized zone. Geophys.Prospect.
22 No.1 22-53.

SAMI SOLIMAN MOHAMED, 1970. Induced polarization, a method to study
water collecting properties of rocks. Geophys.Prospect.
18 supplement 654-665.

SCHOEPPEL, R.J. and THRASHER, J.E.,1966. Laboratory study of induced
polarization in sandstone rocks with varying salinity and
shalyness. Trans.Soc.Prof.Well log Anal. Seventh Annual Logging
Symposium 1-42.

SIEGEL, H.O.,1959. Mathematical formulation and type curves for
induced polarization. Geophysics 24 547-565.

SPIEGLER, K.S.,YOEST,R.L., and WYLLIE, M.R.J.,1956. Electric
potentials across porous plugs and membranes - ion exchange
resin-solution systems. Discuss. Faraday Soc 21 174-185.

STALDER, P.J., 1973. Influence of crystallographic habit and aggregate
structure of authigenic clay minerals on sandstone permeability.
Geologie.Mijnb. 52 217-220.

TOPPING, J. 1972. Errors of observation and their treatment. 4th ed.
Chapman and Hall Ltd. London.

VACQUIER, V., HOLMES, C.R., KINTZINGER, P.R., and LAVERGNE, M., 1957.
Prospecting for groundwater by induced electrical polarization.
Geophysics 22 No. 3 660-687.

WINSAUER, W.O. and McCARDELL, W.M., 1953. Ionic double-layer
conductivity in reservoir rock. Trans.Am.Inst.Min.metall.Engrs.
198 129-134.

WORTHINGTON, P.F.,1970. Geophysical investigation of a Permo-Triassic
sandstone aquifer. Ph.D. thesis unpublished. University of
Birmingham.

_____ 1971. The use of resistivity logging to estimate borehole yield
from a matrix-conducting sandstone. Q.J.Eng.Geol.4.No.4 263-279.

_____ 1972. A geoelectrical investigation of the drift deposits in
northwest Lancashire. Geol.J., 8 Pt 1 1-16.

_____ 1976. Hydrophysical properties of parts of the British Trias.
Geophys.Prospect. 24 No.4 672-695.

_____ 1977. Permeation properties of the Bunter sandstone of northwest
Lancashire, England. J. Hydrol. 32 295-303.

_____ and BARKER, R.D. 1972. Methods for the calculation of true
formation factors in the Bunter sandstone of northwest England.
Engng. Geol.6 213-228.

_____ and GRIFFITHS, D.H., 1975. The application of geophysical methods
in the exploration and development of sandstone aquifers.
Q.J. Eng.Geol.8 73-102.

WYLLIE, M.R.J. and GREGORY, A.R. 1953. Formation factors of unconsolidated
porous media; influence of particle shape and effect of
cementation. Trans.Am.Inst.Min.metall.Engrs. 198 103-110.

_____ and SOUTHWICK, P.F. 1954. An experimental investigation of the S.P.
and resistivity phenomena in dirty sands. Trans.Am.Inst.Min.metall.
Engrs. 201 43-56.

APPENDIX

Fortran Programme for the least squared errors

solution of equation 7.3
(for N, scaling factor = 1)

VARIABLE	DESCRIPTION
A	z
AINC	decremental step of z
B	k
C	k'
DAT	two dimensional array (2 x 20)
DAT (N -)	pore water conductivity σ_w x 100
DAT (- N)	chargeability Vs/Vp (not percentage)
DE	inequality of equation 7.4
DTE	d^2E/dz^2 (see 7.c)
N	number of σ_w data for sample
NST	number of samples
SET	sample number

SEQUENCE OF INPUT

VARIABLE	FORMAT STATEMENT
NST	111
SET, N, A, AINC	112 e.g. put A = 1.0, AINC = 0.1
DAT (1,1)	113
⋮	
DAT (N,N)	

Programme description

Using the input value of A(z) the programme solves for
B (k) and C (k') through equations 7.7 and 7.8 and
returns these values to 7.4 to determine the
inequality (DE). For A greater than true A, DE is
negative. In this case A is reduced by AINC and the
process is repeated. (If the inputted A is too low,
the sample (SET) is rejected and the programme accepts
the next.) As A is progressively reduced, DE eventually
becomes positive. The previous A is then reduced by
AINC/10 and the process repeats using decrements of
AINC/10. When AINC is reduced to 0.0001, the programme
calculates DTE and outputs SET,A,B,C, DTE and DE, the
error of A being within +0.001.

```
      DIMENSION DAT(2,20), DS(8), DP(8)
      REAL*8 DS,DP,DCFA,DCFB,DCFC
      READ (5,111) NST
      WRITE (6,115)
      DO 99 M=1,NST
      DTE=0
      READ (5,112) SET, N, A, AINC
      READ (5,113) ((DAT(I,J),I=1,2),J=1,N)
      AL=A
   50 CONTINUE
      DO 98 K=1,8
      DS(K)=0
      DP(K)=0
   98 CONTINUE
    5 DO 1 I=1,N
      DS(1)=DS(1)+DAT(2,I)*DAT(1,I)**(A+1)
      DS(2)=DS(2)+DAT(2,I)*DAT(1,I)**(A*2+2)
      DS(3)=DS(3)+DAT(2,I)*DAT(1,I)**(A+2)
      DS(4)=DS(4)+DAT(2,I)*DAT(1,I)**(A*2+1)
      DS(5)=DS(5)+DAT(2,I)*DAT(1,I)**(A*2)
      DS(6)=DS(6)+DAT(2,I)*DAT(1,I)**A
      DS(7)=DS(7)+DAT(1,I)**(A*2)
      DS(8)=DS(8)+DAT(1,I)**(A*2+1)
      DLG=ALOG(DAT(1,I))
      DP(1)=DP(1)+DAT(2,I)*DAT(1,I)**(2*A)*DLG
      DP(2)=DP(2)+DAT(2,I)*DAT(1,I)**(2*A+1)*DLG
      DP(3)=DP(3)+DAT(2,I)*DAT(1,I)**A*DLG
      DP(4)=DP(4)+DAT(2,I)*DAT(1,I)**(A+1)*DLG
      DP(5)=DP(5)+DAT(1,I)**(A*2)*DLG
    1 CONTINUE
```

\#

```
C
C       CALCULATE B C AND DE
C

        DCFA=DS(1)*DS(2)-DS(3)*DS(4)
        DCFB=DS(6)*DS(2)-DS(3)*DS(5)+DS(3)*DS(7)-DS(1)*DS(8)
        DCFC=DS(4)*DS(6)-DS(1)*DS(5)-DS(6)*DS(8)+DS(1)*DS(7)
        C=SNGL((DSQRT(DCFB**2-4*DCFA*DCFC)-DCFB)/(DCFA*2))
        B=SNGL((DS(7)-DS(5)-DS(4)*C)/(DS(1)*C+DS(6)))
        DE=SNGL(DP(1)+DP(2)*C+DP(3)*B+DP(4)*B*C-DP(5))
C
C       TEST FOR DE=0
C
        IF (DE) 2,3,4
      2 A=A-AINC
        GO TO 50
      4 AINC=AINC/10
        IF (AINC.LE.0.0001) GO TO 3
        A=A+AINC*9
        IF (A.GT.AL) GO TO 99
        GO TO 50
      3 CONTINUE
C
C       CALCULATE D2E/DA2 = DTE
C
        DO 97 L=1,N
        DATP=DAT(1,L)**A
        DTE=DTE+(((1+C*DAT(1,L))*(DATP**2-B**2)*DAT(2,L)-DATP**2+DATP*2*B)
     1*2*B*(ALOG(DAT(1,L))**2)*DATP/((1+C*DAT(1,L))**2*(DATP+B)**4))
     97 CONTINUE
        WRITE (6,114) SET, A, B, C, DTE, DE
     99 CONTINUE
    111 FORMAT (I3)
    112 FORMAT (A4,2X,I2,2X,2F4.0)
    113 FORMAT (2F5.0)
    114 FORMAT (1H ,6X,A4,7X,F6.4,3X,F7.4,2X,F6.4,2X,F10.4,6X,F15.8)
    115 FORMAT (1H1,6X,6HSAMPLE,5X,1HA,8X,1HB,8X,1HC,8X,7HD2E/DA2,5X,2HDE)
        STOP
        END

#
```

APPENDIX

Solution to equation 7.3 for the data in 4.c (FIG.12)

using the Fortran programme (Scaling factor = 1)

Sample	z	k	k'	d^2E/dz^2	DE	Fylde borehole
1	0.236	45.72	0.005	0.13	0.0062	T52
2	0.335	14.53	0.019	0.62	0.0236	T37
3	0.398	5.81	0.218	0.20	0.0017	T48
4	0.480	5.67	0.218	0.29	0.0013	T52
5	0.334	4.84	0.158	0.32	0.0041	T44
6	0.284	3.62	0.083	0.68	0.0062	T31
7		input data rejected				T44

APPENDIX

Field data calculated as $m_{(a)}$ $\rho_{A(a)}$ and $\rho_{B(a)}$.

Units-spacing a ft; apparent chargeability $m_{(a)}$%;
apparent resistivity $\rho_{(a)}$ ohm.ft.

a	$m_{(a)}$	$\rho_{A(a)}$	$\rho_{B(a)}$		a	$m_{(a)}$	$\rho_{A(a)}$	$\rho_{B(a)}$
1. SD	**4739**	**4038**	**NOV 73**		**4. SD**	**4695**	**4164**	**NOV 73**
6	0.53	155	29413		8	0.44	148	33148
8	0.50	134	26586		16	0.65	149	22762
16	0.56	138	24443		32	0.65	144	22137
32	0.75	177	23358		64	0.92	170	18426
64	1.11	221	19776		128	1.30	219	16591
128	1.59	273	16920		192	1.71	273	14086
256	2.45	269	10622		256	2.06	270	12850
512	1.45	289	19551		384	2.23	319	14000

a	$m_{(a)}$	$\rho_{A(a)}$	$\rho_{B(a)}$		a	$m_{(a)}$	$\rho_{A(a)}$	$\rho_{B(a)}$
2. SD	**4715**	**4102**	**NOV 73**		**5. SD**	**4717**	**4198**	**NOV 73**
8	0.58	171	29362		8	0.84	212	24911
16	0.81	173	21093		16	0.66	184	27807
32	1.06	167	15511		32	0.59	134	22622
64	1.25	185	14661		64	0.69	150	21459
128	1.66	206	12067		128	1.00	208	20513
192	1.89	201	10457		192	1.47	250	16926
256	1.99	187	9172		256	1.54	262	16846
384	1.71	217	12513		384	1.70	309	17711
512	1.23	225	18193					

a	$m_{(a)}$	$\rho_{A(a)}$	$\rho_{B(a)}$		a	$m_{(a)}$	$\rho_{A(a)}$	$\rho_{B(a)}$
3. SD	**4695**	**4141**	**NOV 73**		**6. SD**	**4702**	**4240**	**NOV 73**
8	0.52	158	30382		8	0.84	257	30132
16	0.57	212	37153		16	0.57	219	37865
32	0.51	138	26747		32	0.67	181	26747
64	0.85	157	18404		64	1.05	239	22398
128	1.44	220	15046		128	1.87	212	11112
192	1.83	257	13822		192	2.52	200	7679
256	1.78	312	17524		256	2.65	214	7798
384	1.50	383	25085		384	1.90	–	–
512	1.64	399	24201					

a	$m_{(a)}$	$\rho_{A(a)}$	$\rho_{B(a)}$
7.	SD 4710	4230	NOV 73
8.8	0.64	235	36191
16	0.50	185	36486
32	0.54	175	31937
64	1.04	183	17313
128	1.50	154	10041
192	2.07	216	10268
256	2.69	164	5920

a	$m_{(a)}$	$\rho_{A(a)}$	$\rho_{B(a)}$
8.	SD 4800	4376	NOV 73
8	1.20	254	20911
16	1.30	277	20961
32	1.34	320	23565
64	1.20	284	23527
128	1.27	252	19554
192	1.52	337	21777
256	1.85	281	14922
384	2.09	358	16586

a	$m_{(a)}$	$\rho_{A(a)}$	$\rho_{B(a)}$
9.	SD 5047	4527	NOV 73
8	1.42	403	27800
16	1.97	573	28224
32	2.88	656	22025
64	4.13	600	13869
128	4.85	329	6460
192	3.29	266	7822
256	2.37	249	10216
384	0.86	525	59984

a	$m_{(a)}$	$\rho_{A(a)}$	$\rho_{B(a)}$
10.	SD 4977	4102	NOV 73
8	0.47	179	37858
16	0.64	254	39265
32	0.96	267	27467
64	1.67	273	16127
128	3.56	290	7860
192	3.85	309	7722
256	3.53	338	9230
384	2.00	431	20932

a	$m_{(a)}$	$\rho_{A(a)}$	$\rho_{B(a)}$
11.	SD 5240	3688	NOV 73
8	0.92	440	47469
16	0.94	538	56206
32	0.90	409	45268
64	1.17	303	25511
128	1.76	330	18420
192	1.86	354	18632
256	1.72	381	21638
384	1.42	448	30887

a	$m_{(a)}$	$\rho_{A(a)}$	$\rho_{B(a)}$
12.	SD 5010	3611	NOV 73
8	0.26	113	44122
16	0.26	118	44627
32	0.42	140	34317
64	0.65	190	29067
128	1.06	226	21108
192	1.36	228	16549
256	1.41	303	21210
372	2.43	354	13966

a	$m_{(a)}$	$\rho_{A(a)}$	$\rho_{B(a)}$
13.	SD 4896	4340	NOV 73
8.	0.48	152	31244
16	0.65	176	26999
32	1.05	239	22310
64	1.98	276	13582
128	3.66	293	7692
192	4.29	325	7228
256	4.76	358	7130
384	3.54	456	12431

1. SD 4830 4156 JUNE 74

t_p, t_d incorrect

a	$m_{(a)}$	$\rho_{A(a)}$	$\rho_{B(a)}$	a	$m_{(a)}$	$\rho_{A(a)}$	$\rho_{B(a)}$

2. SD 4915 4131 JUNE 74

a	$m_{(a)}$	$\rho_{A(a)}$	$\rho_{B(a)}$
16	0.55	455	82648
32	0.83	571	68595
64	1.16	429	36419
128	1.49	363	23944
192	1.97	339	16449
256	2.53	304	11691
384	4.18	253	5760

6. SD 5014 4003 JUNE 74

a	$m_{(a)}$	$\rho_{A(a)}$	$\rho_{B(a)}$
8	0.67	374	55258
16	1.02	415	40126
32	1.50	351	22956
64	1.85	254	13397
128	2.51	225	·8711
192	2.73	275	9807
256	1.67	344	20301
384	1.44	502	34431

3. SD 4985 4050 JUNE 74

a	$m_{(a)}$	$\rho_{A(a)}$	$\rho_{B(a)}$
8	0.28	127	44845
16	0.54	175	32374
-32	1.04	221	20948
64	2.08	234	10960
128	3.02	254	8139
192	3.16	280	8573
256	2.8	315	10899
384	2.62	367	13590

7. SD 5082 3995 JUNE 74

a	$m_{(a)}$	$\rho_{A(a)}$	$\rho_{B(a)}$
8	0.94	537	56756
16	1.26	550	43188
32	1.48	356	23761
64	2.11	248	11490
128	2.90	268	8974
192	3.12	264	8207
256	2.85	285	9696

4. SD 5033 4068 JUNE 74

a	$m_{(a)}$	$\rho_{A(a)}$	$\rho_{B(a)}$
8	1.19	689	57408
16	1.59	515	31960
32	1.38	377	26819
64	1.65	365	21695
128	2.58	267	10041
192	2.84	274	9345
256	2.21	355	15675

8. SD 4969 4144 JUNE 74

a	$m_{(a)}$	$\rho_{A(a)}$	$\rho_{B(a)}$
8	0.37	242	64347
16	0.62	192	30826
32	0.86	231	26812
64	1.23	270	21734
128	2.55	249	9500
192	3.23	243	7273
256	3.31	282	8220
384	3.44	333	9363

5. SD 5001 4019 JUNE 74

a	$m_{(a)}$	$\rho_{A(a)}$	$\rho_{B(a)}$
8	0.96	695	71865
16	1.13	601	54885
32	2.48	461	18136
64	5.28	284	5091
128	4.64	254	5212
192	2.91	287	9477
256	3.09	288	9020

9. SD 5052 3975 JUNE 74

a	$m_{(a)}$	$\rho_{A(a)}$	$\rho_{B(a)}$
8.	0.69	406	58097
16	0.60	434	71343
32	0.85	398	46644
64	1.63	514	30897
128	2.49	368	14381

a	$m_{(a)}$	$\rho_{A(a)}$	$\rho_{B(a)}$

10. SD 5007 3917 JUNE 74

a	$m_{(a)}$	$\rho_{A(a)}$	$\rho_{B(a)}$
8	0.21	248	117944
16	0.33	441	133397
32	0.62	579	92968
64	1.14	639	55522
128	2.22	479	21038
192	2.84	354	12105
256	2.85	362	12329
384	3.22	355	10560

11. SD 5000 3920 JUNE 74

a	$m_{(a)}$	$\rho_{A(a)}$	$\rho_{B(a)}$
8	0.26	126	49076
16	0.42	143	34077
32	0.93	180	19016
64	1.66	230	13610
128	2.47	283	11148
192	2.60	313	11727
256	2.66	355	12981

12. SD 4989 3876 JUNE 74

a	$m_{(a)}$	$\rho_{A(a)}$	$\rho_{B(a)}$
8	0.37	125	33753
16	0.60	167	27801
32	1.23	234	18776
64	2.02	258	12520
128	2.79	292	10164
192	2.82	308	10623
256	3.09	315	9884
384	3.05	362	11494

13. SD 4973 3870 JUNE 74

a	$m_{(a)}$	$\rho_{A(a)}$	$\rho_{B(a)}$
8	0.20	117	58831
16	0.35	115	32342
32	0.77	166	21551
64	1.45	223	15119
128	2.45	288	11437
192	2.93	315	10442
256	2.98	322	10495

14. SD 4999 3835 JUNE 74

a	$m_{(a)}$	$\rho_{A(a)}$	$\rho_{B(a)}$
8	-0.1	110	- ve
16	0.24	112	46690
32	0.56	152	26840
64	1.12	222	19591
128	1.93	290	14634
192	2.71	324	11618
256	2.38	352	14480
384	2.34	440	18305

15. SD 5032 3814 JUNE 74

a	$m_{(a)}$	$\rho_{A(a)}$	$\rho_{B(a)}$
8	0.79	334	41933
16	0.52	189	36154
32	0.86	217	25056
64	1.46	258	17287
128	2.12	288	13239
192	2.15	315	14215
256	2.00	331	16202

16. SD 5083 3806 JUNE 74

Excessive 50 HZ noise

17. SD 5107 3728 JUNE 74

a	$m_{(a)}$	$\rho_{A(a)}$	$\rho_{B(a)}$
8	0.21	96	45286
16	0.22	104	47826
32	0.23	139	59575
64	0.36	208	57107
128	0.57	290	50581
192	1.42	346	23918
256	1.78	341	18790
384	2.63	392	13783

18. SD 5050 3723 JUNE 74

a	$m_{(a)}$	$\rho_{A(a)}$	$\rho_{B(a)}$
8	0.23	136	58454
16	0.40	180	44645
32	0.55	280	51058
64	0.90	390	42845
128	1.44	403	27494
192	1.69	362	20988
256	1.98	349	17114
384	1.62	493	29371

a	$m_{(a)}$	$\rho_{A(a)}$	$\rho_{B(a)}$

19. SD 5039 3696 JUNE 74

a	$m_{(a)}$	$\rho_{A(a)}$	$\rho_{B(a)}$
8	0.20	107	52635
16	0.17	98	56824
32	0.36	125	34558
64	0.91	162	17616
128	1.84	207	11070
192	2.33	246	10284
256	2.57	286	10764
384	3.86	307	7549

20. SD 5018 3756 JUNE 74

a	$m_{(a)}$	$\rho_{A(a)}$	$\rho_{B(a)}$
8	0.00	91	00
16	0.20	97	47701
32	0.55	129	23490
64	1.58	183	11384
128	2.20	252	11148
192	2.47	274	10771
256	2.05	327	15527

21. SD 4996 4020 JUNE 74

a	$m_{(a)}$	$\rho_{A(a)}$	$\rho_{B(a)}$
8	1.28	851	65681
16	1.08	522	47593
32	1.28	430	33246
64	1.93	391	19841
128	2.91	315	10499

22. SD 5175 3416 JUNE 74

Excessive noise

23. SD 5136 3364 JUNE 74

a	$m_{(a)}$	$\rho_{A(a)}$	$\rho_{B(a)}$
16	0.03	current	
32	0.33	recording	
64	0.61	error	
128	0.98		
192	1.07		
256	1.28		

24. SD 5170 3433 JUNE 74

a	$m_{(a)}$	$\rho_{A(a)}$	$\rho_{B(a)}$
8	0.20	134	66412
16	0.27	161	58938
32	0.41	273	66606
64	0.69	364	52118
128	0.98	372	37479
192	1.11	377	33493
256	1.34	358	26462

25. SD 5160 3450 JUNE 74

a	$m_{(a)}$	$\rho_{A(a)}$	$\rho_{B(a)}$
8	0.70	201	28366
16	0.70	177	22032
32	0.74	191	25440
64	0.83	218	26037
128	0.69	261	37684
192	1.14	268	23163

26. SD 4880 4407 JUNE 74

a	$m_{(a)}$	$\rho_{A(a)}$	$\rho_{B(a)}$
8	0.72	269	37133
16	0.79	236	29656
32	0.98	228	23169
64	1.18	228	19184
128	1.63	261	15696
192	1.75	281	15752
256	1.88	315	16444

27. SD 5137 3521 JUNE 74

a	$m_{(a)}$	$\rho_{A(a)}$	$\rho_{B(a)}$
8	0.24	122	51217
16	0.24	114	48404
32	0.30	163	55112
64	0.39	246	62481
128	0.73	294	40048
192	0.88	259	32282

28. SD 5052 3545 JUNE 74

a	$m_{(a)}$	$\rho_{A(a)}$	$\rho_{B(a)}$
8	0.10	86	83511
16	0.10	84	85589
32	0.18	110	62012
64	0.32	176	54489
128	0.74	226	30289
192	1.08	246	21860

a	$m_{(a)}$	$\rho_{A(a)}$	$\rho_{B(a)}$

29. SD 4900 4105 JUNE 74

a	$m_{(a)}$	$\rho_{A(a)}$	$\rho_{B(a)}$
8	0.73	165	22424
16	0.64	162	25329
32	0.68	194	28332
64	0.88	268	30258
128	1.43	307	21125
192	2.05	311	14881
256	2.37	292	12053
384	1.77	413	22573

30. SD 5034 4121 JUNE 74

a	$m_{(a)}$	$\rho_{A(a)}$	$\rho_{B(a)}$
8	1.48	707	47100
16	1.56	1035	65418
32	1.54	1078	68985
64	1.65	871	51853
128	2.07	542	25683
192	2.36	359	14827

31. SD 5033 4367 JUNE 74

a	$m_{(a)}$	$\rho_{A(a)}$	$\rho_{B(a)}$
8	1.73	1302	73879
16	2.13	1387	63485
32	2.31	912	38376
64	2.27	447	19226
128	2.35	264	11035
192	3.54	227	6210
256	1.92	239	12210

32. 4769 4522

a	$m_{(a)}$	$\rho_{A(a)}$	$\rho_{B(a)}$
8	0.23	100	43811
16	0.33	122	36722
32	0.66	166	24967
64	1.05	226	21304
128	1.51	295	19226
192	1.66	328	19455
256	1.95	358	17913
384	1.78	500	27880

33. SD 4823 4457 JUNE 74

a	$m_{(a)}$	$\rho_{A(a)}$	$\rho_{B(a)}$
8	0.21	73	33909
16	0.43	93	21420
32	0.63	133	21099
64	0.91	177	19216
128	1.25	212	16809
192	1.50	246	16106
256	1.63	249	14924

34. SD 4971 4343 JUNE 74

a	$m_{(a)}$	$\rho_{A(a)}$	$\rho_{B(a)}$
8	0.83	255	30487
16	1.16	228	19484
32	1.54	211	13490
64	1.79	167	9113
128	2.34	216	8968
192	2.14	251	11473
256	2.69	264	9420